Mef2c transcription factor is required for the development of medium spiny neurons of the mouse striatum

A thesis submitted for the degree of doctor of Philosophy

At

Cardiff University

School of Medicine

Heba Ali

2022

Thesis Summary

Medium spiny neurons (MSNs) are the major projection of the striatum and are the neurons predominantly degenerating in Huntington's disease. Understanding normal striatal MSNs development is important for several areas of applied research; it is key in understanding the pathological conditions affecting this area of mouse brain, and for improving protocols for differentiating MSNs from pluripotent stem cells for use as cell models of disease or for generating cells for cell-based therapy of neurodegenerative diseases like HD. We have shown the transcription factor Mef2c to be significantly upregulated in the striatum over a period encompassing peak generation of medium spiny neurons (MSNs). Here I present data that suggest a significant functional role of Mef2c in the survival of MSNs in the mouse striatum

The spatiotemporal expression of Mef2c in embryonic and postnatal mouse striatum was determined, Mef2c was found to be expressed predominantly in MSNs of the striatal matrix compartment. To investigate the role of Mef2c in MSNs development, a striatal-specific Cre mouse line was used to knockout Mef2c in the mouse striatum (CKO) during embryonic development. The histological effects on mouse striatum were assessed in a developmental series between P2 and 12 months, which showed a significant reduction in striatal volume and MSNs count in CKO striatum at P14 onward and a mild, yet significant effect on dendritic spine development. Behavioral testing of 12-month-old CKO mice showed a significant impairment in motor functions and in the exploratory behavior of new environments, demonstrating the functional importance of Mef2c in MSN development.

The mechanism underlying the loss of MSNs was explored and a significant increase in apoptotic activity was observed in P3 CKO striatum, with more apoptotic cells in matrix compartment. This was accompanied with a significant reduction in the anti-apoptotic factor Bcl-xl. Suggest that Mef2c loss impacted MSNs survival in matrix compartment through altering Bcl-xl mediated pathways.

In conclusion, this thesis investigated the functional role of Mef2c in the development of mouse striatum through studying a striatal specific CKO mouse model and showed that Mef2c is required for the survival of a subpopulation of matrix MSNs.

Acknowledgement

Firstly, I would like to thank my supervisors Professor Anne Rosser and Dr Michael Taylor for having me in the BRG during the last four years. Words cannot express my gratitude for your invaluable patience and feedback especially during the last few months. I am extremely grateful for all the invaluable advice and the continuous guidance and support not only through my PhD but also through the difficult moments I've been through. This endeavour would not have been possible without your support.

I would also like to thank Dr Sophie Rowlands for all the technical assistance at every stage of my research project, for the emotional support and for lifting my spirits and motivation high in my most difficult times. Without your tremendous encouragement and patience in the past few years, it would be impossible for me to complete my study.

Special thanks for Dr Mariah for being always reachable for any help and support and for the valuable advice you provided in statistics.

I would also like to thank Anne-Marie for all the help you provided through the past years and for lending ears to listen to my early morning complaints and keep reminding me how strong I am.

I would like also to thank all the members in BRG, Rachel Hills, thanks for all the technical help and support you provided through the last four years. Thanks to my ''old'' roommates Charlie, Patricia, and Firas, I am sure you all will do brilliant in the rest of your Ph.D. Thanks also to Rachel Sellick, Oly, Kyle, Kubra, and Olivia. It is your kind help and support that have made my study in the UK a wonderful time.

I would also like to thank Dr Emma Lane for the valuable advice you provided every lab meeting.

Very big thanks go to my big family, my devoted and compassionate Mum, thanks for being a second mother while I am away. And to my sisters Lina, Lara, Shere, and Ala, and to my brothers, Ashraf and Ahmad, there is no way I would have got through my PHD without your help and support. And for my small family, my beloved husband Hazem, thanks for the love, understanding and patience. To my lovely boys, Ghazi and Ashraf, thanks for making me the luckiest Mum ever and thanks for all the entertainment you always made to me Ashraf! I promise we will never be apart again; and remember our best days together are yet to come.

And finally, I dedicate this thesis to the person who will never read these words, to my father, I will always love and miss you until we meet.

Abbreviations

ANOVA: Analysis of variance

BDNF: Brain-Derived Neurotrophic Factor

BrdU: Bromodeoxyuridine / 5-bromo-2'-deoxyuridi

BSA: Bovine serum albumin

Caspase3: Cysteine-aspartic acid protease 3

CGE: Caudal ganglionic eminence

ChAT: Anti-Choline Acetyltransferase

CKO: conditional knockout

CNS: Central nervous system

Ctip2: COUP TF1-interacting protein 2

CV: cresyl violet

D1 and D2: Dopamine 1 and 2 receptors

DAB: 3,3'-Diaminobenzidine

Darpp32: Dopamine and cyclic AMP-regulated phosphoprotein

DIV: days in vitro

DMEM: Dulbecco's modified eagle medium

DNA: Deoxyribose nucleic acid

dNTP: Deoxyribonucleotide triphosphates DNA

E12: embryonic day 12

E14: embryonic day 14

E16: embryonic day 16

E18: embryonic day 18

EdU: 5-ethynyl-2'-deoxyuridine

FCS: Foetal calf serum

FoxP1: Forkhead Transcription Factor 1

GABA: Ɣ-aminobutyric acid

GP: Globus Pallidus

Gsx2: Genetic-Screened Homeobox 2

HCL: Hydrochloric acid

HD: Huntington's Disease

HDAC: Histone deacetylase

hESCs: human embryonic stem cells

IHC: Immunohistochemistry

KDa: kilodalton

Ki67: Antigen KI-67

LGE: Lateral ganglionic eminence

MAP2: Microtubule associated protein 2

MEF2: Myocyte Enhancer Factor

MGE: Medial ganglionic eminence

MOR1: mu opioid receptor1

mRNA: Messenger RNA

MSNs: medium spiny neurons

NeuN: Neuronal nuclei

NPCs: Neural precursor cells

P0: Post-natal day 0

P2: Post-natal day 2

P7: Post-natal day 7

P14: Post-natal day 14

PBS: Phosphate buffered saline

PD: Parkinson's disease

PDL: Poly-D-Lysine

PFA: Paraformaldehyde

Poa: preoptic area

PV: parvalbumin

RGCs: Radial glial cells

RNA: Ribonucleic acid

ROI: Region of interest

RT: room temperature

RT qPCR: reverse transcriptase quantitative poly chain reaction

SGZ: sub-granular zone

SNc: substantia nigra pars compacta

SNr: substantia nigra pars reticulata

STN: subthalamic nucleus

SVZ: subventricular zone

TAD: transcriptional activation domains

TBST/TxTBS: Tris-buffered saline

TF: transcription factor

TUNEL: Terminal deoxynucleotidyl transferase (TdT) dUTP Nick-End Labelling

WT: wild type

Table of Contents

Table of Figures

List of Tables

Chapter 1 General Introduction

1.1 Introduction

The focus of the work in this thesis is to understand more about striatal development, in particular differentiation and organisation of striatal medium spiny neurons (MSNs). MSNs are the major projection neuron of the striatum and constitute more than 95% of neurons in the adult mouse striatum. Several conditions can lead to loss of MSNs, in particular the neurodegenerative condition, Huntington's disease (HD), in which MSNs are preferentially affected very early in the disease course. Understanding more about MSN development is important in order to facilitate efforts to produce more accurately specified MSNs for cell culture models and as donor cells for cell replacement therapy and may also contribute to an enhanced understanding of striatal function.

The striatum is complex and striatal MSNs are not homogeneous. Producing an appropriate balance of properly specified MSNs is particularly important for cell replacement therapy in which the approach is to transplant into the disease striatum cells that have the capacity to develop into MSNs and take over the function of the cells that have degenerated. Donor MSNs need to be immature, as fully mature MSNs cannot survive the transplantation process. One source of immature MSNs is foetal ganglionic eminence, often referred to as whole ganglionic eminence (WGE), as it comprises two parts; the lateral GE (LGE) and medial GE (MGE). There is extensive evidence from animal studies that transplantation of foetal-derived MSNs can result in reconstruction of neural circuitry and proof of concept that the approach can improve function in HD patients (Dunnett and Rosser, 2011; Rosser and Bachoud-Lévi, 2012; Olsson et al., 1995). However, use of foetal tissue is associated with ethical and practical challenges. Therefore, there is a pressing need for better protocols to direct human pluripotent stem cells (hPSCs) into MSNs for replacement therapy. This requires an in-depth and comprehensive understanding of the MSN differentiation program to generate mature MSNs reliably and precisely from hPSCs.

Our interest in Myocyte enhancer factor C, Mef2c, in the context of MSN differentiation, arose from a microarray study undertaken in our lab (Affymetrix technology, MAS5.0) that revealed that one of the MEF2 TFs family, Mef2c isoform, is among the most highly upregulated genes during embryonic striatal neurogenesis (Precious et al., 2016) and Jeyasingham 2005, PhD thesis).

Mef2c is a TF that was originally identified as having a key role in muscle differentiation (Taylor and Hughes, 2017), but more recently has been shown to have an important role in neuronal development, maturation and survival of various brain regions in human and rodents (Leifer et al., 1993; Kamath and Chen, 2019; Adachi et al., 2016). However, little is known about the role of Mef2c in the development of the striatum. Therefore, my aim in this thesis was to identify the role of Mef2c in the development of the mouse striatum using conditional striatal Mef2c knockout mice as the main experimental model, with the future aim of using this information to improve on existing protocols to differentiate MSNs from hPSC populations (Li et al., 2008e). To the best of my knowledge, this work is the first attempt to understand the role of Mef2c in the development of MSNs.

1.2 Adult striatum

1.2.1 Adult striatal architecture

The striatum (or neo-striatum) is the largest subcortical structure and the main input structure of the basal ganglia and is involved in motor, cognitive and emotional functions. It consists mainly of the caudate nucleus and putamen in human and non-human primates, while in rodents it is one structure. The major neuronal component of the mouse striatum, about 95%, is the MSNs which form the major projection output of the striatum and use the inhibitory neurotransmitter γ-aminobutyric acid (GABA). The remaining 5% of neurons are mostly interneurons (Jain et al., 2001; Lanciego et al., 2012). This interneuron population consists mainly of two populations choline acetyltransferase (ChAT)-positive cholinergic interneurons as well as parvalbumin (PV) positive interneurons (Tepper et al., 2010). The striatum receives afferents by its integration with different parts of the brain, including cerebral cortex, thalamus, substantia nigra and other parts of the basal ganglia (Albin et al., 1989; Jain et al., 2001).

The striatum can be subcategorized into the dorsal striatum, and the ventral striatum, the latter of which comprises the nucleus accumbens and part of the olfactory tubercle. The dorsal striatum receives a huge glutamatergic input from the cortex and thalamus. These excitatory glutamatergic cortical fibers innervate distinct regions of the striatum; for example, input from sensorimotor cortical areas innervate the dorsal striatum, while fibers from limbic cortical areas innervate the ventral striatum (Lanciego et al., 2012).

Dopaminergic inputs from the substantia nigra pars compacta also synapse with striatal fibers, releasing dopamine onto D1 receptors in the direct pathway and D2 receptors in the indirect pathway (Svenningsson et al., 2004; MarionYger and Girault, 2011). This anatomical arrangement illustrates the importance of the direct and indirect striatal pathways; pathologies that result in alterations in this arrangement within the striatum include Parkinson's disease (PD) and HD that lead to abnormalities in multiple neurological domains such as motor and cognitive functions.

1.2.2 The organisation of matrix-striosomes in the mouse striatum

The mouse striatum has a mosaic organisation and can be divided anatomically and neurochemically into two main divisions, the striosomes (also called patches) and the matrix, **Figure 1.1A**. In the adult mouse striatum, the striosomes form a labyrinth-like structure that is embedded in the larger part, the matrix. The striosomes compartments constitute about 10-15% of the overall striatum and are occupied by the early born MSNs, formed between E11 and E13, while the later-formed MSNs, between E13-E16, will occupy the matrix compartment which constitutes about 85-90% of the striatal volume (Graybiel and Ragsdale, 1978; van der Kooy and Fishell, 1987; Mason et al., 2005; Brimblecombe and Cragg, 2017; Johnston et al., 1990; Matsushima and Graybiel, 2020), **Figure 1.1B**.

These two compartments differ in the neurochemical markers they express, in addition to differences in their afferent and efferent connectivity. Striosomes are enriched with the mu opioid receptor marker 1 (MOR1) and substance P (Delfs et al., 1994; Nakamura et al., 2009), while the matrix is enriched with acetylcholinesterase, calbindin D-28K, somatostatin and enkephalin (Graybiel and Ragsdale Jr, 1978; Gerfen and Young III, 1988; Gerfen, 1992). A summary of molecules expressed differentially in the striosomes, and matrix of mouse striatum are shown in **Table 1.1.**

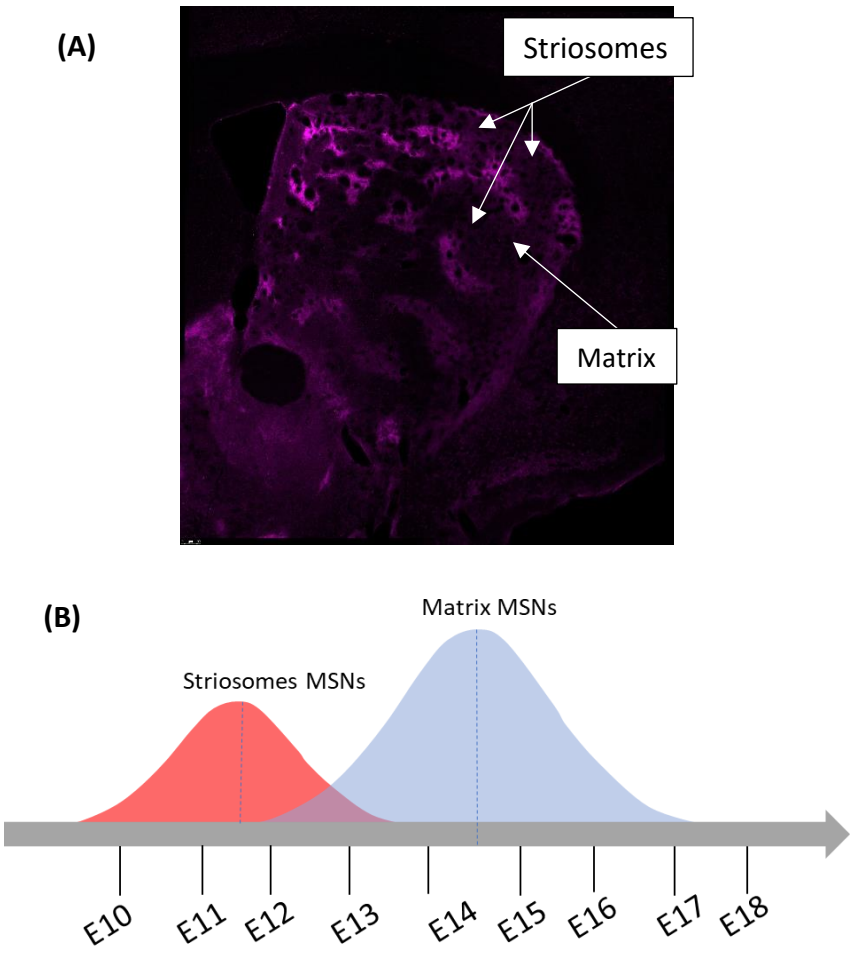

Figure 1.1: A: the organisation of matrix and striosomes in adult mouse striatum shown by MOR-1 immuno-staining, White arrows show the two different compartments. **(B)** schematic illustration of striatal embryonic neurogenesis that contributes to the two striatal compartments: striosomes and matrix. Adapted from (Lebouc et al., 2020).

Molecule	***Full name***	***Reference***
Striosomes		
5HT2a	Serotonin receptor type 2a	(López-Giménez et al., 2002)
AADC	Aromatic, l-amino acid decarboxylase	(Kim et al., 2002)
C3HC4	Membrane-associated ring finger 4	(Hatten et al., 2003)
CALB2	Calretinin	(Davis and Puhl, 2011)
DARPP-32	Dopamine and cAMP-regulated phosphoprotein 32 kDa (P0 striatum only)	(Arlotta et al., 2008a)
Drd1	Dopamine receptor D1 (early postnatal only)	(Kim et al., 2002)
Drd4	Dopamine receptor D4	(Rivera et al., 2002)
GluR1	Glutamate receptor, ionotropic, AMPA 1	(Arlotta et al., 2008)
MOR1	Opioid receptor, mu 1	(Herkenham and Pert, 1981)
NR4a1	Nuclear hormone receptor	(Davis and Puhl, 2011)
Pdyn	Prodynorphin	(Hatten et al., 2003)
Matrix compartment		
CALB1	Calbindin 1, 28 kDa	(Ito et al., 1992, Davis and Puhl, 2011)
CalDAG-GEFI	Calcium/diacylglycerol-regulated guanine nucleotide exchange factor I	(Crittenden et al., 2010)
ChAT	Choline O-acetyltransferase	(Graybiel et al., 1986)
Htr4	5-hydroxytryptamine (serotonin) receptor 4	(Hatten et al., 2003)
Preproenk	Enkephalin	(Koshimizu et al., 2008a)

Table 1.1 A Summary of the most known makers of striosomes and matrix in mouse striatum.

1.2.3 The direct and indirect pathways

The striatal MSNs can be categorised according to which dopamine receptors they express into D1- and D2-receptor MSNs. Dopamine receptor 1 (D1) is functionally associated with the direct excitatory pathway whereas dopamine receptor 2 (D2) is associated with the indirect inhibitory pathway (Gerfen et al., 1990; DeLong and Wichmann, 2009; Keeler et al., 2014). The direct pathway (also called the striato-nigral pathway) provides direct input to the substantia nigra pars reticulata (SNr) and the globus pallidus internus (GPi) while the indirect pathway (also called the striato-pallidal pathway) provides input to the globus pallidus externus (GPe) that in turn connects the striatum to the SNr indirectly (Gerfen, 1992). D1 and D2 MSNs are distinct immunohistochemically with substance P and dynorphin being enriched in MSNs projecting to GPi and SNr in the direct pathway while the neuropeptide enkephalin is enriched in MSNs projecting to GPe in the indirect pathway in matrix compartment. Ebf1 TF was shown to be important for the differentiation of D1 MSNs in matrix compartment(Lobo et al., 2008), on the other hand, the TF SP9 was shown to be important for the development of D2 MSNs (Zhang et al., 2016; Xu et al., 2018). A recent investigation has shown a new marker of D1 MSNs during LGE development which is Zfhx3 (Zhang et al., 2019a).

The mouse striatum receives glutamatergic input from the cortex and thalamus and dopaminergic input from the SN. The two striatal compartments, matrix and striosomes, are distinct with striosome MSNs receiving input mostly from the insular limbic cortex and matrix MSNs receiving input from the sensorimotor and associative cortex (Flaherty and Graybiel, 1994; Lui et al., 2011). However, both of the striatal compartments, matrix and striosomes, contribute to the direct and indirect pathways with an assumption that D1 MSNs are more abundant in striosomes (Miyamoto et al., 2018) and tracing studies have also shown that striosome MSNs send monosynaptic fibers to SNc (Fujiyama et al., 2011; Nambu et al., 2002; Lévesque and Parent, 2005; Fujiyama et al., 2011; Crittenden et al., 2016) **(Figure 1.2).**

(a)

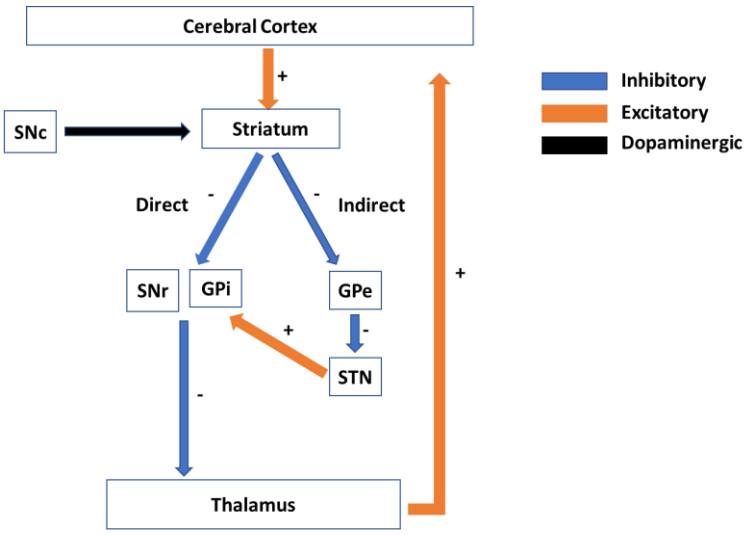

(b)

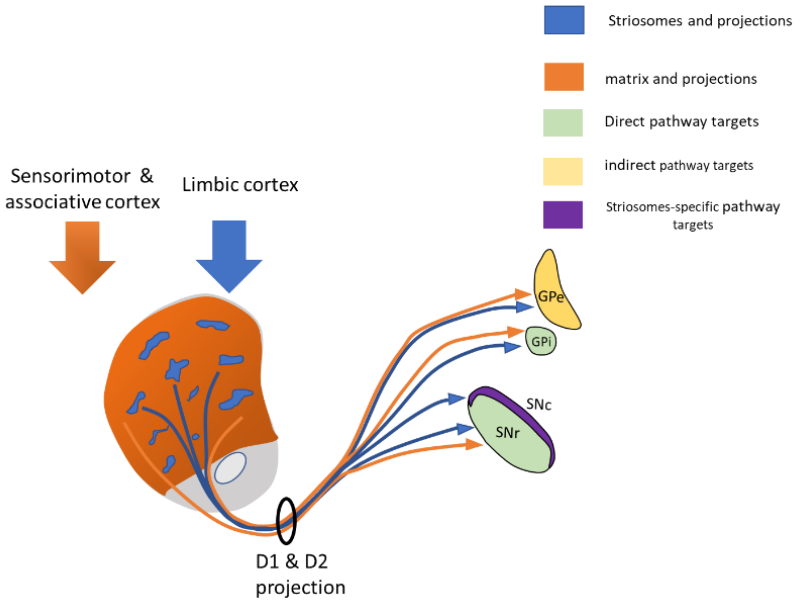

Figure 1.2: **(a)** Schematic diagram of mouse striatum connections in direct and indirect pathway. **(b)** Basal ganglia connections in respect to matrix and striosomes MSNs. Adapted from (Crittenden and Graybiel, 2011). STN-subthalamic nucleus, GPe/GPi globus pallidus external/internal, SNr/SNc Substantia Nigra pars reticulata/compacta

1.3 Mouse striatal development

The development of the central nervous system (CNS) is a highly conserved process among mammals (Puelles et al., 2000; Rubenstein et al., 1998). It starts with neural induction, which is the formation of the neural plate at the dorsal end of the embryo, with the brain and cerebellum formed from the rostral end and the spinal cord from the caudal end. This is followed by neurulation, during which the neural plate folds and the neural tube is formed. Regional patterning of the neural tube results in identification of distinct subdivisions: telencephalon that will further divide into pallium (also called dorsal telencephalon) and sub pallium (also called ventral telencephalon), with the striatum developing from the sub pallium (Jain et al., 2001); diencephalon (from which thalamus and subthalamus will develop); mesencephalon (midbrain); and rhombencephalon (hindbrain). The structure surrounding the developing telencephalon is the ventricular zone (VZ) located on the lateral ventricles and subventricular zone (SVZ), which is unique to the telencephalon and extends from the basal region of the VZ. The WGE is formed as an intraventricular bulge of proliferative zones in the subpallium and composed of the MGE medially and LGE laterally **(Figure 1.3)**.

1.3.1 Striatal neurogenesis, migration, and maturation during embryonic development and early postnatal period

The mouse WGE consists of lateral, medial, and caudal ganglionic eminences, (LGE, MGE and CGE respectively). Striatal MSNs are derived from different populations of neural progenitors that reside in the neuroepithelium of the LGE, from where the bulk of the striatum will be formed. MSNs develop from LGE as a population of *Ascl1+, Gsh2+* and *Dlx1/2/5/6+* precursors that reside and proliferate in the VZ and SVZ, and among these, Gsx2 is responsible for the neuronal progenitor establishment of the LGE (Deacon et al., 1994; Waclaw et al., 2010) **Figure 1.3**. Following proliferation, neurons migrate to the mantle zone (MZ) of the developing striatum, where they become postmitotic and then differentiate to MSNs.

At E9.5 the LGE starts to be evident in the mouse brain, with the ventricular region enriched with neuroepithelial cells (NECs) that express the TFs Gsx1/2. NECs will give rise cells that will form the radial glial cells (RGCs) that express the TFs Gsx1/2 and Tis21, all striatal MSNs will later form the RGCs (Sousa and Fishell, 2010).

The MSNs of the striosomes and matrix are generated sequentially in two waves (or expansions as described in (Lebouc et al., 2020)) at which D1 and D2 MSNs are intermixed in each compartment. In the early expansion phase that takes place between E10-E13, RGCs will give rise a specific neural progenitor cell called apical intermediate progenitors (aIPs) that are restricted to form D1 and D2 MSNs that will occupy striosomes compartment. While in the second later, and longer, expansion phase that takes place between E13-E17, RGCs will differentiate first to aIPs and then into another neuronal type called basal intermediate progenitors (bIPs), that will eventually form the D1 and D2 MSNs of matrix compartment. aIPs and bIPs can be distinguished according to the markers they express, with aIPs are only expressing Ascl1 while bIPs express both Ascl1 and Dlx1 which means that Dlx1 is downstream to Ascl1 (Martín-Ibáñez et al., 2012; Kelly et al., 2018).

There are many TFs that are expressed downstream to Dlx1 and Ascl1 for the specification of striosomes and matrix MSNs and to define MSNs in direct and indirect pathways. The TFs insulin gene enhancer protein (Islet-1), Early B-Cell Factor (Ebf1) and SRY-Box Transcription Factor 8 (Sox8) are required not only for the development of D1 MSNs in striosomes compartment but also for the early postnatal striatonigral connection (Ehrman et al., 2013; Lobo et al., 2008).

The migratory process of MSNs from the LGE to the mantle zone will shape the mosaic structure of the striatum and is still not fully understood. MSNs that will occupy striosomes migrate first and those in the matrix will migrate later. Tangential migration of D2 MSNs to the developing striosomes and matrix compartments in mantle zone (later called striatum) is important to ensure their intermixing with D1 MSNs that migrated with radial glial cells. FoxP1 was shown in (Anderson et al., 2020b) to be required for the migration of D2 MSNs in striosomes compartment, a finding that raised the question whether it is also required for the migration of other MSNs since its expressed in both D1 and D2 MSNs.

The maturation of striosomes MSNs takes place during late embryonic period and until the early postnatal period, while the maturation of matrix MSNs takes place over the first postnatal week (Fishell and van der Kooy, 1989). Input from brain cortical, nigral and thalamic brain regions is important for this process. The earliest input arrives to striosomes MSNs and D1 MSNs also starts sending projection to the substantia nigra between E17 and postnatal day 0 (P0). Cortical neurons project to striatal MSNs in mouse at postnatal day 3 (P3) while the process of dendritic spines formation is still ongoing, but by P9 all striatal MSNs receive cortical and thalamic input (Sohur et al., 2014; Krajeski et al., 2019).. Mature MSNs in early mouse striatum are expressing Darpp32 in striosomes compartment (Chen et al., 2016). During the maturation period of MSNs, a period of neuronal cell death that is responsible for the loss of about 30% of MSNs in matrix and striosomes compartment, however, it was found that MSNs that send projections to the SN and GPe are less susceptible to cell death.

The globus pallidus, striatal and cortical interneurons will develop from the MGE. Mef2c expression is shown to be highly increased in the developing WGE between E12-E16 (Precious et al., 2016, and Jeyasingham 2005, PhD thesis). It was also found to play a key role in the development of parvalbumin positive cortical interneurons that originate from the MGE (Miyoshi et al., 2015; Mayer et al., 2018; Zhao et al., 2022). Cortical interneurons are generated from the MGE and CGE (Wichterle et al., 2001, Xu et al., 2004; Rubin et al., 2010), and from the pre-optic area (Poa) (Gelman et al., 2009; Gelman et al., 2011) Radial glial (RG) cells embedded in the LGE generate fate restricted intermediate progenitors (IPs) that mediate neurogenesis of the striosomes and matrix through two phases of neurogenesis, the first one is through apical IPs to form striosome MSNs and the second phase is through basal IPs to form the pool of matrix MSNs (Kelly et al., 2018).

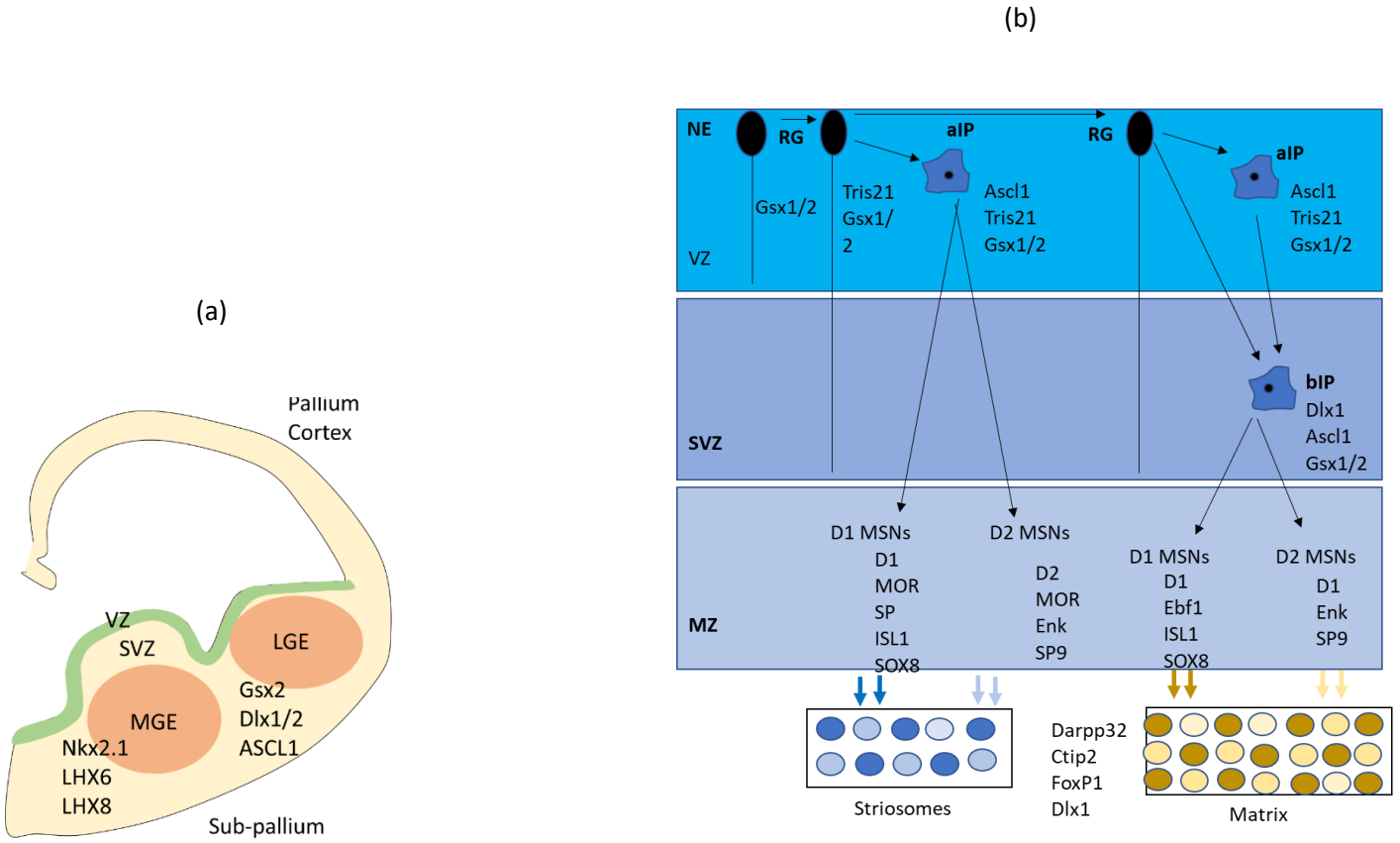

Figure 1.3: (a) Schematic representation of E12.5 brain illustrating the developing telencephalon with gene expression. Adapted from (Osório and Rétaux, 2008). **(b)** LGE region magnified showing the different expansion phases with TFs expressed at each phase adapted from (Lebouc et al., 2020).

1.3.2 Thymidine analogues in the study of proliferation and neurogenesis in rodent's brain

Thymidine analogues have been used for decades as proliferative markers with BrdU, 5-Bromo- dioxyuridine, the most commonly used one. Tritiated-thymidine autoradiography was used in the past for birth dating neurons and neurogenesis in the developing and adult brain, however, the drawbacks of using H^3-thymidine, including the need for a radiolabeled material, and the time-consuming process necessitate the need to use new thymidine analogues (Duque and Rakic, 2011). The greatest advantage of using BrdU over H^3-thymidine is the permanent incorporation of BrdU into the adult genome and the ability to track these newly born cells and identify their phenotypes through co-labeling of BrdU with other cellular and neuronal markers using immunohistochemistry, which makes it possible to study neurogenesis at specific time points. BrdU has been widely used to investigate proliferation and neurogenesis in humans and rodents. Post-mortem studies of patients who received BrdU as part of their treatment, as a radiosensitizer, revealed the retention of BrdU within dividing neurons in their brains (Eriksson et al., 1998). One of the most significant drawbacks of using BrdU as a proliferative marker is the need for unmasking the genetic material using relatively aggressive techniques that might harm the cellular contents.

5-ethynyl-2'-deoxyuridine (EdU), can be also used as a proliferative marker that incorporates into the genome permenantly during S-phase. In contrast to BrdU, detection of EdU does not require harsh tissue treatment to denature DNA double strands, since the small-sized fluorescent azides can easily diffuse through DNA and bind the alkyl group of EdU in a copper-catalyzed reaction ''click reaction'' (Zeng et al., 2010).

Combinations of two thymidine analogues provide a better understanding of cell proliferation at two different time points in the same experimental animal. BrdU and EdU, and Cldu (chloro-deoxyuridine) and Idu (iodo-deoxyuridine) are the most commonly used combinations of proliferative markers and their specific antibodies show no interactions. For example, injections of XX can be administered to label cells undergoing proliferation in

S-phase, while Idu injections label cells exiting S-phase (Tuttle et al., 2010; Anda et al., 2014). Retrospective birth-dating studies and subsequent immunohistochemical tests in humans that received the thymidine analogue Idoxuridine (Idu) revealed that many cells were labelled in the hippocampus and the expression of the neuroblast marker DCX was similarly high in both the hippocampus and the striatum, which may indicate the presence of active adult neurogenesis in both regions (Hyo Jung et al., 2011, Ernst et al., 2014).

Protocols used BrdU in studying neurogenesis are widely variable in terms of the age studied, BrdU injection protocol; dose, route of administration and the number of injections, in addition to variation in the DNA denaturation step, as BrdU is detected only in single stranded DNA.

Table (1.2) summarises various methodology in published work using BrdU in neurogenesis studies. In most of these studies animals are injected intraperitoneally with BrdU with a dose range of 10-100 mg/kg of BrdU concentration from 10-25 mg/ml and perfused at different time points for immunohistochemical analysis. However, other administration routes are also available by directly injecting BrdU solution into the lateral ventricle of newborn mouse or rat pups by stereotaxic surgery instead of a periphral injection (Wright et al., 2013).

Author-Date	*species*	*Part of the brain*	*Aim of BrdU experiment*	*Age at time of injection*	*Method og BrdU administration*	*Perfused at*	*Unmasking*	*Co-labled with*
(Rivera et al., 2019)	*Rat*	*Striatum & SVZ*	*The role of OEA[(1)] on the ethanol-induced inhibition of striatal neurogenesis & gliogenesis*	*10-12 weeks*	*8 injections (twice per day over 4 days) 50mg/Kg 15mg/ml IP*	*Two weeks later ?*	--	*GFAP, NeuN, β3-tubulin or Iba-1*
(Rodgers et al., 2018)	*Mouse*	*Striatum*	*Neurogenesis in juvenile mouse brain following ischemic injury*	*3-4 weeks (juvenile brain)*	*Two injections in two days* *50mg/Kg* *IP*	*30 days after*	2 N HCl for 20 min at 37 C, neutralized with 0.1 M borate buffer (pH 8.5, 3X 15 min)	*DCX, NeuN, TUNEL, GFAP & Olig2*
(Martín-Ibáñez et al., 2017)	*Mice*	*Striatum*		*E13.5* *E14.5* *E16.5*	*Single injection* *50mg/Kg* *IP*	*E18.5*		
(Wright et al., 2013a)	*Rat*	*Striatum*	*Neurogenesis in the neonatal rat brain under normal physiological conditions*	*P0, P2 or P5*	*-single injection -single I.p injection -50mg/Kg (20mg/ml)* *-150mg/kg Intra-ventricular (stereotaxic surgery) + I.P*	*At the age 4 weeks*	50% de-ionised formamide for 2 h at 65°C 2 M HCl for 30 min at 37°C, washed for 15 min in sodium borate buffer (pH 8.0)	*NeuN, Darpp-32*
	Mouse	*Striatum and SVZ*		*4weeks*	*14 injection over 2 weeks, 100mg/Kg, IP*	*8weeks*		βIII-tubulin

Table 1.2 A summary of the most commonly used methodology for studying embryonic and postnatal neurogenesis in different species.

1.4 1.4 MSNs development and MSN markers

1.4.1 DARPP-32

Dopamine- and cAMP-regulated phosphoprotein-32 kDa (DARPP-32, also known as proteinphosphatase-1 regulatory subunit, PPP1R1B), was first identified by (Walaas and Greengard, 1984). It is a cytosolic signalling molecule in MSNs that plays a crucial role in brain dopaminergic signalling pathaways with functions that include ion channel permeability and synaptic plasticity. In addition it acts as a messenger molecule which mediates shuttling between the nucleus and the cytoplasm. DARPP-32 is highly enriched in MSNs with dense dopamine and glutamate innervation in both direct and indirect pathways (Ouimet and Greengard, 1990). It is first detected at E18.5 in the rat striatum and reaches peak levels after three weeks postnatally (Foster et al., 1987; Yger and Girault, 2011). DARPP-32 is considered as a "gold standard'' marker of mature MSNs in the striatum, although it was found to only label around 65% of FoxP1 MSNs in the adult mouse striatum (Precious et al., 2016; Arber et al., 2015; Ivkovic and Ehrlich, 1999) . Distribution of Darpp32 and its mRNA is relatively similar among different species including human, monkeys, rats and mice and it was shown to be enriched in brain regions with dopaminergic terminals; i.e. it is enriched in dopaminoceptive neurons but absent in the dopaminergic neurons themselves (Ouimet et al., 1984; Svenningsson et al., 2004; Schalling et al., 1990).

Darpp32 phosphorylation is regulated by opposing molecular mechanisms. Darpp32 can act as protein phosphatase1 inhibitor after stimulation of D1 receptors that results in Darpp32 phosphorylation on Th34, which is a protein required for regulating a range of phosphoproteins including voltage-dependant sodium and calcium channels and neurotransmitter receptors. Or, it can be a protein kinase inhibitor if phosphorylated at Thr-75 by cyclin-dependant kinase 5 (CDK5) which results in the inhibition of protein kinase A (PKA), increasing phosphorylation of PKA substrates and thereby mediating peak voltage-gated calcium currents (Yger and Girault, 2011). Targeted deletion of Darpp32 in the mouse brain has been implicated in psychiatric disorders and impairments in learning and memory functions (Fienberg et al., 1998)(Albert, Hemmings et al. 2002)(Heyser et al., 2000). In

humans, Darpp32 was significantly decreased in the dorsolateral prefrontal cortex circuit in patients with schizophrenia (Foster et al., 1987).

1.4.2 Ctip2

Also called COUP TF1-interacting protein 2, Ctip2 is expressed in various regions of the CNS including neocortex, the hippocampus, the olfactory bulb, and the striatum, from early embryonic stages of development (Leid et al., 2004). Ctip2 is a transcription factor important for axonal and dendritic growth of subcortical neurons and differentiation of MSNs. Ctip2 also plays an important neuroprotective role; in an *in vitro* study using S-nitroso-N-acetyl penicillamine, Ctip2 knockout cells revealed more apoptosis than Ctip2 wild type cells, suggesting that Ctip2 could play a neuroprotective role in MSNs (Fjodorova et al., 2019). Darpp32 has binding sites for Ctip2 located ~6.5 kb upstream of the Darpp-32 transcription start site and therefore its expression was found to be absent in a Ctip2 CKO mouse model (Arlotta et al., 2005). Ctip2 labels MSN precursor cells as well as mature MSNs and co-localizes with FoxP1 in 99% of MSNs (Arlotta et al., 2008; Precious et al., 2016). Ctip2 is expressed in the WGE of mice at E12.5 in MSNs and this expression continues through to adulthood in mature MSNs of patch and matrix compartments (Arlotta, et al., 2005). Ctip2 loss caused abnormalities in striosomes and matrix organization with Ctip2 mutant mice lacking patches and having large aberrant cellular aggregates (Arlotta, et al., 2005). It has been shown that Ctip2 is expressed in cortical interneurons, however, in mouse striatum it is only expressed in MSNs (Nikouei et al., 2016). Ctip2 with Darpp-32 and FoxP1 are recognized as key markers of mature MSNs.

1.4.3 FoxP1

Forkhead-box P1 (FoxP1) is a member of the FoxP gene family that encodes four transcription factors, FoxP1, FoxP2, FoxP3 and FoxP4. All are expressed in the nervous system except FoxP3. FoxP1 is highly expressed in the developing and adult mouse striatum, in both striato-nigral and striato-pallidal neurons. A microarray analysis of developing mouse striatum revealed FoxP1 to be the most highly upregulated gene between E12 and

E16 (Precious et al., 2016). Whilst Darpp-32 is the "gold -standard" marker of mature MSNs, FoxP1 marks a greater number of MSNs, including mature and precursor MSNs. FoxP1 co-localizes with Darpp-32 and is required for its expression (Precious et al., 2016). FoxP1 does not co-localize with interneurons, indicating its importance as a specific MSN marker (Tamura et al., 2004). During embryonic neural development, FoxP1 plays an important role in neuronal migration, morphogenesis, and MSN differentiation (Bacon et al., 2015; Xue et al., 2015; Precious et al., 2016). In embryonic life, expression of FoxP1 is high in the WGE early from E12.5 and remains high to adulthood in mature MSNs (Precious et al., 2016). FoxP1 complete null is embryo lethal in mouse, therefore, CKO mouse models were generated. Studies of conditional knockout (KO) of FoxP1, show that the total number of surviving cortical and striatal MSNs was significantly reduced, indicating the neuroprotective anti-apoptotic role FoxP1 plays in survival of these neurons (Bacon and Rappold, 2012; Titus et al., 2017). Furthermore, it is required for normal dendritic formation and dendritic pruning, as studies of FoxP1 KO in cortex using a nestin-cre mouse has been shown to significantly affect dendritic length, dendritic maturation and also results in significantly shorter axonal lengths (Xue et al., 2015). In addition, striatal neurons cultured from E15 FoxP1 mice revealed an abnormal increase in dendritic branching (Bacon et al., 2015). However, FoxP1 knockout studies in cortical neurons revealed no effect on the proliferation and differentiation of cortical neurons (Xue et al., 2015). This further supports the unique role FoxP1 plays on MSNs in striatum but not cortex. Cortical-targeted FoxP1 CKO via shRNA results in delayed neuronal migration in the developing cerebral cortex (Konstantoulas et al., 2010; Palmesino et al., 2010; Bacon et al., 2015), the effects of which appear to be long-lasting and are not self-correcting. In another investigation, *FoxP1 CKO* via the nestin-promoter and *cre/loxP* complex also caused significant structural alterations of the striatum and caused mice to exhibit autism-like behavior (Harrington et al., 2016a).

1.5 Mef2c

1.5.1 Mef2c overview

The myocyte enhancer factor 2 (Mef2c) gene is a member of the MEF2 family of MADS (MCM1, agamous, deficiens, serum response factor) box transcription factors family that in vertebrates includes four distinct genes, Mef2a, Mef2b, Mef2c, and Mef2d (Breitbart et al., 1993; Martin et al., 1994; Yu et al., 1992). The N-terminal of MEF2 proteins consists of the MADS-box domain which is a 57-amino acid and MEF2 domain that is a 29 amino acids extension that is responsible for high-affinity DNA binding and dimerization, and facilitates interaction with other cofactors (Potthoff and Olson, 2007b). While the C-terminus, that is subjected to complex patterns of alternative splicing, contains the transcriptional activation domain (TAD) (Wu et al., 2011b). A recent study provided evidence for the ability of MEF2 TFs to compensate for each other; for example, it has been shown that MEF2D loss was fully functionally compensated by MEF2A (Majidi et al., 2019).

MEF2 TFs are involved in many biological processes including proliferation, differentiation, survival and apoptosis in different peripheral tissue types including muscle, bone, cartilage, immune cells, craniofacial development and central nervous system (Potthoff and Olson, 2007; Rashid et al., 2014; Arnold et al., 2007; Verzi et al., 2007; Mao et al., 1999). Mef2c was first recognised for its role as a major regulator of skeletal muscle development and differentiation (Gossett et al., 1989; Potthoff and Olson, 2007; Taylor and Hughes, 2017). Mef2c is also expressed in the brain microglia, which are responsible for maintaining neuronal and synaptic function, removing the apoptotic debris in the brain and spinal cord and mediating, under strict regulations, the immune response in the central nervous system (Speliotes et al., 1996). Interferon type I (INF-1) downregulates Mef2c in microglia with ageing, which results in an increased pro-inflammatory response in microglia after inducing immune stimuli, and causes a significant effect on mouse behaviour and immune response, suggesting the importance of Mef2c in maintaining homeostasis in the brain (Deczkowska et al., 2017a). In bone, Mef2c was shown to regulate osteoclastogenesis (Fujii et al., 2021). And its loss in Col2-Cre expressing chondrocytes caused impairments in cartilage

hypertrophy and cartilage angiogenesis (Arnold et al., 2007). Mef2c plays an important role in the proliferation and survival of B cells and its knockout in these cells resulted in significant impairment of these biological processes.

1.5.2 Mef2c gene

The mouse Mef2c gene is a protein coding gene that is located on chromosome 13. It consists of a total of 13 exons, three of them are alternative splicing sites; the mutually exclusive exons α1/α2, the skipping/inclusion exon β, and the 3' splice site region γ (Zhang et al., 2015) **(Figure 1.4).** Alternative splicing is an important process for the regulation of gene expression and diversity in transcriptional activity (Kelemen et al., 2013). Six isoforms of *Mef2c* are generated in mouse, *Mef2c* α1 was found to be expressed in muscular cardiac tissue while *Mef2c* α2 was strongly expressed in skeletal muscle tissue (McDermott et al., 1993; Sekiyama et al., 2012) and to a lesser extent in non-muscular tissue like spleen. Inclusion of β exon was shown as the main transcript in the CNS but not in non-neural tissue (Hakim et al., 2010), with skipping β exon expressed in non-neural tissue. Mef2c α1β isoform is expressed in neuronal tissue (Sekiyama et al., 2012).

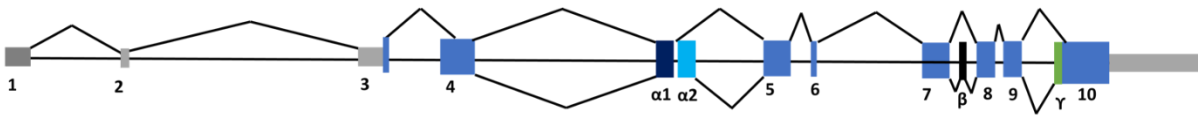

Figure 1.4: mouse *Mef2c* gene structure. Schematic representation of the Mef2c gene shows that it has 10 conventional exons and three alternative splicing exons. The mutually exclusive α1 and α2 exons, the skipping/inclusion β exon and the 3' splice site ϒ exon. Adapted from (Hakim et al., 2010).

1.5.3 *Mef2c* exons

The mutually exclusive α exon: *Mef2c* exon α1 and α2 are located just adjacent to the MEF2 domain. Either α1, α2 or no α is expressed, with α1 is typically expressed in heart muscular tissue and neurons while the alternatively spliced exon α2 transcript is expressed in muscle-specific manner in adult mouse, with minor expression in spleen (McDermott et al., 1993; Hakim et al., 2010). Mef2c mRNA transcripts that lack α exons show increased transcriptional activity (Infantino et al., 2013). **The skipping inclusion exon β**: Mef2c isoform could include or skip exon β. This exon is in the middle of the transcriptional activation domain. It was reported that inclusion exon β is found in adult tissue, including the brain, and transcripts including exon β are exclusively expressed in the brain (McDermott et al., 1993; Zhu et al., 2005). The splicing regulator Fox-1 is enriched in neural tissue and regulates inclusion exon β expression in this type of tissue. **The 3' splice site selection**, **the ϒ region**: this exon is located at the last exon of Mef2c gene, exon 10, and it is thought to encode a transcriptional repression domain (Zhu et al., 2005). Mef2c isoforms that lack this exon show enhanced interaction with the myoblast determination protein 1 (MyoD1) which is important for skeletal muscles development (Zhu and Gulick, 2004). According to (Sekiyama et al., 2012) there are six isoforms of Mef2c transcripts in mice, with Mef2c α1β the most common in the brain and Mef2c α2 transcripts in the skeletal muscles**, (Figure 1.5).**

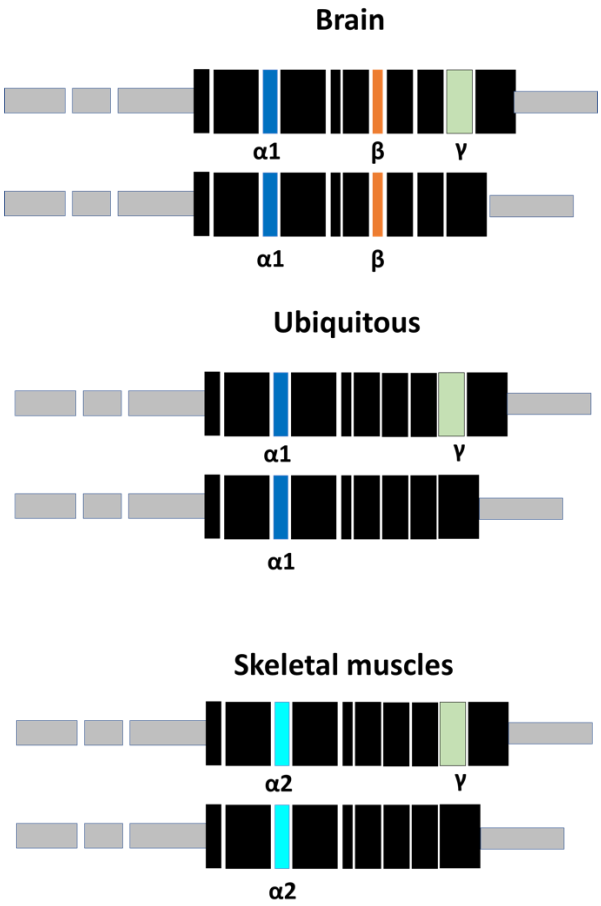

Figure 1.5: tissue-specific isoforms of Mef2c in mouse. Adapted from (Sekiyama et al., 2012).

1.5.4 Mef2c protein structure

Mef2c has a sequence motif located most frequently in TFs, which forms a DNA-binding domain. This domain is located towards the N-terminus of the Mef2 protein and is adjacent to the MEF2 domain, **Figure 1.6** It is the combination of these two domains which characterise the Mef2 family, and these domains are present in both the invertebrate form of Mef2 and its mammalian orthologs Mef2a, b, c and d. Mef2c can recognize DNA and interact with different transcription factors to mediate a range of cellular and nuclear events (Potthoff and Olson, 2007a). The C-terminus regions in all forms of Mef2 are highly divergent and function as transcriptional activation regions, allowing for several alternative splicing patterns to occur along with the modulation of transcriptional activity (Wu et al., 2010). The human Mef2c protein consist of five core domains; MADS domain, MEF2 domain, transcriptional activation domains 1 (TAD1) and 2 (TAD2), as well as the nuclear localization signal (NLS). Mef2c α1 is the most common Mef2c isoform in human brain (Infantino et al., 2013).

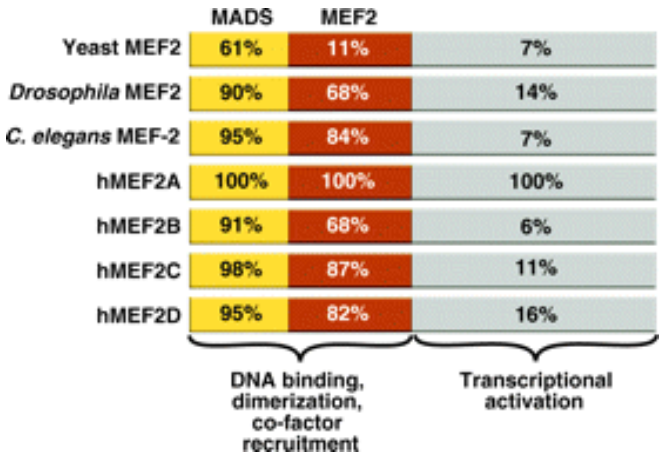

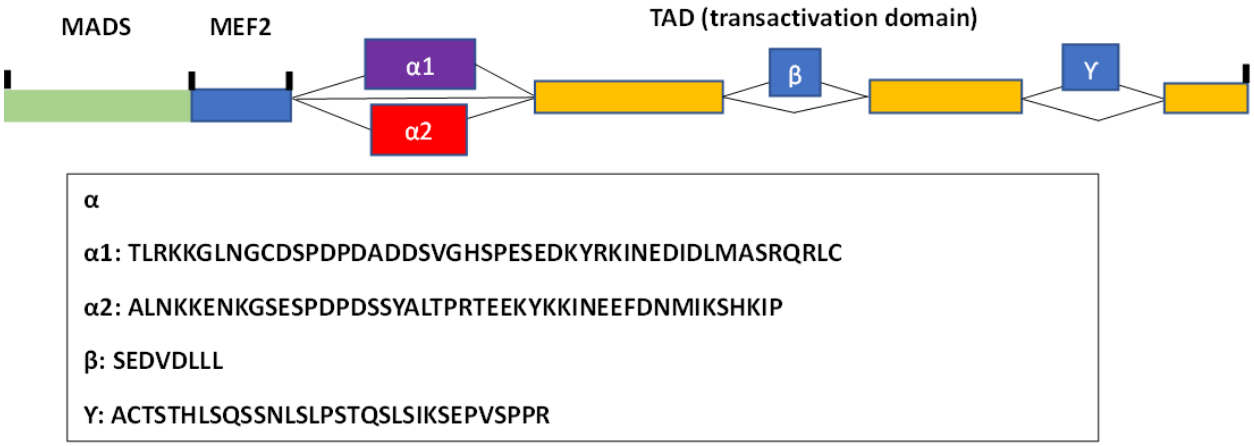

Figure 1.6: **(a)** The MADS and MEF2 domains are highly conserved between Drosophila and mammalian orthologs. The percentage is normalized to hMEF2A. Adapted from (Potthoff and Olson, 2007a). **(b)** The structure of the Mef2c protein in mouse showing the three alternative exons with their sequences of the amino acids. Adapted from (Zhang et al., 2015).

1.5.5 Variations between the four MEF2 TFs

Although there are four variants of the *Mef2* TFs in vertebrates Mef2a, b, c and d, Mef2c genes are expressed differentially both spatially and temporally from the embryo through to adulthood with some overlap in the mouse brain (Edmondson et al., 1994; Assali et al., 2019) **(Figure 1.7**). *Mef2c* is the first to be expressed in the CNS (Leifer et al., 1994; Lyons et al., 1995; Li, McKercher et al. 2009). Mef2a, c and d are highly similar in gene structures and alternative splicing patterns between coding exons, while Mef2b gene sequence is different downstream of the MADS/MEF2 toward the c terminus domains and differs in its expression patterns. Mef2c is the only MEF2 gene that has an alternative splice acceptor in the last exon that generates Mef2c transcripts that include or exclude γ domain; Mef2c γ− isoforms are enriched in heart tissue (Zhu and Gulick, 2004). Because of this γ region present within Mef2c, eight variants are possible, referred to as α1, α1β, α1γ, α1βγ α2, α2β, α2γ or α2βγ (Zhu and Gulick, 2004). Only two isoforms of Mef2b exist, named as A and B with distinct c terminal domains (Ying et al., 2013).

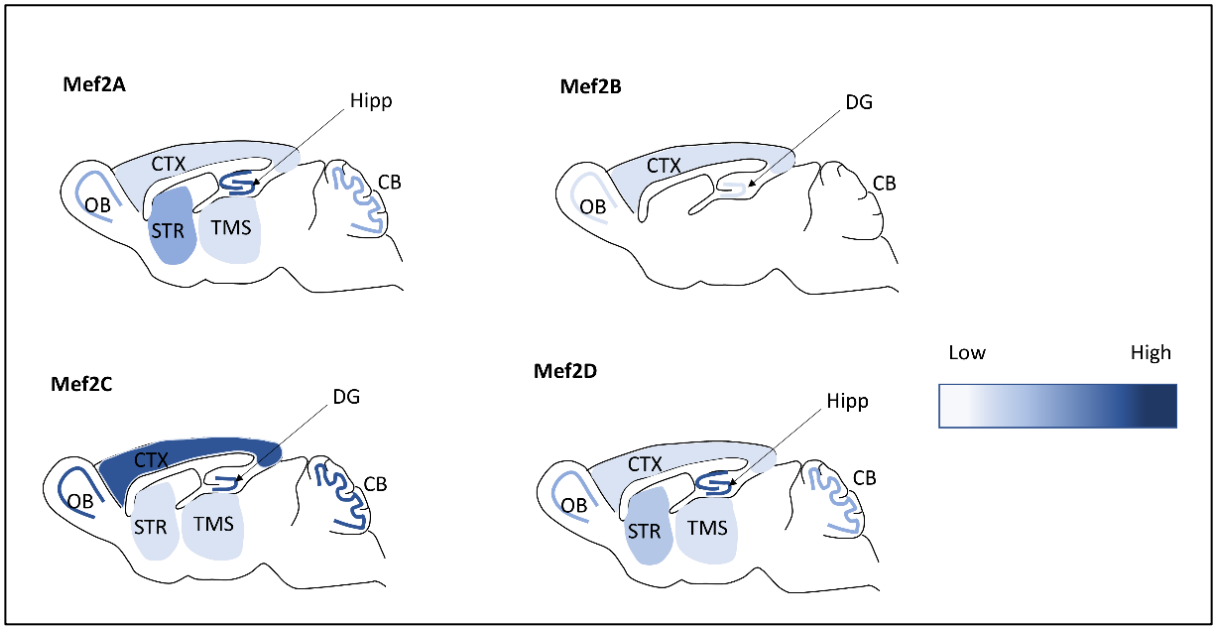

Figure 1.7: Illustration of Mef2 isoform expression in the adult mouse brain, adapted from (Assali et al., 2019)

1.5.6 Regulation of Mef2c

Mef2c regulation can occur at various stages including transcription, translation, and protein degradation (Okamoto et al., 2002; Zhu and Gulick, 2004). In yeast, Drosophila and in invertebrates, mitogen-activated protein kinase signalling pathways (MAPKs) were shown to play an important role in regulating MEF2 factors (Han and Molkentin, 2000; Han et al., 1997). The alternative splicings at Mef2c exons α, β, or ϒ is regulated by cis elements and trans factors through serine/arginine-rich (SR) proteins that are important for the regulation of both constitutive and alternative splicing and are involved in pre-mRNA splicing. These proteins are widely expressed in different tissue types but they are thought to work in a concentration-dependant manner (Hastings and Krainer, 2001). Examples of regulators of splicing that affect Mef2c are Nova proteins. These are regulators of alternative splicing but in a tissue-specific manner. For instance, Nova 1 and Nova 2 proteins are expressed in neural tissue (Buckanovich et al., 1993), although Nova 2 is weakly expressed in the heart. Nova proteins have RNA-binding sites called hnRNP K homology (KH) domain (Jensen et al., 2000). Fox1 is another regulator of alternative splicing that acts in a tissue -specific manner. This protein contains RRM-type RNA-binding domain, which specifically binds to the GCAUG sequence. Fox-1 is expressed in neuronal and muscular tissue. HDAC5 was also shown as a regulator of gene expression in neurons by binding and suppressing the activity of Mef2c (Dietrich et al., 2012; Wein et al., 2015; Assali et al., 2019). Knockdown of HDAC5 induces neurites elongation in P19 cells (Gu et al., 2018).

1.6 Mef2c CKO models used to alter Mef2c expression in the central nervous system

The functional roles of Mef2c have been extensively studied in the mouse brain through using different mouse models. Complete null of Mef2c is lethal during embryonic development due to impairment in cardiovascular development (Lin et al., 1997a), therefore, different *Mef2c CKO* mouse models were developed to allow for temporal and tissue-specific deletion of Mef2c without affecting the development of the heart. Mef2c het mice (Mef2c $^{-/+}$) that have exon 2 deleted were generated by Olson's lab (Lin et al., 1997b). Exon 2 is responsible for DNA binding and dimerization. These mice showed reduced survival and were used as a model of Mef2c haploinsufficiency syndrome (MCHS) (Tu et al., 2017a). A significant reduction in survival was also reported in a *Nestin-Cre Mef2c CKO* model in which only 60% of *CKO* mice survived to adulthood (Li et al., 2008b), suggesting that deletion of *Mef2c* across the whole CNS could contribute to lethal phenotypes. *Mef2c* floxed mice (*Mef2c* $^{fl/fl}$) were generated to have exon 2 flanked by two loxP sites oriented in the same direction to ensure that *Mef2c* will be excised after recombination as described in (Arnold et al., 2007; Vong et al., 2005). This mouse line was used in this thesis and in (Harrington et al., 2016; Bjorness et al., 2020; Harrington et al., 2020; Chen et al., 2016; Arlotta et al., 2008; Barbosa et al., 2008).

Mef2c deletion was targeted in different cell lines and tissues at specific time points according to the Cre mouse line used. The expression of the promotor used is a determining factor to the extent and timing of the recombination. For example, nestin-Cre mouse line can induce recombination early during embryonic development in immature cortical neurons at the stage of neural stem/progenitor cells (NSCs) as described in (Li et al., 2008c). In contrast, using Emx1 cre, Prm1 cre and GFAP cre allow for Mef2c knockout at later stages of development (Barbosa et al., 2008; Harrington et al., 2016; Harrington et al., 2020). CKO of Mef2c was also done in postnatal cortical excitatory neurons using Camk2a-Cre to study the role of Mef2c in sleep loss functions as described in (Bjorness et al., 2020a). The work outlined in this thesis is the first to study Mef2c functions in the development of MSNs using Gsx2- Cre induced recombination.

A summary of Cre mouse models used to knockout Mef2c is in **Table 1.3.**

Cre mouse line	***Promoter name***	***Reference***
Camk2a-Cre	calcium/calmodulin dependent protein kinase II alpha	(Bjorness et al., 2020b),(Adachi et al., 2016a)
N-Cre	Nestin	(Li et al., 2008c), (Chen et al., 2016) & (Latchney et al., 2015)
hGFAP-Cre	human glial fibrillary acidic protein	(Barbosa et al., 2008a)
Emx1-Cre	Empty Spiracles Homeobox 1	(Harrington et al., 2016b)
Prm-Cre	protamine 1	(Harrington et al., 2020a)
Cx3cr1-Cre	C-X3-C Motif Chemokine Receptor 1	(Deczkowska et al., 2017b)
VGAT-Cre	vesicular GABA transporter	(Cho et al., 2022)

Table1.3: A summary of Mef2c mouse models used in the literature to study mouse brain.

1.7 Clinical conditions associated with Mef2c

Members of MEF2 family have been implicated in several neuropsychiatric genetic disorders in humans and are considered as one of the risk genes involved in autism spectrum disorders (ASD) (Novara et al., 2010; Vrečar et al., 2017; Neale et al., 2012) . Mutations in the *Mef2c gene* have been shown to be involved in multiple motor, developmental, autistic, and mental syndromes. Patients with microdeletions of Mef2c are diagnosed with haploinsufficiency syndrome (MCHS) and present with intellectual disabilities, abnormal motor movement and autistic like symptoms (Le Meur et al., 2010a). Mef2c could also play an important neuroprotective role in human brain, as it was shown to be a potential regulator of APP (amyloid-protein precursor protein) proteolysis at which Aβ (Amyloid β) is produced, thought to be a central initiator of Alzheimer's disease (Burton et al., 2002). However, recent reports have Aβ might not be the causative factor of AD based on the failure of all clinical trials targeting this protein in the treatment of this disease. Mef2c haploinsufficiency is also implicated in Rett syndrome that was shown to be triggered by MeCP2 mutations (Li et al., 2011), however, Mef2c mutations were found in 44 patients who presented with the symptoms of Rett syndrome in the absence of any MeCP2 gene mutations (Wang et al., 2019). Mef2c target sites were found in the heritable risk factors associated with Schizophrenia, a severe mental disorder characterised by cognitive impairments.

1.8 Mef2c role in proliferation, neurogenesis, differentiation, and survival of neurons.

The MEF2 family of transcription factors are known for their key roles in various biological processes in different types of tissues including CNS and outside the nervous system such as; skeletal muscles and immune cells (Sandau et al., 2008). These roles involve proliferation and neurogenesis, synaptic formation, and survival of neurons. *In vitro* analysis of the effect of Mef2c on the development of hNPCs revealed that Mef2c overexpression in these cells using lenti-MEF2c viral vectors resulted in more than threefold increase in DCX positive cells by 32 (days post infection), while on the other hand, its loss at the rosette neural stem cell stage (R-NSC; before the formation of NSCs) caused a delay of neurogenesis. Mef2c overexpression in the P19 cell line was shown to enhance neurogenesis in these cells (Skerjanc and Wilton, 2000). Furthermore, its knockout resulted in a significant increase in TUNEL positive cells at 14 DIV and adverse effects on neurogenesis at R-NSC/NPCs of hESC-derived (incomplete) (Cho et al., 2011).

In another study, it was reported that overexpression of Mef2c in a mouse D3 ES cell line resulted in a significant increase in the expression of mature and immature neuronal markers and a reduction in the expression of the glial cell marker GFAP. This strongly suggested that Mef2c enhances the differentiation of cells towards a neuronal fate. They also found that the survival of cells overexpressing Mef2c was significantly enhanced compared with controls (Li et al., 2008e). *In vivo*, Mef2c knockout in Nestin expressing progenitor cells in mouse brain caused abnormal compaction of cortical cell layers, with no effect on neuronal neurogenesis or survival (Li et al., 2008b) (Latchney et al., 2015). In hippocampus, adult neurogenesis was significantly reduced in Mef2c het mice, with those neurons generated exhibiting smaller soma and alterations in dendritic development (Tu et al., 2017b). Table 1.5 summarises the literature of Mef2c involvement in different biological processes through neuronal development.

MEF2 TFs are required for normal axonal and dendritic spine development. Viral-mediated loss of Mef2a and Mef2d in primary hippocampal neurons caused a significant increase in dendritic spines density (Flavell et al., 2006). *Mef2c* plays a key role in controlling neuronal

excitation and inhibition through regulating dendritic spine formation. Alterations in Mef2c levels through using various CKO mouse models or through viral-mediated over- or under-expression result in a wide range of anatomical changes in the growth and pruning of axons, dendrites, and dendritic spines. In the mouse hippocampus, early embryonic deletion of *Mef2c* in the forebrain causes impairment of hippocampus-dependant learning and memory by increasing the density of dendritic spines on dentate granule neurons of the hippocampus dentate gyrus (Barbosa et al., 2008a). Similarly, postnatal loss of Mef2c in granule cells between P10-14 using CaMKII-Cre93 causes a significant increase in the number of spines (Adachi et al., 2016a). *Mef2c* loss in the cortical excitatory pyramidal neurons of the forebrain had an effect that suggests a specific role for Mef2c on the density of GABAergic synapses (Harrington et al., 2016a). In cerebellum, Mef2c CKO during early postnatal development caused a significant increase in dendritic tree complexity (Kamath and Chen, 2019b). In mouse striatum, loss of Mef2c at P2 resulted in a significant increase in spine density (Chen et al., 2016).

An increase in dendritic spine density and dendritic complexity was observed in the visual cortex of environmentally enriched (EE) mice, with Mef2c TF shown to be involved in the molecular mechanisms underlying these findings. Specifically, EE resulted in downregulation of HDAC5 which is responsible for suppressing the activity of Mef2c through binding the MEF2 binding domain. *Mef2c* regulates spine formation by acting as a suppressor TF, since Mef2c was released from this suppression, its binding to the co-factor Arc and Egr1 that are involved in synaptic plasticity alongside with Mef2c enhanced increase in the spines density (Puang et al., 2020).

A summary of the current literature of MEF2 TFs role in Neurogenesis and survival in neuronal tissue in **Table 1.4**, and Mef2c role in dendritic spines development and dendritic tree complexity in **Table 1.5**.

Author-Date	Model used	Neurogenesis	Differentiation	Cell death
(Okamoto et al., 2000)	*P19 cell line* *Mef2c overexpression*	*No difference in proliferation of multipotent cells*	*XX*	*Enhanced survival* *Loss caused MAP2 + cells*
(Skerjanc and Wilton, 2000)	*P19 cell line* *Mef2c overexpression*	*Initiate neurogenesis in P19 cells*	----------	----------
(Li et al., 2008d)	*In vitro, Mouse D3 ESC cell line* *Overexpres*		*Enhanced (electrophysiology)*	*Enhanced survival*
(Cho et al., 2011)	*In vitro, hNPC Overexpression* *Knockout*	*3.2-fold increase in DCX*	*2.4-fold? Increase in DA neurons*	------ *~ 2 Increase*
(Li et al., 2008a)	*In vivo, Nestin-Cre Mef2c KO mouse model* *Cre loxp knockout*	*No difference*	----------	*No difference*
(Latchney et al., 2015)	*Inducible KO in NPCs in adult mouse brain* *Tamoxifen-induced Mef2 (a, c, d) KO in Hippocampus*	----------	----------	----------
(Tu et al., 2017a)	*Mice* *Mef2c het -null*	*Reduced adult neurogenesis in Hippo.* *Downregulation of neurogenesis genes*	*Reduced soma size* *Reduced number of NeuN*	----------

Table 1.4: A summary of Mef2c genetic alterations in the literature. The role of *Mef2c* TF in dendritic spine development and the pattern and complexity of dendritic tree.

author/year	***Part of brain***	***Mouse model***	***Methodology***	***Soma size***	***Sholl analysis***	***Overall Dendritic length***	***Primary dendrites***	***Secondary dendrites***	***Spine density***
(Flavell et al., 2006)	*Primary hippocampal neurons*	*Mef2a and MEF2d KO*	*shRNAs*	*-*	*-*	*-*	*-*	*-*	*↑in KO mice*
(Chen et al., 2016)	*Striatum*	*Postnatal day 2 KO*	*HSV-Cre-GFP virus*	*-*	*-*	*-*	*-*	*-*	*↑in KO mice*
(Puang et al., 2020)	*Visual cortex*	*Mef2c overexpression*	*FD Rapid GolgiStain™ Neurolucida*	*n=4*	*↑ in EE neurons (n=4)*	*-*	*-*	*-*	*↑ in EE neurons*
(Tu et al., 2017b)	*Hippocampus*	*Mef2c haploinsufficiency (Mef2c het)*	*FD Rapid GolgiStain kit, Neurolucida*	*↓in het (het)=71 (WT)=28*	*↓ in het n=4*	*↓ in het n=4*	*No difference (Confocal)*	*↓ in het n (het)=55 n(WT)=25*	*-*
(Barbosa et al., 2008a)	*Hippocampus Dentate gyrus)*	*hGFAP Cre*	*FD Rapid Golgi Stain Kit*	*-*	*-*	*-*	*-*	*-*	*↑in KO mice*
(Harrington et al., 2016b)	*Cortex and hippocampus*	*Emx1IRES-Cre⁺) mice*			*N. S*	*-*	*-*	*-*	*↓in KO mice*
(Rajkovich et al., 2017)	*Neocortical L2/3 Pyramidal Neurons*	*AAV-Cre-GFP*	*Biocytin*	*-*	*N. S*	*N. S*	*-*	*-*	*↓ on basal dendrites only*

(Kamath and Chen, 2019a)	*Purkinje cells (Mouse cerebellum)*	*Mef2c KO using shRNA lentivirus*	*SNT Fiji*	-	*↑in KO mice*	*↑in KO mice*	-	-	*↑in KO mice*
(Adachi et al., 2016a)	*Frontal cortex & hippocampus*	CaMKII-Cre93	*FD Rapid Golgi Stain Kit*	-	-	-	-	-	*↑in KO mice*

Table 1.5: Summary of the literature reviewed on the effect of MEF2 TF loss on dendritic spine development and dendritic complexity in different parts of the mouse brain using various CKO models.

1.9 The involvement of Mef2c in transcriptomic analysis in human and mouse brain

Understanding the transcriptome of the human and mouse genome has greatly enhanced our understanding of the differential expression of different existing and novel transcripts in human and mouse brains in health and disease. Mef2c functional roles on different biological pathways was extensively studied using this approach. In humans, a recent transcriptomic analysis study has shown Mef2c to be involved in the neurodevelopment of human and mouse brain, (Zhao et al., 2022). Mef2c was shown as one of the TF required for the normal development of the human GE, particularly in the MGE, in a study included three human foetuses at the second trimester. Human transcriptome analysis in ASD brains showed that Mef2c is one of the TFs that has binding motifs to the up-stream regions of ASD gene-enriched modules (Parikshak et al., 2013; Voineagu et al., 2011). Genome-wide transcriptional profiling of Mef2c regulated genes in human neural progenitor/stem cells hNPCs derived from H9 human embryonic cells revealed that 1880 unique genes were differentially expressed among these genes, 1121 genes were up-regulated and 759 genes downregulated (Chan et al., 2015). Most of these genes were shown to be involved in pathways of neuronal development and function.

In mice, an investigation that involved a set of 1052 genes that were differentially expressed in mouse brain lacking Mef2c expression early during embryonic development using Emx1 Cre, Mef2c was shown to be involved in neurodevelopmental diseases by changes in gene expression that affects multiple types of cortical excitatory neurons. Enrichment analysis of gene expression from two scRNA-seq data sets included a total of 830 cell types from scRNA-seq data of mouse brain (Zeisel et al., 2018; Saunders et al., 2018) conducted in (Cosgrove et al., 2019) showed that D2 MSNs (indirect pathway) were enriched in Mef2c gene set. Although the differentially expressed genes are from the analysis of cortex, they were also found enriched in mouse brain parts like hippocampus and striatum. Another extensive transcriptomic changes were reported in Mef2c CKO mouse model (Camk2a-Cre) in which postnatal loss of Mef2c in cortical neurons has caused large transcriptional changes in non-neuronal genes following sleep deprivation in mice (Bjorness et al., 2020b).

1.10 Diseases affecting the striatum

Degeneration of striatal MSNs is a component of multiple movement disorders including Parkinson's disease (PD), HD, and dystonia. A balance between direct and indirect pathways is required for the successful generation of movement. HD is a progressive neurodegenerative disease with an autosomal-dominant inheritance that is caused by a repeat of the CAG trinucleotide in the huntingtin (Htt) gene. HD was first described by George Huntington in 1872 (Wexler et al., 2016). The age of onset of this disease is between 30-40 years and patients are presented with motor, cognitive and psychiatric disturbances. MSNs are selectively affected in HD, with D2 MSNs initially affected, followed by MSNs in the direct pathway (Plotkin and Surmeier, 2015), due to several molecular mechanisms including, the direct toxicity of the aggregates of mutant Htt (mHtt) protein on different cellular functions (Ross and Tabrizi, 2011). HD is currently an untreatable condition, for some behavioural phenotypes, patients are provided with certain drugs to reduce the severity of chorea. Neural transplantation has been shown to be effective in replacing diseased MSNs and bringing about some level of functional recovery (Rosser and Bachoud-Lévi, 2012).

PD is another neurodegenerative disorder caused by the selective loss of dopaminergic neurons in the substantia nigra and subsequent loss of dopamine in the striatum. Striatal dysfunction is also associated with non-motor disorders due to an imbalance in the neurochemicals of striatal MSNs, these disorders include mode changes, depression, motivation problems, attention-deficit hyperactivity disorder (ADHD), compulsivity and obsessive-compulsive disorder (OCD), and drug addiction.

1.11 Aims and objectives of this thesis

The literature outlined in this chapter demonstrates that Mef2c is involved in many areas of neuronal development. Furthermore, results from the microarray analysis performed in our lab revealed that Mef2c is one of the most upregulated TFs in the WGE during embryonic striatal development between E12-E16. Taken together, it is evident that Mef*2c* plays an essential role in neuronal development, including in the mouse striatum. Therefore, in this thesis the effect of *Mef2c* knockout on the developing and adult mouse striatum was investigated.

My aim was to investigate the role of Mef2c in the development of the mouse striatum, and in particular striatal MSNs, using a range of tools including a novel conditional KO of Mef2c in the mouse striatum.

Main objectives:

- To fully characterize *Mef2c* expression pattern in embryonic, postnatal, and adult wild type mouse striatum using IHC and RT qPCR, and to compare this expression to the well-known markers of MSNs and matrix-striosomes compartments.
- Study the effects of *Mef2c* loss during embryonic development on the mouse striatum using a novel CKO mouse model in a developmental series between postnatal day 2 and 12-months old, and to identify whether *Mef2c KO* mouse shows any evidence of ongoing striatal neurodegeneration (as well as affecting development) by examining the striatum at 12 months
- To assess dendrites and dendritic spine development in the Mef2c CKO and controls using Golgi cox staining.
- To investigate if there is any effect of Mef2c loss on matrix-striosomes compartments through using IHC of the most known matrix and striosomes markers.
- Assess proliferation, neurogenesis, and survival of striatal MSNs *in vivo* and *in vitro* using different proliferation and cell death assays.
- Conduct behavioural testing of Mef2c CKO mice and controls with focus on motor functions to see if Mef2c loss will result in functional deficits.

Chapter 2: Materials and Methods

2.1 Mice

All animal experiments were performed in agreement with local ethical guidelines and accepted animal care according to the UK Animals (Scientific Procedures) Act 1986 and its subsequent amendments. All mice were housed in groups of 3–5 in standard cages at 24 ± 2 °C under a 12 h light–dark cycle (lights on from 7:00 to 19:00) with ad libitum access to food and water.

2.1.1 Mouse lines

Three transgenic mouse lines were used in this project to delete *Mef2c* in mouse striatum using *Cre-loxP* recombination technology, which is a tissue specific recombination used to induce deletions, insertions, or translocations in certain genes of the mouse genome. When the two loxP sites are oriented in the same direction cre recombinase, under the control of a specific promotor, will induce excision of the loxP-flanked part of the gene. In this research the first mouse line is Mef2c floxed mice, the second is Gsx2-Cre line and the third is tdTomato reporter mice. All mouse lines, allele types and their sources are listed in table 2.1.

Mouse line	**Type of allele**	**Source/ origin**	**Location/ loxP orientation**
Mef2c floxed	Two loxP sites/ same direction	Eric Olson's lab	Same direction
Gsx2-Cre	Cre recombinase	(Kessaris et al., 2006)	-
Reporter mouse line (Ai9) tdTomato	Cre reporter	Gift from Trevor Dale and Eider Valle-Encinas, Cardiff University	Gt(ROSA)26Sor locus

Table 2.1 mouse lines used in this thesis

2.1.1.1 Mef2c floxed mouse line

The *Mef2c loxP/loxP* mouse line was a gift from Eric Olson's lab, based at the Southwestern medical centre at the University of Texas (Lin et al., 1997a). In this line two loxP sites oriented in the same way are flanking *Mef2c* coding exon 2, therefore, after cre recombination only exon 2 is removed leaving the remaining part of the transcript intact.

2.1.1.2 Gsx2-Cre mouse line

Gsx2-Cre mice were originally generated in (Kessaris et al., 2006). The Cre line was generated through the creation of a P1 artificial chromosome containing a codon improved Cre recombinase with a nuclear signal fused to the initiation codon, with expression recapitulating endogenous expression in the WGE. Gsx2 is expressed in the telencephalon from E9.5 and is involved in the establishment of LGE, from which all striatal MSNs are derived (Deacon et al., 1994).

2.1.1.2.1 Why Gsx2-Cre?

The homeobox gene Gsx2 (also known as Gsh2) is highly expressed in the LGE NPCs from as early as E9.5 during embryonic development and is responsible for the establishment of dorsal-ventral patterning in the LGE (Szucsik et al., 1997; Rubenstein and Rakic, 2013). During telencephalic embryonic neurogenesis, Gsx2 was found to be required for the temporal specifications of striatal and olfactory bulb neurogenesis, with striatal neurogenesis occurring between E11-E16 while olfactory bulb neurogenesis starting at later embryonic stages with the majority born during early postnatal development (Waclaw et al., 2009). The Gsx2-Cre mouse line was chosen in this research work to induce striatal-specific Mef2c loss early during embryonic development. Gsx2 expression in the developing E12 telencephalon is shown in **Figure 2.1.** Gsx2 is expressed in a high-dorsal to low-ventral gradient in the VZ multipotent progenitors of the LGE and MGE (Corbin et al., 2000; Toresson et al., 2000; Waclaw et al., 2009).

Gsx2 is expressed in the septum of mouse brain, although the Gsx2-Cre mouse line used in (Qin et al., 2016) did not show any Gsx2-Cre reporter expression in the septum.

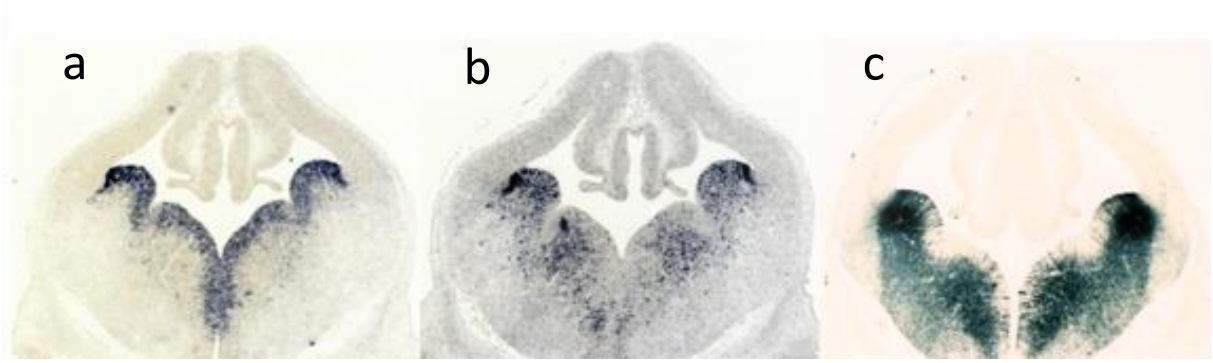

Figure 2.1 (a) In situ hybridization for endogenous Gsh2 expression in E12.5, (b) Gsh2-Cre mice and (c) galactosidase enzymatic labelling in Gsh2-Cre/ Rosa26R-lacZ embryos. Adapted from (Kessaris et al., 2006)

2.1.1.3 Reporter mouse line (Ai9) tdTomato

This mouse line was a gift from Trevor Dale and Eider Valle-Encinas, Cardiff University; it is also available in the Jackson laboratory (Stock No. 007909). Ai9 is a Cre reporter allele that has a loxP-flanked STOP cassette preventing transcription of a CAG promoter-driven red fluorescent protein variant (tdTomato), inserted into the Gt (ROSA)26Sor locus. Ai9 mice express robust tdTomato fluorescence following Cre-mediated recombination. When bred to mice that express Gsx2-Cre recombinase, the resulting offspring will have the STOP cassette deleted in the tissue where cre is expressed, resulting in robust tdTomato fluorescence. Because this CAG promoter-driven reporter construct is inserted into the Gt (ROSA)26Sor locus, robust tdTomato expression is present in those tissue(s) which express Cre recombinase.

2.1.2 Breeding strategy

To generate conditional knockout mice (*Gsx2-Cre* $^{(+)}$ *Mef2c* $^{(fl/fl)}$, the Cre-LoxP system was used, where the Cre-recombinase transgene, under the control of the Gsx2 promoter (Gsx2-Cre mice) is responsible for deletion of *Mef2c* in tissues expressing Gsx2. Also,

TdTomato reporter mice were used to determine the location of Cre expression. The breeding strategies used in this research work are listed below:

2.1.2.1 Breeding strategy to generate Mef2c conditional knockout mice (*Gsx2-Cre $^{(+)}$ Mef2c (fl/fl)*)

First, Gsx2-Cre mice were crossed with Mef2c floxed mice. To generate litters with both *Mef2c* conditional knockout mice and wild type littermate control mice, females that expressed the Gsx2-Cre transgene and had two loxP sites (*Gsx2-Cre $^{(+)}$ Mef2c$^{(fl/fl)}$* (experimental females) were crossed with males that were homozygous for loxP sites and were cre negative (*Gsx2-Cre $^{(-)}$ Mef2c$^{(fl/fl)}$*, **Figure 2.2a**. It was important that male mice were negative for the Cre to avoid the deletion of Mef2c by expression of Gsx2 in the germline at testes level. I found that when using a male breeder that expresses Gsx2-Cre and has loxP sites, a cre mediated recombination of Mef2c TF at the germline level has occurred and resulted in complete null of *Mef2c* in one of the alleles only. This observation was only noticed in the offspring of males positive for Gsx2-Cre suggesting a strong expression of Gsx2, the cre driver, in the testes and resulted in an unwanted fully recombinant null allele of Mef2c during the process of spermatogenesis. A similar observation when using females hGFAP cre positive was reported in (Zhang et al., 2013). Since this has prevented maintain brain-restricted recombination and subsequently complicated the genotyping results, I avoided using male breeders cre positive throughout the work in this thesis.

Control mice (also called wild type, WT mice) were those that had loxP sites and were cre negative (*Gsx2-Cre $^{(-)}$ Mef2c $^{(fl/fl)}$*) as the presence of only loxP sites does not cause any effect at the genetic level (Harrington et al., 2020a). Experimental mice (also called CKO mice) were cre positive and had loxP sites (*Gsx2-Cre $^{(+)}$ Mef2c $^{(fl/fl)}$*).

Using this breeding strategy, 50% Mef2c CKO and 50% WT were generated. To keep the colony, only males that were *Gsx2- Cre* negative were used for breeding, **Figure 2.2, b**.

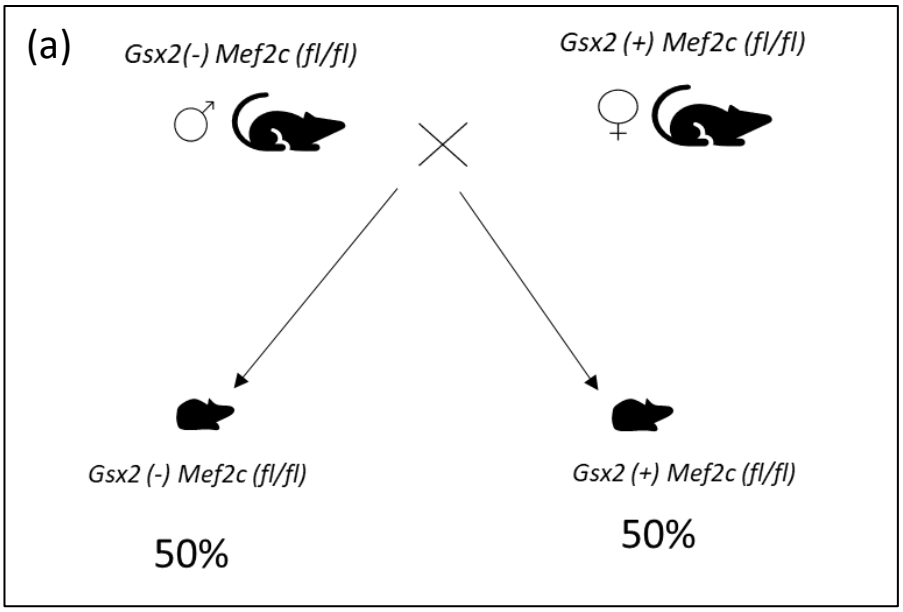

(b)

Mef2c floxed status	**CRE status**	**Genotype**	**% In progeny**	**Used as breeder?**
HOM floxed	+	*Gsx2-Cre* $^{(+)}$ *Mef2c* $^{(fl/fl)}$ Experimental *Mef2c CKO*	50%	Only females
	-	*Gsx2-Cre* $^{(-)}$ *Mef2c* $^{(fl/fl)}$ Control	50%	Only males

Figure 2.2: a: Breeding strategy used to generate *Mef2c CKO* mice. **b:** genotypes resulting from breeding, and genotypes used in breeding.

2.1.2.2 Breeding strategy to generate tdTomato *Mef2c (fl/fl)* mice

Mice homozygous for tdTomato reporter were crossed with mice homozygous for Mef2 loxP sites *(Mef2c fl/fl)*. All progenies were tdTomato heterozygous (+/-) and Mef2c floxed heterozygous *(Mef2c fl/wt).* The second stage of this breeding strategy involved either *(i)* crossing two mice of the same genotype: *tdTomato* $^{(+/-)}$ *Mef2c(fl/wt)*; or (ii)

crossing a *tdTomato HOM* $^{(+/+)}$ mouse with a *tdTomato* $^{(+/-)}$ *Mef2c(fl/wt)* mouse, to get the possible genotypes shown in **Figure 2.3**. Only *tdTomato HOM Mef2c (fl/fl)* or tdTomato HOM (fl/wt) were used for breeding. Mice with the genotype tdTomato (HOM) Mef2c (wt/wt) were used for breeding to maintain the mouse line described above in 2.1.1.3.

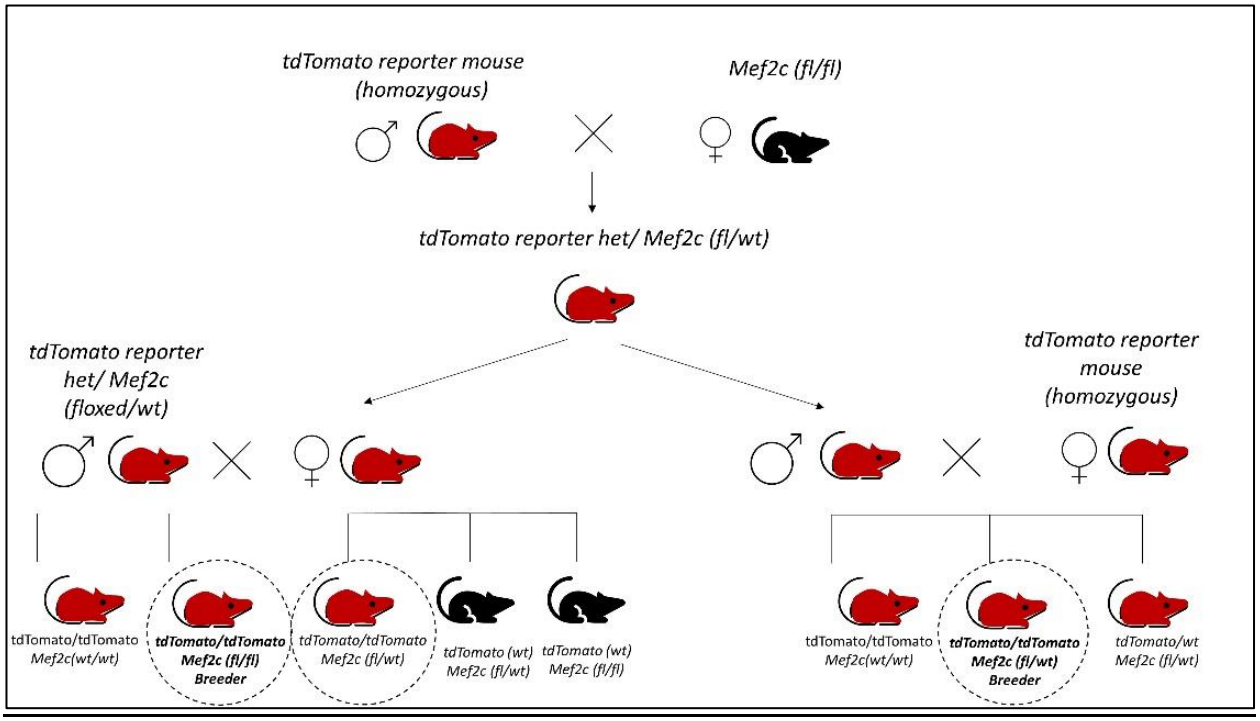

Figure 2.3 Schematic representation of the breeding strategy used to generate tdTomato reporter/ Mef2c floxed mouse line.

2.1.2.3 Breeding strategy to generate *tdTomato* $^{(+/-)}$*/ Gsx2-Cre* $^{(+)}$ *Mef2c*$^{(wt/wt)}$

Mice of the genotype *tdTomato* $^{(+/-)}$*/Gsx2-Cre* $^{(+)}$ *Mef2c*$^{(wt/wt)}$*)* were used to validate the Gsx2 Cre used in this thesis by characterising the expression of RFP in tissues expressing Gsx2. To generate mice with this genotype tdTomato $^{(+/+)}$ *Mef2c*$^{(wt/wt)}$ mice were crossed with mice *Gsx2-Cre* $^{(+)}$ *Mef2c*$^{(wt/wt)}$. All progenies were heterozygous for tdTomato and

either positive or negative for the Gsx2- Cre. After genotyping, only mice that were Gsx2-Cre positive were used, **Figure 2.4**.

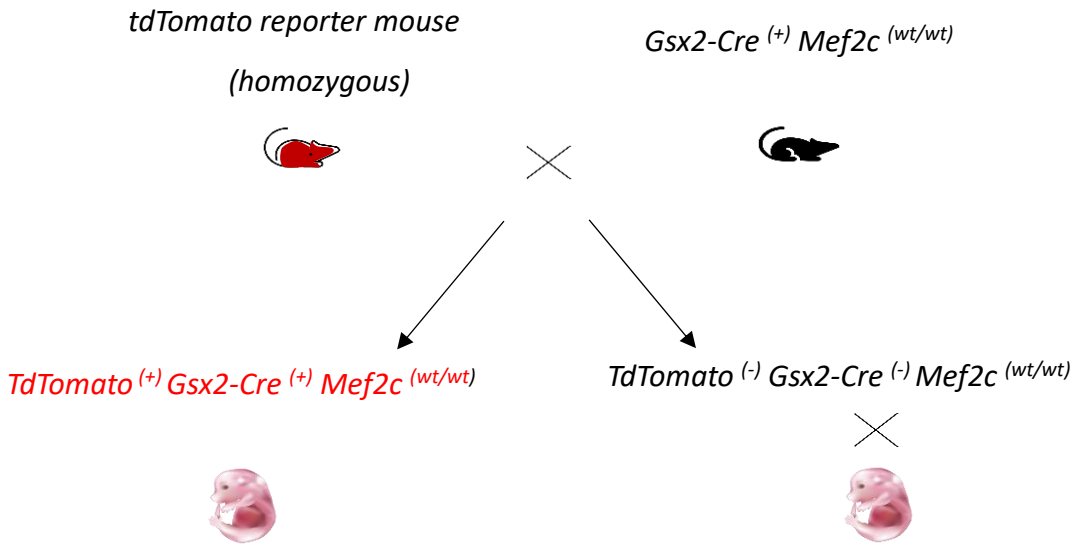

Figure 2.4: Breeding strategy to validate Gsx2-Cre mouse line used in this thesis.

When embryonic tissue was needed at certain time point, mice were paired at 5:00 pm and checked early the next morning for the presence of a vaginal plug between 8:00 – 9:00 am. The day a plug was detected was considered as embryonic day (E) 0.

2.1.3 Genotyping

Mice were weaned at one month of age. After weaning, mice were genotyped by taking a tail tip sample. Tails were anaesthetized using ethyl chloride spray (Cryogesic©) and about 2-3 mm of the tail was cut using surgical scissors. Bleeding at the area of the cut was stopped using a cauterizing pen (Avoca©). Tail samples were placed in specific 96-wellplate to be sent to Transnetyx for genotyping (https://www.transnetyx.com). The primer sequences are a proprietary of Transnetyx company and can be provided upon request.

2.1.4 Administration of reagents to assess proliferation (BrdU and EdU)

The work outlined in chapter 5 involved comprehensive assessment of proliferation and neurogenesis in Mef2c CKO and WT mice. Two proliferative markers; 5-Bromo-2´-Deoxyuridine (BrdU) and 5-ethynyl-2'-deoxyuridine (EdU), were used to permanently incorporate into proliferating cells at S phase of the cell cycle.

2.1.4.1 Preparation of BrdU and EdU solutions

For BrdU solution preparation, 25mg/ml solution was prepared by dissolving 250 mg BrdU powder (Sigma-Aldrich, B9285) was dissolved in 10ml 0.9 saline at 37°C for several hours then aliquoted and stored at –20°C. On the day of injection BrdU solution was thawed and warmed to 37°C. For EdU solution preparation for *in vivo* use, 50 mg Edu powder (™Invitrogen) was dissolved in 5ml 0.9 saline to produce a working solution of 10mg/ml. This solution was stored at -20°C until use.

2.1.4.2 Intraperitoneal injections

For the assessment of proliferation in WT and CKO postnatal and adult mouse striatum, the proliferative marker BrdU was used. Administration of BrdU was by i.p. injection in both postnatal pups and adult mice. For pups, care was taken when handling each pup and when returning to their home cage, to avoid rejection by the dam, by rubbing in nesting from their cage and anaesthetising the dam during the procedure. Specific details of the injections, groups and timings are in chapter 5.

2.2 Tissue harvesting and preparation

2.2.1 Perfusion

To obtain adult mouse tissue for histological analysis, mice were transcardially perfused. Initially, they were terminally anaesthetized by intraperitoneal (i.p) administration of 0.3ml of 0.2mg/ml solution of sodium pentobarbital (Dolethal) (Vetoquenol©). Absence of withdrawal reflexes were confirmed before proceeding (tested by pinching the paws). Thereafter mice were perfused with ice-cooled prewash solution (PBS, pH7.3) for two minutes (or until fluid ran clear) followed by 4% paraformaldehyde (PFA) for six minutes. Then brains were removed from the skull, placed in brain pots with 4% PFA, post-fixed

for four hours and preserved in 25% sucrose solution (Sigma) for cryoprotection at room temperature for 48 hours or until sunk**.** Brains were cut into 40 µm sections using a freezing microtome after removing cerebellum and olfactory bulb. Sections were collected in 48 well plates (Thermo, Fisher Scientific) filled with antifreeze solution and kept at –20°C until use. For free-floating section staining, a one in twelve series of sections (or 1 in 6 for P7 tissue) was placed into an immuno-pot in PBS overnight to remove excess anti-freeze solution.

2.2.2 Embryonic and postnatal (earlier than P14) tissue collection

When embryonic tissue was needed, time-mated pregnant dams were culled by cervical dislocation (Schedule 1) and embryos removed quickly from the uterine horns and collected in Hanks Balanced Salt Solution (HBSS) (Gibco).

For RNA extraction or cell culture experiments, the LGE was dissected in a laminar flow hood as described in **Figure 2.5**, at different ages and then snap-frozen or collected in Eppendorf tubes for further processing *in vitro*.

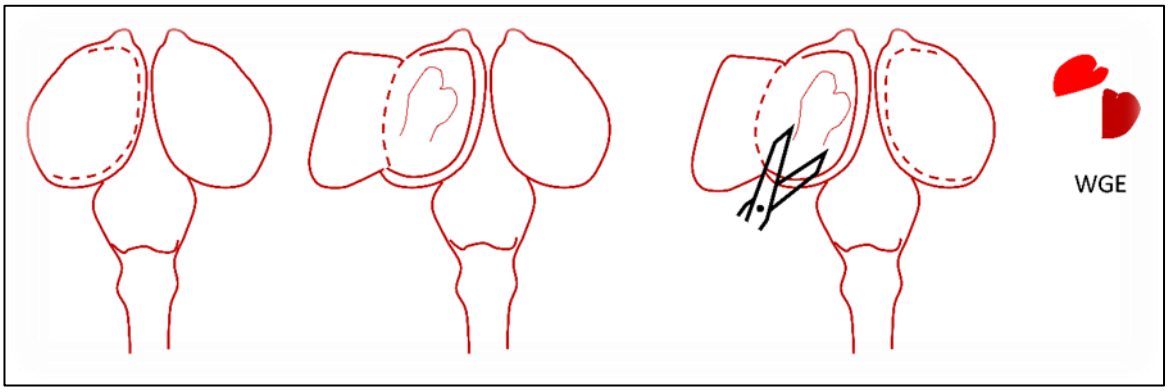

Figure (2.5): Schematic representation of E14.5 mouse brain illustrating the technique used to dissect whole ganglionic eminence (WGE). Adapted from (Dunnett and Björklund, 1992).

For immunohistochemistry, brains (whole heads for embryonic and P0 age groups) were transferred to ice cold 4% PFA overnight and then replaced with 25% sucrose solution

for cryoprotection until tissue had sunk. Embryonic and P0 brains were cut into 50micron thick sections and kept in anti-freeze solution until use.

For cutting P7, P14, 3- and 12-month brains were mounted onto a freezing stage sledge microtome and cut, coronally at 40 µm. Brain sections were stored in antifreeze in 48-well plates in one in twelve series until used.

For sectioning using Leica cryostat, embryos or P0 brains were embedded O.C.T and left to freeze for a minimum of 30 minutes in Leica cryostat, sectioned at 15 µm and mounted directly onto super frost plus slides (ThermoFisher). Slides were left to dry for 10 minutes at room temperature and then used immediately for staining or stored at -20°C.

2.2.3 Dissection of fresh mouse brain tissue P0-3months

P0, P3 and P7 pups were culled by decapitation while P14 and adults were sacrificed by cervical dislocation (Schedule 1). Brains were carefully removed from the skull and transferred to a metal plate placed on ice to cool the brains directly. Cortex and striatum were dissected out, placed in screw-cap tubes, snap-frozen in liquid nitrogen and stored at -80°C until use.

2.2.4 Tissue collection for dendritic spines analysis

Mice aged between 3-6 months were culled by cervical dislocation (schedule 1). The brains were removed gently and quickly and washed for 10 seconds in normal saline and then transferred to the Golgi cox solution in a glass pot.

2.3 Histological methods

2.3.1 Cresyl violet (CV)

Adult brain sections from one in twelve series (or 1 in 6 for P7 tissue) were mounted onto double subbed slides and allowed to dry overnight. Cresyl violet staining was automated using a Shandon tissue processing machine: 5 minutes in 70% industrial methylated spirits (IMS) alcohol, 5 minutes in 95% IMS, 5 minutes in 100% IMS, 20 minutes of agitation in chloroform: alcohol (50:50), 5 minutes in 95% IMS, 5 minutes in

70% IMS, 5 minutes in distilled water, 5 minutes in cresyl violet solution (Sigma) and 5 minutes in distilled water. Sections then underwent dehydration through increasing concentrations of IMS alcohol-70%, 95% and 100%- then 5 minutes in xylene and finally cover-slipped using DPX mounting medium.

2.3.2 Golgi-Cox

2.3.2.1 Preparation of Golgi-Cox solution

Golgi cox solution preparation protocol previously developed in our lab was used (described in (Bayram-Weston, Olsen et al. 2016). This method impregnates neurons in whole brains. Solutions used in this protocol are the following: Solution A (SolA): 5% Potassium Dichromate solution, prepared by dissolving 5g potassium dichromate stirred into 100ml warm dH2O; Solution B (SolB): 5% Mercuric Chloride solution, prepared by dissolving - 5g Mercuric chloride stirred into 100ml hot dH2O; Solution C (SolC) 5% Potassium Chromate solution: prepared by dissolving 5g Potassium chromate solution stirred into 100ml cold water. To make Golgi cox working solution; 100ml of SolA is added to 100ml SolB. And 80ml of SolC is added to 200ml dH2O. Then, SolA-B mixture is slowly poured into diluted SolC, being constantly stirred until dissolved. Red-yellow precipitate should form. The solution should be stored in the dark for 3 days and filtered before use. It is important to make sure that only plastic forceps are used throughout the process and to avoid light and all metals (use glass pots, no aluminium foil etc.).

2.3.2.2 Impregnation of brains in Golgi cox solution

Brains removed as described in **section 2.2.4**, were placed quickly in Golgi cox solution for 14 days, replacing the solution every 1-3 days. At day 14, brains were removed from Golgi cox solution and briefly dried using blotting paper to remove excess liquid before placing them in a specific cryoprotective solution (30% sucrose and 15% glycerol in 100ml prewash solution, 50 ml is needed per brain). Cryoprotectant solution was replaced 3 times over three days or until the solution was clear to minimise brittleness of brains while cutting. Once brains had sunk, they were cut at 100µm using a Leica cryostat. Tissue was collected in TBS, then mounted carefully on double-subbed slides and left to dry at room temperature for 24 hours. Sections were washed in dH_2O for 2 mins, then incubated in 20% ammonium solution (Sigma-Aldrich) for 10 mins and then

washed in dH_2O for 2 mins. Sections were dehydrated in increasing alcohol solutions, 50%, 70% 95% and 100% followed by 2 xylene steps of 10 mins each. Sections were cover slipped with DPX.

2.3.3 Antigen retrieval

Two methods of antigen retrieval were used depending on the antibodies being used.

2.3.3.1 HCL antigen retrieval

For BrdU staining, sections were pre-treated with 2N HCL for 30 minutes at 37°C followed by 3x10 min washes in 0.1 M sodium borate buffer solution (3.8 g sodium borate in 100 ml distilled water, pH adjusted to 8.5 with NaOH).

2.3.3.2 Sodium citrate antigen retrieval

This was used for mild antigen retrieval. 10mM Sodium citrate buffer was made by adding 2.94 g dihydrate tri-sodium citrate to 1000 ml of distilled water, pH adjusted to 6.0 with 1N NaOH. Sections were placed in glass pots and about 2ml of the buffer solution was added to each pot. Pots were placed in a pre-heated water bath (80°C) for 30 minutes, after which sections were allowed to cool to room temperature then washed 3x10 mins in TBS.

2.3.4 Immunohistochemistry (IHC) - Free-floating method

Brain sections were washed in tris-buffered saline (TBS) 3x10 minutes. Endogenous peroxidase activity was quenched for 5 minutes using 30% hydrogen peroxide H_2O_2 (VWR, West Sussex, UK) and 10% methanol (Sigma-Aldrich, Dorset, UK) in distilled water, followed by 3x 10 min TBS washes. To block non-specific binding sites, sections were incubated with 3% normal goat serum in Triton-X tris-buffered saline (TXTBS) for 1 hour. Afterwards, blocking solution was removed and, without washing, sections were incubated with the primary antibody in 10% normal goat serum in TXTBS over night at room temperature with continuous stirring. The next day sections were washed 3x10 mins in TBS and incubated in biotinylated secondary antibody in TBS with 10% goat serum for 3 hours. Sections were then washed 3 x 10 mins in TBS, and ABC kit (Vector Laboratories Ltd, Peterborough, Cambridgeshire) was added, using a 1:200 dilution of both solutions A and B (made-up as manufacturer's instructions) in 10% normal goat

serum in TBS for 2 hours. Sections were then washed 3 x 10 mins in TBS and 2 x 10 mins in TRIS non-saline (TNS) (6g Trizma base (Sigma) in 1L of dH_2O). Immuno-positive cells were visualised with addition of the chromogen 3-3'-diaminobenzadine (DAB) (DAKO). Stock solution of DAB was defrosted at room temperature in the absence of light with the 2ml vial (0.66mg/ml) then added to 40ml of fresh TNS in the presence of 12µl of H_2O_2. This solution was then further diluted to a 1:5 concentration in fresh TNS. 2-3ml of this working DAB solution was added to the tissue sections. The reaction was allowed to develop until the stain could be clearly seen under a light microscope, with time kept consistent for each primary antibody. Sections were washed in TNS first to dilute the reaction and then washed in TBS to stop the reaction before being mounted on to double-subbed 1% gelatinized slides (Thermo Scientific, Menzel Gläser). Slides were air dried overnight before dehydration in an industrial methylated spirit (IMS) alcohol ladder of increasing concentrations (70%, 95% and 100%). Samples were then cleared in 100% xylene and cover slipped using distyrene plasticizer and xylene mounting medium (DPX) (Thermo Scientific, Raymond Lamb, Leicestershire, UK) and allowed to dry for at least 48 hours in a fume hood.

2.3.5 IHC – On-slide method

15-micron thick embryonic tissue sections were washed twice with TBS, and the same steps as for the free-floating method were applied here with the exception that slides were placed in a humidified chamber while covered with thin films during primary and secondary antibody incubations to avoid evaporation.

All primary and secondary antibodies (both biotinylated and fluorescent) used through the course of this project are listed in Table XX.

Primary antibodies	Species	Supplier + (Cat. number)	Conc.
BrdU	Rat	Abcam (Ab6326)	1:500
Calbindin	Rabbit	Swant (300PUR)	1:500
ChAT	Rabbit	Abcam(ab181023)	1:2000
Cleaved caspase 3	Rabbit	Cell signalling (9664)	1:1000
Ctip2	Rabbit	Abcam (ab240636)	1:500
Ctip2	Rat	Abcam (ab18465)	1:500
Darpp32	Mouse	Cornel university (gift)	1:200
Darpp32	Rabbit	Santa Cruz (sc-271111)	1:500
DCX	Rabbit	Abcam (ab18723)	1:500
FoxP1	Rabbit	Abcam (ab16645)	1:500
FoxP1	Mouse	Abcam (ab32010)	1:500
GFAP	Rabbit	DAKO (Z0334)	1:2000
GFAP	Mouse	Abcam (ab279290)	1:500
Gsx2	Rabbit	Sigma (ABN162)	1:500
Iba-1	Rabbit	WAKO (4987481428584)	1:8000
Ki67	Rabbit	Abcam (ab15580)	1:500
Mef2c	Rabbit	Proteintech (18290-1-AP)	1:200
Mef2c	Rabbit	Abcam (ab211493)	1:500
MAP2	Mouse	Sigma (M4403)	1:200
MOR1	Rabbit	Abcam (ab134054)	1:500
MOR1	Rabbit	Immunostar (24216)	1:8000
NeuN	Mouse	Millipore (MAB377)	1:1000
NeuN	Rabbit	Abcam (ab177487)	1:2000
Parvalbumin	Mouse	Swant (235)	1:1000
RFP	Rabbit	Rockland (200-101-379)	1:500

Secondary antibodies	Species	Supplier	Conc.
Alexa fluor anti rabbit 488	Goat	Invitrogen (A32723)	1:200
Alexa fluor anti rat 488	Goat	Invitrogen (A-11006)	1:200
Alexa fluor anti mouse 488	Goat	Invitrogen (A-11001)	1:200
Alexa fluor anti rabbit 594	Goat	Invitrogen (A-11012)	1:200
Alexa fluor anti mouse 594	Goat	Invitrogen (A-11005)	1:200
Alexa fluor anti Rabbit 647	Goat	Invitrogen (A-21244)	1:200
Alexa fluor anti mouse 647	Goat	Invitrogen (A-21247)	1:200
Biotinylated goat anti rabbit	Goat	Invitrogen (31820)	1:200
Biotinylated rabbit anti rat	Rabbit	Invitrogen (31834)	1:200

Table 2.3 Primary and secondary antibodies used in this thesis.

2.3.6 Detection of Edu in P0 tissue sections

To visualise EdU in tissue sections, P0 mouse sections collected as described in **section 2.2.2,** were kept in PBS overnight to clear from anti-freeze solution. At day two, sections were placed using a small pipettor into a 48-well plate, each brain in one well, and permeabilised as described in the protocol in 0.5% Triton X-100 for 30 minutes, followed by 3 x 5 minutes washes in PBS, carefully to avoid losing the sections. 300µl of the EdU cocktail (prepared as described in the protocol with amendments to the suggested concentrations of CuSO4 and azides - these were halved without any effect on the staining outcomes) was added to each well and incubated in the dark for 30 minutes. Afterwards, 3 x 5min washes with PBS were done.

2.3.7 Imaging and Quantification

2.3.7.1 Imaging and microscopy

In this thesis three types of microscopes were used for imaging. An Olympus Canada Inc. Q-Imaging Microscope was used for all stereological quantifications; an Upright Leica DM6000 B microscope was used for fluorescent imaging and cell culture experiment quantification; and an Axioscan scanner for semi-automated quantification with Fiji was used for BrdU, EdU, golgi cox, optical density and striosome analysis. Images were taken using the Axioscan Z1 slide scanner equipped with plan-Apochromat 20X/0.8 M27 objective lens. Z-stacks were 1um spaced (total of 16 slices were taken per section) for at least 4 slices of striatum per mouse, for BrdU, EdU, optical density and striosome analysis; or 0.5µm spaced (40 slices taken per section) for Golgi-cox slides to clearly visualise dendritic spines.

2.3.7.2 Quantification and analysis

2.3.7.2.1 Unbiased stereological analysis and striatal volume estimates

Rigorous cell counts throughout the entire striatum were performed using stereological quantification: cells expressing MSN markers, Neun, BrdU & Ki67 were counted using Visiopharm Integrator System (VIS, version 4.4.6.9) software on an Olympus Canada Inc.

Q-Imaging Microscope. Striatal sections were initially photographed using a 1.25X objective lens under a Leica DFC420 Camera using the Leica Application Core V3.6 software to generate a super-image of multiple brain sections. Regions of interest (ROIs) were then defined by drawing around the striatal areas in each brain section. These defined striatal sections were then randomly sampled from a grid via the software under a consistent step length, with cells counted manually with oil and optical condenser under the 40X objective lens to improve resolution. A 300 μm^2 counting frame size was used with cells either within the frame or touching the green lines included in the count and cells that touched either of the red lines excluded as shown in **Figure 2.6** below:

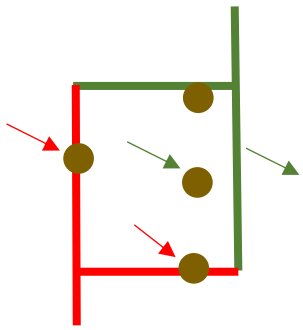

Figure 2.6: illustration of which cells are included or excluded within the 300μm^2 counting frame. Red arrows indicate those rejected; green arrows indicate those accepted.

The total number of cells (C) in each striatal section was calculated using the following formula: $\mathbf{C = \Sigma c \times (\Sigma A \times (\Sigma n \times a)) \times f}$

Where:

C = estimated total number of cells

Σc = total number of cells counted

ΣA = sum of all striatal areas

Σn = total number of frames allocated to the included striatal area

a = area of sampling user grid (300µm2)

f = frequency of sectioning

x= multiplication

Striatal volume estimates:

To determine the striatal volume of Mef2c CKO mice and their WT littermates, the striatal area, of both hemispheres was drawn around at 1.6X magnification using the Leica Application Core V3.6 software microscope. Five anatomically matched striatal sections from rostral to caudal that are 480µm spaced were analysed for all brains. Striatal volume was then calculated using the formula:

V = (Σa*M)/f Where: V = Volume, a = area (mm^2), M = section thickness (40µm) and f = frequency of sampled sections (1:12 or 1:6).

2.3.7.2.2 Semi-automatic Quantification using Fiji software

In this method, z-stacks of fluorescent stained sections were obtained using Axioscan scanner as described above, and all image quantification was done using Fiji image processing package. Reconstructed serial stacked images were transformed from CZI format to TIFF format and exported to Fiji software for processing. In Fiji, images were converted to greyscale (8 bit) and threshold adjusted as in **Figure 2.7**. Striatal regions were outlined using free-hand selection tool. The second method was using manual counting of Edu positive cells under the microscope within 512 x512 pixel field (4 fields per section for three sections).

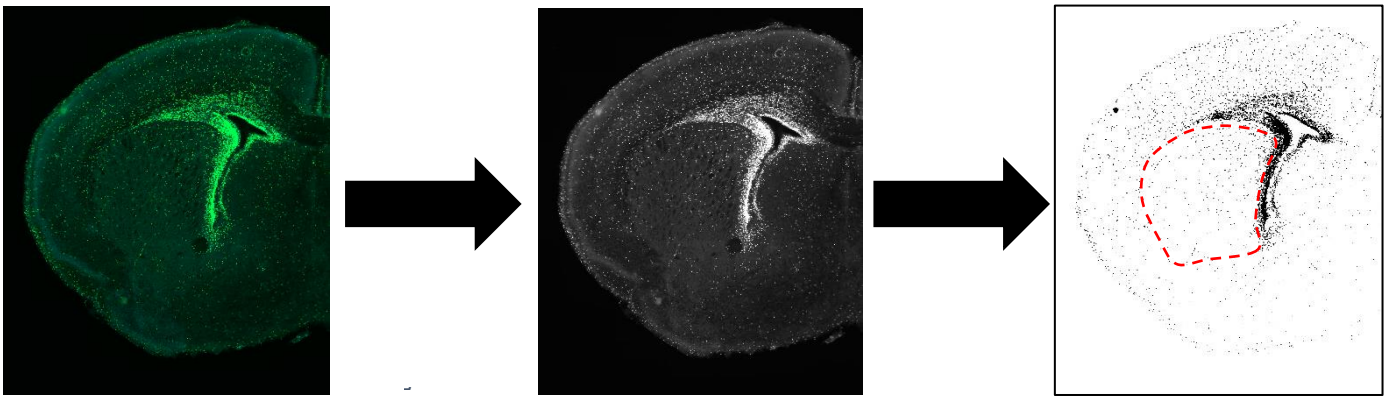

Figure 2.7: Illustration of converting images from CZI files into Tiff files, and then in Fiji. 8-bit images were threshold adjusted for semi-automatic quantification. Red-dashed region shows striatum, SVZ was not included in the analysis.

2.3.7.2.3 Processing Golgi cox slides using Fiji software

Bright field z-stack images were acquired using a Zeiss Axioscan Z1 slide scanner running Zeiss Zen Software (Carl Zeiss Microimaging, Jena, Germany) equipped with a 40x objective. Between 10-14 frames were imaged at dorsomedial and dorsolateral parts of the striatum from at least eight 100µm-thick coronal sections per mouse brain for at least three animals per genotype. Images were processed using Zen lite software and exported in Tagged Information File Format (TIFF) to Fiji software for processing. Images were opened in Fiji by File>>>import>>>image sequence >>ok and converted to 8-bit grayscale and scale bars were set. For each neuron assessed, soma area was measured by measuring the maximum cross-sectional area of that neuron, the number of primary dendrites was counted manually and the number of spines per µm was also counted directly from bright field z-stacks in ImageJ as the total number of spines per ~ 50µm of about 10 dendritic segments. Ten neurons per mouse from three mice per group were analysed. Analysis of dorsomedial and dorsolateral sides were done individually, **Figure 2.8.**

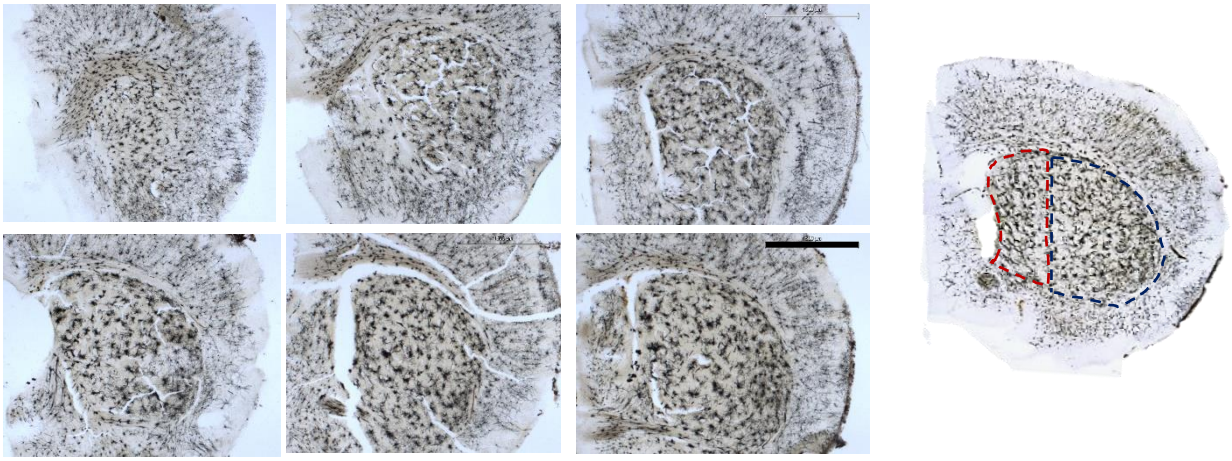

Figure 2.8: Golgi cox-stained coronal mouse brain sections at different Bregma levels from anterior to posterior. Quantification and analysis were done for both dorsomedial (red) and dorsolateral (blue) individually. Scale bar is 1500µm

2.3.7.2.4 Sholl analysis

To quantify the complexity of dendritic arborization in individual neurons from both genotypes, Sholl analysis was performed to count the number of intersections at a fixed distance from the cell body. For semi-automated tracing of dendrites, simple neurite tracer (SNT) plugin ((https://imagej.net/SNT) was initialized, by running plugin>neuroanatomy>SNT. Sholl analysis was done as described in (Welsh et al., 2020). Only neurons with clear and continuous dendritic branches and minimum overlapping with surrounding neurons were included in this analysis as shown **Figure 2.9** below. From user interface parameters, 3 pane views were chosen (Default: XY, ZY and XZ VIEWS)

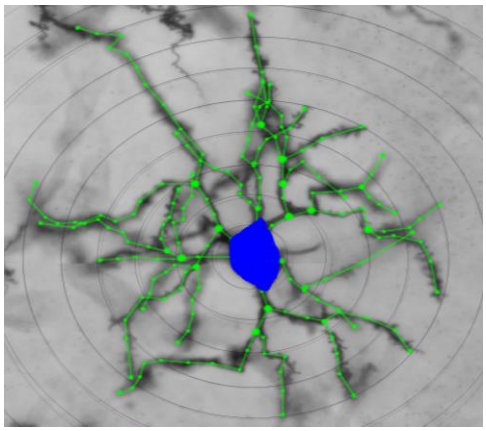

Figure 2.9: 3D-Sholl analysis of an individual neuron using simple neurite tracer plugin in Fiji at 150 µm from the centre of the cell body (blue).

2.3.7.2.5 Optical density analysis

For optical density measurements, the method described in https://imagej.nih.gov/ij/docs/examples/calibration/ and in (Kelm-Nelson et al., 2018) was used. Briefly, a calibrated optical density step tablet to calibrate an image was downloaded. Images were opened in ImageJ and the mean grey value of the background was measured and the first 18 bands, **Figure 2.10.**

Figure 2.10 Calibrated optical density step table.

Then, from Analyse/Calibrate, the 19 measurements are automatically entered into the left column in the dialog box. Optical density (OD) values are manually pasted into the right column and select "Rodbard" from the "Function" popup menu, enter "O.D." into the "Unit" field, then press "OK". ImageJ then generated and displayed the calibration curve. Open the image of interest and convert it to 8-bit image. The OD of the region of interest was measured using the free hand tool of ImageJ and the OD of the background was subtracted from the final measurements. Values per genotype were averaged.

2.3.7.2.6 Striatal striosomes and matrix area measurements

To quantify the percentage area of striosomes, z-stacks of sections immuno-stained with MOR1 receptor were analysed directly in ZEN lite software. Areas of striosomes (MOR1+) and overall areas of striatal sections were measured directly in Zen lite software using region tracing tool. The overall number of striosomes were counted manually in the same images. To quantify percentage area of matrix, area of immunoreactive to calbindin D-28K (CB) was quantified.

2.4 Molecular methods

2.4.1 RNA extraction and removal of genomic DNA

LGE was dissected as described in **2.2.1.2 section** and P0, P3, P7 P14 and adult striatal and cortical tissue dissected as described in **2.2.1.3**. were used for RNA extraction. At the start of the protocol, the dissected sample tissue was weighed, and RNA was extracted using the Qiagen RNAeasy Mini Kit, RNAse-free DNAse set and QiaShredder (all Qiagen, West Sussex, UK) according to manufacturer's instructions. Following extraction, the RNA yield and quality was tested using a Nanodrop Spectrophotometer (1µl) and used for subsequent cDNA synthesis. For pure RNA, 260/280 is ~2. To remove genomic DNA, we used ezDnase kit (Invitrogen) after completing the column RNA extraction step, this was done according to the manufacturer instructions.

2.4.2 cDNA synthesis

For first strand synthesis, RNA samples were standardised by amount and a maximum of 1 µg of DNase-treated RNA was incubated with random primers (100ng) (Invitrogen) and 10mM dNTP mix (Bioline) for 5 minutes at 65˚C. Following a brief chill on ice, 5X first strand buffer, 0.1M DTT, RNase OUT (40 u/µl) (all Invitrogen) were added with Superscript IV (200 u) (Invitrogen) was added and incubated at 23˚C for 10 minutes, 55˚C for 10 minutes and finally 80˚C for 10 minutes. cDNA was used for subsequent PCR reactions. RT-ve controls were also generated by substituting superscript with water.

2.4.3 QPCR (quantitative polymerase chain reaction (RT-PCR) and the ΔΔCt method

For QPCR, 1μl of cDNA from first strand synthesis was combined with a PCR master mix that consisted of 10μl PowerUp SYBR Green master mix x2 (Invitrogen), with 1μl of forward and reverse primers of the target gene at 100pmol (all primers were from Eurofins) and 7μl nuclease-free water (Invitrogen), to make a 20μl final volume reaction per well of a 96 well plate (MicroAmpTM Fast Optical 96-well reaction plates) (Applied Biosystems). The plate was sealed with MicroAmpTM Optical Adhesive Film (Applied Biosystems) and centrifuged for 20 seconds. Plates were run in a StepOnePlusTM Real-Time PCR System (Applied Biosystems) using StepOneTM Software under the following amplification conditions: 95°C for 15 minutes, and then 40 cycles of 95°C, 58°C, and 72°C for 30 seconds each. Melt curves were generated from readings every 0.5°C between 53°C and 95°C.

Samples (1μl cDNA templates) were each run in triplicate for each primer pair assessed, including the house-keeping gene, and a negative control (where cDNA template was substituted for RT -ve control) was included in a fourth well. All primers used are shown in **Table 2.4**.

Primers used:

Primer	Forward	Reverse
Mef2c exon2	GTGCTGTGCGACTGTGAGAT	CTCCACAATGTCTGAGTTTGTC
Mef2c	AGGACAAGGAATGGGAGGAT	GCAGTGTTGAAGCCAGACAG
Mef2c	GTCGGCTCAGTCATTGGCTAC	CGCTACTCAGAGAGTACTCAG
Caspase 3	AGCAGCTTTGTGTGTGTGATTCTAA	AGTTTCGGCTTTCCAGTCAGAC
Caspase 9	TCCTGGTACATCGAGACCTTG	AAGTCCCTTTCGCAGAAACAG
Cytochrome c	AGGCTGCTGGATTCTCTTACAC	CAGGGATGTACTTTTTGGGATT
Bcl-2	GTGGATGACTGAGTACCTGAACC	AGCCAGGAGAAATCAAACAGAG
Bcl-xl	CTTTCGGGATGGAGTAAAC	AGGTGGTCATTCAGATAGG
Bad	CAGCCACCAACAGTCATC	CTCCTCCATCCCTTCATCC
GAPDH	TAACATCAAATGGGGTGAGG	GGAGATGATGACCCTTTTGG
Bactin	GCTGTCCCTGTATGCCTCT	GTCTTTACGGATGTCAACG

Table 2.4 sequence information for all primers used in this thesis.

2.5 *In vitro* methods

2.5.1 Tissue processing and preparation of single cell solution

Tissue was dissected as described in section **2.2.1.2**, washed once with Dulbecco's modified Eagle's medium (DMEM F12) supplemented with dornase alpha (DA), then transferred to ™TrypLE Express (Gibco, Life Technologies) supplemented with DA (20u/1ml) and incubated for 10 minutes at 37°C with gentle agitation after the first 5 minutes. Then, tissue was washed twice with DMEM F12/ DA, and 200µl of DMEM/F12 was added for the trituration step. To get a single cell suspension tissue was gently triturated between 10-15 times with a 200 µl Gilson pipette.

Cells were counted using a haemocytometer and trypan blue (0.4% trypan blue solution, ThermoFisher) to assess cell viability. Specifically, 10 µl of cell suspension was diluted in a 40µl drop of DMEM F12, then 10µl of this diluted cell suspension was further diluted in 10µl of Trypan blue and transferred to a haemocytometer (™Marienfeld) with a glass cover slip and viewed under the microscope. Cells in the centre square and the 4 corner

squares were counted and the number of cells per µl was calculated, as well as total cell number, taking the dilution factor into consideration. The following formula was used:

Cells/Number of squares x 10 x Dilution Factor (10) = number of cells/µl

Cells were re-suspended in neuronal differentiation media (DMEM/F12 with 2% B27 supplement, 1% foetal calf serum, 1%PenStrep, a cocktail of Penicillin and Streptomycin, and BDNF) seeded onto PDL-coated cover-slips (prepared by adding 300ul of PDL to each cover slip, then washing in dH_2O and drying under UV) at a final density of 50,000 or 100,000 cells in a total volume of 30 µl per well. Plates were transferred to the incubator at 37°C and after the cells had adhered to the coverslips (~2-4 hours) the wells were flooded with 500ul of differentiation media. Cells were maintained at 37°C in humidified 5% CO2 and 95% atmospheric air. Differentiation media was replaced after 3 days of incubation.

2.5.2 Adding Edu to the cells

The proliferative marker EdU (5-ethynyl-2'-deoxyuridine) (Click-iT™ EdU Cell Proliferation Kit for Imaging, Alexa Fluor™ 488 dye) was added to the differentiation media after cells had settled on the cover slips for ~2 hours. EdU (10 µg/ml) was added to the neuronal differentiation medium 24 hours before fixation. Cells were either fixed at 24 hours or 6 DIV.

2.5.3 Fixing cells and immunocytochemistry

After the end of the culture period, cells were washed once with phosphate buffered saline (PBS; Gibco) and fixed in 3.7% PFA (Millipore) for 15 minutes at room temperature (5ml of 40% PFA was added to 45ml of PBS). Once fixed, cells were washed three times with PBS, and stored in 500µl of PBS at 4°C for immunocytochemistry. **For EdU detection,** tissue was permeabilized with 0.5% Triton-X-100 for 30 minutes followed by 3 x 5-minute washes with PBS. EdU cocktail was prepared according to manufacturer's instructions, by mixing the following for 500µl per sample: 430µl of click it reaction buffer, 20µl of CuSO4, 1.2µl of Alexa fluor azide and Reaction buffer additive. Tissue was incubated in the EdU cocktail for 30 minutes in the dark. The reaction cocktail was removed, and the tissue was washed 3 x 10 mins in TBS. Staining with additional antibodies was performed after this, as in section XX. For terminal deoxynucleotidyl

transferase-mediated dUTP nick end labelling **(TUNEL)** death assay protocol, this assay was started immediately after EdU protocol. TUNEL death assay (™ThermoFisher) was performed according to the manufacturer's instructions except that the permeabilization step was already done for the EdU protocol. Briefly, 100µl of TDT buffer was added to each cover slip and incubated at 37°C for 10 minutes. Then, coverslips were incubated for 60 minutes at 37°C in TdT Reaction mixture, (for 1 coverslip, prepared in the following order: TdT reaction buffer 47µl, EdUTP 1µl, TdT enzyme 2µl).

After 60 minutes, coverslips were washed twice with 3% Bovine serum albumin (BSA) in PBS for 5 minutes each. Click-iT™ Plus TUNEL reaction cocktail prepared according to the manufacturer's instructions was added to 10X Click-iT™ Plus TUNEL Reaction buffer additive prepared by diluting the 100X solution 1:10 in deionized water (this solution must be prepared fresh and used on the same day). Components were mixed well by vortexing, and solution must be used within 15min of preparation. 50 µL of the Click-iT™ Plus TUNEL reaction cocktail was added to each cover slip and the solution was allowed to spread completely over the surface. Samples were incubated for 30 minutes at 37°C, protected from light. Click-iT™ Plus TUNEL reaction cocktail was removed, then each coverslip was washed with 3% BSA in PBS for 5 minutes.

2.5.4 Imaging and Quantification of cells

were performed live using Leica DM6000 B microscope. For each cover slip, between 5-9 frames were quantified for EdU tdTomato and TUNEL.

2.6 Behavioural tests

2.6.1 Nesting

Mice were placed individually in new cages provided with a square shaped nesting material for two hours. The mouse was removed, and the nest analysed. The amount of the shredded and non-shredded material was weighed.

2.6.2 Marble burying

The test was conducted in a plastic box measuring 30 cm by 50 cm by 15 cm which was filled with 5 cm of non-allergenic bedding sawdust. For the assessment of anxiety related behaviour 20 glass marbles were evenly spaced out in 5 rows of 4 (5 cm apart) (**Figure 2.11**) in the centre of a novel cage with enough sawdust to allow burying; a mouse's normal response is to bury marbles. 5 test stations were set up, allowing 5 mice to be tested simultaneously. Animals were left for 30 minutes in the cage, with a plastic lid over the top so that they could not escape or climb on it. The experimenter was not in the room whilst testing occurred. Following the 30 minutes, mice were removed, individual cages were photographed, and the number of marbles buried were counted. Marbles were categorised into four classes; not buried, <50% buried, >50% buried and completely buried. Only those that are > 50% buried and completely buried were included in the final analysis.

Figure 2.11 Initial set up of the marbles in the plastic cages

2.6.3 Automated activity boxes

Animals were tested using automated clear activity boxes, Med Associate hardware (Med Associates, St Albans VT, USA) and MED PC (IV) software over a period of 32hours to assess activity during full light and dark phases. 18 mice (10 CKO and 8 WT) were placed in individual plastic cages (L42 cm, W26 cm and D 19cm) with fitted water bottles and adequate powdered food. Beam breaks of three infrared beams crossing the base of each cage were recorded, and the total number of beam breaks was totalled per each animal and averaged for the two genotypes. Animals were tested using automated activity boxes over a period of 26 hours.

2.6.4 Rotarod

This test has been used as a measure of motor coordination and balance. The moving apparatus of the rotarod (Ugo Basile, Varese, Italy) (**Figure 2.12**) rotates in a gradually accelerating speed (4-44 rpm over 300 seconds). The mice were handled over two days to acclimatize and tested at day 3 over 8 trials with a 30-minute interval between each two successive trials. The time when the mouse fell off was recorded as the end of experiment.

Figure 2.12: Rotarod apparatus. Up to 5 mice were tested simultaneously, a 300 second cut-off per trial was used.

2.6.5 Open field tests

This test is used to determine different aspect of locomotor activity, anxiety, and exploratory mouse behaviour by scoring several parameters using video camera. The open field arena is 80 x 80 cm and can be divided into a central zone and a peripheral

zone. Animals were acclimatized to the testing arena for two days before the day of testing and 10 minutes on the day of testing (data were not collected at this time). The experiment for each mouse was run over another 10 minutes in the arena (80 cm x 80 cm) divided into the Centre zone (40 cm x 40 cm) and the peripheral zone (measuring about 20 cm from the edge of the arena) (**Figure 2.13**). Data were automatically collected via Ethovision software and selected parameters were transferred to excel sheets for analysis.

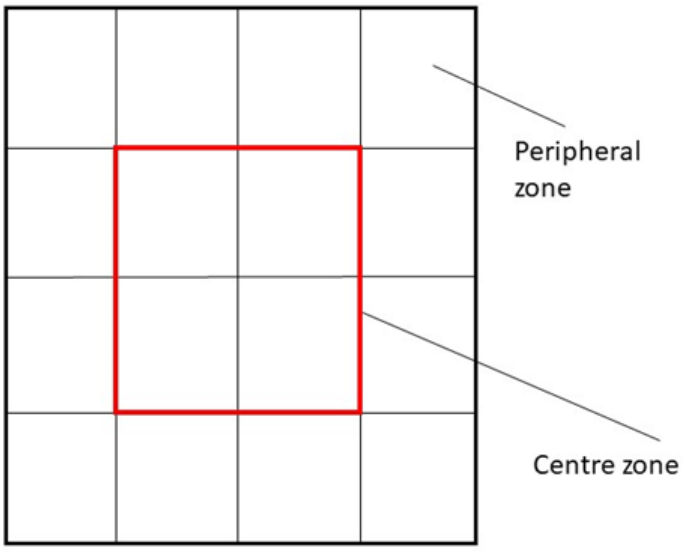

Figure 2.13 illustration of the open field test arena. The middle four squares represent the centre zone.

2.6.6 Inverted cage grip strength test

This test is used to measure the strength of the fore and hind limbs of the mice using a metal grid. The mouse was placed on the grid and then carefully inverted and placed over 30 cm height stands with bedding towels placed underneath to soften falls. The time the mouse spent grasping the grid without falling was recorded, a maximum cut-off of 1 minute was used and analysed.

2.7 Statistical analysis

SPSS V.25 and Graph Prism9 were used to carry out statistical analysis of all data. For immunohistochemical analysis of developmental series, Two-way ANOVA (analysis of variance) with Bonferroni correction was used. For behavioural data analysis, either Student's t-test (weight, Nesting, marble burying, OFT) or repeated measures Two-way ANOVA followed by Bonferroni post hoc (Rotarod and activity boxes) were used.

Chapter 3: Characterization of Mef2c TF expression in WT mouse striatum

3.1 Summary

Mef2c is a transcription factor (TF) that was originally identified as having a key role in muscle gene expression, but more recently has been shown to have an important role in neuronal development, maturation and survival in various brain regions in human and rodents. An Affymetrix microarray analysis performed in the host lab, which investigated gene expression in the mouse WGE over the period between the ages E12-E16, revealed that Mef2c is one of the most upregulated genes during embryonic striatal development (Precious et al., 2016). However, little is known about its spatiotemporal expression in the developing and postnatal mouse striatum. In this chapter, I show, using immunofluorescence, IHC and RT qPCR, that Mef2c has a narrow window of expression in the mouse striatum and is downregulated in the adult striatum.

A complete null of Mef2c is lethal at E9.5 as a result of cardiac deficits (Potthoff and Olson, 2007; Lin et al., 1997) therefore, a striatal-specific Mef2c conditional knockout mouse model using Cre-recombinase under the control of Gsx2 promotor was utilised in this study. The Gsx2- Cre mouse line used was shown to be specifically expressed in the mouse striatum and the CKO (Gsx2- Cre line crossed with Mef2c floxed line) results in a specific reduction of Mef2c levels in the CKO mouse striatum only, without affecting its levels in the cortex.

3.2 Introduction

The four *Mef2* genes, *a-d*, encode four different transcription factors that are crucial for neuron and muscle differentiation (Kamath and Chen, 2019; Adachi et al., 2016; Leifer et al., 1993; Piasecka et al., 2021; Taylor and Hughes, 2017). Among these, Mef2c transcription factor (TF) has emerged as an important regulator of neuronal development and survival. Many research studies have successfully characterised the expression pattern and functional role of Mef2c in the cortex, hippocampus and cerebellum by utilizing different *CKO* mouse models, i.e *Camk2a-Cre*, *Emx1 IRES-Cre* and *hGFAP-cre* (Bjorness et al., 2020; Harrington et al., 2016; Barbosa et al., 2008; Li et al., 2008; Kamath and Chen, 2019). However, its role in mouse striatum and striatal development is still unexplored.
According to gene expression analysis performed previously (Precious et al., 2016), *Mef2c* is amongst the most upregulated genes during embryonic striatal development, however, the pattern of its expression in the striatum is largely unknown. Therefore, I aim in this chapter to characterise the temporal pattern of Mef2c expression within the developing and adult striatum further and at earlier time points, and the spatiotemporal expression of Mef2c protein in the same period. This will form a foundation towards a better understanding of the role of Mef2c in striatal development.

IHC, immunofluorescence, and RT qPCR were used to characterize Mef2c protein and mRNA expression patterns in the mouse striatum over a developmental series that covered different time points during embryonic and postnatal development and the results were compared with its expression in the cortex. I also aimed to compare the expression of Mef2c with the three well-known MSN markers, Ctip2 and Darpp32, in early postnatal (P0 and P3) brain.

I used the Cre-loxP recombination system under the control of the *Gsx2* promotor, to generate mice that specifically lack *Mef2c* in the striatum during early embryonic development. *Gsx2* is expressed from approximately embryonic day 10 (E 10)(Toresson et al., 2000). Complete null of *Mef2c* is lethal between E9.5 and E10.5 due to an impairment in heart development and vascular angiogenesis (Lin et al., 1997; Potthoff

and Olson, 2007). Before undertaking different histological and behavioural analyses on this mouse line, the *Gsx2-Cre* mouse line used in this project needed to be validated to confirm that the CKO had been generated successfully. Therefore, I show here that Mef2c protein and mRNA expression have been reduced significantly in the CKO striatum, while the cortex is unaffected.

Understanding the expression profile of Mef2c in the mouse striatum provides valuable information before attempting to understand the functional roles of this TF in the mouse brain. Therefore, the main objectives of this chapter were:

1. To characterise Mef2c RNA and protein expression in WT developing, postnatal, and adult mouse striatum and compare its expression to the expression of other MSNs markers
2. To assess the spatiotemporal expression of Mef2c in embryonic and postnatal WT brain sections.
3. To validate the Gsx2-Cre mouse model used in this project using tdTomato reporter expression.
4. To compare the expression of Gsx2-Cre reporter in the mouse striatum with the expression of FoxP1 and Mef2c, in addition to the most known interneuronal markers; PV and ChAT.
5. To confirm the absence of Mef2c expression in Gsx2-Cre reporter positive cells outside the striatum.
6. To confirm that Gsx2-induced recombination of Mef2c was sucessful in the striatum with no effect on Mef2c levels in the cortex.

3.3 Experimental procedures

To characterize the spatiotemporal expression of Mef2c in WT embryonic mouse striatum, time-mated dams were culled by schedule 1, and tissue was collected for RT qPCR and IHC as described in **2.2.2.** For postnatal analysis, striatae were either dissected for molecular analysis as in **2.2.3**. or perfused for IHC as in **2.2.1**. Free-floating IHC of Mef2c was done as described in **2.3.4**. Optical density and stereological analysis were performed as described in **2.3.7.2.1.** and **2.3.7.2.5.** To validate Gsx2-Cre used in this thesis, breeding strategy described in **2.1.2.3** was used and IF with MSNs and interneuronal markers was performed.

To confirm striatal Mef2c CKO, striatal and cortical tissue were dissected from WT and CKO mice generated from the breeding strategy described in **2.1.2.1**. RT qPCR was conducted as described in **2.4** and Mef2c IHC was conducted using specific Mef2c antibody.

Statistical analysis was done using GraphPad prism 9.4.1 software. One-way ANOVA was performed with Tukey's post hoc test and significance was set at 0.05 level. Multiple t-test was conducted with Holm-Sidak correction.

3.4 Results

3.4.1 Mef2c expression in WT mouse striatum peaks at P0 and decreases through adulthood.

Little is known about the expression of the Mef2c TF in the mouse striatum. Therefore, the aim of this section was to assess the expression of *Mef2c* RNA and protein in WT mouse striatum in a developmental series between E12 through to adulthood. RT qPCR and IHC were carried out at different ages throughout development. Time-points assessed were embryonic days E12, E14, E16 and E18, in addition to the postnatal time points P0, P3, P7 and P14, and the adult mouse (3 months). These ages were chosen, firstly, to assess Mef2c expression during a period encompassing striatal MSN neurogenesis and maturation, and secondly, to assess Mef2c expression within the early postnatal and adult striatum, as viral-induced *Mef2c CKO* in MSNs in the early postnatal period was shown to result in morphological changes in the striatum (Chen et al., 2016), indicating that Mef2c could play a distinctive role during postnatal development.

3.4.1.1 *Mef2*c RNA expression from embryonic day E12 through to adulthood.

First, the *Mef2c* gene expression profile in mouse LGE and striatum was examined by RT qPCR in a developmental series including E12, E14, E16, E18, P0, P3, P7, P14 and adult age groups**, (Figure 3.1 a)**. mRNA levels were normalized to the level of GAPDH and βactin housekeeping genes and values were compared to the minimum relative expression seen at E12. Overall, the levels of *Mef2c* expression were significantly variable across development (One-way ANOVA, $F_{(8, 18)} = 11.72$, $p<0.0001$). Specifically, *Mef2c* RNA was minimal at E12, but then became evident at E14 and increased by E16. The levels were similar at E18, after which a significant increase occurred with peak expression at P0 (One-way ANOVA with Tukey's post hoc, $p < 0.00001$). This was followed by a gradual reduction until it was expressed minimally in the adult striatum.

In the cortex, *Mef2*c RNA levels started to increase gradually during embryonic development and reached a plateau of expression in the postnatal cortex **(Figure 3.1b**). *Mef2c* levels were significantly different across age groups (One-way ANOVA, $F_{(8,18)} = 7.466$, $p = 0.0002$). Pairwise comparison using Tukey's post hoc test revealed that,

except for the significant difference between both E12 and E14 with adult (p = 0.0012 and p = 0.0023, respectively), no significant differences in cortical *Mef2c* expression were found between E16, E18, P0, P3, P7, or P14 and adult cortex (E16 and adult p = 0.0799; E18 and adult p=0.1687; P0 and adult p=0.8833; P3 and adult p=0.9654; P7 and adult p=0.9971; and lastly, P14 and adult p=0.9952)**.**

Next, I compared *Mef2c* RNA expression between the striatum and cortex (**Figure 3.1 c)**. The two factors "Age" and "brain region" were analysed using a Two-way ANOVA test followed by Bonferroni tests. A significant difference in *Mef2c* RNA levels was found between these two mouse brain regions across different age groups (Age x brain region; $F_{(8, 36)}$ =6.823, p<0.0001). *Mef2c* expression was significantly greater in the cortex than the striatum (brain region; $F_{(1, 36)}$ = 144.7, p <0.0001) and there was an increase in expression with age, (Age; $F_{(8, 36)}$ =8.157, p <0.0001). Bonferroni Post hoc tests showed a significant difference in *Mef2c* gene expression between cortex and striatum at E18, P0, P3, P7, P14 and adult (p= 0.0233, p=0.0003, p=0.0001, p=0.0001, p=0.0001, and p=0.0001, respectively).

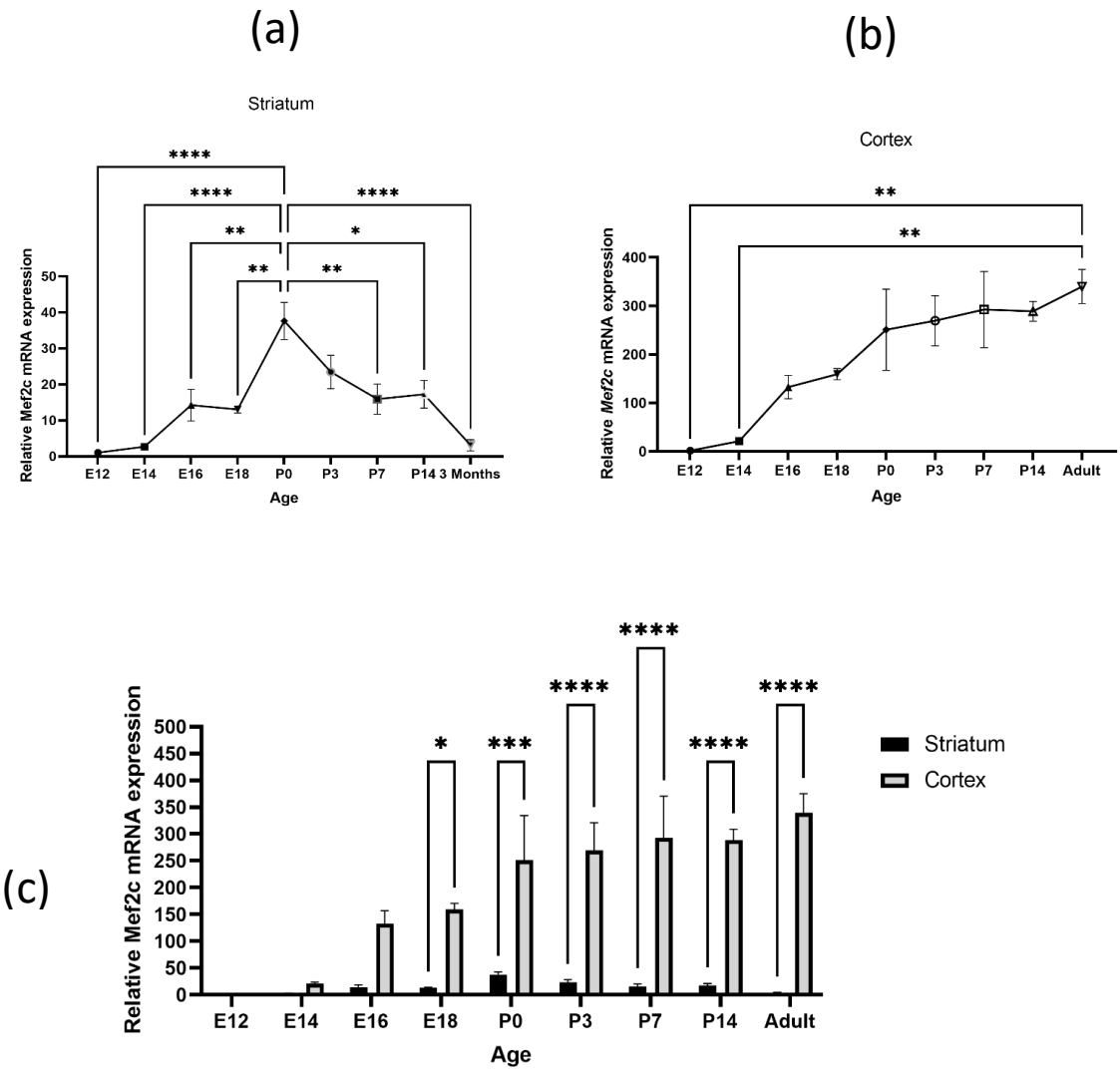

Figure 3.1 RT qPCR analysis of *Mef2c* RNA expression in the developing WT striatum and cortex from embryo to adulthood.

(a) *Mef2c* expression peaks at P0 in the striatum and then decreases towards adulthood (****p < 0.0001). **(b)** *Mef2c* levels increase significantly in the developing cortex through embryonic and postnatal development, with continued high expression in adult cortex. (**c**) Graphical representation of *Mef2c* expression showing that *Mef2c* RNA levels are significantly higher in the cortex than the striatum. Data are presented relative to *Mef2c* gene expression at E12. n= 3 per group. * p<0.05, ** p<0.01, ***p<0.001,****p<0.0001.

3.4.1.2 Mef2c protein expression in embryonic and postnatal mouse striatum

In the previous section *Mef2c* RNA expression was minimal at E12, then first clearly expressed at E14, and increased greatly at E16, with little change at E18. In this section, embryonic mouse brain sections were analysed to see if protein expression correlated with RNA expression. First, embryonic tissue sections were stained using IHC with a specific Mef2c antibody against amino acids 268-281 of mouse Mef2c to perform a qualitative assessment of protein expression during embryonic development (**Figure 3.2)**.

No immunoreactivity for Mef2c was found in the LGE (or MGE) at E12, while weak expression was observed in the cortical plate **(Figure 3.2a)**. Mef2c expression was first evident in the dorsolateral aspects of the mantle zone at E14, whilst still undetectable in the germinal zone (GZ) and with strong immunoreactivity observed in the cortex **(Figure 3.2b).** At E16, the immunoreactivity became stronger and distributed over a wider area of the developing striatum (mantle zone) **(Figure 3.2c)**. By E18, Mef2c positive cells were to a great extent equally distributed over the striatum **(Figure 3.2d)**.

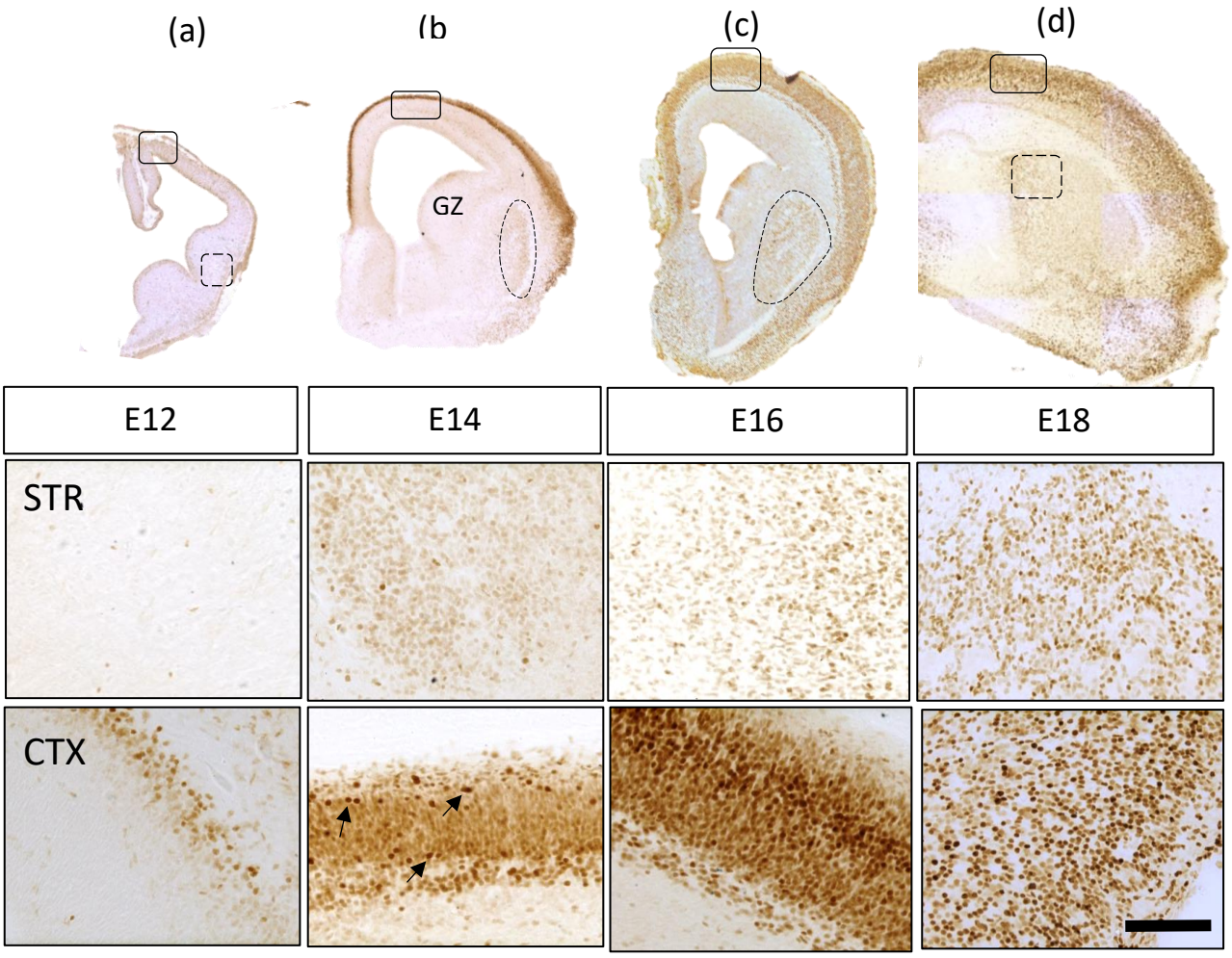

Figure 3.2 Mef2c protein expression is first evident at E14, increases at E16, and remains unchanged at E18.

Mef2c DAB IHC in the embryonic mouse striatum at E12 **(a)**, E14 **(b)**, E16 **(c)** and E18 **(d)**. Areas (LGE or striatum) with a black dashed outline in each section are shown at high magnification in the upper panel below, and areas (cortex) outlined with a continuous black line are shown at higher magnification in the lower panel below. Mef2c was first expressed at E14, specifically in the dorsolateral aspects of the LGE (dashed area in b). At E16, Mef2c immunoreactivity increased and covered more area of the developing striatal mantle, while at E18 it became expressed in more cells across the whole striatum. In the cortex, Mef2c was weakly expressed at E12 **(a)**, strongly expressed in many cells at E14 (arrows in **b**), while at E16 **(c)** the immunoreactivity increased and labelled more neurons right across all cortical layers at E18 **(d)**. Scale bar is 100µm.

3.4.1.3 Mef2c expression is heterogenous in early postnatal mouse striatum along the medio-lateral and rostro-caudal axes.

Here I have assessed the Mef2c spatiotemporal expression pattern in postnatal striatum. Mef2c expression varied significantly between medial to lateral and rostral to caudal aspects of the striatum **(Figure 3.3).** Mef2c was expressed more highly medially (**a** and **c**) than laterally (**b**), with the densest staining of Mef2c observed at the most ventral-lateral aspect of the striatum **(d**) in (**Figure 3.3B)**. Mef2c expression also varies along the rostro-caudal axis **(Figure 3.3C)**, with Mef2c being almost completely absent in the most rostral striatum (**a'**), then increasing gradually (**b'**), until it is strongly expressed in the caudal striatum **(c'**).

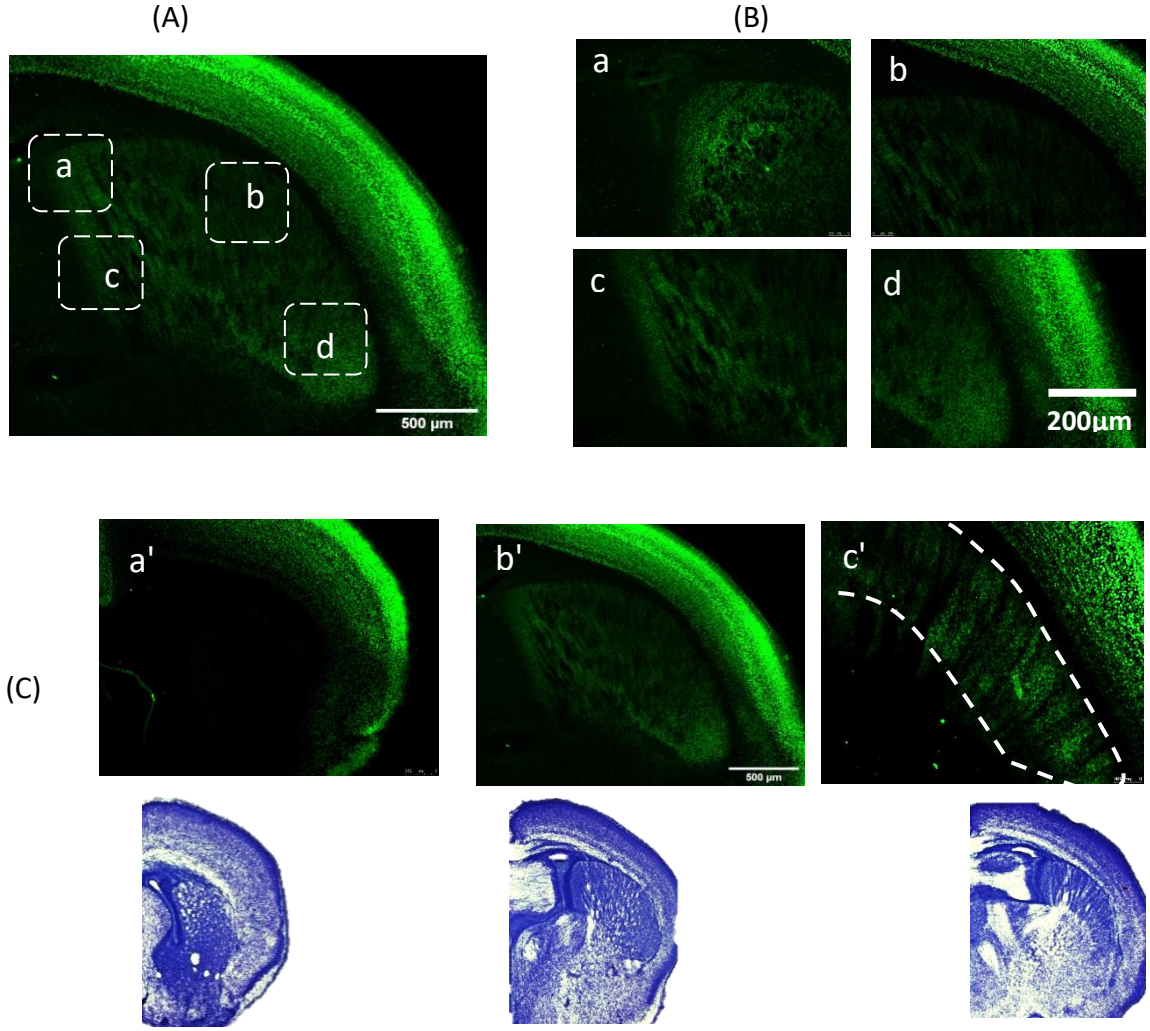

Figure 3.3 Mef2c is heterogeneously expressed along the medio-lateral and rostro-caudal axes of P0 mouse striatum.

Immunofluorescence of Mef2c in WT mouse striatum at postnatal day 0 showed regional heterogeneity of Mef2c expression. Higher magnification of dashed areas in **(A)** are shown in **a, b, c and d**. Mef2c expression decreased from **a** to **b**. A strong intensity of Mef2c staining was observed in **d,** which is the most ventral aspect of this brain section. **(B)**, Mef2c expression altered across the rostral-caudal axis, with very low Mef2c in the most rostral section **(a'),** more prominent expression observed in **(b')** with the strongest staining caudally in **(c').** Corresponding CV- stained sections in **C** illustrate at which level along the rostral-caudal axis images were taken.

3.4.1.4 Mef2c expression decreases from medial to lateral in postnatal P0 – adult mouse striatum.

The graded pattern of Mef2c protein expression observed in P0 striatum in the preceding section prompted an assessment of the spatiotemporal expression of Mef2c in brain sections at other postnatal time points (P3, P7, P14 and adult), along with P0.

Mef2c protein expression was determined at two levels in DM and DL striatum in coronal sections (**Figure 3.4 a**). The highest Mef2c immunoreactivity was in the DM aspect of P0, while the lowest was observed in the DL aspect of P14 and adult, with almost undetectable levels at P14 and adult striatum **(Figure 3.4 a (A-D).** Mef2c expression in the cortex **(Figure 3.4 a (E))** was used as a positive control as Mef2c is highly expressed in this region and no significant difference was observed in its RNA levels over postnatal development as shown in the first section.

Quantification of Mef2c protein expression was performed using two methods, stereological analysis, and optical density, to see if changes in protein level and RNA expression showed similar patterns. This was done first for the whole striatum, and then for DM and DL parts individually by dividing the striatum into DM and DL (based on (Martín-Ibáñez et al., 2017) **(Figure 3.4b).** A two-way ANOVA was conducted with age and part of striatum as the two factors assessed**.**

Stereological analysis of numbers of Mef2c expressing cells per mm^3 in the whole striatum revealed a significant decline across the five developmental ages ($F_{(4, 24)}$ =82.80, p<0.0001), **(Figure 3.4c)**. The peak of Mef2c positive cells was seen at P0 (*p*<0.0001). Analysis of DM and DL separately **(Figure 3.4d**), also demonstrated a significant decline in the number of cells expressing Mef2c per mm^3 over this developmental period (2-way ANOVA showed a significant effect of age, $F_{(4.48)}$ =130.7, p<0.0001) and a significant difference between DM and DL ($F_{(1, 48)}$ = 29.66, p<0.0001). There was no interaction (Age x part of striatum, $F_{(4, 48)}$ =1.440, p =0.235) indicating that the decrease in Mef2c positive cells was consistent between DM and DL over this developmental period and not specific to certain age.

Optical density analysis of whole striatum also showed a significant difference across the five developmental ages ($F_{(4, 26)}$ = 45.19, p <0.0001, One-way ANOVA) **(Figure 3.4.e**).

There was also a significant difference in Mef2c intensity between DM and DL across the five ages (Age x part of striatum, $F_{(4, 51)} = 3.649$, $p= 0.0109$) **(Figure 3.4.f**). Bonferroni post hoc tests revealed a significant reduction in Mef2c staining intensity between DM and DL regions at both P3 and P7, of about 53% and 69%, respectively ($p <0.0001$ and 0.0017).

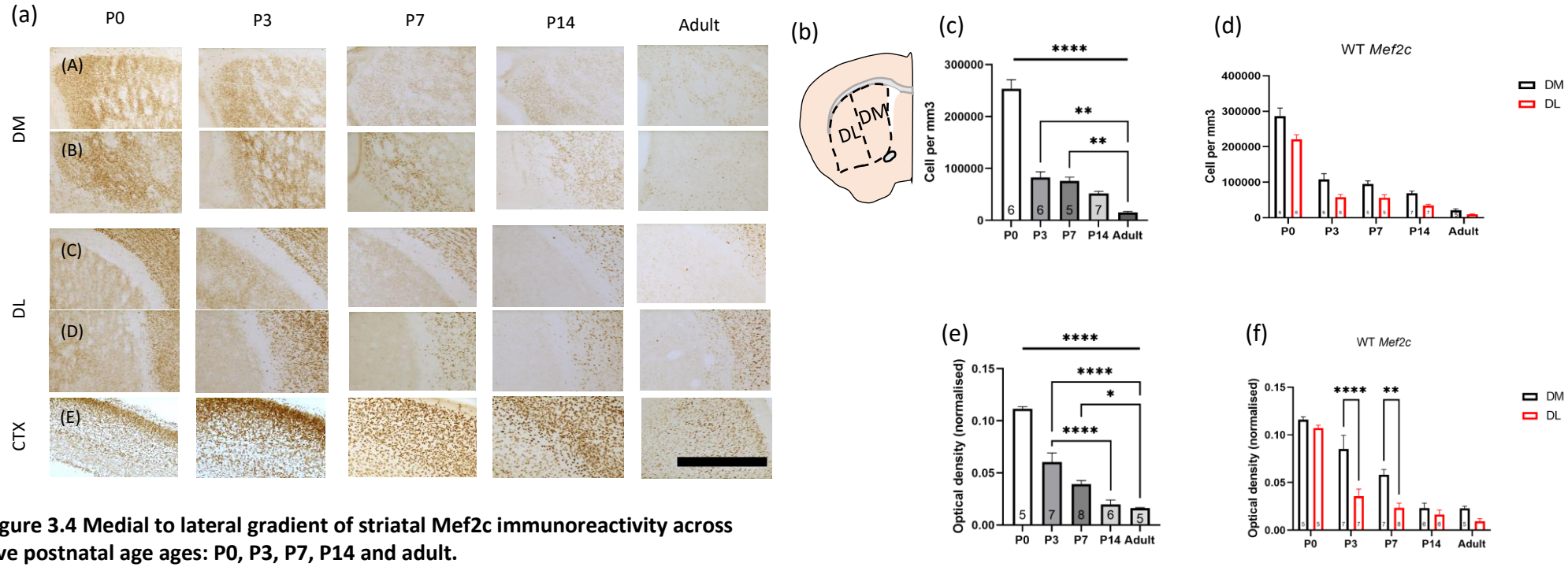

Figure 3.4 Medial to lateral gradient of striatal Mef2c immunoreactivity across five postnatal age ages: P0, P3, P7, P14 and adult.

(a): Mef2c IHC in coronal brain sections at P0, P3, P7, P14 and adult, showing images of dorsomedial striatum (**A** and **B**), dorsolateral striatum (**C** and **D**) and cortex (**E**), showing a clear reduction of Mef2c expression between DM and DL, with almost undetectable Mef2c in the DL at P14 and adult striatum in D. Images were taken at magnification of 100x, scale bar is 500µm. **(b):** Schematic showing how coronal brain sections were divided into DM and DL. (c): Stereological quantification of Mef2c positive cells per mm3 in whole striatum at P0, P3, P7 and P14 and adult, showing peak expression at P0 ($p<0.0001$). (d): stereological quantification of Mef2c positive cells in DM and DL individually showing consistent reduction in Mef2c expression in both DM and DL toward adulthood. (e): Optical density analysis showed similar decline as in c with peak Mef2c expression at P0 ($p <0.0001$). (f): Optical density analysis of DM and DL showed less expression in DL compared to DM; however, this was statistically significant only at P3 and P7 ($p< 0.0001$ and 0.0017, respectively). Bars represent means ± SEM. **** = $p < 0.0001$, * = $p < 0.05$, numbers at the bottom of each bar represents n per group.

3.4.1.5 Mef2c RNA and cells per mm^3 are positively correlated in postnatal mouse striatum

Mef2c RNA expression reached a maximum expression in the neonatal mouse striatum, at P0 and then downregulates through postnatal development. Cells expressing Mef2c in the overall striatum were also shown to be the maximum at P0 and then this number significantly reduced through adulthood. Therefore, to see if Mef2c expression correlates with Mef2c expressing cells in postnatal WT mouse striatum, I performed a correlation test using Pearson's correlation coefficient. There was a positive correlation between RNA and protein expression (r= 0.8520, p<0.001) as shown in **(Figure 3.5).**

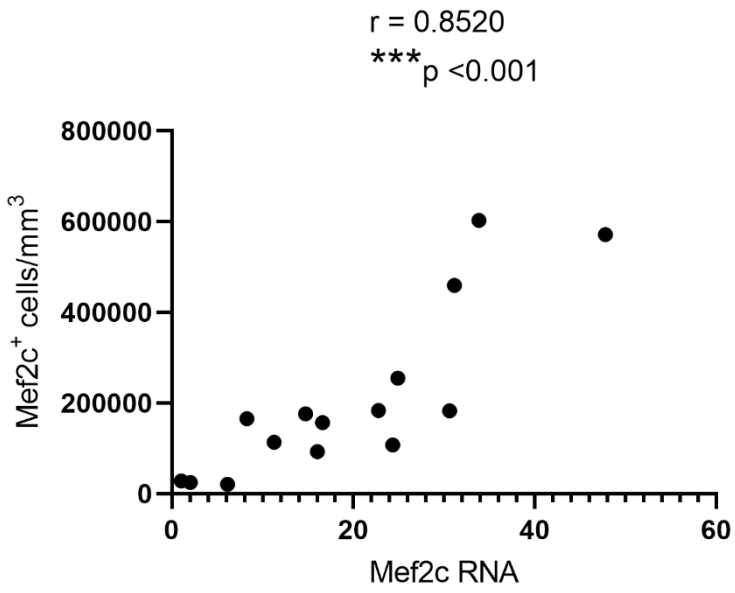

Figure 3.5 Mef2c RNA is positively correlated with Mef2c positive cells per mm3 in WT postnatal mouse striatum (r=0.852, p<0.001).

3.4.2 At the time of peak Mef2c expression (P0) all Mef2c positive cells are Ctip2-positive, but Mef2c is not co-expressed with Darpp32.

As a first step to exploring which striatal cells express Mef2c, co-labelling of Mef2c with the well-known MSN markers Darpp32, and Ctip2 was performed at P0, when Mef2c expression is at its peak **(Figure 3.6).** Ctip2 TF is expressed in striatal MSNs from early development through to adulthood (Arlotta et al., 2008; Precious et al., 2016). Darpp32 is another important marker that is expressed only in mature MSNs at P0 (Ivkovic and Ehrlich, 1999; Precious et al., 2016).

At P0, all Mef2c-positive cells appeared to be Ctip2 positive (**Figure 3.6a**). There are Ctip2 cells that are Mef2c negative (white arrows in **a**), indicating that although the vast majority of Mef2c positive cells appeared to be of MSN origin, not all MSN progenitors at this stage co-express Mef2c.

Another observation was that Mef*2c* did not co-localise with Darpp32 at this stage. The pattern of Darpp32 expression is ''patchy'' and it is not expressed evenly throughout the striatum (white arrows in **b** in **Figure 3.6**). Darpp32 expression at P0 in the mouse striatum was seen only in striosomes. To confirm this, double immunofluorescence of Darpp32 and MOR1, which is specifically expressed in striosomes (Chen et al., 2016), was performed. The results showed complete co-localisation between these two markers **(Figure 3.6c)**.

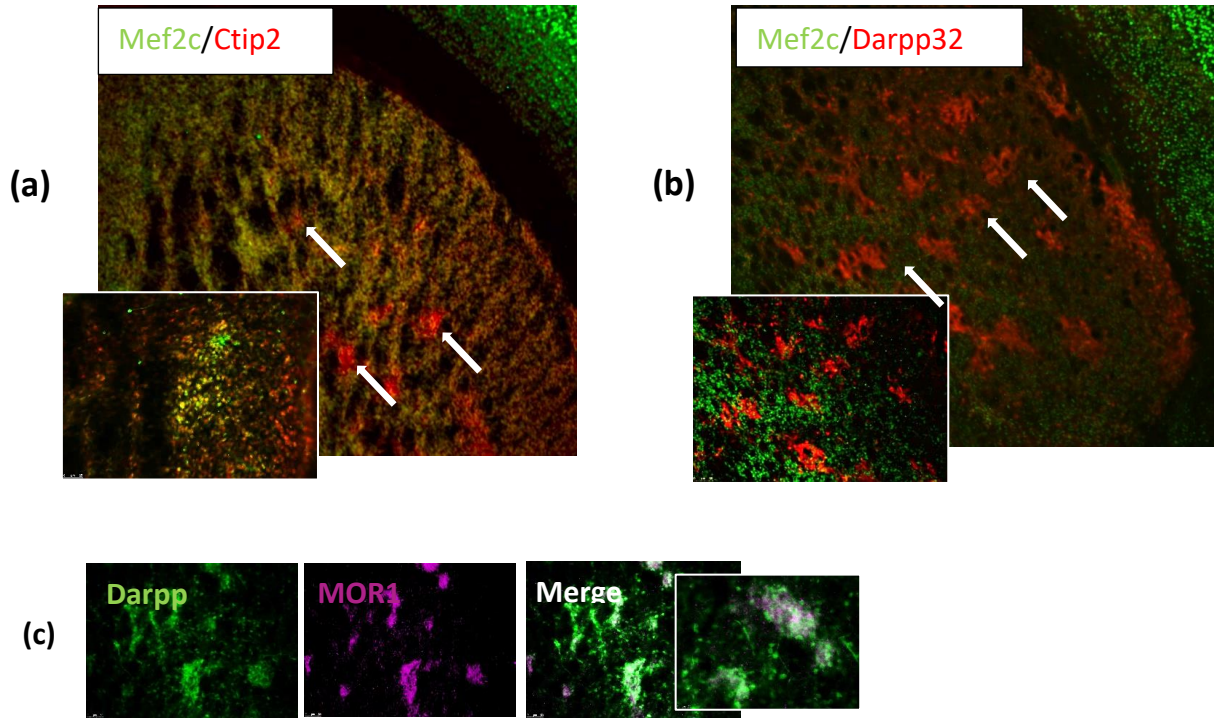

Figure 3.6 Mef2c colocalises with Ctip2 but not Darpp32 at postnatal day 0.

Fluorescent immunostaining comparing Mef2c expression relative to the MSN markers, Ctip2**(a)** and, Darpp32**(b)** in P0 mouse striatum. All Mef2c-positive cells are Ctip2-positive, except for regions indicated by white arrows in (a). In contrast, there is minimal co-localisation between Mef2c and Darpp32. White arrows in **b** indicate the ''patchy like'' Darpp32 positive regions. **(c)**: Double immunofluorescence of Darpp32 and MOR1 at P0 shows complete co-localisation, indicating all Darpp32 positive regions at P0 are striosomes. All low magnification images were taken at 100x magnification while high magnification in **a**, **b,** and **c** were taken at 400x magnification.

3.4.3 Mef2c is expressed only in neurons in WT cultured E16 LGE.

In the previous section Mef2c was shown to fully colocalise with Ctip2, suggesting that it is found exclusively in neuronal progenitors and differentiated neurons at this developmental stage. Previous studies have shown Mef2c to be expressed in microglial cells of the mouse cortex which are a non-neuronal modified form of macrophages that act as immune cells in the CNS (Deczkowska et al., 2017a). In this experiment, E16 LGE cells were cultured for 24hours or 7 days to assess Mef2c expression over these time points. Double immunocytochemistry of Mef2c (purple) with the neuronal marker MAP2 (green) was done at 24hrs and 6DIV, **Figure 3.7** (first and second panels). *In vitro* analysis of Mef2c expression showed that it was only expressed in neurons with all *Mef2c* positive cells expressing MAP2 (a neuronal marker) but not in GFAP positive cells, indicating that Mef2c is only expressed in neurons in E16 cultured LGE.

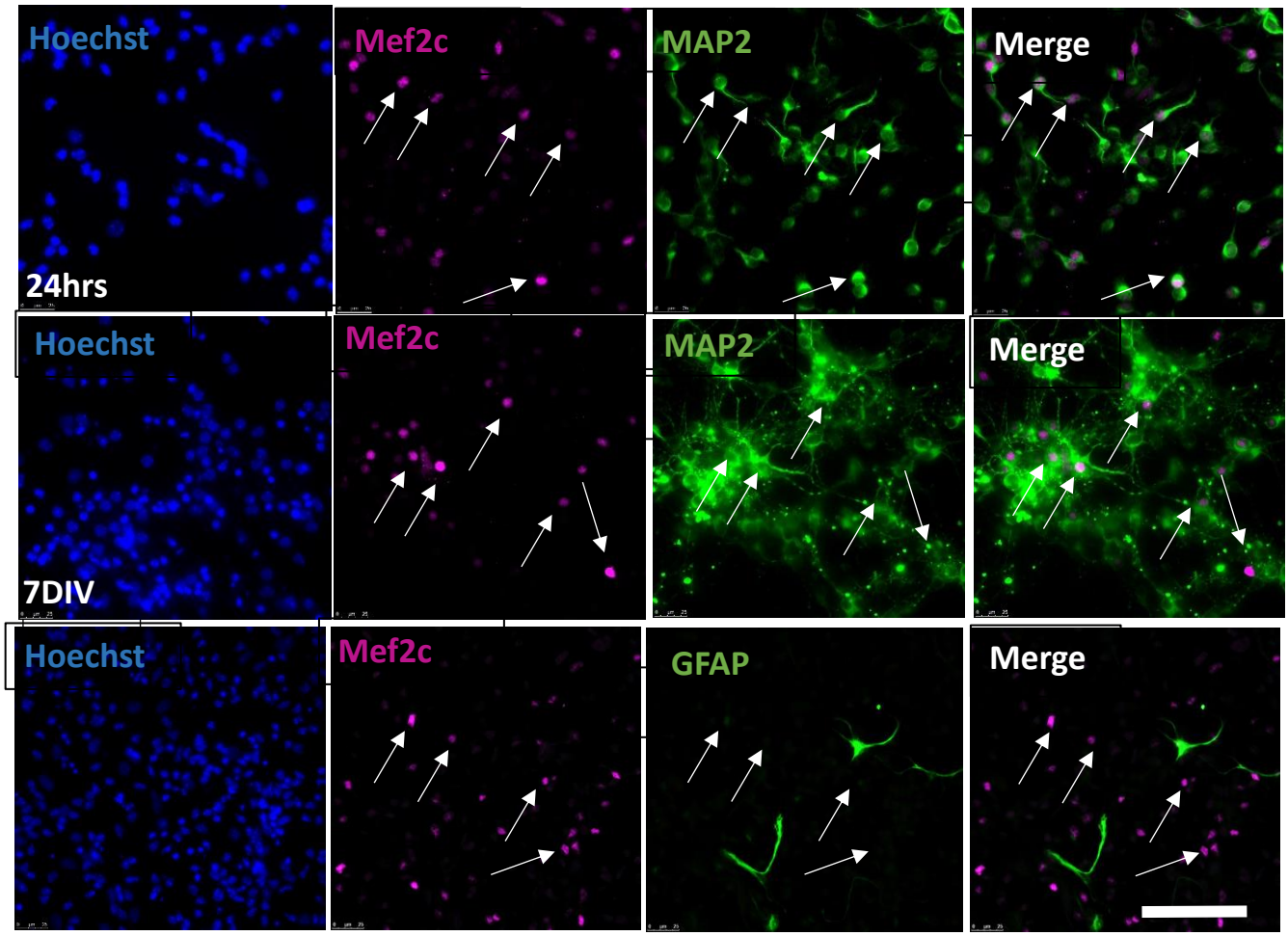

Figure 3.7 All Mef2c-positive cells are MAP2 positive.

Double immunocytochemistry of Mef2c (purple) and the neuronal marker *MAP2* and non-neuronal marker GFAP (green) reveals complete co-expression between Mef2c and the mature neuronal marker MAP2 at both 24hrs and 7DIV, but no co-expression with GFAP. Scale bar is 100µm.

3.4.4 Validation of *Gsx2-Cre* line used in this project

The focus of this thesis is on the role of Mef2c TF in the development of MSNs in the mouse striatum. An essential tool was the Gsx2-Cre used to induce recombination of the *Mef2c^{loxP}* alleles to make the striatal *Mef2c CKO*. Therefore, it was important to show that *Gsx2-Cre* is expressed specifically in MSNs and hence that recombination is likely to occur in these cells.

I first needed to confirm that in the *Gsx2*-Cre line used, Gsx2-Cre is indeed expressed in the striatum. *Gsx2-Cre $^{(+)}$* mice were crossed with tdTomato reporter mice **(Figure 3.8a)**. Mice positive for *Gsx2-Cre* and tdTomato showed a robust red autofluorescence signal in the striatum (**Figure 3.8b)**. In contrast, expression in the cortex was undetectable except for uncertain very weak expression at the most outer cortical layer as illustrated with the white arrow in **(Figure 3.8b).** A strong tdTomato protein signal was seen homogeneously expressed along the rostro-caudal and medio-lateral axes of both dorsal (DS) and ventral (VS) aspects of adult mouse striatum as shown in the coronal brain sections imaged at different distances from Bregma in **(Figure 3.8c)**.

Reporter expression was also observed in the olfactory bulb and cerebellum, which is expected since the LGE is a source of the inhibitory interneurons populating these brain regions (Qin et al., 2016). Expression was also observed in the septum (**Figure 3.8 d),** which was not reported in the Gsx2- Cre mouse model used by (Qin et al., 2016). Septal neurons contribute to the interneurons of the olfactory bulb with a proposed role of Gsx2 in this process (Qin et al., 2017).

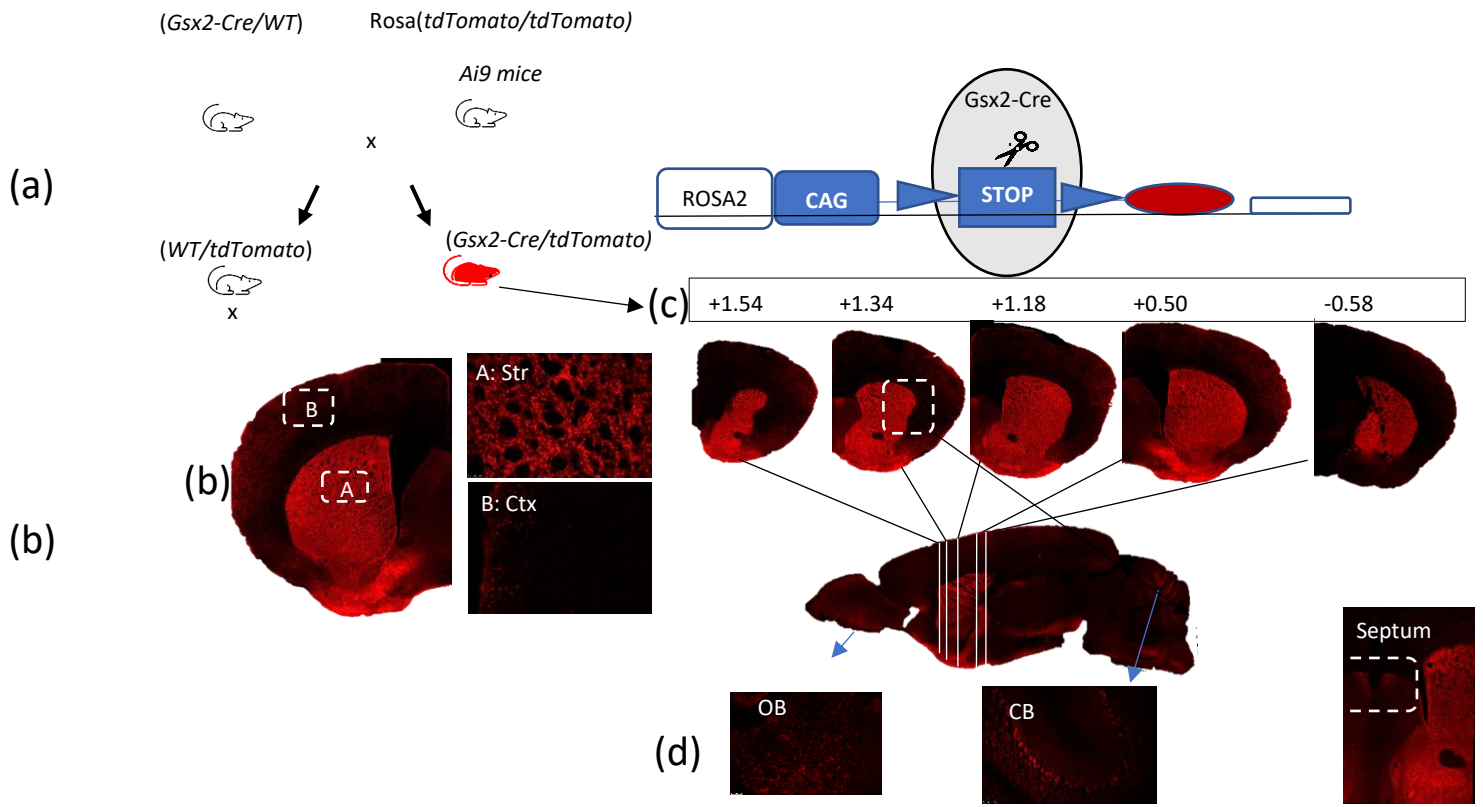

Figure 3.8 Gsx2- Cre is expressed in the adult mouse striatum.

(a): Schematic representation of the breeding strategy used to generate Gsx2-Cre tdTomato mice by crossing Gsx2-Cre positive and Rosa tdTomato positive mice. **(b):** Coronal brain section showing auto-fluorescence of tdTomato reporter expression in the striatum but no expression in the cortex except for minimal uncertain expression at the outer layers; dotted areas A and B are shown in higher magnification (200x). **(c):** Series of coronal sections along the rostral-caudal axis, showing strong expression in the striatum at different distances from bregma; images were taken at magnification 50x**. (d)** Cre expression was also observed in the olfactory bulb (OB), cerebellum (CB) and septum (within dotted area).

3.4.4.1 *Gsx2-Cre* is co-expressed in medium spiny neurons with FoxP1 *and* Mef2c

It was shown in the previous section that Gsx2-cre was expressed across the striatum. In this section I explored whether Gsx2-Cre is expressed specifically in the MSNs of adult striatum by double immunofluorescence with FoxP1 which is expressed only in striatal MSNs and not in interneurons. TdTomato protein is expressed in *Cre-expressing* cells constitutively through cre transgene and its fluorescence can be visualised under the microscope, facilitating double immunofluorescence with other specific cell markers.

Quantification of 500 FoxP1 positive cells in two striatal sections of each mouse brain (n=5) showed that approximately 97% of FoxP1 positive cells were tdTomato positive (**Figure 3.9 a)**.

To see if Gsx2-Cre is co-expressed with Mef2c, double immunofluorescence of Mef2c and *tdTomato* was performed in early postnatal mouse striatum (P3 in this case) as I showed earlier in this chapter that *Mef2c* is highly expressed at this time. All Mef2c positive cells were also tdTomato positive in the P3 mouse brain**, (Figure 3.9b)**. However, not all tdTomato positive cells were also positive for Mef2c (tdTomato only regions indicated by white dashed lines in Figure 3.8 b). Given the finding illustrated above in figure 3.5d, that Mef2c did not co-localise with Darpp32^{+}/MOR^{+} areas, it seems likely that these *tdTomato*$^{+}$*/Mef2c*$^{-}$ regions are striosomes.

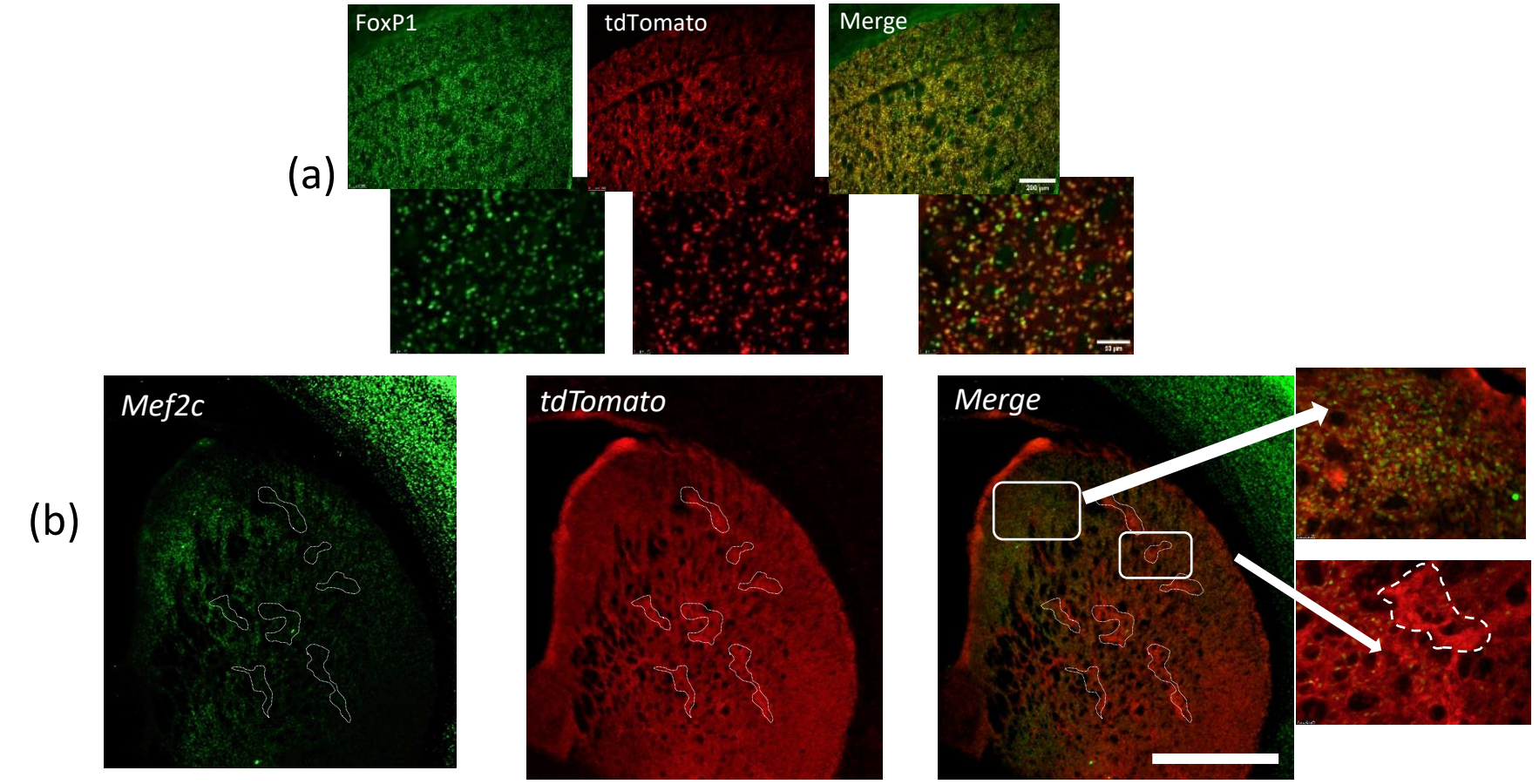

Figure (3.9): (a): 97% of tdTomato positive cells are also FoxP1 positive; double immunofluorescence of tdTomato with FoxP1 shows almost complete co-localisation of FoxP1 positive MSNs (green) with tdTomato positive cells (red). **(b):** All Mef2c positive cells in P3 mouse striatum are tdTomato positive, but there are *tdTomato*$^{+}$ regions that do not express Mef2c (white-dotted regions). The scale bars in a are 200 µm (upper) and 50 µm (lower) and scale bar in b is 1000µm in low magnified images and 100µm in high magnified images in white boxes.

3.4.4.2 Mef2c is expressed in striatal parvalbumin positive interneurons but Gsx2- Cre is not.

I have shown in the previous section that Mef2c is expressed in the neurons of the developing striatum and appears to exclusively co-label with Ctip2 and FoxP1, which are well recognised MSN markers. However, it is known that Ctip2 and FoxP1 are also expressed in neuronal progenitors in the developing brain (Precious et al., 2016; Arlotta et al., 2008a) and it is therefore theoretically possible that some of these cells may go on to generate interneurons. Only about 5% of adult mouse striatal neurons are interneurons, and these sparsely distributed cells are extremely important in modulating motor functions of MSNs (Lee et al., 2017). The most important classes of striatal interneurons are the GABAergic inhibitory parvalbumin (PV)-positive interneurons and the cholinergic (CH) interneurons (Gritton et al., 2019). PV positive interneurons are concentrated at the DL aspects of mouse striatum (Luk and Sadikot, 2001), while CH positive interneurons are a major source of acetylcholine (Graveland and Difiglia, 1985; Kawaguchi et al., 1995). Less common populations are calretinin and serotonin positive interneurons.

Mef2c has been shown to be expressed in PV positive interneurons in the cortex, which originate almost entirely from the MGE (Anderson and Wonders, 2006), and also in hippocampal somatostatin (SST)- and PV-positive interneurons (Pai et al., 2020). In the striatum, most PV^+ interneurons express Nkx2.1 and originate from the MGE and preoptic area (POa) (Marin et al., 2000). Therefore, it was important to assess whether Mef2c is expressed in striatal PV interneurons and if so, whether these cells also expressed the Gsx2- Cre and thus whether PV interneurons are at risk of being affected in the Gsx2-Cre induced CKO.

Triple immunofluorescence of adult mouse striatal sections was performed with Mef2c (green), PV (purple) and tdTomato (red) **(Figure 3.10 a).** High power images showed that Mef2c was expressed in both striatal and cortical PV interneurons, but no PV^+/$tdTomato^+$ neurons were seen. Thus, it is highly unlikely that these cells would be affected by the CKO. A total of 570 PV+ cells were counted in three striatal coronal sections of 3-month-old mice with a total of three mouse brains, and all were negative for tdTomato (Figure **3.10 b).**

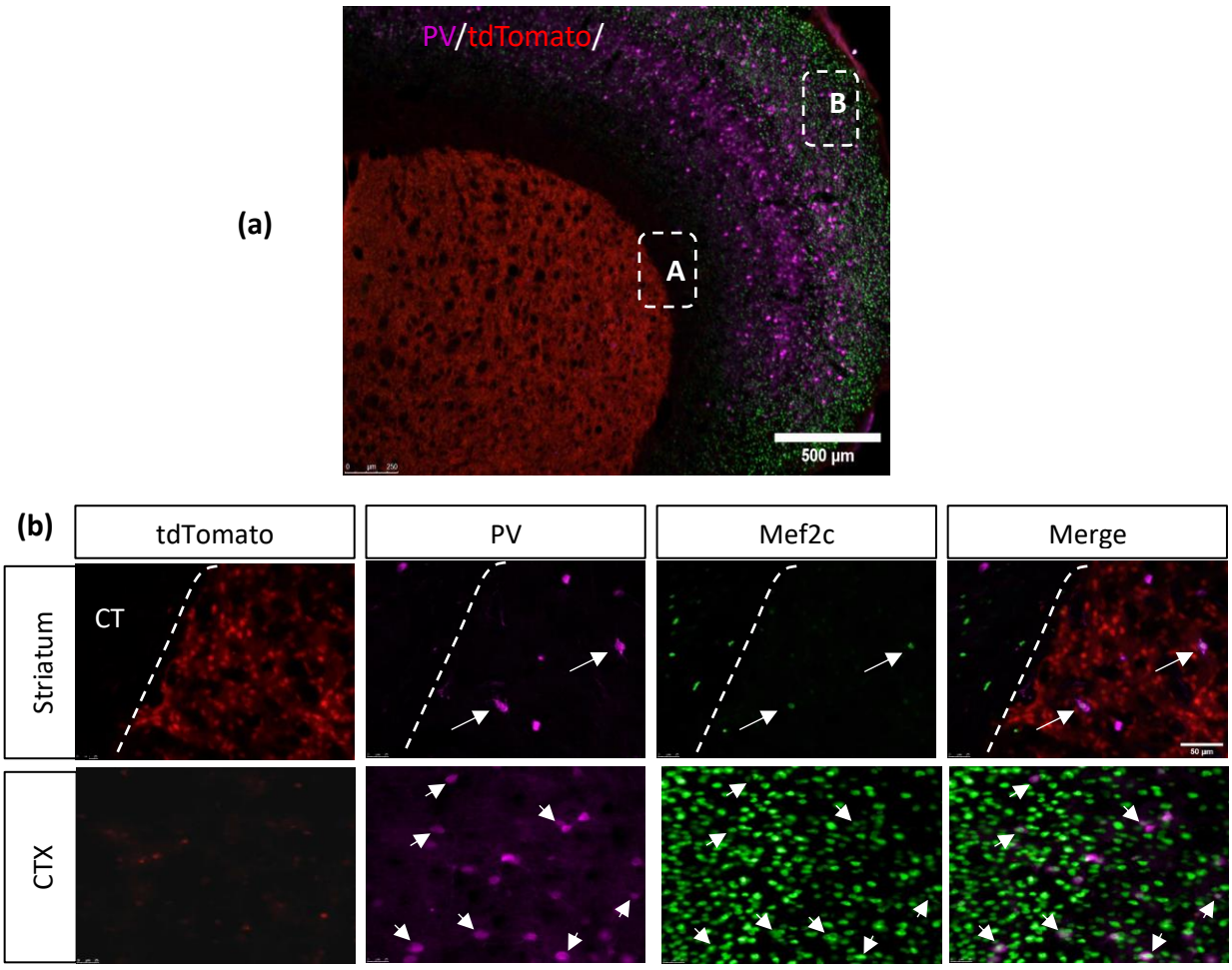

Figure 3.10 **Mef2c is expressed in striatal PV-positive interneurons, but Gsx2-Cre is not.**

(a): Triple immunofluorescence of tdTomato (red), the interneuronal marker Parvalbumin (purple) and Mef2c (green) in an adult mouse coronal brain section. The white dashed area **A** of the striatum is magnified in the upper panel in **b**, and the white dashed area **B** of the cortex is magnified in the lower panel in **b**. **(b)** Upper panel shows that Mef2c is expressed in PV-positive interneurons (white arrows)**,** but there is no co-expression of *tdTomato* and PV in the striatum. In the cortex (lower panel), all Mef2c-positive cells are PV+ (white arrows). Scale bars are 500 and 50 µm in **a** and **b**, respectively.

3.4.4.3 *Gsx2*- Cre is not expressed in acetylcholinesterase positive striatal interneurons.

To further characterise the expression of Gsx2-Cre in mouse striatal interneurons, immunofluorescence of the IN-marker CHAT was performed with tdTomato in adult mouse striatum **(Figure 3.11).** There was no colocalization of tdTomato with CHAT+ interneurons, which means that the Gsx2-Cre used in this thesis is only expressed in MSN progenitors.

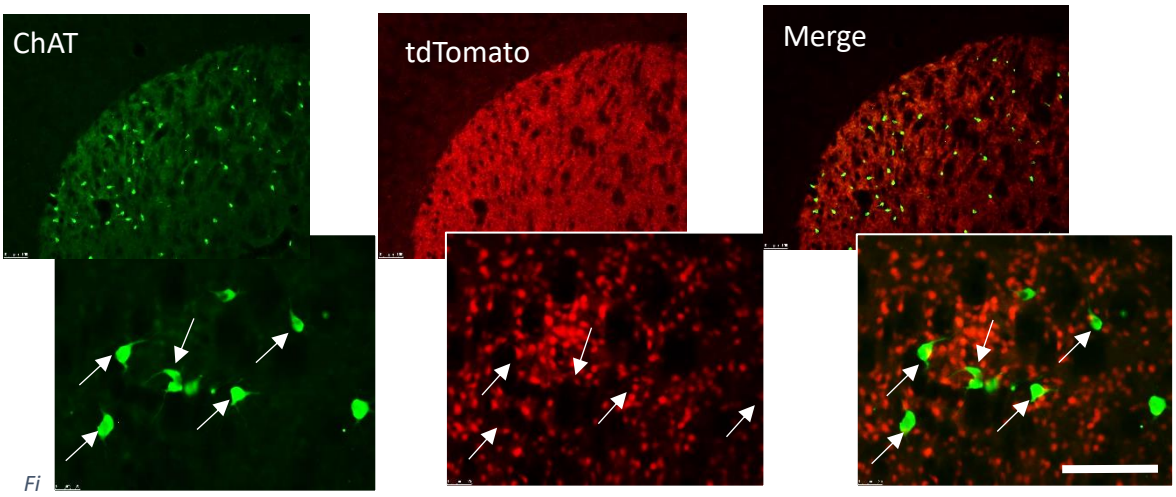

Figure 3.11: *Gsx2-Cre* is not expressed in acetylcholinesterase positive striatal interneurons. Double immunofluorescence of ChAT (green) with tdTomato (red) in adult mouse striatum. (White arrows in high magnification images show no colocalization between ChAT+ interneurons with Gsx2-Cre/tdTomato. Scale bar is 200µm.

3.4.4.4 Gsx2-Cre is not expressed in Mef2c positive cells in the cortex, nor in the septum.

Mef2c *TF* is expressed in different areas in the developing and adult mouse brain (Assali et al., 2019). Since Mef2c is abunduntly expressed in the cortex, it was important to make sure that Gsx2- Cre is not expressed in these cells, even though I have shown in the previous section that tdTomato expression in the cortex is almost undetectable. Furthermore, Mef2c was also shown to be expressed in the septum, and I have shown before that the tdTomato is expressed in the septum (Figure 3.7, d), making it necessary to see if Mef2c is co-expressed with Gsx2 in the septum. To assess this, a double immunofluorescence of Mef2c and tdTomato was undetaken in adult mouse coronal sections (**Figure 3.12)**. There was no co-expression of tdTomato and Mef2c positive cells in the cortex (**a**) nor in the septum (**b**), which means that the mouse model used here is specifically altering Mef2c expression in the striatum only.

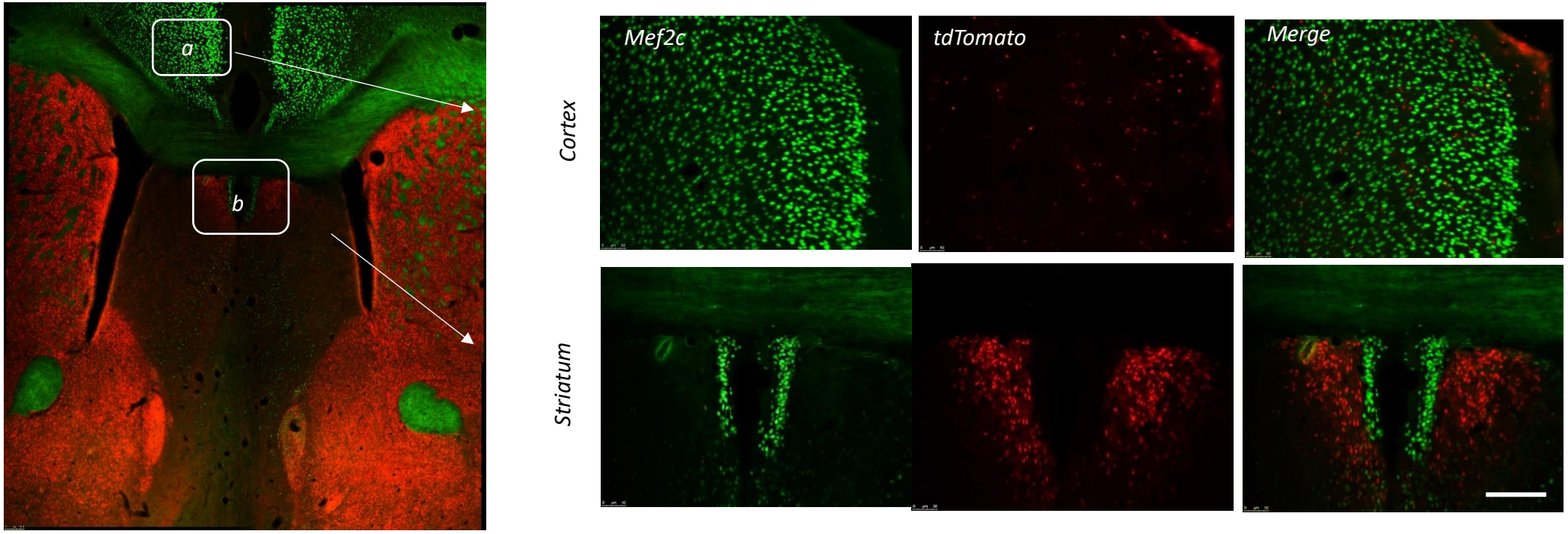

Figure 3.12: No colocalization between Gsx2-Cre reporter and Mef2c was observed in the cortex or the septum. Double IF of Mef2c and tdTomato in the adult mouse brain showing no co-labelling of Mef2c (green) and tdTomato (red) positive cells in the cortex (white outlined region a, magnified in the upper panel) nor in the septum (white outlined region b, magnified in the lower panel). Scale bar is 200µm.

3.4.5 Confirmation of *Mef2c* CKO

3.4.5.1 Reduced *Mef2c* mRNA and protein expression in *CKO*

Following initial characterisation of *Mef2c* expression in WT striatum, the next step was to demonstrate that *Mef2c* expression was lost in the *CKO* striatum. To confirm this, WT and CKO tissue was collected from breeding *Gsx2-Cre*$^{+}$ *Mef2c fl/fl* females with *Gsx2-Cre* $^{(wt)}$ *Mef2c fl/fl* males as described in chapter 2. Striatal tissue was collected at four ages (P0, P3, P7 and P14) for RT qPCR and histological analysis. IHC of P3 mouse coronal sections showed clear reduction in *Mef2c* immunoreactivity in the striatum with no difference in the cortex **(Figure 3.13, a)**.

To further confirm the loss of *Mef2c*, stereological quantification and optical density analysis were performed to assess protein expression at dorsomedial and dorsolateral aspects individually, in P3, P7, and P14 striatum **(Figure 3.13b-e).** Stereological analysis showed a significant reduction in the number of cells expressing *Mef2c* in the DM in the CKO at P3, P7 and P14 (**Figure 3.13b and c**). A percentage reduction of about 61%, 58% and 57% was observed in P2, P7 and P14 respectively, (p=0.03, p=0.001 and p<0.0001, respectively). A significant reduction was also observed at DL aspects, about 86%, 79% and 78%, (p =0.003, p<0.0001 and p<0.0001) in P3, P7 and P14, respectively.

Optical density analysis also demonstrated a significant reduction of Mef2c immunoreactivity in CKO striatum (**Figure 3.13 d and e**). In the DM, a percentage reduction of 72%, 70% and 76%, was observed at P3 (p=0.0035), P7 (p=0.0018) and P14 (p=0.0001), respectively; and in the DL, a percentage reduction by 60%, 62% and 68% was reported at P2, P7 and P14, however, the only significant reduction was observed at P7 (p=0.04).

A summary of means, SEM, p values and n per group is shown in the **Table 3.1** below.

			Mean WT	Mean CKO	N WT	N CKO	P-value
Optical density	DM	P3	0.085	0.02522	7	6	0.0035**
		P7	0.053	0.01589	8	6	0.0019**
		P14	0.02646	0.006357	6	7	0.0001***
	DL	P3	0.03903	0.02217	6	6	0.1018
		P7	0.02707	0.01284	7	8	0.0444*
		P14	0.01689	0.006048	6	7	0.1018
Stereology (cell counts)	DM	P3	107493	41800	6	3	0.0389*
		P7	94955	39547	5	7	0.0011**
		P14	68790	29439	7	7	0.0006***
	DL	P3	57738	8173	6	3	0.0036**
		P7	56080	11646	5	7	0.0003***
		P14	34429	7238	7	7	0.000006****

Table 3.1: A summary of optical density and stereological quantification analysis of *Mef2c* protein performed to confirm CKO of *Mef2c* in each of the DM and DL aspects of the mouse striatum.

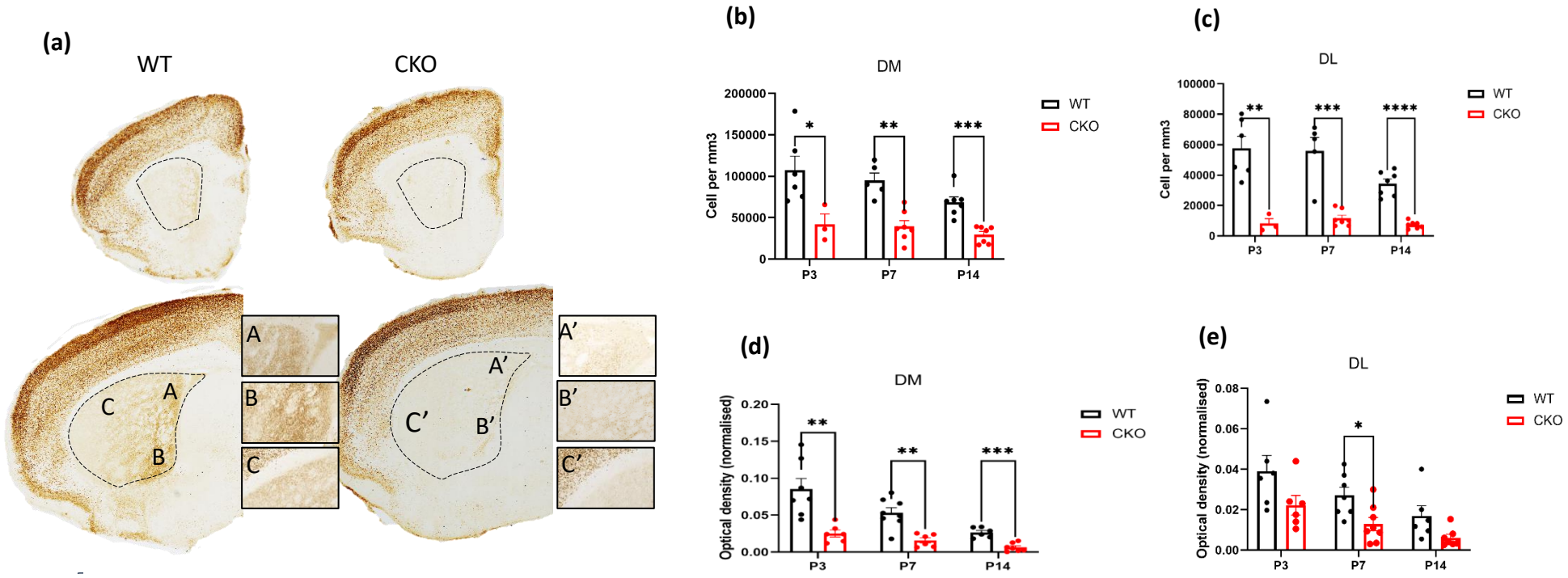

Figure (3.13): Mef2c expression is significantly reduced in the striatum in the CKO. (a): Mef2c IHC of coronal brain sections of mouse striatum at P3 of WT and CKO. Higher magnification of WT (A, B & C, left) and CKO (A', B'& C', right) show a reduction in Mef2c immunoreactivity in the CKO. Stereological quantification in WT and CKO shows a significant reduction in Mef2c positive cells in CKO P3, P7 and P14 in both DM **(b)** and DL **(c)** striatum. Optical density assessment of Mef2c immunoreactivity was quantified in DM **(d)** and DL **(e)** striatum individually. Bright field coronal sections were imaged at 100x magnification, and the higher magnification in A-C, A'-C' were at 200x. Bars represent means ± SEM. * = p< 0.05, ** = p <0.01, *** = p< 0.001, **** = p<0.0001 in multiple t-tests using Holm-Sidak correction. N per group for optical density and stereology is at least 6 per group.

Furthermore, there is a significant reduction in *Mef2c* mRNA and protein expression in *CKO* mice in P0, P3 and P14 striatum **(Figure 3.14)**. *Mef2c* mRNA levels at P0, P3 and P14 are significantly lower in *CKO* mice, by 89% (p=0.00001), 64% (p=0.000071) and 81% (p=0.000027), respectively (using multiple unpaired t tests using Holm-Sidak correction).

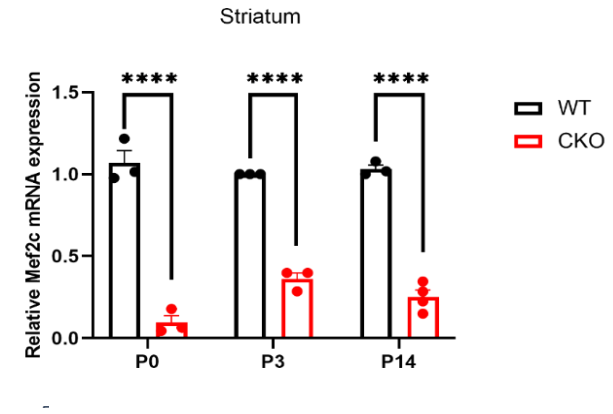

Figure 3.14: Mef2c mRNA expression is significantly reduced in the CKO striatum at P0, P3 and P14. Relative to the expression of two housekeeping genes GAPDH and βactin, **** = p <0.0001. n=3 per group.

Immunofluorescence of *Mef2c* in the DL striatum of WT and CKO at P7 showed a significant reduction of *Mef2c* fluorescence intensity in *CKO* (lower panel). It is worth noting that CKO showed reduced numbers of Hoechst positive cells, which will be explored further in chapter 4 to see if this is incidental or if Mef2c loss is associated with cellular loss (**Figure 3.15)**.

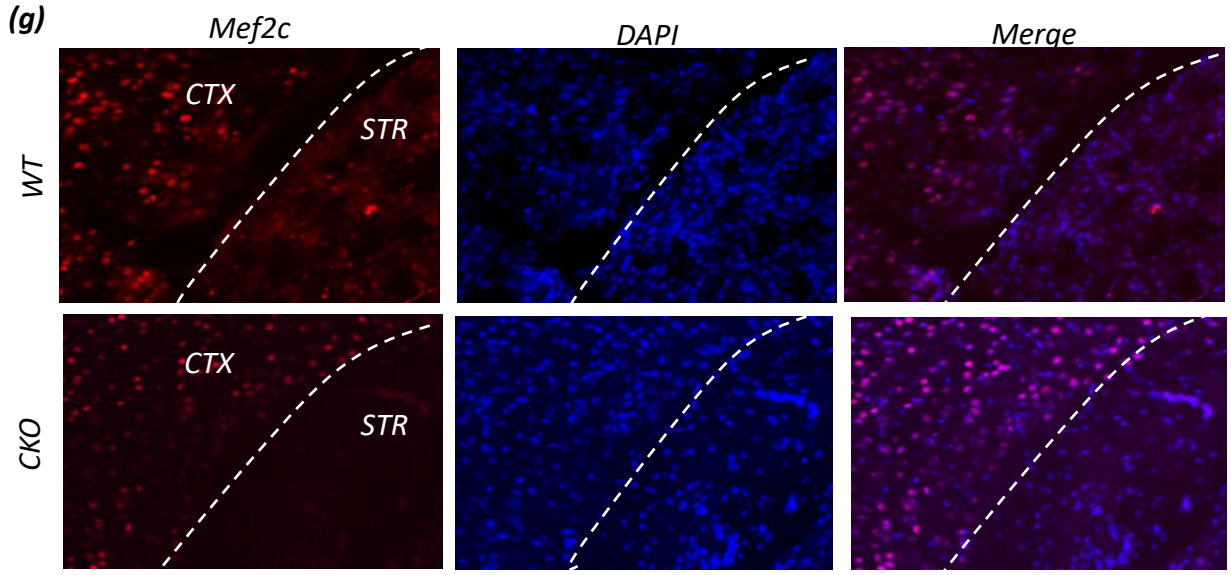

Figure 3.15 Mef2c expression (red) in WT (upper) and CKO (lower) mouse striatum at P7, showing absence of Mef2c signal in CKO mice, and fewer cells in the DL aspect of the CKO striatum as seen by fewer DAPI-positive cells (blue).

3.4.5.2 Mef2c expression is not reduced in the cortex of *CKO* mouse

Mef2c is abundantly expressed in the developing cortical plate and adult mouse cortex, specifically in the frontal cortex, entorhinal cortex, dentate gyrus, and amygdala (Leifer et al., 1994; Lyons et al., 1995). Mef2c loss in cortical excitatory neurons using different mouse models resulted in significant morphological and behavioural alterations in KO mice (Rajkovich et al., 2017). Therefore, I aim in this section to see if there is any effect on Mef2c expression levels in the cortex of the Gsx2-Cre CKO mouse. No effect would indicate that any cellular and behavioural phenotype in this project does indeed result from loss of Mef2c in the mouse striatum.

IHC and qPCR followed by optical density and fold-change analysis were used to quantify Mef2c protein and mRNA in WT and CKO mouse cortex (**Figure 3.16**). *Mef2c* expression in cortical neurons appeared unaffected in the CKO model used here. *Mef2c* mRNA expression in cortical tissue at P3, P7 and P14 was not significantly reduced in CKO mice compared to WT mice (**Figure 3.16 b**; P3 p= 0.814; P7 p=0.870; P14 p =0.912; multiple unpaired t-test with Holm-Sidak correction). Likewise, protein expression did not significantly change in the cortex of CKO mice compared to WT mice (**Figure 3.16 c**; P3 p =0.9898, P7 p=0.83011, and P14 p=0.8106, multiple unpaired t-tests with Holm-Sidak).

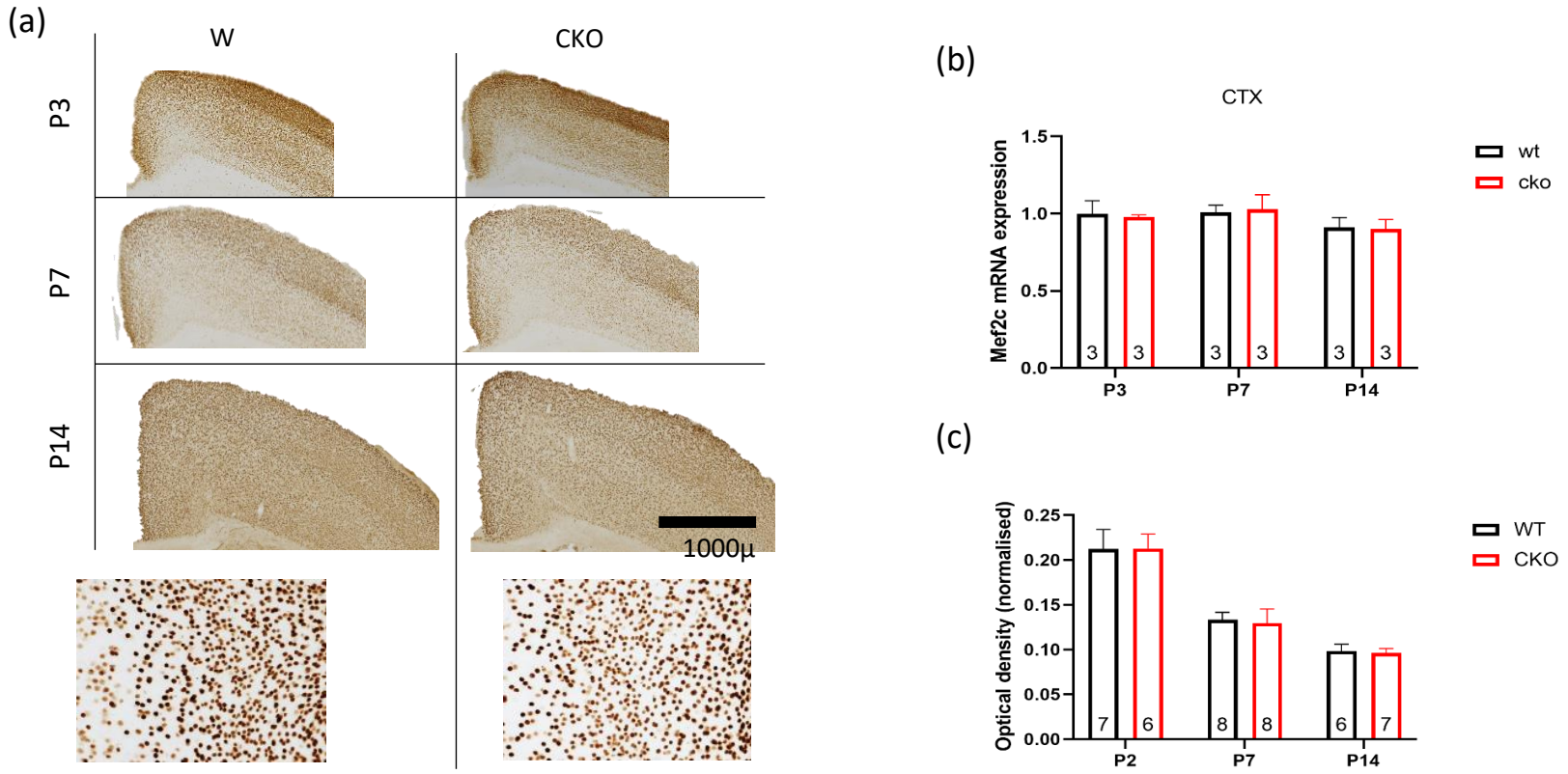

Fig 3.16: No effect on cortical Mef2c RNA and protein levels in the CKO mouse brain. **(a)** Mef2c IHC of WT and CKO cortex at P3, P7, and P14 showed no obvious difference in Mef2c expression. **(b)** qPCR of dissected cortex shows no difference in *Mef2c* mRNA expression between WT and CKO. **(c)** Optical density analysis of Mef2c protein in WT and CKO also shows no significant difference between the two genotypes. Coronal brain sections are imaged at 100x magnification. Bar graphs show Means ± S.E.M. Scale bar is 1000µm. n per group is the number in each bar.

3.5 Discussion

Mef2 TFs are expressed widely and differentially in the mouse brain during development and adulthood. Mef2c is the first Mef2 subclass to be expressed in the cortex and its levels remain high through development (Lyons et al., 1995). Little is known about the expression of Mef2c in the mouse striatum and MSNs. This gap is addressed in this chapter, which provides data on the spatiotemporal pattern of Mef2c expression in the embryonic, postnatal and adult striatum. Mef2c expression relative to the well-known MSN markers, Darpp32, and Ctip2 was also analysed. Furthermore, I have shown that the *Gsx2-Cre* mouse line is ideal to study genetic alterations in mouse striatum. In particular, it drives recombination throughout the striatum, but not the cortex.

The pattern of Mef2c expression in the embryonic and postnatal mouse striatum was characterised using IHC, immunofluorescence and RT qPCR techniques. In embryonic LGE, *Mef2c RNA* was expressed at extremely low levels at E12 and was almost undetectable by IHC in brain sections. At E14, it was quantitatively detectable. This is consistent with the peak of matrix MSN neurogenesis that was shown using BrdU birth-dating experiments during embryonic development in (Gerfen, 1992; Mason et al., 2005). In E14 brain sections stained with Mef2c, expression was limited to the lateral aspects of the mantle zone, but not the germinal or SVZ , suggesting that Mef2c could be expressed in postmitotic neurons, as there are many of them, rather than the proliferating NPCs. By E16, *Mef2c* RNA expression had more than tripled compared to E14 and cells expressing Mef2c had become distributed more medially and ventrally within the mantle zone. Peak expression occured around birth and then a gradual reduction occurred through to adulthood. The spatial pattern of Mef2c expression suggests the involvement of Mef2c in the maturation and differentiation of precursor MSNs toward mature MSNs. Progenitors in the LGE produce striatal postmititic neurons that migrate radially and tangentially to the mantle zone that will develop later into the striatum. Although IHC of Mef2c with the markers of NPCs in mouse LGE like, Dlx1/2, Gsx2, and Meis2 was not done, the co-expression of Mef2c with Ctip2 at P0 could suggest that Mef2c is also expressed in immature MSNs.

A graded pattern of expression was observed along the medio-lateral striatum, being high in medial aspects and low in lateral aspects, and along the rostro-caudal axis,

increasing toward the caudal aspects. This observation was first apparent at P0, but not at E18. Mef2c was preferentially expressed in the medial and ventral parts of the dorsal striatum. Furthermore, the expression of Mef2c decreased postnatally, especially in the dorsolateral and ventrolateral parts of the P14 and adult striatum. The expression of *Mef2c* mRNA correlated with protein expression between E12 and adulthood. It is worth mentioning here that this is, to the best of my knowledge, the first research work that describes Mef2c expression in the striatum during embryonic development. The DM-DL gradient expression of Mef2c in the dorsal striatum could have important implications in in the behavioural functions. Both regions receive input from motor and sensory cortex, however, DMS receives more cortical input from associative frontal cortical areas, such as orbitofrontal cortex (Hunnicutt et al., 2016; Hintiryan et al., 2016). Directed-lesion studies in DMS caused impairments in goal-directed behaviour while habitual behaviour was maintained (Yin et al., 2005), illustrating the different functional roles of these striatal regions. However, it was shown that both the goal-directed and habitual formation functions were developed in parallel and are both required to control motor functions (Kupferschmidt et al., 2017; Robbins and Costa, 2017).

The spatio-temporal pattern of Mef2c expression can be discussed in the context of different biological events that take place in the mouse striatum during embryonic and postnatal development. Among these, striatal MSN neurogenesis is one of the most important. The neurogenesis of the two striatal compartments occurs over two waves: striosome MSN neurogenesis peaks at E12, and matrix MSN neurogenesis, which peaks at E14. The maturation period of MSNs extends into the first week of postnatal development (Matsushima and Graybiel, 2020).Immunofluorescence staining of Mef2c with two well-known markers of MSNs (Ctip2 and Darpp32) was performed in this chapter to qualitatively assess and compare their expression in the mouse striatum. Mef2c was clearly shown to be expressed in MSNs by showing complete co-localization with Ctip2. However, in P0 mouse striatum, there was minimal co-expression of Mef2c and Darpp32 which means that Mef2c might only expressed in precursors MSNs.

I have also shown that, at the developmental age P0, all Darpp32 positive cells were positive for the striatal striosomes marker MOR1. Darpp32 expression in early postnatal

striatum is limited to the striosomes because MSNs occupying this compartment mature first and so express the mature MSN marker Darpp32 earlier than other MSNs (Passante et al., 2008; Chen et al., 2016). The fact that Mef2c was not expressed in these Darpp32 postive patches in the neonatal mouse striatum raised the question as to whether Mef2c plays a role in one striatal compartment, the matrix, but not the other, striosomes. To further investigate this, suitable markers of striosomes and matrix must be used to assess Mef2c expression in these two compartments, and this has to be performed as early as possible in postnatal striatum while Mef2c levels are still relatively high. MOR1 is considered as the canonical marker of striosomes, and calbindin-D28K is abundantly expressed in striatal matrix neurons. However, in early postnatal striatum calbindin is also expressed in striosomes, and it is not until adulthood that this marker can be used as a specific matrix marker (Liu and Graybiel, 1992a). Here, this was not possible as Mef2c is expressed only at a very low level, if at all, in adult striatum as shown in this chapter. Other evidence that showed Mef2c is not expressed in all MSNs, is from Mef2c/Gsx2-reporter double labeling which showed tdTomato^{+}/Mef2c^{-} regions within the striatum, which is a novel finding that was not reported before in the literature that further indicates that Mef2c is only expressed in a subpopulation of MSNs, and this could be matrix MSNs.

Postnatally, Mef2c expression peaked at P0 and then started to decrease gradually, until it was almost undetectable in the P14 DL striatum, with weak persistent expression in the DM striatum. The early postnatal period is critical for functional development and maturation of striatal connections with the cortex and thalamus. For example, motor learning and habit formation and mouse corticostriatal circuitry undergoes extensive maturation during this period. This includes the dendritic arborisation of specific neuronal subtypes like PV positive interneurons, which are fully mature by the end of P10 (McGuirt et al., 2021). Mef2c is expressed in DM striatal regions during this period which indicates that a region-specific effect of Mef2c might be taking place.

The cell culture approach provides an excellent tool to monitor the expression of TFs in cells at different developmental stages. Using this system I was able to culture WT E14 mouse LGE to look at the expression of Mef2c compared to the expression of the mature neuronal marker MAP2. The analysis showed that all Mef2c expressing cells

were also MAP2 positive following 24hrs and 7DIV indicating that in cluture, Mef2c is expressed exclusively in neurons. This was confirmed with the absence of Mef2c expression in GFAP positive cells. These findings were in line with the expression of Mef2c in brain sections with Ctip2 which is only expressed in neurons in striatum. Unfortunately, I couldn't comapre these finding with published work due to the lack of current literature on striatal Mef2c expression in vitro.

The specificity of *Gsx2-Cre* induced recombination was confirmed with Mef2c loss in the CKO model shown to be specific to the striatum, without affecting its expression in the cortex. This makes the *Gsx2-Cre* ideal to study Mef2c function in the striatum. This is important as CKO of cortical Mef2c results in a significant structural and functional outcome (Adachi et al., 2016; Rajkovich et al., 2017; Bjorness et al., 2020). In addition, although Mef2c+/PV+ interneurons were detected in the adult mouse striatum, our *Gsx2-Cre* was not expressed in interneurons and so Gsx2-mediated recombination is very unlikely to cause alterations in Mef2c in the PV+ interneurons in the mouse striatum. This makes Mef2c expression in PV- positive interneurons less significant for phenotypic interpretation in this project. *Mef2c* was shown before in a microarray analysis at E18.5 to be enriched in MGE-derived, but not in CGE-derived, cortical interneurons (Miyoshi et al., 2015). This further explains why Gsx-2 cre is not expressed in $Mef2c^{+}/PV^{+}$ as these are derived from the MGE.

In the literature, only one paper has reported on Mef2c expression in the WT mouse striatum (Chen et al., 2016). My data are consistent with some aspects of this paper, but not all. Although analysis in Chen et al (2016) was limited to three postnatal age groups, P0, P4 and P14, and the total number of mice per group was low (only 3), we are in agreement that Mef2c is poorly expressed in striosomes, by showing that it is not expressed in Darpp32-positive striosomes at postnatal day 0. Work presented in this chapter that is also consisent with Chen et al is the number of Mef2c expressing cells decreased from P0 to P14. However, Chen et al showed that Mef2c intensity, based on fluorescence intensity of a polyclonal antibody, increased in matrix MSNs from P0 to P14, while in this thesis I showed that mRNA and protein levels decreased with advancing age. Since no RNA analysis of Mef2c expression was performed and no

representative images were shown in the Chen et al paper, I assume that a non-specific Mef2c antibody was used as its production has been discontinued.

TFs that are essential for production and differentiation of neurons during embryonic development are either highly expressed during embryonic development and maintain high levels of expression through postnatal development, for example FoxP1 and Ctip2, or they are highly expressed during neuronal formation and maturation and then decrease significantly through adulthood. Examples of the latter are Helios TF, which was found to play an important role in the proliferation of matrix MSNs (Martín-Ibáñez et al., 2017), and Ikaros, which is abunduntly expressed during embryonic striatal neurogenesis and decreases postnatally (Martín-Ibáñez et al., 2010). Mef2c can be listed in the second group, as its expression decreases after the production and maturation period of MSNs ends.

Genetic manipulation in mice is one of the most powerful tools to study gene functions. Complete deletion of some genes is associated with early lethality during embryonic development. For instance, a complete null of *Mef2c* is lethal at embryonic day 9.5 (E9.5) due to failure of angiogenesis and heart development (Lin et al., 1997; Potthoff and Olson, 2007; Li et al., 2008). This issue can be avoided by the generation of site-specific CKO mouse models using the *Cre/loxP* recombinase system by crossing mice in which the gene of interest is flanked by two loxP sites to mice harboring a Cre recombinase gene. Gene deletion or inactivation will occur only in tissues where the Cre is expressed, without affecting other tissues of the mouse body. In the cortex, the effect of Mef2c expression in different cell populations of excitatory and inhibitory neurons has been studied through using different Cre lines, including *Camk2a-Cre* (Adachi et al., 2016; Bjorness et al., 2020), *nestin-Cre* (Li et al., 2008b), and *hGFAP-Cre* (Barbosa et al., 2008a). However, to the best of my knowledge, this is only the second study to use a Cre mouse model to knockout *Mef2c* expression in the striatum during embryonic development. The only other published work is a study of Foxp2 and Mef2c that showed *Foxp2* and *Mef2c* knockdown in early postnatal striatum, but used *Nestin-cre* which causes recombination in various neuronal types in the mouse brain and thus is not striatal specific (Chen et al., 2016).

There are many Cre-lines that have been used to knockout genes specifically in the adult mouse striatum, such as Drd1 and Drd2-Cre lines to knockout the expression of specific genes in striatonigral and striatopallidal MSNs in direct and indirect pathways, respectively in mouse striatum (Benthall et al., 2020; Anderson et al., 2020b). CaMKIIα-Cre was used to induce recombination of Darpp32 (Dragatsis and Zeitlin, 2000), however, this Cre is expressed late during postnatal development and not striatal specific. Gpr88-Cre Tg mice were also used to induce knockout in caudo-putamen, nucleus accumbens and olfactory tubercle neurons (Hisatsune et al., 2013). In this project, a *Gsx2-Cre* mouse line (Kessaris et al., 2006) was used to specifically delete *Mef2c* in the striatum. Gsx2 is expressed from E9 in the LGE with limited expression in the MGE (Toresson et al., 2000). This mouse line was also used to look at the heterogeneity of cells in the olfactory bulb (Young et al., 2007), and to explore the migration pattern of GABAergic neurons in (Wu et al., 2011a).

Several reporter mouse strains have been developed to identify the efficiency of Cre expression in the tissue of interest, and here we used a tdTomato reporter mouse which was crossed with *Gsx2-Cre* $^{(+/-)}$ *Mef2c* $^{(wt/wt)}$ mice to assess the expression of the red fluorescent protein. I found that, in the adult mouse, Gsx2-Cre reporter is expressed in the striatum along the rostro-caudal and medio-lateral axis, while it is absent in the cortex, except for a very minimal expression at the most outer layers of the cortex, that is probably associated with certain population of cortical interneurons originating from the dorsal half of the MGE or POa of CGE, (Qin et al., 2016).

3.6 Conclusion

This chapter characterised Mef2c expression in the mouse striatum during embryonic and postnatal development using different tools. Knowledge was successfully generated, and this is the first research work looking at Mef2c expression in mouse striatum in this detail. Mef2c was found to reach peak expression at P0, and it is only expressed in a subpopulation of MSNs. Furthermore, Mef2c might be necessary for the development of matrix MSNs rather than striosomes as it was shown to be absent in the $MOR1^{+}$/$Darpp32^{+}$ MSNs in P0 mouse striatum. The importance of the research work outlined in this chapter is not only to confirm that Mef2c does co-localise with established MSNs markers, but it also promotes Mef2c as differentially expressed in matrix MSNs and suggests a specific function of Mef2c in MSNs development. Furthermore, I show here that Mef2c is a developmentally regulated TF in the mouse striatum, being relatively highly expressed during late embryonic/early postnatal development and downregulated significantly through adulthood. This suggests important role of Mef2c in the development of MSNs.

As a result of the embryonic lethality associated with complete null of Mef2c, Gsx2- Cre recombinase was used to study the functional role of Mef2c in the mouse striatum. This mouse line was first assessed using a reporter mouse and it was shown to be specifically expressed in MSNs and in Mef2c expressing cells, making it suitable to conditionally delete Mef2c in mouse striatum. The CKO mouse model was successfully generated and further characterised in the following chapters of this thesis to understand more about the roles of Mef2c in striatal development.

Chapter 4: The morphological consequences of Mef2c loss in the mouse striatum

4.1 Summary

Mef2c mRNA analysis showed that it is expressed between E14 to P14, with peak expression at P0, in correlation with Mef2c protein expression in mouse striatum with a significant downregulation toward adulthood. Mef2c was shown to be expressed in striatal MSNs with evidence suggesting it is expressed only in matrix compartment but not in striosomes. To investigate the functional role of Mef2c in the development of striatal MSNs, Gsx2-Cre mouse line was used to specifically knockout Mef2c in the striatum and histological analysis of a developmental series was conducted between P2 to 12 months. Dendritic spine development was also investigated at DM and DL aspects of the striatum separately to see if there is a region-specific effect. And finally, immunohistochemical markers of striosomes and markers were used to assess the development of these compartments in both WT and CKO adult mouse striatum.

I showed here that the striatum of adult CKO mouse is significantly smaller than WT, this was accompanied with a significant reduction in the number of cells expressing NeuN, and three MSN markers. The percentage area of striosomes has significantly increased in CKO striatum compared with WT striatum, while the percentage area of the matrix compartment was significantly decreased. Except for the significant effect of Mef2c loss observed on the dendritic tree complexity, no significant effect of Mef2c loss was observed on density of dendritic spines.

4.2 Introduction

The pattern of *Mef2c* expression in the developing WT mouse striatum presented in chapter 3, suggests that *Mef2c* could be important in the development of MSNs, particularly matrix MSNs. Here I explore this further by knocking down *Mef2c* in the developing striatum using a *Gsx2*-driven *Cre LoxP* (Kessaris et al., 2006), which I showed in Chapter 3 to be specifically expressed in MSNs of the developing striatum. Preliminary unpublished results from the host lab found that at 3-months both striatal volume and the MSNs count in *Mef2c CKO* mice were significantly lower than WT.

Mef2c loss in cortical neurons has previously been found to result in several morphological changes. Cortical *Mef2c* loss using *Nestin Cre* was shown to cause significant reduction in brain volume and cortical thickness, and abnormal organisation of cortical layers (Li et al., 2008b).

Furthermore, in the mouse cortex, *MEF2* genes were found to be directly involved in synaptogenesis and the growth and pruning of axons and dendrites. This role was established using an *in vitro* approach in which *Mef2a* and *Mef2d* were knocked down in primary hippocampal neurons, which resulted in a significant increase in synapse number, suggesting that MEF2s are essential regulators of dendritic spine formation (Flavell et al., 2006). Subsequent studies found a similar role for *Mef2c* using different mouse models to delete or overexpress *Mef2c* during embryonic or postnatal development. A significant increase in synapse number was found when Mef2c expression was reduced in cerebral cortex (Harrington et al., 2016; Puang et al., 2020), dentate gyrus of the hippocampus (Adachi et al., 2016; Barbosa et al., 2008), and cerebellum (Kamath and Chen, 2019a). Although, a similar role is still largely unexplored in the mouse striatum, one paper studied the effect of loss of Mef2c at postnatal day 2 in the mouse striatum on dendritic spine development and found a significant increase in the density of dendritic spines without specifying any regional or compartment-specific differences (Chen et al., 2016).

Given the importance of *Mef2c* in the biological processes described earlier in several brain regions and the previous results from the host lab, the main objectives of this chapter were:

1. To assess the development of MSNs in WT and CKO striatum through a comprehensive histological analysis of developmental series between P2 and 12months using *cre loxP* recombination under the control of *Gsx2*. By specifically assessing striatal volume and the expression of the three classical MSNs markers (FoxP1, Ctip2, Darpp32) and the neuronal marker NeuN.
2. To assess the effects of Mef2c CKO on striosomes and matrix compartments in the adult mouse striatum, based on the proposed role of *Mef2c* in the development of matrix MSNs, but not striosome MSNs, from findings in chapter 3.
3. To undertake full analysis of the dendritic tree and dendritic spines of MSNs in adult WT and CKO adult mice.

4.3 Experimental design

A total of ~ 80 mice of WT and Mef2c CKO were used in the comprehensive histological characterisation conducted in this chapter. Striatal CKO used in this chapter was generated using the breeding strategy described in **2.1.2.1.** To clearly visualise the boundaries of the striatum for volumetric analysis, CV staining was performed as described in **2.3.1.** For immunohistochemical and stereological analysis of the developmental series P2, P7, P14, 3months and 12months of WT and CKO mouse brains were collected, fixed, and sectioned as described in Chapter 2 sections **2.2.1** and **2.2.2.** Free-floating IHC of NeuN, FoxP1, Ctip2, and Darpp32 was conducted as described in section **2.3.4** and unbiased stereological quantification was conducted according to section **2.3.7.2.1**. For matrix- striosomes analysis, MOR1 and CB immunoreactivity was used to visualise striosomes clearly and precisely and matrix respectively. Percentage areas of striosomes and matrix were quantified as described in **2.3.7.2.6**.

Dendrites and dendritic spines analysis Golgi-cox staining were performed to visualise neural dendrites and spines as in section **2.3.2** of methods chapter. Analysis was undertaken in Golgi-Cox-stained sections in DM and DL striatum individually to see if there is a region-specific effect of Mef2c loss in respect to the pattern of Mef2c expression. Quantification and Sholl analysis were done semi-automatically using SNT plugin in Fiji software as described in sections **2.3.7.2.3** and **2.3.7.2.4**.

Two-way ANOVAs were used to analyse the developmental series. When significant interaction exists, post hoc Bonferroni correction was applied. All data analysed are normally distributed (confirmed using Shapiro-Welk test), with equal variances (Levine's test is non-significant). Significance was determined at the level of 0.05.

4.4 Results

4.4.1 Mef2c loss has significant developmental effect on MSNs in mouse striatum

Mef2c was shown previously in this thesis to be expressed in striatal MSNs, suggesting that it could play an important role in their development. To assess this proposed role, the striatal volume, NeuN and the three classical MSN markers, FoxP1, Darpp32, and Ctip2, were assessed in WT and striatal CKO mice in a developmental series between P2 to 12 months. The reason behind choosing these time points was to perform comprehensive histological analysis with an unbiased stereological approach to characterise the role that Mef2c is having over a period covering different events of MSNs development from early neonatal until late adulthood.

4.4.1.1 The WT striatal volume increases over the postnatal period, and this increase is significantly less in *Mef2c CKO* mice

Striatal volume is an important predictive factor to assess the health status of the striatum, and striatal atrophy is considered as one of the hallmarks of HD pathology that precedes motor deficits (Aylward et al., 2012). The analysis of the striatal volume in *Mef2c CKO* and WT mice was measured from the anatomically matched CV-stained brain cross-sections, using stereological methods, at P2, P7, P14, 3 months and 12 months (a total of 44 WT and 46 CKO brains) (**Figure 4.1 A**).

Mef2c CKO has a significant effect on the striatal volume across the five age groups **(Figure 4.1 B).** A two-way ANOVA test conducted with age and genotype as the factors being assessed revealed a significant interaction between them (Age x Genotype: $F_{(4, 80)} = 2.617$, p=0.0411). A significant effect of the main factor Age ($F_{(4, 80)} = 137.5$, $p<0.0001$) and the main factor genotype ($F_{(1, 80)} = 18.89$, $p <0.0001$) was also found. Pairwise comparisons using Bonferroni test revealed that striatal volume was significantly increased over postnatal development in both *WT* and *CKO* mice. An increase of about 3.5-fold occurred between P2 and 3 months (*WT* from **3.17 ± 0.18 mm^3** at P2 to **11.06 ± 0.38 mm^3** at 3 months, $p <0.0001$; *CKO* from **2.47 ± 0.31 mm^3** at P2 to **9.05 ±0.43 mm^3** at 3 months, $p < 0.0001$). This was followed by a mild, non-significant reduction in striatal volume between 3 and 12 months: about 10% reduction in WT, from **11.06 ± 0.38 mm^3**

at 3 months to **9.85 ± 0.36 mm^3 at** 12 months (p=0.79), compared to about 6% reduction in CKO, from **9.05 ± 0.43mm^3** at 3 months to **8.53± 0.41mm^3** at 12 months (p=0.99).

No significant difference in the striatal volume was observed between *WT* and *CKO* at P2 nor at P7 (0.789 and 0.99). At P14, a 14.6% reduction was observed in the CKO compared with the WT, however this was not statistically significant (p= 0.137). At 3 months, a significant reduction was reported (~18.2%, *p*=0.0003) in CKO compared to WT and this was accompanied by enlargement of the lateral ventricle (black arrow in **Figure 4.1 A**). There was no significant difference between WT and CKO at 12 months (*p*=0.09) (**Figure 4.1 B**).

A summary of the means ± SEM of striatal volume for *WT* and *CKO* mice and the percentage difference in volume between them are shown in Table 4.1.

	Mean ± SEM		***% Difference***	***p***
Groups	***WT***	***CKO***		
P2	3.17±0.184	2.47±0.31	-22.19%	0.789
P7	4.59±0.19	4.73±0.12	-1.10%	0.99
P14	8.07±0.22	6.89±0.39	-14.63%	0.1371
3 months	11.06±0.38	9.05±0.41	-18.20%	0.0003 ***.
12 months	9.85±0.36	8.53±0.41	-13.36%	0.09

Table 4.1 A summary of means, SEM, and % difference of striatal volume (mm3) at five age groups in WT and CKO.

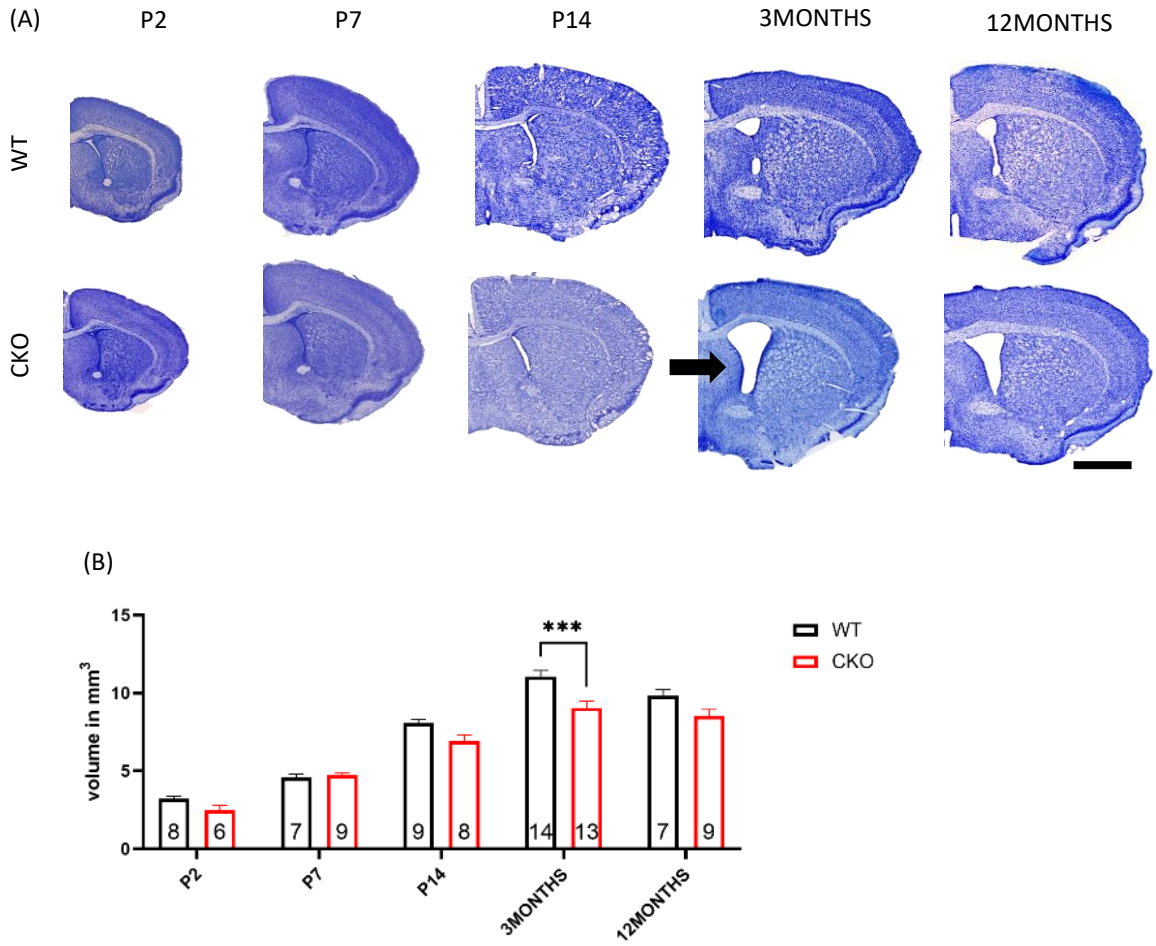

Figure 4.1 The increase in striatal volume over postnatal period is significantly less in Mef2c CKO mice.

(A) representative images of CV-stained brain sections at equivalent anatomical levels shows increase in striatal volume (and overall brain volume) across five different age groups P2, P7, P14, 3 months and 12 months in WT and CKO mice. Striatal volume is significantly smaller in CKO striatum at 3 months, and larger lateral ventricles are observed (black arrow). (B) graphical representation of striatal volume in the five age groups showing a significant difference in striatal volume between WT and CKO mice at 3-months (***p<.0003). Numbers at the bottom of each bar are n per group. Bars are means ± SEM. Scale bar is 1000µm.

4.4.1.2 NeuN count is significantly reduced in *CKO* mice

To see whether the reduction of striatal volume resulted from neuronal loss, the total NeuN-positive cell count was determined in *WT* and *CKO* mouse striatum of a developmental series between P2 and 12 months (**Figure 4.2a)**. The expression of NeuN is not exclusive to MSNs, but it is also expressed in the interneurons (Gusel'nikova and Korzhevskiy, 2015).

There was a significant effect of *Mef2c* loss across the five age groups (Genotype x Age: $F_{(4, 66)} = 2.842$, p=0.0308, two-way ANOVA) (**Figure 4.2b**). Furthermore, the main factor Age with NeuN count was found to be significantly increased between P2 and P14 (Age: $F_{(4, 66)} = 58.40$, P<0.0001). For the main factor genotype, the NeuN count was significantly decreased in *CKO* striatum (genotype: $F_{(1, 66)} = 19.55$, P<0.0001).

The results of the pairwise comparison using Bonferroni test were described firstly based on the changes observed at each of the different ages assessed between each genotype and, secondly, for each of the two genotypes comparisons across the five age groups.

Pairwise comparisons comparing each of the five ages assessed, across the two genotypes showed that the number of NeuN positive cells was significantly reduced in P14 *CKO* by 17% (p=0.027), in 3 months by 20% (p =0.003), and in 12 months by 18% (p =0.002), each compared to WT at the same age. There was no significant difference in NeuN positive cells between CKO and WT striatum at the early postnatal time points, P2 and P7 (p=0.408 and 0.40, respectively). A summary of NeuN count means ± SEM and percentage difference between WT and CKO is in Table 4.2 below.

	Means ± SEM		***% Difference***
Groups	***WT***	***CKO***	
P2	470531.53±38615.19	490455.03±39952.29	4.23%
P7	618270.04±50561.05	573902.18±26512.99	-7.18%
P14	1011280.80±52154.81	839724.57±19028.78	-16.96%
3Months	1024694.97±30878.54	828097.26±53419.62	-19.19%
12Months	1072259.56±38496.45	880285.63±43278.55	-17.90%

Table 4.2 NeuN count (as overall count per striatum) and % difference between WT and CKO.

In WT mice, a non-significant increase (of about 31%) was observed in NeuN positive cells between P2 and P7. Whereas, in CKO the increase was only 17% (p=n.s.). Furthermore, there was a significant increase between P7 and P14 of about 64% ((p<0.0001) in WT compared to 46% in CKO (p<0.0001). This increase in WT mice might happened because of postnatal neurogenesis or the presence of progenitor cells that are not expressing the postmitotic neuronal marker NeuN yet at the earlier time point(s). Taking together, this indicates that the increase in NeuN expression is significantly less in CKO mice and Mef2c might be acting early between P2-P14.

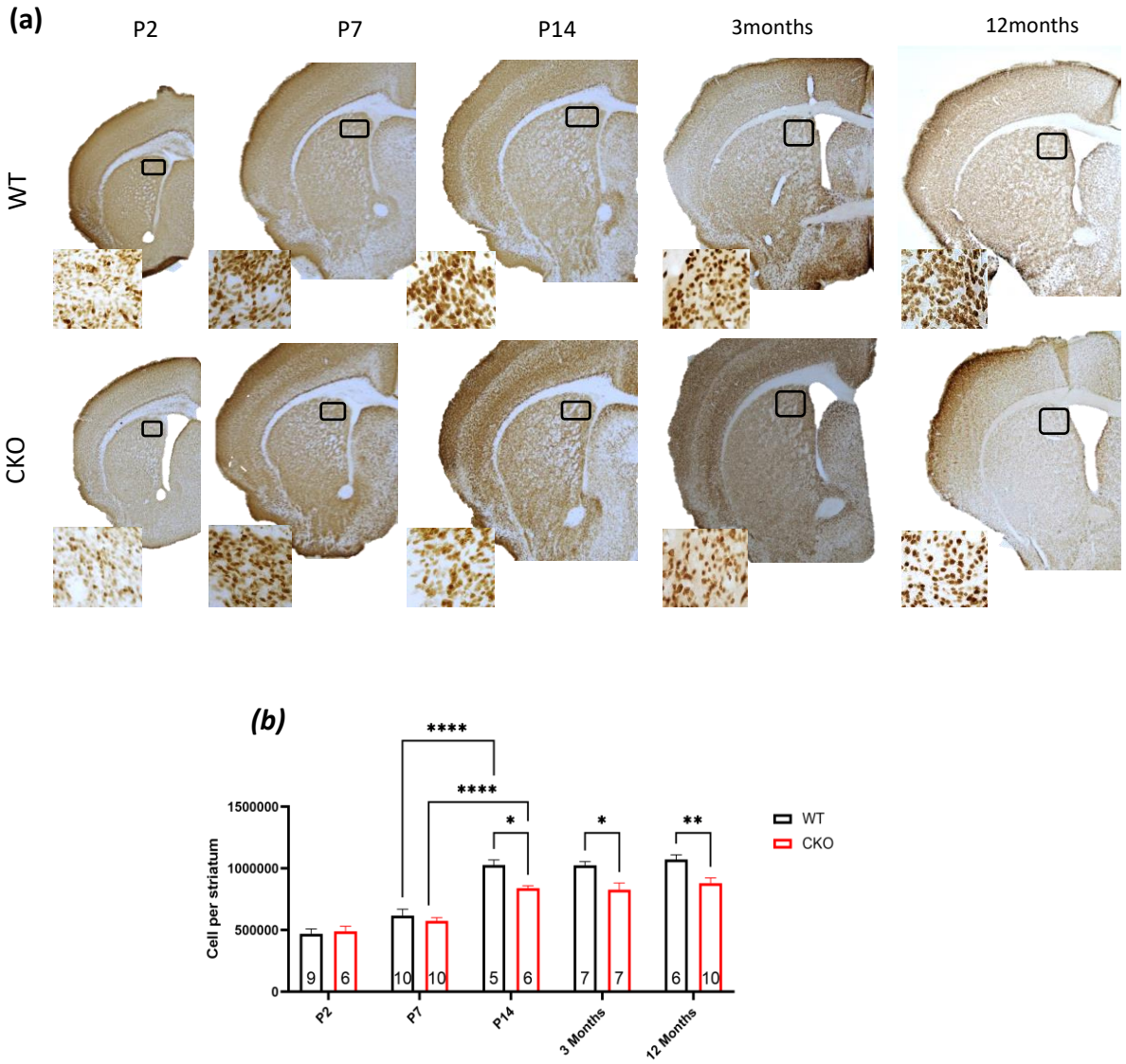

Figure 4.2 NeuN count is significantly reduced in CKO mouse striatum compared to WT at P14, 3-months and 12-months.

(a) representative images of NeuN immunohistochemical staining in mouse brain coronal sections at P2, P7, P14, 3months, and 12 months, WT (upper) and CKO (lower panel) striatum. Images were taken at magnification of 12.5 in low magnification while magnified black outlined regions were imaged at 400x. (b) a graphical representation of NeuN quantification per mouse striatum shows a significant effect of Mef2c CKO on overall NeuN count across the five age groups (age x genotype: $p<0.0308$), with NeuN significantly less at P14, 3months and 12months. NeuN count has significantly increased between P7 and P14 in WT and CKO ($p<0.0001$), but the percentage increase in CKO is less (46% compared to 64% in WT). Bars are means ± SEM. Numbers at the bottom of each bar graph are n per group. *$p<0.05$, **$p<0.01$, ****<0.0001

4.4.1.3 FoxP1-positive cells significantly decrease in *CKO* mouse striatum

In the previous section, it was shown that the NeuN count was significantly less in the striatum in *Mef2c CKO* mice compared with *WT*. NeuN labels both neurons and interneurons (INs). However, the fact that the percentage of striatal INs in mouse striatum is less than 5% (Graveland and DiFiglia, 1985), while the average reduction was 20% in *CKO* 3-month striatum, indicates that there is loss of MSNs that contributes to the reduction in *NeuN* count. rather than INs (To assess this, a specific MSNs marker named FoxP1 was assessed that is exclusively expressed in MSNs, but not in interneurons (Tamura et al., 2004; Precious et al., 2016). The overall FoxP1 positive cell number was quantified in *WT* and *CKO* mouse brain sections stained with FoxP1 using unbiased stereology in a developmental series between P2 and 12 months **(Figure 4.3 a)**.

The overall FoxP1 count was shown to be significantly less in CKO striatum than in WT **(Figure 4.3 c)**. A Two-way ANOVA test revealed a significant effect of the main factors, genotype ($F_{(1, 68)} = 21.69$, $p<0.0001$), and age ($F_{(4, 68)} = 18.84$, $p<0.0001$), but there was no significant interaction between them ($F_{(4, 68)} = 0.5802$, $p=0.6780$). This indicates that the effect of Mef2c loss is non-progressive across the age groups tested, and the reduction of FoxP1 expression was maintained over time.

Although pairwise comparisons were not possible as no significant interaction was found in the ANOVA, a percentage reduction in FoxP1 count in *CKO* striatum was observed at P14 (13.01%), 3 months (17.13%) and 12 months (14.89%).

NeuN is expressed in all neurons, however, in P2 WT striatum, FoxP1 was found to label 32% more MSNs than *NeuN* (690946.00 ± 12325.97 FoxP1- positive cells compared with 470531.53 ± 38615.19 NeuN-positive cells) and 21% more FoxP1 than NeuN at P7 (779576.33 ± 27148.77 FoxP1-positive compared with 618270.04 ± 50561.05 NeuN-positive cells). In contrast, no percentage difference in MSNs expressing NeuN and FoxP1 was found at later age groups.

One interesting observation at P2 was that cells expressing FoxP1 were morphologically different between *WT* and *CKO* **(Figure 4.4).** There are more cells that look distorted and non-uniformly shaped in the CKO. These cells could be undergoing the early stages of apoptosis, and not completely washed off from the striatum section. However, this requires further analysis to confirm this suggestion.

A summary of FoxP1 count means and SEM is in the **Table 4.3** below.

	means ± SEM		**% Difference**
Age	WT	CKO	
P2	690946.00 ± 12325.97	613242.67 ± 55117.65	-%11.25
P7	779576.33 ± 27148.77	718999.25 ± 64771.26	-%7.80
P14	977935.00 ± 51750.94	850741.60 ± 42588.23	-%13.01
3 months	1060494.67 ± 46962.58	878839.00 ± 36890.02	-%17.13
12 months	996410.00 ± 25705.09	848029.83 ± 17249.44	-%14.89

Table 4.3 A summary of FoxP1-positive striatal cell counts in a time series between P2 and 12 months in WT and CKO Mef2c mice.

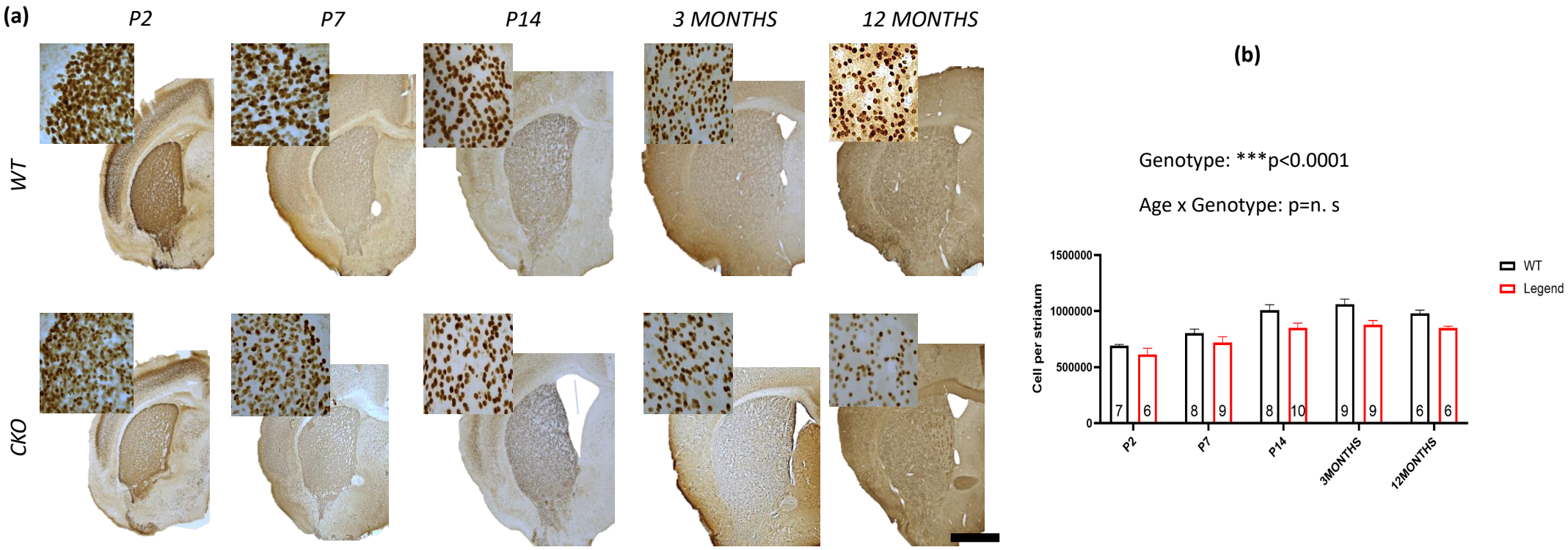

Figure 4.3 FoxP1-positive cells significantly decrease in CKO mouse striatum

(a) representative images of mouse coronal sections stained with FoxP1 at P2, P7, P14, 3 months and 12 months were imaged at 12.5x magnification, (Black-dashed regions were imaged at 400X). **(b)** graphical illustration of total FoxP1-positive cell count per striatum shows a significant reduction in CKO mouse striatum (Genotype; ***p<.0001), but no significant interaction between Age and genotype (p=n.s.). Bars represent Means ± S.E.M. Numbers at the bottom of each bar are the "n" per group.

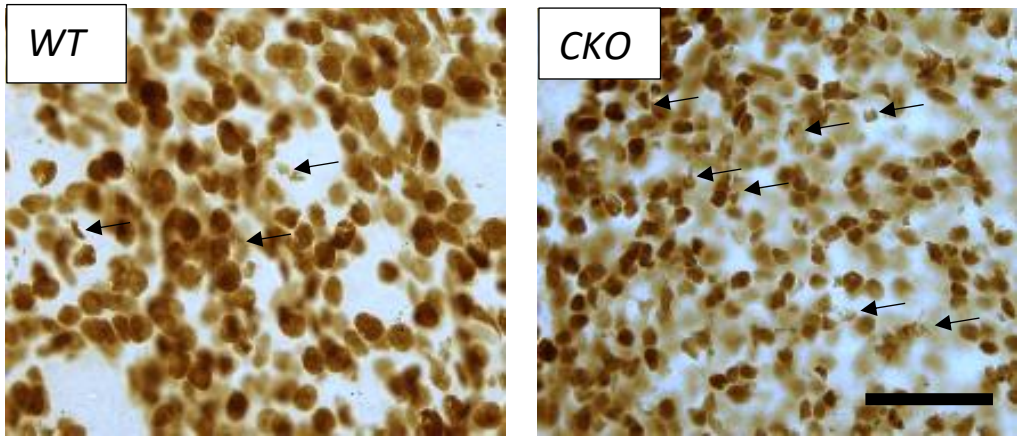

Figure 4.4 FoxP1 expression at P2 shows that there are more distorted cells in CKO striatum (indicated by black arrows). Scale bar is 50µm.

4.4.1.4 Ctip2-positive cell number is significantly reduced in CKO mouse striatum

Ctip2 is one of the MSNs markers that is expressed early in MSNs through development, but not in striatal interneurons (Arlotta et al., 2008b). Only two time points, P7 and 3 months, were analysed using IHC and subsequent stereological quantification **(Figure 4.5)**.

Consistent with the striatal volume measurement, the overall area of Ctip2 immunoreactivity looked smaller in 3-month *CKO* mouse striatum compared to WT striatum (**Figure 4.5 a**). A Two-way ANOVA revealed no significant interaction between Age and Genotype ($F_{(1, 21)} = 1.704$, $p=0.205$), indicating that Mef2c has no effect on the overall count of Ctip2 over the two age groups However, a significant effect of the factor genotype, was observed between WT and CKO ($F_{(1, 21)} = 4.948$, $p=0.0372$) **(Figure 4.5 b).**

Age	***Means ± SEM***		***% Difference***
	WT	*CKO*	
P7	*804105.91±11074.15*	*756290.71±42043.82*	*-5.9%*
3months	*1030738.99±46660.66*	*845953.22 ±43588.31*	*-17.9%*

Table 4.4 A summary of Ctip2 counts and SEM in WT and CKO P7 and 3-month mouse striatum.

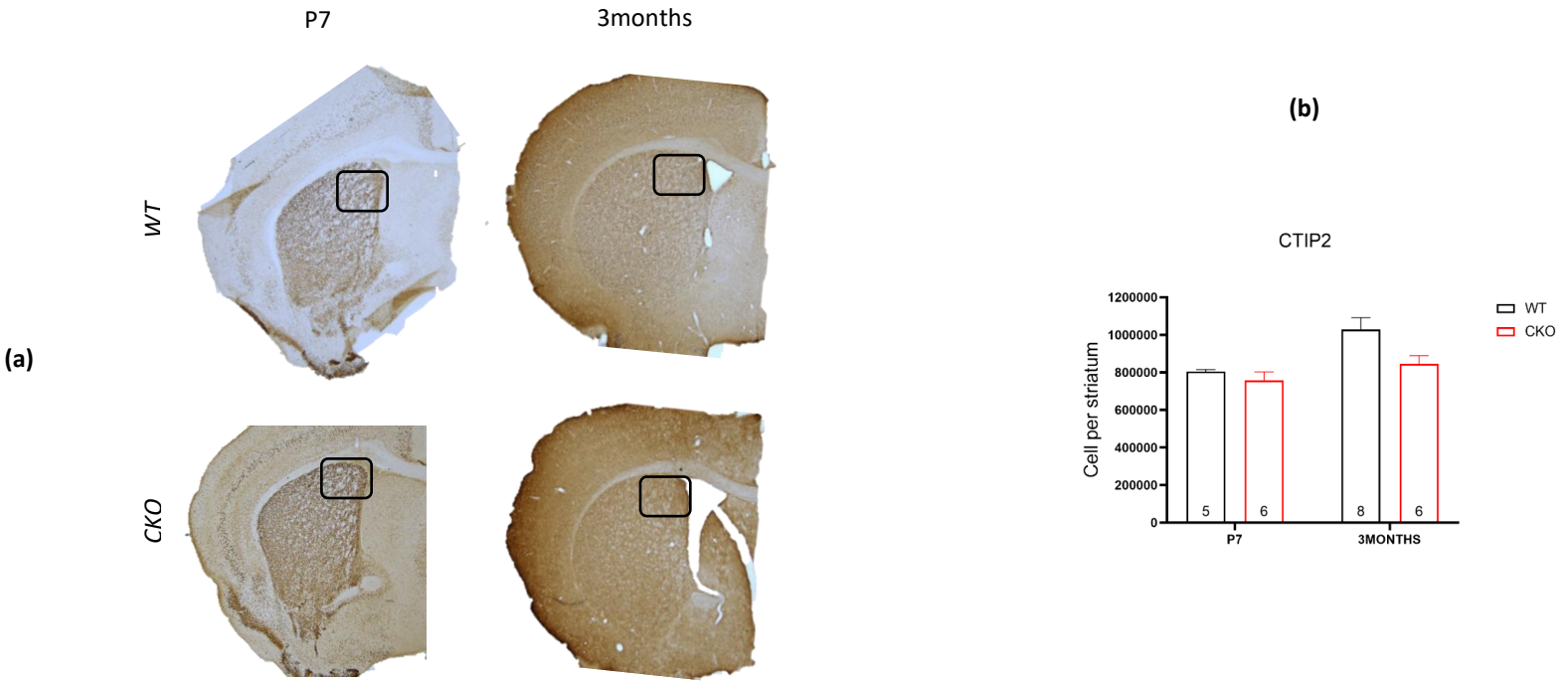

Figure 4.5 The overall count of Ctip2-positive cells per striatum is significantly less in CKO mouse striatum.

(a) representative images of WT and CKO Ctip2-stained mouse brain sections at P7 and 3 months images at 12.5X in low magnification and 400X at high magnification. **(b)** graphical representation of Ctip2 count in WT and CKO striatum at P7 and 3 months shows significant reduction in overall Ctip2 count in *CKO* ($p=0.037$). Bars are means $\pm$ SEM.

4.4.1.5 Mef2c loss in mouse striatum has no effect on FoxP1 and Ctip2 co-localisation

In the WT more than 99% of Ctip2-positive cells are also FoxpP1-positive (Arlotta et al., 2008b). In the previous two sections FoxP1 and Ctip2 cell numbers were found to be significantly decreased in 3 months CKO striatum, by about 17% and 18% respectively. This indicates a similar effect of Mef2c loss on cells expressing these two proteins. To confirm this and exclude any differential effect on one transcription factor but not the other, double immunofluorescence of Ctip2 and FoxP1 using specific antibodies was performed. Ctip2/FoxP1-positive cells were quantified in both DM and DL aspects, to relate to the Mef2c expression pattern described in Chapter 3 (**Figure 4.6).**

Again, the mouse striatum is smaller in the CKO (white-dashed regions in **Figure 4.6 a**). However, no significant difference was observed in the percentage of Ctip2+/FoxP1+ MSNs between WT and CKO in either the DM ($t(4)= 0.827$, $p=0.45$) or DL ($t(4)= 0.39$) aspects of the striatum (**Figure 4.6b)**.

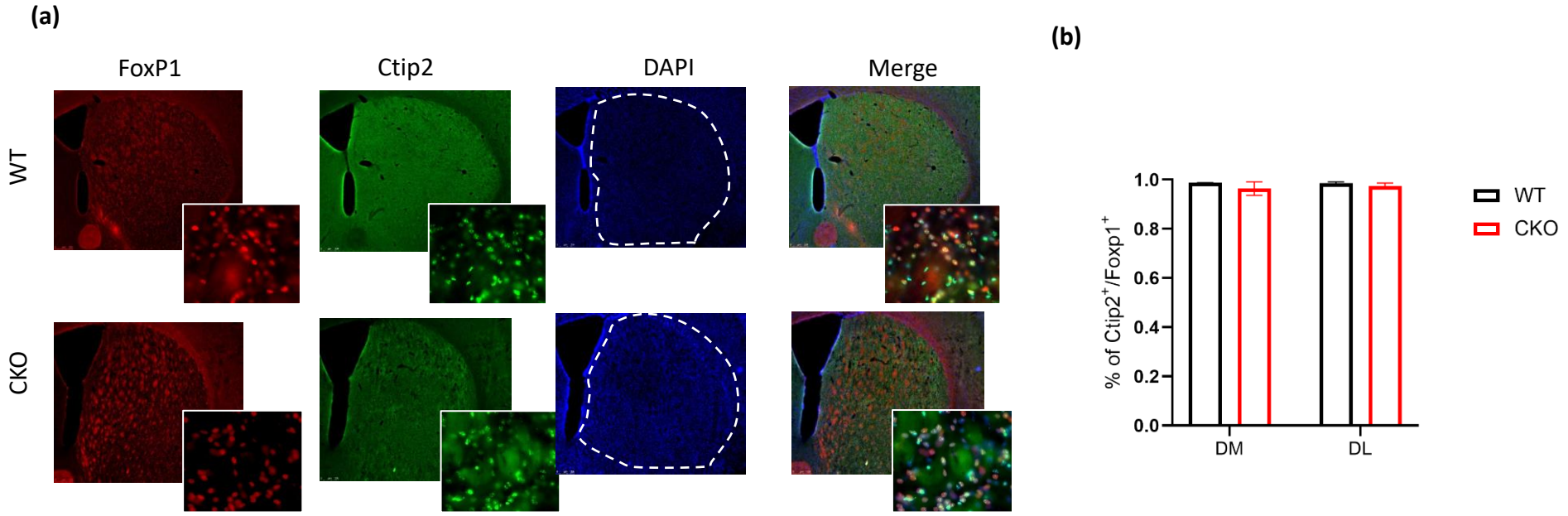

Figure 4.6 No significant difference in the percentage of Ctip2+/FoxP1+ MSNs between WT and CKO in 3-month mouse striatum.

(a) Double immunofluorescence of Ctip2 (green) and FoxP1(red) in WT and CKO mouse striatum sections shows reduced striatal area in CKO (white-dashed regions). High magnification images in boxes show no difference in Ctip2/FoxP1 co-localisation between WT and CKO. **(b)** Graphical representation of Ctip2/FoxP1-positive cells in DM and DL aspects shows no significant difference. Scale bars are 500 µm in low and 100 µm in high magnification. Bars are means ±SEM.

4.4.1.6 *Darpp32*-positive cells are significantly reduced in *CKO*

In the previous sections, the *CKO* mouse striatum was shown to be significantly smaller than the WT mouse striatum, with fewer NeuN-, FoxP1- and Ctip2-positive cells, indicating that *Mef2c CKO* could cause a loss of MSNs. In this section, the expression of a third MSN marker, Darpp32, which is only expressed in the mature MSNs, was assessed to see if Mef2c loss affects mature MSNs. Free-floating IHC of Darpp32 followed by stereological quantification for both *WT* and *CKO* mice was used at P2, P7, P14, 3 months and 12 months (**Figure 4.7)**. A Two-way *ANOVA* was conducted with age and genotype as the two main factors assessed, followed by a Bonferroni *post hoc* test.

Unlike FoxP1 and Ctip2, Darpp32 expression in the WT striatum is not homogenously distributed throughout the striatum **(Figure 4.7 a).** At P2, *DARPP*-32 expression in the *WT* mouse striatum was localised mainly to specific ''patchy-like'' regions, which are very likely to be striosomes (black arrows in **Figure 4.7 a**). MSNs occupying this compartment will mature first and express the mature MSN marker Darpp32 earlier than MSNs occupying the matrix compartment (Anderson et al., 1997). With advancing age, Darpp32 becomes homogenously expressed throughout the striatum.

Mef2c loss was found to significantly affect Darpp32 expression over the five age groups (Age x Genotype: $F_{(4, 68)} = 3.706$, p=0.008) (**Figure 4.8**). In the WT striatum Darpp32 significantly increased (by about 147.93%) between P2 and P7 (p= 0.0001), with a further increase (by about 77.63%) between P7 and P14 (p<0.0001). No further increase or any difference in Darpp32 count was observed between P14, 3 months and 12 months (p=n.s.).

A significant effect of age ($F_{(4, 68)} = 85.12$, $P<0.0001$) and genotype ($F_{(1, 68)} = 26.03$, $P<0.0001$) was also found. Post-Hoc comparisons using a Bonferroni test indicated that there is a significant difference in Darpp32 expression between *WT* and *CKO* at P14 (p =0.027), 3 months (p <0.0002) and 12 months (p < 0.002). In contrast, there was no significant difference between WT and *CKO* mice at P2 or P7 (p, n.s.) **(Figure 4.8 b).**

A summary of the means and SEM of total Darpp32 count for each group and percentage difference between WT and CKO is in **Table 4.5** below.

Groups	***Means ± SEM***		***% Difference***
	WT	***CKO***	
p2	99514.31 ± 9304.496	91954.75 ± 6777.84	-8%
P7	246729.38 ± 5692.465	238761.20 ± 4251.055	-3%
P14	438268.58 ± 4251.055	358398.48 ± 26677.78	-18%
3months	477976.94 ± 22070.18	345770.53 ± 21922.52	-28%
12 months	493843.74 ± 21965.34	373350.79 ± 25629.84	-24%

Table 4.5 A summary of Darpp32 count measured as total cells per striatum, means ± SEM and % difference between WT and CKO.

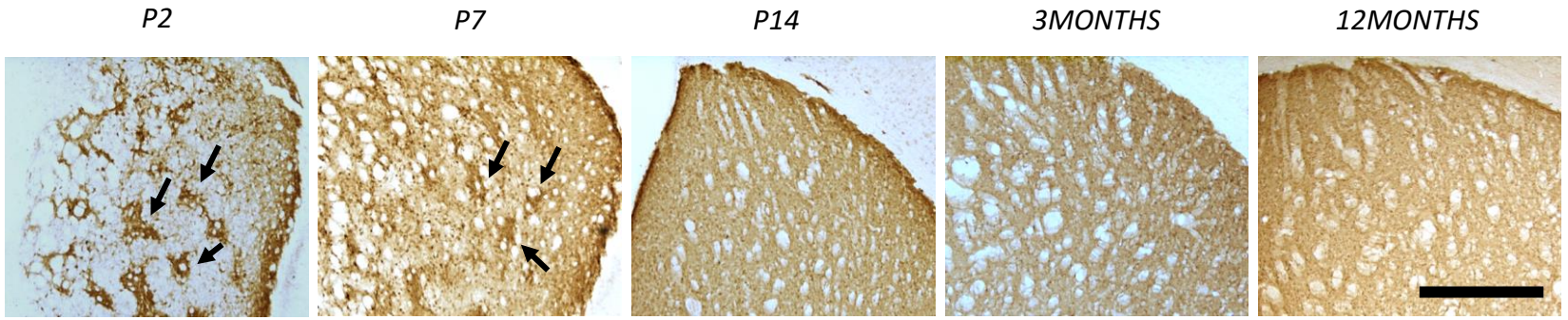

Figure 4.7 Representative photomicrographs from WT mouse coronal sections at P2, P7, P14, 3 months and 12 months, taken at magnification of 100x, show the distribution of Darpp32-positive cells across the five age groups

---

Representative photomicrographs from WT mouse coronal sections at P2, P7, P14, 3 months and 12 months, taken at magnification of 100x, show the distribution of Darpp32-positive cells across the five age groups, with ''patchy'' like appearance of Darpp32 at P2 and P7 (black arrows) that becomes more evenly distributed across the striatum at later age groups.

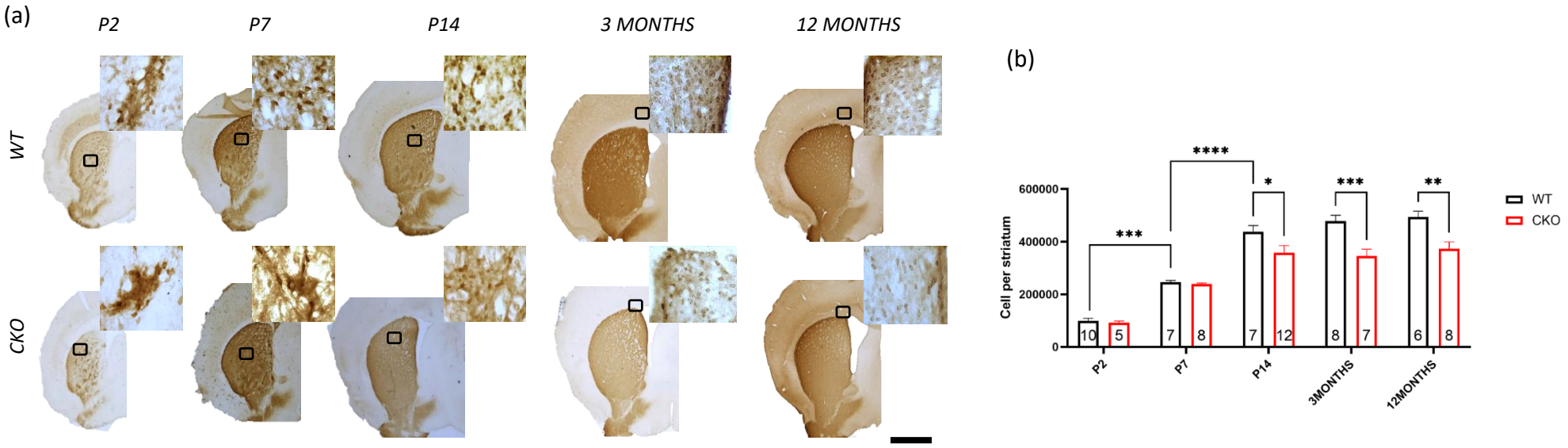

Figure 4.8 Reduced Darpp32 positive cells in Mef2c CKO mouse striatum.

(b) IHC of Darpp32 in WT (upper panel) and CKO (lower panel) at Five age groups P2, P7, P14, 3 months and 12 months. **(c)** a graphical representation of Darpp32 quantification per mouse striatum shows a significant effect of Mef2c loss on overall count of Darpp32 across the five age groups (Age x genotype: *P*=0.0087) and a significant increase in the number of cells expressing Darpp32 in both WT and CKO by adulthood (Age: p<0.0001), n per group. Scale bars are, 500µm in **a**, and 1000 µm in (low magnification) and 50 µm (high magnification) in **b**. bars are means ± SEM. *p<0.05, **p<0.001, and ***p<0.0001.

4.4.1.6.1 *Darpp32* is strongly expressed in striosomes MSNs in early postnatal mouse striatum

In the previous section, the overall number of Darpp32-positive cells was shown to significantly increase between P2 and P14 in *WT* striatum. However, this increase does not seem to be because of increased number of cells, but rather as an increase in mature MSNs, since the overall FoxP1-positive cell number was shown to be higher compared to Darpp32 in the same age groups. Mef2c loss was also shown to have no effect on Darpp32 count in P2 and P7 mouse striatum.

Darpp32 was shown before to be expressed in the striosomes compartment in the early postnatal striatum (Chen et al., 2016). To confirm this, a double immunofluorescence of Darpp32 and MOR1 (the classical striosomes marker described in chapter3) was undertaken in WT striatum at P0, P2 and P7 (**Figure 4.9).** The images show complete co-expression between Darpp32 and MOR1 at P0 and P2 WT striatum, with very minimum expression of Darpp32 in MOR1-ve regions (white-dashed regions in Figure 4.8). While at P7 Darpp32 expression becomes more distributed throughout the striatum, but still with strong expression in striosomes.

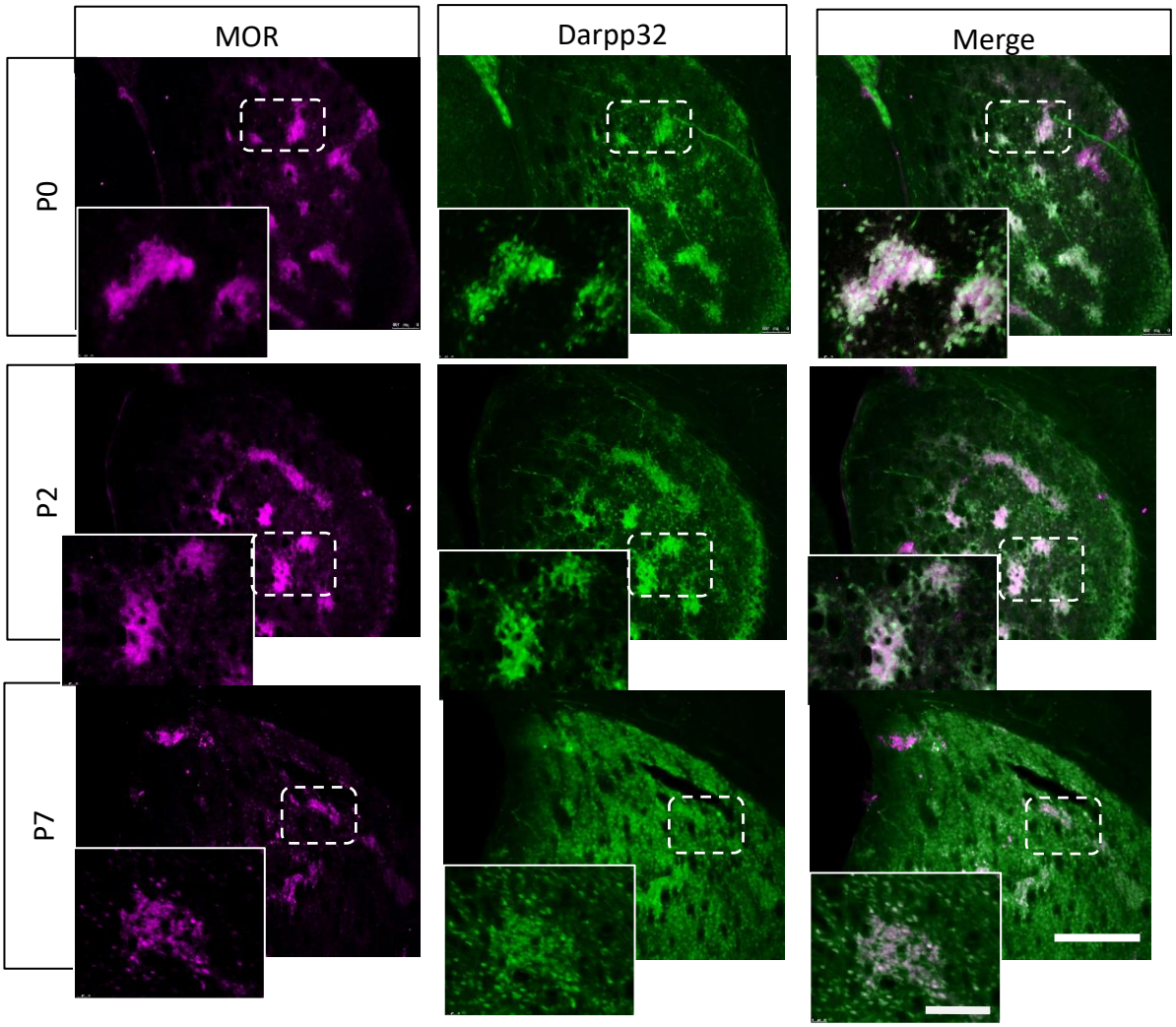

F

Figure 4.9: Darpp32 expression in early postnatal striatum is restricted to the striosomes compartment. Double immunofluorescence of Darpp32 (green) and MOR1 (purple) in coronal mouse brain sections at P0 (upper panel), P2 (middle panel) and P7 (lower panel). The white dashed regions show higher magnification with complete localisation of Darpp32 and MOR1. Scale bars are 300µm in low magnification and 100 µm in high magnification.

4.4.1.7 Further analysis of CKO only

The significant reductions in striatal volume, NeuN-positive cell count, and the count of three MSN markers observed in the previous sections was not progressive toward 12months. This indicates that Mef2c is acting in the early postnatal striatum, sometime in the period up to P14. The absence of significant interaction in some two-way *ANOVA* analyses prevented confirming this with pairwise comparison testing.

Therefore, to confirm one-way *ANOVA* of total count of NeuN, FoxP1 and Darpp32 was conducted in *CKO* only to see if there is any significant difference between the P14, 3 month and 12-month groups, (**Figure 4.10**). Ctip2 was not included as I do not have data for P14.

One-way ANOVA test followed by Tukey's post hoc test showed that, no significant difference between P14, 3 months and 12 months in NeuN, FoxP1, and Darpp32 count (p=n.s.).

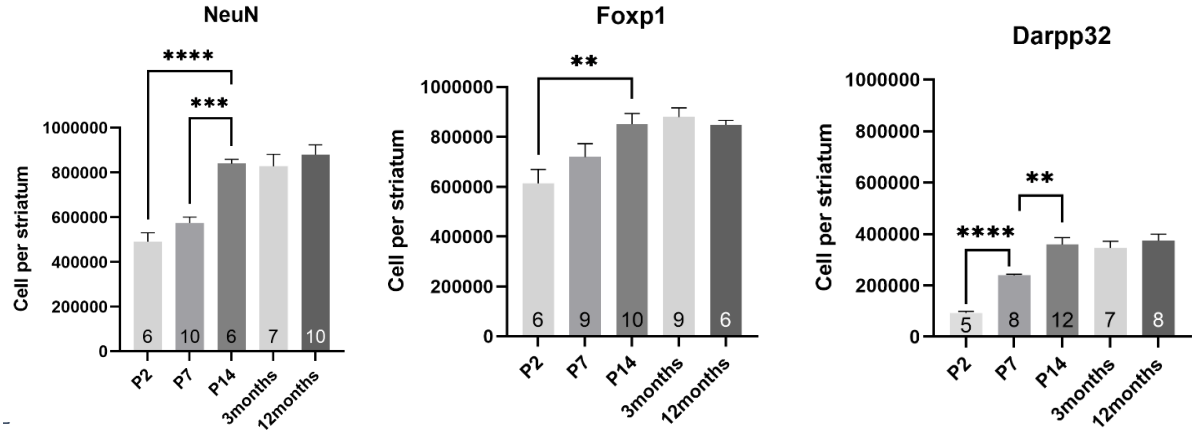

Figure 4.10: No significant difference in the overall NeuN-, FoxP1- and Darpp32-positive *cell* count between P14, 3 months and 12 months in *CKO* mouse striatum. *p<0.05, **p<0.01, ***p<0.001. n per group is at the bottom of each bar.

4.4.2 Mef2c loss has a differential effect on the matrix/striosome MSNs

In chapter 3, I provided data that suggest Mef2c is not expressed in striosomes MSNs, among these is that Mef2c expression is not expressed in all MSNs: it is expressed minimally during peak striosomes MSNs neurogenesis at E12, and does not colocalise with Darpp32, which is expressed only in striosomes MSNs in WT P0 mouse striatum. I therefore hypothesize that Mef2c might not play a role in the development of the striosome compartment of the striatum, and its effect is only on matrix MSNs.

Therefore, the aim of this section was to characterise the organisation of striatal striosomes in P2 and adult *WT* and Mef2c *CKO* mouse striatum through using immunohistochemical localisation of the classical marker of striosomes, MOR1, which is specifically enriched in the striosomes only (**Figure 4.11 a)**. The overall number of striosomes was quantified first, and then the percentage striatal area occupied by striosomes was measured (as detailed in chapter 2, section 2.3.7.2.5).

Immunofluorescence of MOR1 at different levels of bregma in WT and CKO P2 and adult striatum is shown in **Figure 4.11 a.** Mef2c loss significantly affects the percentage area occupied by striosomes over the two age groups (two-way ANOVA Age x Genotype: $F_{(1, 19)} = 8.577$, p=0.0086) (**Figure 4.11 b)**. A significant increase in *CKO* mice was observed in the percentage area of striosomes. (Genotype: $F_{(1, 19)} = 6.600$, p=0.0188). Post hoc test using Bonferroni correction showed a significant increase in the percentage area of striosomes in adult mice (p=0.0026), but not in P2 mice (p= n.s.).

Mef2c loss has no significant effect on the overall number of striosomes in P2 or in adult mouse striatum **(Figure 4.11 c)**. Two-way ANOVA revealed no significant effect of the main factor genotype on the overall number of striosomes (Genotype: $F_{(1, 29)} = 0.01085$, p=0.9178), nor the main effect age ($F_{(1, 29)} = 2.773$, p=0.1066) and no interaction between them (Genotype x Age: $F_{(1, 29)} = 1.182$, p=0.2859).

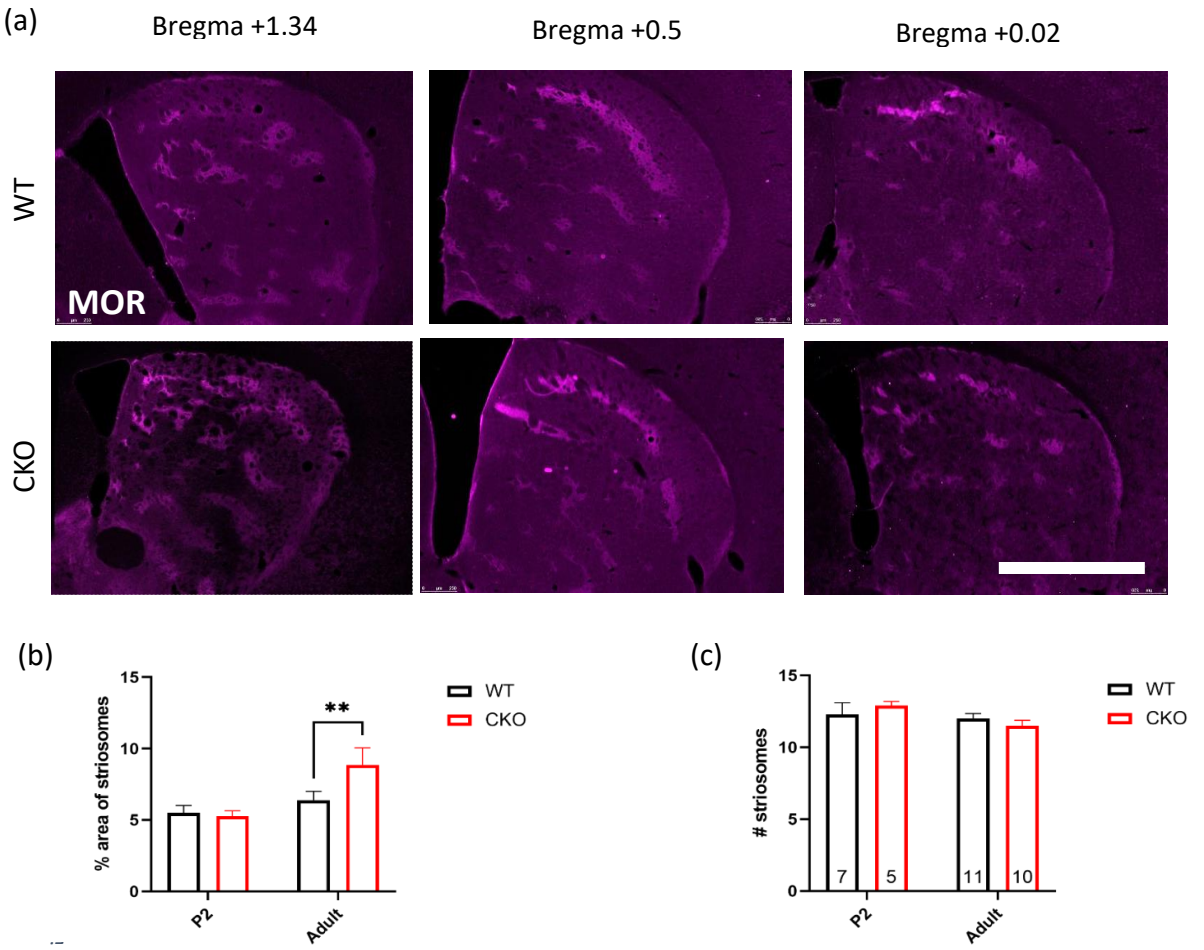

Figure 4.11: Increased percentage area of *MOR1*-positive striosomes in adult *CKO* mouse striatum but not in P2. (a) IHC of (anti MOR1) in *WT* and CKO adult mouse striatum at anatomically matched different levels of bregma. (b) a significant increase in the percentage area of striosomes in *CKO* mice was observed in adult striatum only (p=0.0026). (c) no significant effect of Mef2c loss on the overall number of striosomes per striatum in both age groups. Bars are means ± SEM. Scale bar is 1000µm. **p<0.01.

4.4.2.1 Mef2c loss causes significant reduction in the area occupied by matrix MSNs in adult striatum

The previous section showed that *Mef2c CKO* caused a significant increase in the striatal area occupied by striosomes, while previously I showed that overall striatal volume significantly decreases in the *CKO*. This could mean that the loss of MSNs in the *Mef2c CKO* does not occur in the striosomes compartment and could be in matrix MSNs only. To test this, calbindin (CB) immunofluorescence was performed to visualise the matrix compartment. CB is only expressed in matrix MSNs in adult striatum (Liu and Graybiel, 1992a) and has been widely used to label these cells (Ivkovic and Ehrlich, 1999). However, in the early postnatal striatum it could also be expressed in striosomes(Liu and Graybiel, 1992b). Therefore, only adult striatum was assessed here (**Figure 4.12**).

The percentage area positive for CB was quantified in anatomically matched adult mouse brain sections (**Figure 4.10 a**). The white outlined regions represent CB negative regions that could be striosomes. An unpaired t test was performed, and the results showed that the Mef2c loss caused a significant reduction in matrix MSNs of adult striatum ($t_{(7)=}$ 4.588, , p= 0.0025) (**Figure 4.12 b**).

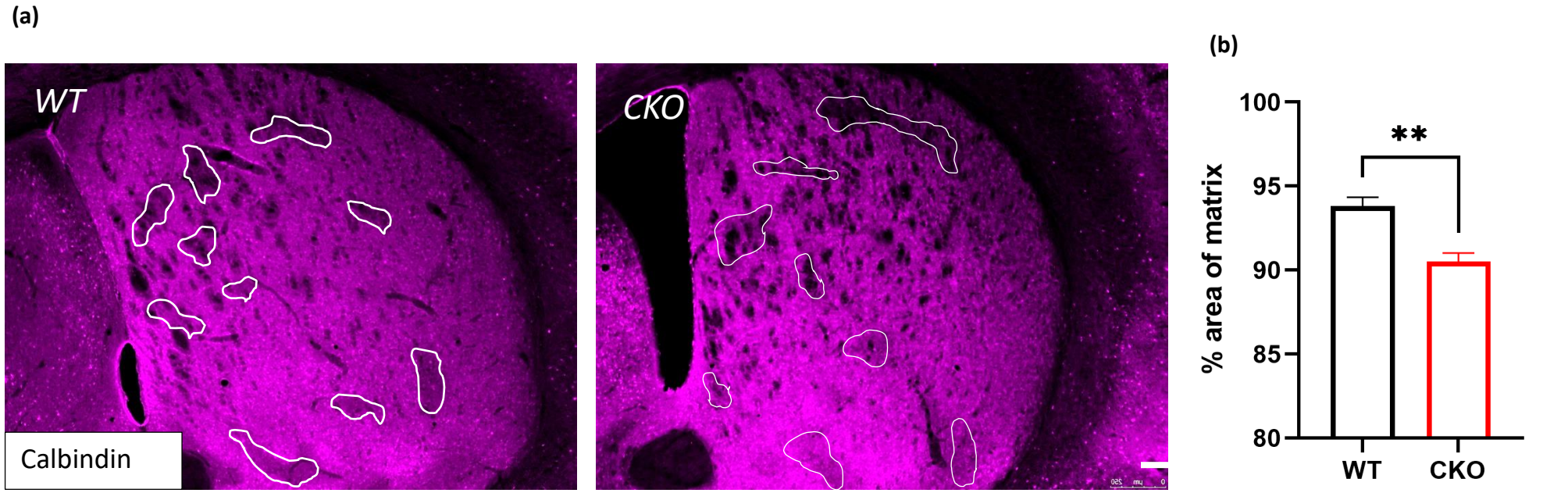

Figure 4.12: Mef2c loss causes significant reduction in the area occupied by matrix MSNs. (a) Immunofluorescence of CB in *WT* and *CKO* adult mouse striatum showing a significant reduction of CB+ve regions in CKO mouse striatum. White-outlined regions show CB-ve regions that represent striosomes. Scale bar is 500µm (b) graphical representation of CB+ percentage area, which shows a significant reduction in CKO (**p<0.01). Bars represent means ± SEM.

4.4.2.2 Mef2c is mostly expressed in MSNs born at embryonic day 14 (E14)

As shown in the previous section, Mef2c loss caused a significant reduction in the area occupied by matrix MSNs. This led me to address the question whether Mef2c expression is associated with a subpopulation of matrix, but not striosomes, as I have shown in the previous section that the percentage area of striosomes increased in CKO mice, while the overall cross-sectional area decreased.

To address this point, I used the proliferation marker EdU to birth-date neurons born during embryonic development. Time-mated pregnant dams received two I.P. injections of EdU at four different time-points E12, E14, E16 and E18, as shown in **Figure 4.13 a**, and pups were collected soon after birth for analysis.

I found that there is a significant difference in the percentage of proliferating cells that express Mef2c at different embryonic time points ($F_{(3, 13)} = 1550$, $p < 0.0001$, One-way ANOVA), **(Figure 4.13 b)**. About 75% of MSNs born at E14 and 24% MSNs born at E16 are Mef2c positive, compared with only 2.02% and 2.16% at E12 and E18, respectively.

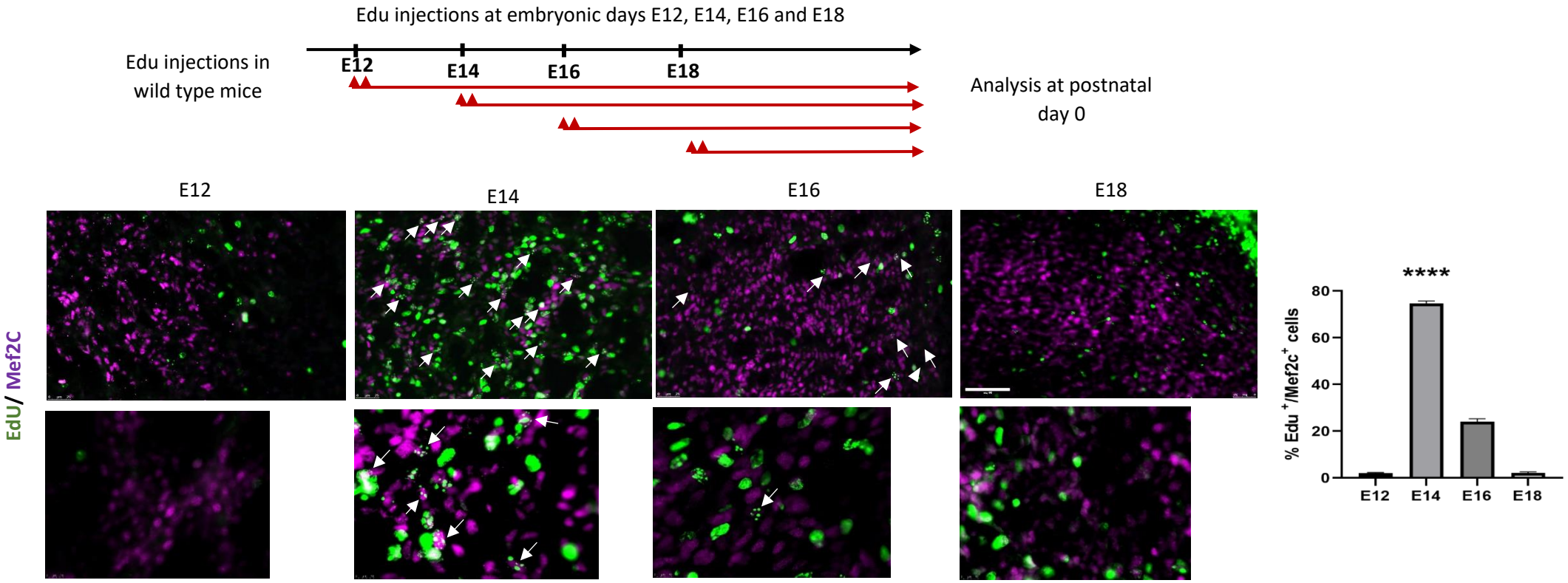

Figure 4.13: **(a)** double labelling of Mef2c and the proliferation marker EdU, injected at four embryonic time points E12, E14, E16 and E18. Mef2c (magenta) is highly co-expressed with EdU(green) in MSNs born at E14, and to a lesser extent at E16, but not at E12 or E18. White arrows represent Mef2c/EdU positive cells**. (b)** graphical representation of the percentages of EdU/Mef2c positive cells at the four time points. The double labelling is the highest at E14 ($p<0.0001$). Scale bar is 100µm. (Higher magnification images are added to this figure)

4.4.3 Mef2c loss significantly increases dendritic tree arborisation in *CKO* mice

Previous findings, outlined in Chapter 3, suggest a role of Mef2c in dendrites and dendritic spine development. Golgi-cox staining was therefore undertaken to visualise the dendritic tree and dendritic spines in adult *WT* and *CKO* mouse striatum to further characterise the morphological consequences of Mef2c loss on mouse MSNs **(Figure 4.14)**.

The technique used was developed and optimised by me in our lab, (as detailed in chapter 2), to clearly visualise these neuronal structures. In this experiment, I looked primarily at dendritic spine density, and dendritic tree arborization through Sholl analysis, in addition to soma size to detect any subtle shifts in neuronal populations (Lingley et al., 2018). The medial and lateral parts of the dorsal striatum were analysed separately to determine if there is a region-specific effect, consistent with the pattern of Mef2c expression in the mouse striatum that was shown in Chapter 3: high in DM and significantly less (or completely lost at some regions) in DL aspects.

Firstly, no significant difference in *WT* and *CKO* soma size was observed in the DM (*WT*=184.6 ±4.4, *CKO* =192.2 ± 3.9; $t_{(118)}$ = -1.296, p =0.198), nor in the DL striatum (*WT*=175.6±4.3, *CKO*= 178.5±5.2; $t_{(118)}$ = -0.429, p =0.696) (t-test with Holm-Sidak correction) (**Figure 4.14 a**).

I then analysed the density of dendritic spines expressed by the number of spines per µm. There was no significant difference in either DM ($t_{(7)}$ = 0.590) p = 0.574, n: 4WT and 5CKO) nor DL ($t_{(6)}$ = 1.910 p = 0.105, n: 3WT and 5CKO) parts of the striatum (**Figure 4.14 b),** indicating that Mef2c loss during embryonic development might not affect dendritic spine density.

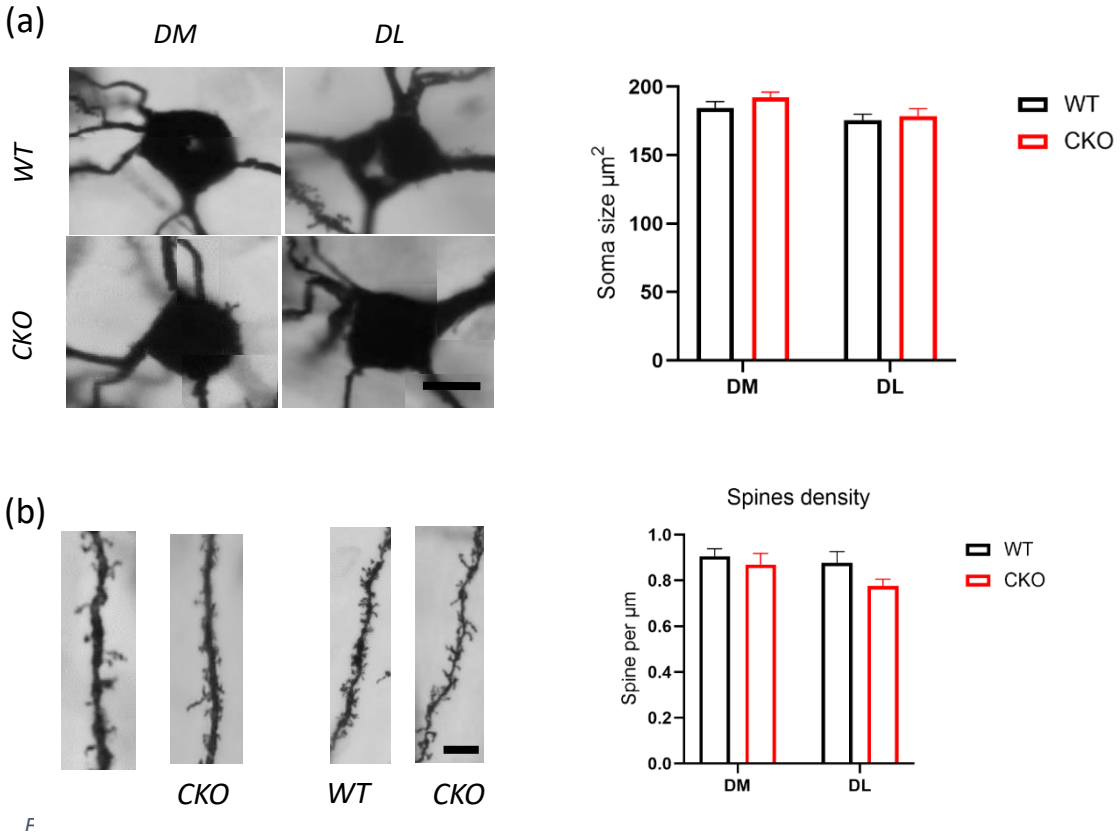

Figure 4.14: Mef2c loss in mouse striatum does not cause any significant change in dendritic spines density. **(a)** No significant effect of Mef2c loss was detected on soma size at DM nor at DL. **(b)** No significant difference in the dendritic spine density (spines per µm) was observed between *WT* and *CKO* in either DM or DL striatum (p =n.s.) bar graphs are means ± SEM. Scale bars are 10µm.

Then, to determine whether Mef2c loss affects dendritic complexity and branching patterns, I undertook 3D-Sholl analysis by counting the number of dendrite intersections in concentric circles at 120 µm from the cell body, (as described in Methods section 2.8.3) (**Figure 4.15 a**).

Two-way repeated measures ANOVA revealed that, in the DM striatum, Mef2c loss caused a significant effect on the number of dendritic intersections at different distances from the neuronal soma (Genotype x distance from soma: $F_{(12, 252)} = 2.790$, $p = 0.001$). Post hoc tests using Bonferroni correction showed a significant increase in the number of intersections at 10, 20 and 30 µm ($p = 0.015$, $p = 0.033$ and $p = 0.019$, respectively) (**Figure 4.15 b)**. In the DL aspect, Mef2c was also found to significantly affect the number of intersections over different distances from cell body (Two-way repeated measures ANOVA: Genotype x distance from soma: $F_{(12, 300)} = 2.853$; $p = 0.001$). However, post hoc tests showed that the only significant difference between WT and CKO was at 10µm distance away from soma (p=0.001) (**Figure 4.15 c**).

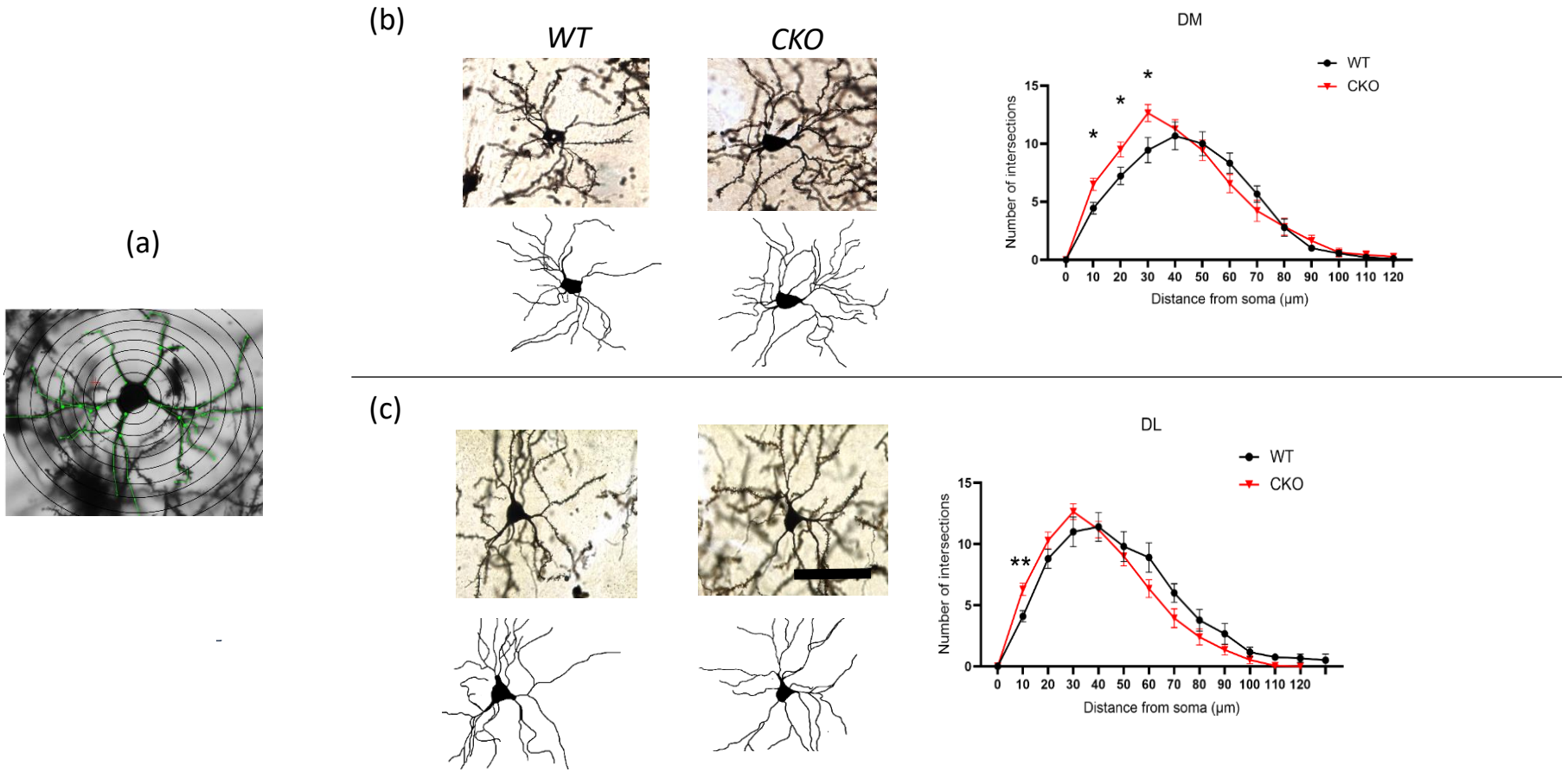

Figure 4.15: Mef2c loss in mouse striatum during embryonic development results in a significant increase in dendritic tree arborisation. Golgi cox analysis of the adult mouse striatum (~ 6months) in *Mef2c CKO* and *WT*.

(a) illustration of the methodology used to quantify the number of dendritic intersections in *WT* and *CKO* striatum. **(b and c)** Golgi Cox-stained *WT* and *CKO* neurons striatum and tracings of these neurons alongside graphical representation of Sholl analysis in individual neurons from DM **and** DL. parts of the mouse striatum. For the Sholl analysis, the number of intersections was semi-automatically quantified between 10 and 120µm from the cell body. For Sholl analysis, the number of neurons per group is: 9 WT and 14 CKO for DM; and 10WT and 17 CKO for DL. * p<.05, **p <0.01. Scale bar is 50 µm.

4.5 Discussion

Genetic manipulation of laboratory mice is a useful tool in investigating the role of different genes *in vivo* and *in vitro*. In this project, I conditionally deleted *Mef2c* in the mouse striatum during early embryogenesis using the Cre-loxP recombination system under the control of the *Gsx2* promotor. *Gsx2* is abundantly expressed in the progenitor cells in the LGE and thus allows specific study of the role of Mef2c in striatal development. I have observed a characteristic anatomical phenotype in the adult Mef2c CKO mouse that strongly suggests a critical role of Mef2c in striatal development.

A comprehensive immunohistochemical assessment of the *CKO* and *WT* striatum was undertaken, mainly by analysing the presence of volumetric changes and the expression of the pan-neuronal marker NeuN and the three MSN markers FoxP1, Darpp32 and Ctip2 in a developmental series between P2 and 12 months. Assessment of striatal volume is an initial measure to assess the health status of the basal ganglia, especially in neurodegenerative diseases (Aylward et al., 2012). In this chapter I show that in the *WT* mouse, striatal volume increases by about 3.5-fold between P2 and 3 months. Most of this increase occurred between P7 and P14 (about 67%), with a further 27% increase occurring between P14 and 3 months as an expansion in striatal volume in medio-lateral direction. Mouse striatum reaches 95% of its adult size by three weeks postnatally. A mild reduction (~10%) in volume was noticed at 12 months, presumably due to age-related changes.

This increase between P2 and 3 months is in parallel with the rodent's whole brain volume, which undergoes a substantial increase between birth and toward adulthood (Bockhorst et al., 2008). Brain volume in rodents reaches 95% of its adult volume at the age of three weeks compared to 2-3 years in humans (Giedd et al., 1999; Semple et al., 2013). One explanation for this normal increase in the volume of mouse striatum, and the mouse brain in general, is the generation of glial cells through early postnatal development (Bandeira et al., 2009b), which peaks between postnatal day 7 and 10 (Catalani et al., 2002a). The striatal volume in *Mef2c CKO* mice also increased over the same period, but there was less of an increase compared to WT mice, resulting in the

striatum at 3 months of age in *CKO* mice being 18% smaller than *WT* mice of the same age.

The increase in striatal volume was associated with an increase in the expression of the neuronal marker NeuN and the mature MSNs marker Darpp32, which indicates an increased number of differentiated neurons. Although the trajectories of the counts of NeuN, FoxP1, Ctip2 and Darpp32 moved in the same direction in both WT and CKO, the increases were significantly less in the CKO. For example, the significant increase in Darpp32 positive cells observed in WT striatum between P2 and P14 was also observed in CKO, but to a significantly lower level (340% in WT compared to 290% in CKO). This applies also to NeuN in which 115% increase in NeuN positive cells occurred in WT compared to 71% in CKO. Unlike NeuN and Darpp32, FoxP1 was shown to label the maximum number of MSNs during development with a significant increase between P2 and P14 of 53%, compared to 43% in CKO. It is worth noting that no significant difference was observed between P14 and other later age groups in either WT or CKO, indicating that Mef2c is acting over the early postnatal period and that the anatomical and cellular changes in *CKO* mice in this thesis are non-progressive and do not worsen with advance of age.

My results are in line with (Zhang et al., 2019b) in which a knocking down of Zfhx3, which is a TF that downregulates through adulthood, causes significant reduction (about 20%) in each of striatal volume and the count of FoxP1 and Ctip2 in early postnatal striatum. But they contrast with other mouse models like *Emx-BDNF* CKO, in which *BDNF* is knocked down in the cortex and results in a significant and progressive reduction in NeuN count by 14% at P35, and by 35% in 1-1.5-year-old mice (Baquet et al., 2004). Assessment of MSNs markers expression provides valuable data about the health and differentiation status of the striatum. FoxP1 and Darpp32 were shown to be significantly downregulated in a mutant mouse striatum that lacked the transcriptional regulator Nolz1 that is expressed in all striatal MSNs; this downregulation was confirmed using transcriptomic analysis of E18.5 mutant mouse striatum (Soleilhavoup et al., 2020). The loss of FoxP1 this study was shown to cause to cause differential effects on gene expression in direct and indirect pathway. Furthermore, the expression of FoxP1 is selectively reduced in R6/2 and R6/1 mouse models of HD and in the caudate of patients

with HD (Louis Sam Titus et al., 2017; Desplats et al., 2006). Over-expression of mut-Htt caused reduced FoxP1, while overexpression of FoxP1 was shown to be protective against the cytotoxicity of mutant Htt. FoxP1 was also shown to be significantly reduced in adult striatum in Mef2c CKO mice in this thesis, about 18% reduction, indicating the major effect of Mef2c on striatal status and suggesting a mild, yet significant striatal neuronal loss.

Darpp32 is often considered as the ''gold standard'' marker of mature neurons (Precious et al., 2016; Gustafson et al., 1992; Ouimet et al., 1998). It is not expressed until E18 in the embryonic mouse striatum where it is expressed in the early-born patch ''striosomes'' neurons, as I have shown in this thesis and as reported in (Anderson et al., 1997; Chen et al., 2016; Anderson et al., 1997; Chen et al., 2016). The expression of Darpp32 in neonatal and early postnatal striatum is limited to MSNs that received input from substantia nigra that starts as early as E14 until P3. In WT, I showed that Darpp32 expression in mouse striatum increases through development and reaches 90% of its maximum expression at around P14, with no significant difference between its levels at P14 and later adult age groups. This suggests that the P14 striatum almost resembles the adult in the sense of mature MSNs content. In rats, a maximum expression of Darpp32 was observed at 3 weeks postnatally (Foster et al., 1987). Moreover, I have shown that almost all Darpp32 positive cells co-express the striosome marker MOR1 at P0, P2 and P7, which means that most mature MSNs at these time points are occupying striosomes. This increase in the expression of Darpp32 over the first two postnatal weeks suggests that the period of MSN maturation is longer than previously thought and certainly extends beyond the embryonic or early neonatal period.

The findings in this chapter suggests a role for the Mef2c TF in the development and maturation of MSNs and/or MSN proliferation. This will be discussed in detail in the next chapter using the proliferative markers BrdU and EdU, which have been introduced into *WT* and *CKO* mice at embryonic and postnatal time points to assess proliferation, neurogenesis, and survival of MSNs. In addition, the abnormal morphology of FoxP1 positive cells at P2 CKO striatum suggests that the effect of Mef2c loss might occur early in postnatal life, but not be detected until development is completed.

As described in chapter 3, the mouse striatum is organised anatomically and neurochemically into two main compartments, striosomes and matrix (Brimblecombe and Cragg, 2017b). Striosomes constitute between 10-15% of the overall striatum and they are occupied by MSNs born early between E11-E13. Striosomes are enriched with different markers, but the most common one is MOR1, which has been used by immunohistochemical methods to visualise striosomes (Anderson et al., 2020; Morigaki et al., 2020). The other striatal compartment is the matrix, which is occupied by the majority of MSNs that are born between E14-E16, and is enriched with calbindin D-28K (Gerfen et al., 1985; Liu and Graybiel, 1992).

The next step was to assess whether *Mef2c CKO* consequences described early in this chapter are specific to the matrix compartment. Calbindin-positive regions were found to be significantly decreased, which supports the conclusion that Mef2c is required for the development of matrix MSNs, but not striosomes. Therefore, in this chapter, I used immunofluorescence of MORI and calbindin to visualise striosomes and matrix respectively.

The importance of investigating the role of Mef2c in matrix-striosomes development arose from the previous findings that showed almost complete absence of Mef2c expression during striosomes MSNs neurogenesis and no co-localisation between Mef2c and Darpp32 in P0 mouse striatum. Here, Darpp32 was shown to be expressed in striosomes only, in early postnatal striatum. Furthermore, the birth-dating experiment using EdU performed in this chapter, showed Mef2c to be expressed in E14, and to lower extent in E16, born MSNs, but not at E12. All of this led me to the conclusion that Mef2c is not required for the normal development of striosome MSNs. The finding that the percentage area of striosomes has increased while the overall striatal volume decreased further supported this conclusion. I found that Mef2c loss has differential effects on the normal organisation of striosome-matrix compartments. In the adult mouse striatum, the percentage of cross-sectional area of striosomes was significantly increased in *CKO*, while the percentage area of matrix was significantly decreased. Alterations in normal striatal development might impact the normal organisation and compartmentation of matrix and striosomes.

Imbalances between matrix-striosomes might contribute to the generation of abnormal behaviour depending on which compartment is mostly affected (Canales and Graybiel, 2000; Saka et al., 2004). For example, conditional knock out of FoxP1 in dopamine receptor D1 (DRD1), DRD2 and both DRD1/DRD2-expressing cells was shown to cause a significant reduction in the percentage striosome area along with a significant reduction in the overall number of striosomes (Anderson et al., 2020b) . Furthermore, the differential loss of dopaminergic neurons in striosomes compartment only in a mouse model of Dopa-responsive dystonia (DRD) was thought to be critical to the motor dystonic symptoms observed (Sato et al., 2008).

Dendritic spines are small bulbous protrusions of dynamic morphological structures along the neuronal dendrites at which neurons form synapses with other neurons. The shape and density of spines are extremely variable according to the location in the brain and synaptic activity, which is crucial in brain development and in learning and memory functions (Parker et al., 2020; Arellano et al., 2007). In the mouse striatum, most of these spines form synapses with glutamatergic excitatory input from the cortex and thalamus, or from dopaminergic input coming from the midbrain (David Smith and Paul Bolam, 1990; Bolam et al., 2000).

Previous studies have shown that MEF2 transcription factors A and D play a role in synaptogenesis and dendritic spine development by acting mainly as suppressors of spine formation (Flavell et al., 2006). This initial finding of *MEF2* TFs involvement in the regulation of synapses in brain regions related to learning and memory functions as frontal and entorhinal cortex and dentate gyrus of hippocampus raised the question whether Mef2c plays a similar role in the striatum. Subsequent research has strongly revealed a strong association between Mef2c expression and neuropsychiatric diseases resulting from the imbalance of excitatory/inhibitory synapses formation (Zhang and Zhao, 2022). I found Mef2c loss causes disruption to the process of dendritic tree resulting in an increase in numbers of dendritic intersections. Alterations in the dendritic tree and spine development in basal ganglia have previously been reported to be involved in impairment of motor learning (Dang et al., 2006).

In my research I used Golgi Cox staining, which is a reliable method for visualising dendritic arborization and dendritic spines (Y, 2013). The Golgi Cox staining method was

amended by me to enhance the visualisation of fine dendritic spines. The Golgi cox analysis of the striatum presented here in adult WT and *Mef2c* CKO mice revealed that Mef2c plays a significant role in the development and complexity of the dendritic tree in DM aspects of the striatum, but a less significant role in the DL. One possible explanation of this selective effect is the continued postnatal expression in DM of Mef2c that extends into postnatal period critical for dendritic spine and axonal development (Bockhorst et al., 2008; Baloch et al., 2009). The age at which the analysis was performed in my research is 3 months to make sure that dendrites and spines are in their mature state. In addition to the finding that Mef2c expression is retained in adult striatum only at the most medial aspects of the striatum, there is minimal/complete loss of Mef2c in the DL aspect from P14 onward. The striatal excitatory input onto MSNs in the DM striatum reaches a maximum maturation period between P10-P18 (Peixoto et al., 2016), and any abnormality in this early postnatal maturation may contribute to the alterations in normal dendritic development.

This effect on the dendritic tree complexity as shown by my Sholl analysis is in line with (Kamath and Chen, 2019a) who found that *Mef2c CKO* in GABAergic cerebellar neurons significantly increased the overall numbers of dendritic intersections in purkinje cells, which are very morphologically complex neurons. No data on number of dendritic spines were published to compare with. No significant effect was observed in the density of dendritic spines in this thesis, which contradicts with other findings in a *Mef2c CKO* in viral-induced P2 mouse striatum that showed a significant increase in spine density (Chen et al., 2016). One contributing factor for this difference could be the timing of knockout, as it was shown before that *CKO* of Mef2c during embryonic development in Emx1-lineage derived excitatory neurons results in a reduction of spine density (Harrington et al., 2016a), while postnatal CKO results in an increase of spine density (Adachi et al., 2016a). This indicates that the consequences of *Mef2c* knock down are distinct depending on whether it occurs during embryonic development or postnatally in postmitotic neurons.

Proper dendritic morphogenesis of striatal MSNs is a key component of the normal development of striatal neural circuitry and the integration of synaptic input. Mef2c has been identified in many published works as an important regulator of dendrites and

dendritic spines formation (**table 1.5**). The relatively small influence of Mef2c loss in mouse striatal MSNs dendritic architecture in this thesis was surprising and the possible explanation of this modest effect as explained earlier could be due to the ''timing'' of the knockout. There are many TFs that play several roles in the regulation of the morphology of synapses in the developing mouse striatum.

4.6 Conclusion

In the light of the results obtained in this chapter, Mef2c TF was found to be required for the normal development of striatal MSNs and its loss results in smaller striatae and disturbs the overall MSN count from P14 onward in the CKO striatum. The effect of *Mef2c* CKO was first statistically significant at P14 but not before, furthermore, NeuN and MSN counts did not further decrease after P14, indicating that Mef2c is acting over a period earlier than P14. It was also shown that the striatal neuronal loss occurs in a compartment-specific manner based on the significant increase in the percentage area of striosomes accompanied by the significant reduction in the percentage area of the matrix compartment, indicating a differential effect on matrix-striosomes pattern in a mouse striatum lacking Mef2c expression. The importance of this finding is that the different cortical projection to these two distinct compartments means that their functional roles will be distinct. Thus, it is anticipated that an aberration in matrix MSNs circuitry could lead to motor dysfunction, and this will be tested in chapter 6.

Chapter 5: Assessment of proliferation, neurogenesis, and survival of MSNs in the mouse striatum

5.1 Summary

Mef2c loss in the mouse striatum was associated with immunohistochemical phenotypes that suggest that Mef2c acts early during the striatal neuromaturation period taking place during the first two postnatal weeks. The loss of MSNs described in chapter 4 was not shown to be progressive over time as no further neuronal loss was observed in the MSNs of the CKO striatum after P14. Previous research showed Mef2c to play an important role in neurogenesis, differentiation and survival of neuronal tissue using an in vitro approach.

Therefore, in this chapter I asked whether Mef2c loss led to changes in proliferation or apoptotic activity in early postnatal mouse striatum. This was assessed using proliferation and cell death assays in vivo and in vitro in cultures of embryonic striatal tissue. No effect on proliferation was seen, but it was shown that Mef2c loss in Gsx2-expressing NPCs in the developing LGE resulted in a significant increase in apoptotic activity in the early postnatal striatum and within the first 24 hours in both E14 and E16 cultured MSNs. These data support the notion that Mef2c is required for neuronal survival in mouse brain, including the striatum.

5.2 Introduction

In chapter 4, it was shown that Mef2c loss in the developing mouse striatum resulted in various histological phenotypes in P14 and adult *CKO* striatum. Among these, a significant reduction in striatal volume that resulted from neuronal loss was observed. This reduction appeared to be predominantly due to the loss of MSNs in the striatal matrix compartment but not in striosomes. In this chapter the functional role of Mef2c in the biological processes proliferation, neurogenesis, and survival of MSNs was investigated *in vivo* and *in vitro*.

In the CNS, Mef2c TF has been demonstrated to be critical for neurogenesis and neural differentiation (Li et al., 2008; Tu et al., 2017; Skerjanc and Wilton, 2000) . Mef2c has also been shown to play a crucial role in neuronal survival by interacting with apoptotic and anti-apoptotic pathways during neuronal differentiation (Mao et al., 1999; Okamoto et al., 2000; Li et al., 2008; Okamoto et al., 2014). The overall number of MAP2 positive neurons was increased and the increased apoptotic neuronal activity after p38 alpha inhibition was rescued after Mef2c overexpression in the P19 cell line (Okamoto et al., 2000). Mef2c was also shown to be necessary for adult neurogenesis in the mouse hippocampus, with *Mef2c* heterozygous mice showing a significant downregulation in neurogenesis genes and reduced NeuN expression observed in the hippocampus of adult mouse (Tu et al., 2017b). The role of Mef2c in striatal neurogenesis has not been previously explored. Although striatal neurogenesis appears to be complete by adulthood, it has been reported that striatal neurogenesis continues during early postnatal life in rats (Wright et al., 2013b), although no similar reports in mouse striatum are available to date.

The compartment-specific and non-progressive reduction of striatal MSNs, combined with our knowledge of the spatiotemporal pattern of Mef2c expression from chapter 3 (peaking at P0 and negligible in the adult striatum) raised the question as to whether *Mef2c* could be acting early during embryonic and early postnatal development. This potential effect could be through affecting neurogenesis and/or cell survival of a subpopulation of matrix MSNs during MSN maturation in the first two weeks postnatally

(Novak et al., 2013; Fishell and van der Kooy, 1987; Fishell and van der Kooy, 1989; Matsushima and Graybiel, 2020; Dehorter et al., 2011).

In the light of the published literature on the involvement of Mef2c in neuronal development and the key results obtained so far in this thesis including our knowledge of the expression pattern of Mef2c, the objectives of this chapter were:

1. To assess the overall proliferation in the postnatal mouse striatum of WT and CKO mice.
2. To assess the proliferation of the NPCs in the WT and CKO LGE during embryonic development.
3. To assess the overall apoptotic activity in WT and CKO early postnatal striatum, and in striosomes and matrix compartments. It is worth mentioning here, that neuronal turnover early after birth is a normal physiological process in all mammals, that is crucial for brain development and learning (Kuan et al., 2000; Buss et al., 2006).
4. To assess the expression of the most known apoptotic and anti-apoptotic genes in postnatal WT and CKO mouse striatum.
5. To assess the proliferation, neurogenesis, and survival of tdTomato positive NPCs in E14 and E16 cultured WT and CKO LGE.

5.3 Experimental procedures

To assess overall proliferation, four groups of WT and CKO mice received three intraperitoneal injections of BrdU as described in **Figure 5.1 a** below. To assess the proliferation of NPCs during embryonic development, time-mated pregnant dams from the breeding strategy described in **2.1.2.1** were injected with the proliferative marker EdU at specific time point during embryonic development as described in Figure **5.1 b.** EdU was used instead of BrdU in the analysis at P0 to avoid the harsh HCL treatment.

To assess overall apoptotic activity in early postnatal mouse striatum, and in matrix-striosomes compartment, free-floating IHC of cleaved caspase 3 and MOR1 in P0, P3, P7 and P14 was conducted as in **2.3.4.** Gene expression analysis of the proapoptotic and anti-apoptotic genes was conducted using the primers listed in table **2.4**.

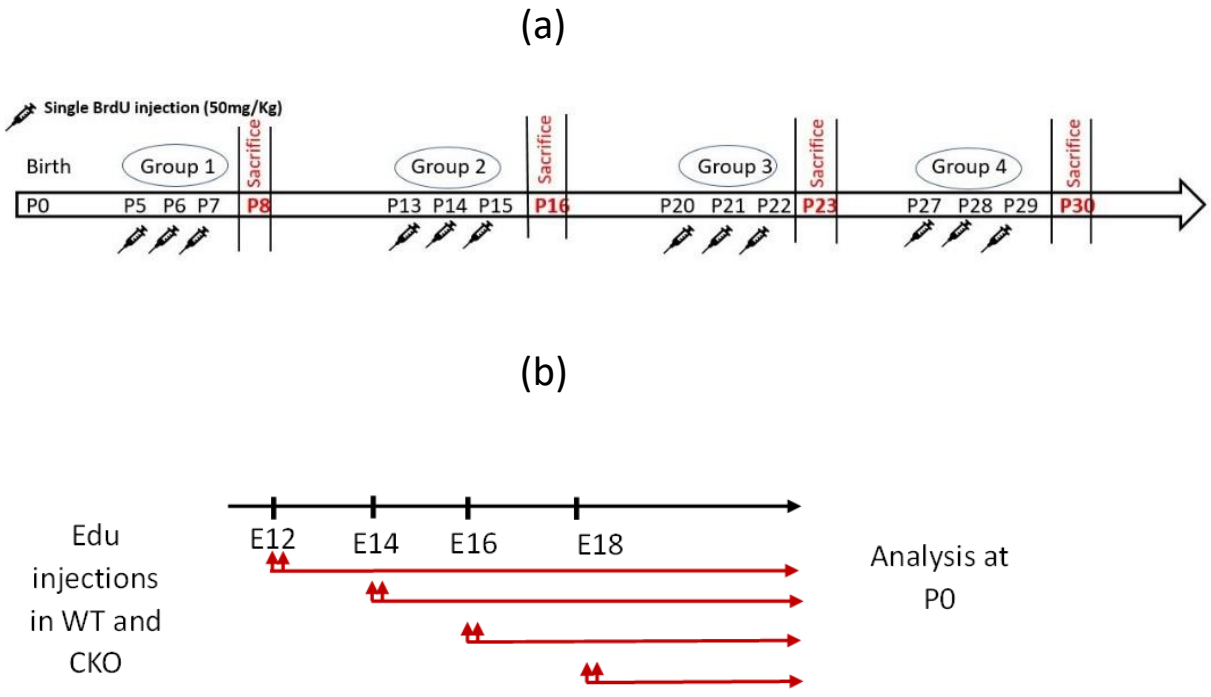

Figure 5.1 Experimental design of BrdU experiment (a) and EdU experiment (b) in this chapter.

5.4 Results

5.4.1 Striatal Mef2c loss has no effect on postnatal proliferation in the mouse striatum compared with *WT* mice.

In the previous two chapters, it was shown that Mef2c CKO mice have smaller striatae with fewer neurons by the end of the 2nd postnatal week, and that Mef2c is most highly expressed in the striatum over this period. Thus, the first step was to ask whether Mef2c loss has resulted in less cell proliferation over this period. This was done using BrdU to label proliferating cells (Tsai et al., 2012), **Figure 5.2**. Since no apparent difference in the distribution of proliferating cells was observed between medial and lateral aspects of the striatum **Figure 5.2a,** all analysis performed in this section was done for the whole striatum. The details of the groups and the timing of *BrdU* injections are summarized in **Figure 5.2b**.

Proliferation in the mouse striatum was quantified and analyzed in the four different postnatal groups. *Mef2c* loss did not show any effect on the overall postnatal proliferation across the four groups (Age x Genotype; $F_{(3, 27)} = 0.0021$, p=0.99, two-way ANOVA) see **Figure 5.2c**. However, there was a significant difference in proliferation between the different groups (Group; $F_{(3, 27)} = 152.7$, $p<0.0001$). The proliferation in mouse striatum in group 1, the group that received three BrdU injections at postnatal days 5, 6 and 7, was significantly higher than the proliferation in the other three groups, as illustrated in **Figure 5.2b**. No significant difference was observed in the total number of BrdU positive cells between *Mef2c CKO* and *WT* (Genotype; $F_{(1, 27)} = 0.001$, $p = 0.973$).

Ki67 expression was assessed in group2 to see if the count of this proliferative marker showed the same pattern of BrdU counts. There was no significant difference in the overall ki67 positive cells between WT and CKO in P16 mouse striatum ($t_{(6)} =0.4162$, p=0.96, unpaired t test), **Figure 5.2d**.

Proliferation in the SVZ, was not quantified but it was clearly highest in group 1, with no apparent changes between groups 2 and 3, and it appeared substantially reduced in group 4, **Figure 5.2a**.

(a)

	BrdU injection timing	Sacrifice
Group 1	P5, P6 & P7	P8
Group 2	P13, p14 & P15	P16
Group 3	P20, P21 & P22	P23
Group 4	P27, P28 & P29	P30

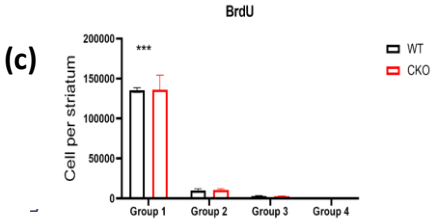

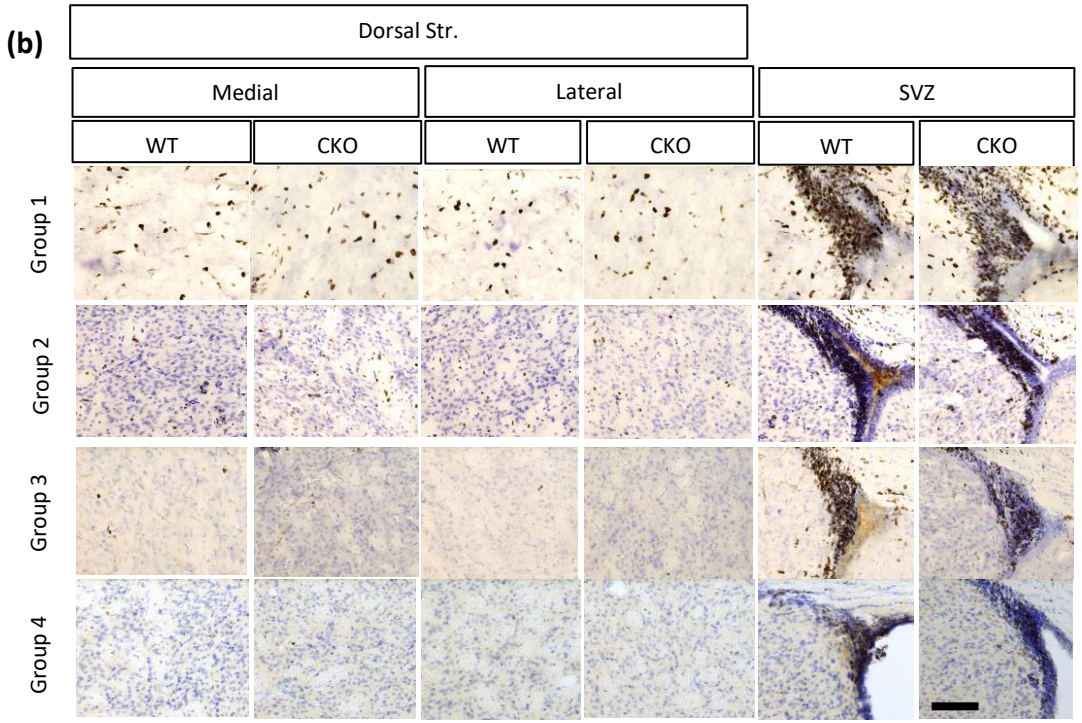

Figure 5.2: Mef2c does not affect overall proliferation in postnatal *CKO* striatum compared with *WT* as measured by BrdU uptake.

(a) The number of injections received and timing of sacrifice per group. **b)** Representative images of BrdU IHC, counterstained with cresyl violet, showing proliferation in mouse striatum and SVZ in four groups. In the striatum, more labelled cells can be seen in group 1, with fewer immuno-positive cells seen throughout medial and lateral aspects of the striatum in groups 2 and 3, and almost complete absence of cell proliferation in group 4. Robust and intense labeling of dividing cells can be seen in the SVZ of group 1,2 and 3, while the proliferative activity is decreased in group 4. Scale bar = 100µm. (**c**) Graphical representation of overall BrdU positive cells in the striatae, showing that BrdU positive cells in group 1 are significantly higher than in other groups (*** p <0.0001). There was no significant difference in the total count of BrdU +ve cells between *Mef2c CKO* mice and wild-type controls (Genotype: p=0.97) and no significant interaction (Genotype x group p=0.99). The graph shows means ± SEM. n = Group 1: (WT=4, CKO=4); group 2: (WT=4, CKO=5); group 3 (WT=5, CKO=4); and group 4(WT=4, CKO=4).

5.4.2 Mef2c has no effect on the proliferation of NPCs in LGE during embryonic development.

Next, we asked the question whether the predominant effect of knocking down *Mef2c* during development is on the proliferation of MSNs during embryonic neurogenesis. To test this, I compared the proliferation of NPCs in *CKO* and *WT* mouse striatum during embryonic development by use of the proliferative marker EdU, **Figure 5.4**. EdU was used instead of BrdU for better compatibility to use with delicate P0 mouse sections (Angelozzi et al., 2021). EdU becomes permanently incorporated into proliferating cells and can then be detected using a Click-iT™ reaction. EdU was injected intraperitoneally in time-mated pregnant females at E12, E14, E16 or E18 and pups were culled at P0 to allow enough time for postmitotic neurons to migrate to their destination and see if they continue to survive until P0.

In *WT* mouse striatum EdU incorporation was significantly different between the four age groups ($F_{(3, 17)} = 14.24$, $p < 0.0001$, one-way ANOVA) see **Figure 5.3**. Pairwise comparison using Tukey's test showed that the maximum incorporation was observed at E14 (P<0.0001, compared to every other age group) and E16 came next (p<0.0001 compared to other age groups). There was no significant difference in EdU positive cells between E12 and E18 (p=0.338). At E12, EdU staining was ''patchy'' in appearance and likely to be occupying striosomes in the mouse striatum (white outlined regions in **Figure 5.4a**).

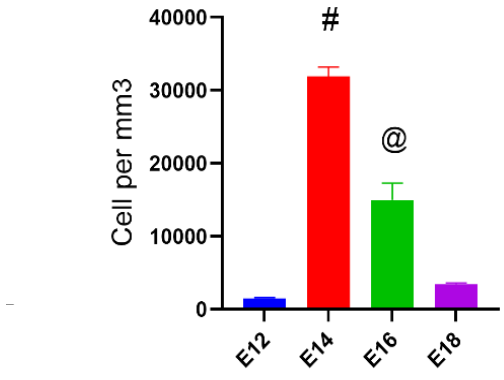

Figure 5.3: EdU Quantification of EdU in WT only striatum revealed peak integration at E14 (p<0.0001). Bar graphs are means ± SEM.

There was no significant difference between *Mef2c* C*KO* and WT in the density of proliferating cells injected with EdU at E12 **(Figure 5.4b),** E14 **(c**), E16 **(d)** or E18 **(e),** per mm^3 in the whole striatum nor when dorsal and caudal striatum were analyzed separately.

Table 5.1 shows a summary of the results of multiple t-tests using Holm-Šídák method and n per group.

	n per group		***P value***		
	WT	***CKO***	***overall***	***Dorsal***	***Caudal***
E12	***5***	***3***	***0.438370***	***0.407959***	***0.891814***
E14	***3***	***3***	***0.212947***	***0.771708***	***0.179816***
E16	***3***	***4***	***0.143678***	***0.838481***	***0.286452***
E18	***7***	***4***	***0.586912***	***0.584114***	***0.701625***

Table 5.1 A summary of n per group and p values at the four time points in WT and CKO.

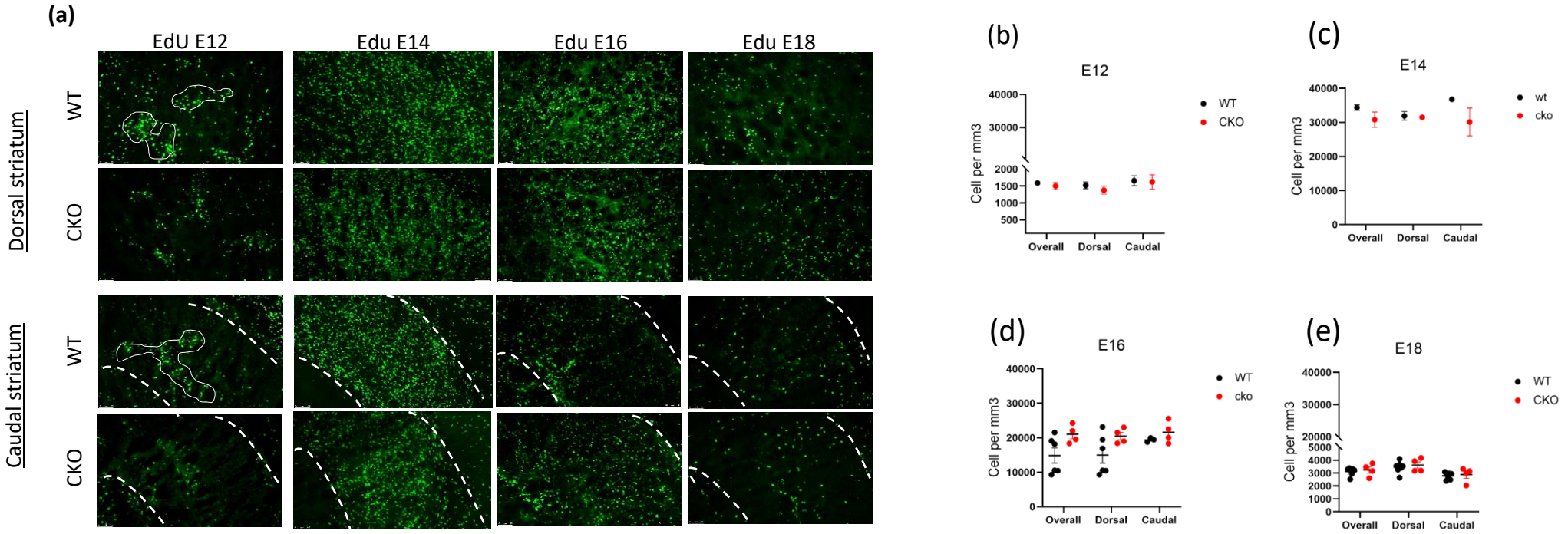

Figure 5.4: No significant effect of striatal Mef2c loss on the proliferation of neural progenitor cells during embryonic development in CKO mouse LGE compared with control.

(a) Detection of the proliferative marker EdU (green) in WT and CKO mouse coronal striatal sections of dorsal (upper two panels) and caudal (lower two panels) of P0 brains, white-dashed areas represent the ''patchy'' appearance of EdU incorporation in E12 mouse striatum and the boundaries of the caudal striatum. (b- e) Graphical representation of the overall number of EdU positive cells per mm3 at E12, E14, E16 and E18 analyzed at P0 striatum with dorsal and caudal striatum analyzed separately to detect any region-specific effects. No significant difference was found between Mef2c CKO and WT. The statistical test performed is multiple t tests with Sidak-Holm correction. Graphs show means ± SEM. **** = $p<0.0001$, n per group and p values are summarized in g.

5.4.3 Mef2c loss induces increased apoptosis in early postnatal mouse striatum

Next, I asked the question whether knock down of *Mef2c* during development affects the cell death of MSNs in the first two weeks of postnatal life**.** Since the proliferation of NPCs in the developing LGE are not different in *Mef2c CKO* and WT mice, survival of MSNs in early neonatal and postnatal mouse brain was assessed to see whether the reduction in striatal MSNs in *Mef2c CKO* mice reported in chapter 4, could be due to alterations in mechanisms regulating MSNs survival, using cleaved caspase 3 IHC. Cleaved caspase 3 is a marker of cell death through apoptosis and considered as an essential factor for mediation and initiation of DNA destruction (Cohen, 1997).

Expression of cleaved caspase 3 was different in mouse striatae at different postnatal ages **(Figure 5.5).** For both WT and CKO, the numbers of cells expressing cleaved caspase 3 rose from P0 to P3, where it peaked, and then fell again by P7, reading the lowest levels by P14. There was a significant effect of genotype over age (Age x genotype $F_{(3, 60)} = 4.086$, $p=0.0105$, two-way ANOVA). Specifically, there was an increased total number of cells undergoing apoptosis in CKO striatum (244± 26.6) compared with WT(139.3±38.9) at P3 (Bonferroni post hoc, $p =0.0017$). There was a trend to an increased number of caspase positive cells at P0 but this did not reach significance.

The high magnification images in (**Figure 5.5d**) show cleaved caspase 3 immuno-positive neurons in the CKO striatum at the four age groups. It clearly shows that at P0 and P3, the apoptotic neurons appear intact, with morphological structure resembling neurons. In contrast, those at P7 and P14 are smaller and more condensed in shape, suggesting that an early stage of apoptosis was taking place at early age groups but not the late ones.

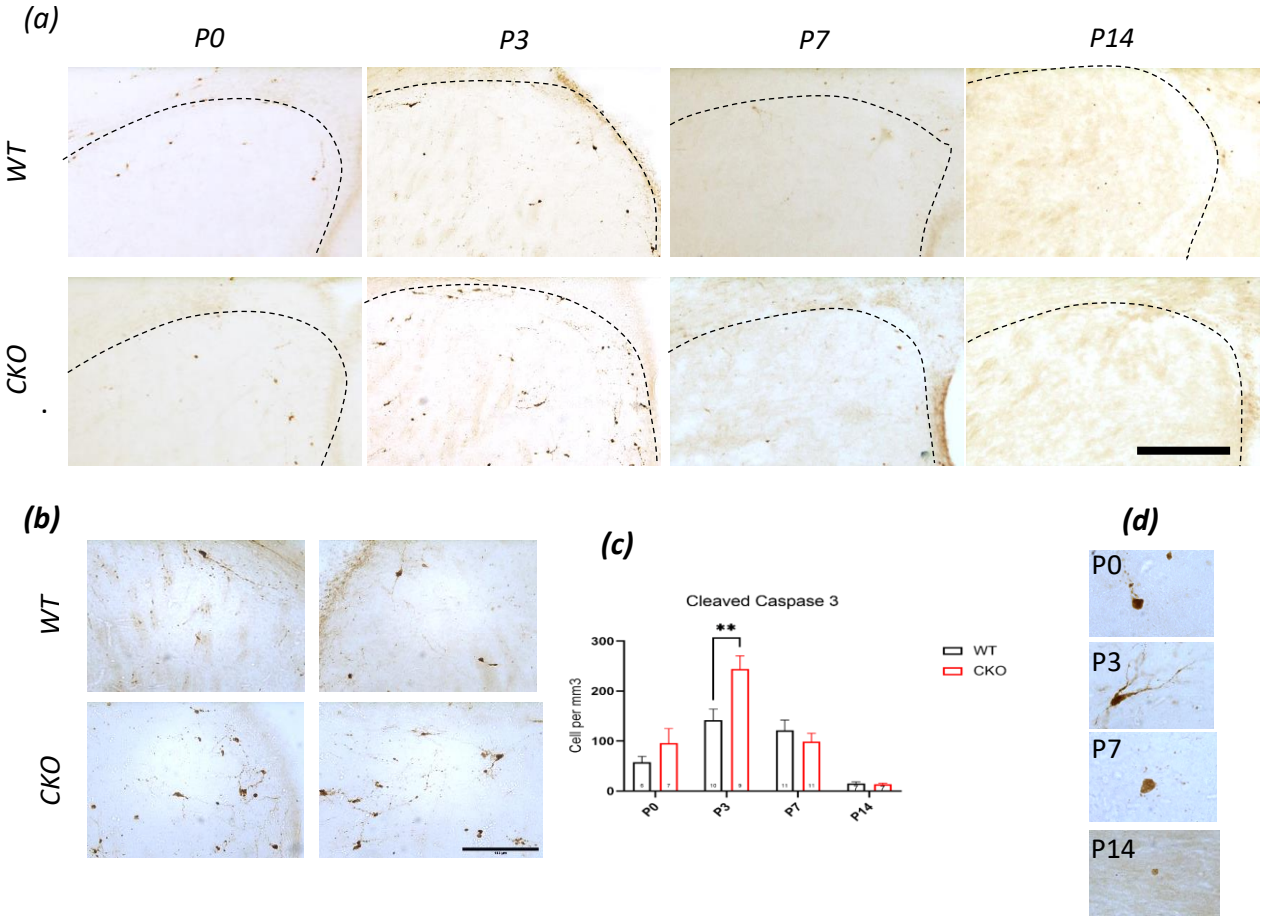

Figure 5.5: IHC of Cleaved caspase 3 in WT and Mef2c CKO postnatal mouse brain at postnatal day 0, 3, 7 and 14.

(a) Mouse coronal sections showing anatomically matched mouse striatae at the four ages with a clear increase in immunoreactivity of cleaved caspase 3 in KO mouse striatum at postnatal day 3 (age X genotype, $p < 0.05$). (b) Higher magnification of P3 in WT (upper panel) and CKO (lower panel). (c) Quantification of number of cleaved caspase 3 positive cells per mm3. (d) Representative neurons stained for cleaved caspase 3 imaged at 630X magnification in P0, P3, P7 and P14 CKO striatum, showing variation in the morphology of the apoptotic cells. Scale bars in a and b are 200 and 100µm respectively. P= 0.0017. The graph represents means ± SEM. n per group is shown at the bottom of each bar graph. ** = $p<0.01$.

5.4.4 Increased apoptotic activity in the matrix compartment of P3 Mef2c CKO mouse striatum but not in striosomes.

MOR1 is the canonical marker of striatal striosomes in postnatal mouse striatum as described in chapter 3. The striatal matrix compartment is enriched with calbindin, but at P3, the time point of interest in this experiment, calbindin is also expressed in striosomes. Therefore, expression of MOR1 was used to distinguish between striosomes and the surrounding matrix to see if there is a compartment-specific effect of Mef2c loss. Double labelling of cleaved caspase 3 and MOR1 was performed on P3 mouse brain sections, and the number of cleaved caspase 3 cells was determined in matrix and striosomes individually, **(Figure 5. 6)**. Black arrows in **(Figure 5.6a**) represent apoptotic cells.

The number of apoptotic cells per mm^3 was significantly higher in CKO compared to WT in the matrix compartment ($t_{(5)} = 5.117$, p=0.007, multiple t-tests with Holm Sidak correction), but no significant difference within the striosomes ($t_{(5)} = 0.5783$, p=0.588) was observed **(Figure 5.6b)**.

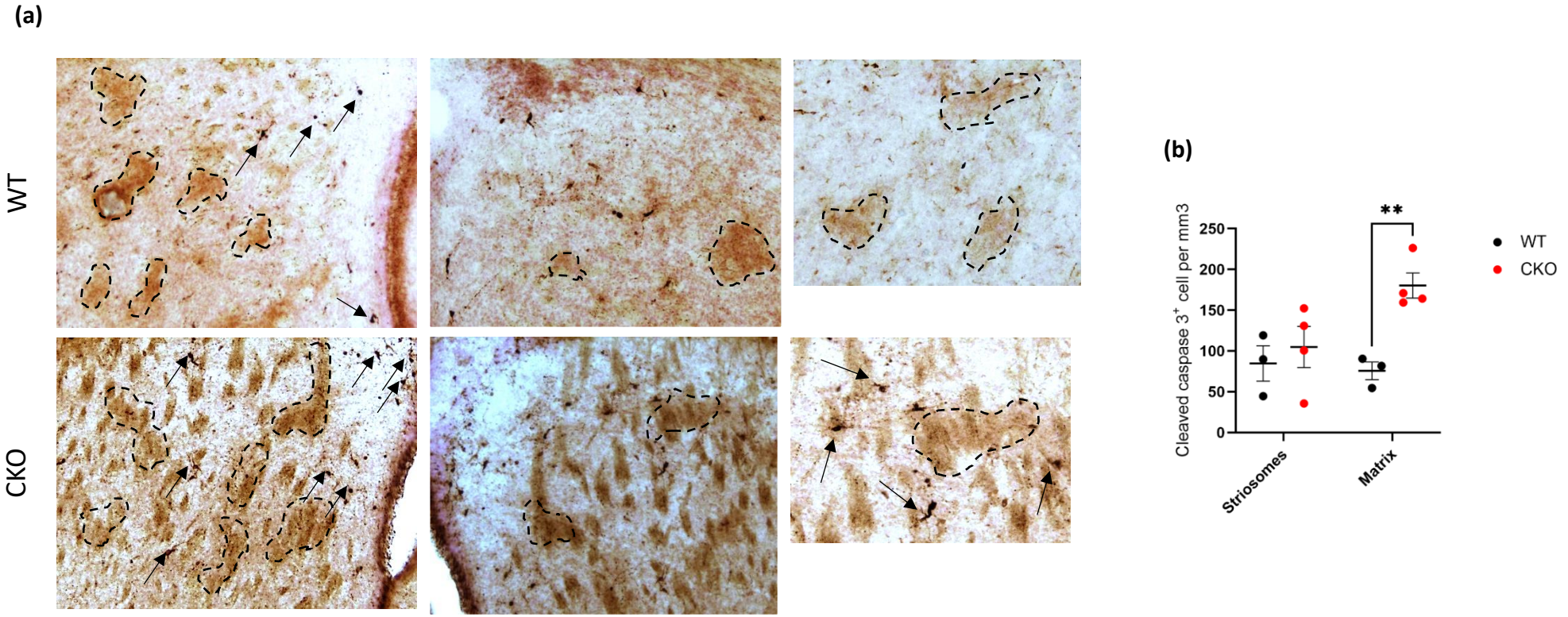

Figure 5.6: Increased apoptotic activity in the matrix compartment of P3 *CKO* mouse striatum but not in striosomes. **(a)** Double IHC of cleaved caspase 3 (black arrows) and MOR1 (black dashed regions) in P3 mouse striatum. **(b)** Quantification of cleaved caspase 3 expressing cells per mm^3 in striosomes ($MOR1^+$) and matrix ($MOR1^-$) revealed a significant increase in the number of apoptotic cells in the matrix compartment of the CKO P3 striatum (**p=0.007) while no difference was observed in striosomes (p=0.588). Dots represent XXX ** = p< 0.01

5.4.5 Assessment of expression of apoptotic and anti-apoptotic genes in the mouse striatum of P0, P3, P7 and P14 using RT qPCR

Along with the assessment of cleaved caspase 3 IHC, RT qPCR of known cell death/survival genes was performed to look for a potential role for Mef2c on the expression of any of these genes. Results are normalized to two housekeeping genes: GAPDH and βactin. Multiple t-tests with Holm-Sidak correction were conducted **(Figure 5.7).**

The expression of caspase 3 was found to be significantly higher in CKO compared to WT at P3, ($t_{(4)}$ =6.580 p = 0.0112) **(Figure 5.7a)**, but no significant difference was observed between WT and CKO in P0, P7 or P14 (p=0.345, 0.678 and 0.654, respectively).

The second gene assessed was Bcl xl gene, which is an anti-apoptotic protein coding gene that was found to interact with *Mef2c* (Li et al., 2008e). The expression of Bcl xl gene was assessed in the four age groups. Despite a trend for Bcl xl expression to be lower in CKO compared to WT across the four age groups, it was significantly reduced in *CKO* mice only at P3 ($t_{(4)}$ = 6.239, p=0.0133) **(Figure 5.7b)**.

Bcl2 is another anti-apoptotic factor that was assessed in this experiment. Interestingly, in contrast to Bcl xl, the expression of this anti-apoptotic factor was not significantly different at P3 (**Figure 5.7c**). At P0, P3, and P14 its level was shown to be increased which was significant only at P7, indicating a proposed compensatory or protective mechanism ongoing in CKO mice at P7.

Fourth, I assessed the expression of BAD gene which is a positive regulator of cell death (promotes apoptosis) and binds to Bcl xl and Bcl2 to deactivate their protective roles (Jiang et al., 2013). The levels of BAD were significantly increased at P0 ($t_{(4)}$ =4.401, p=0.012) (**Figure 5.7d)**. An increase was also observed at P3, but this was not significant (p=0.199). No significant difference was noticed at P7 or P14.

The level of Cytochrome c has increased by 2.5 times at P0 in the CKO; however, this difference was not statistically different between WT and CKO, and there was no significant difference at any age (**Figure 5.7e**). No significant difference in the expression of caspase 9 between WT and CKO was observed in the four age groups (**Figure 5.7f**).

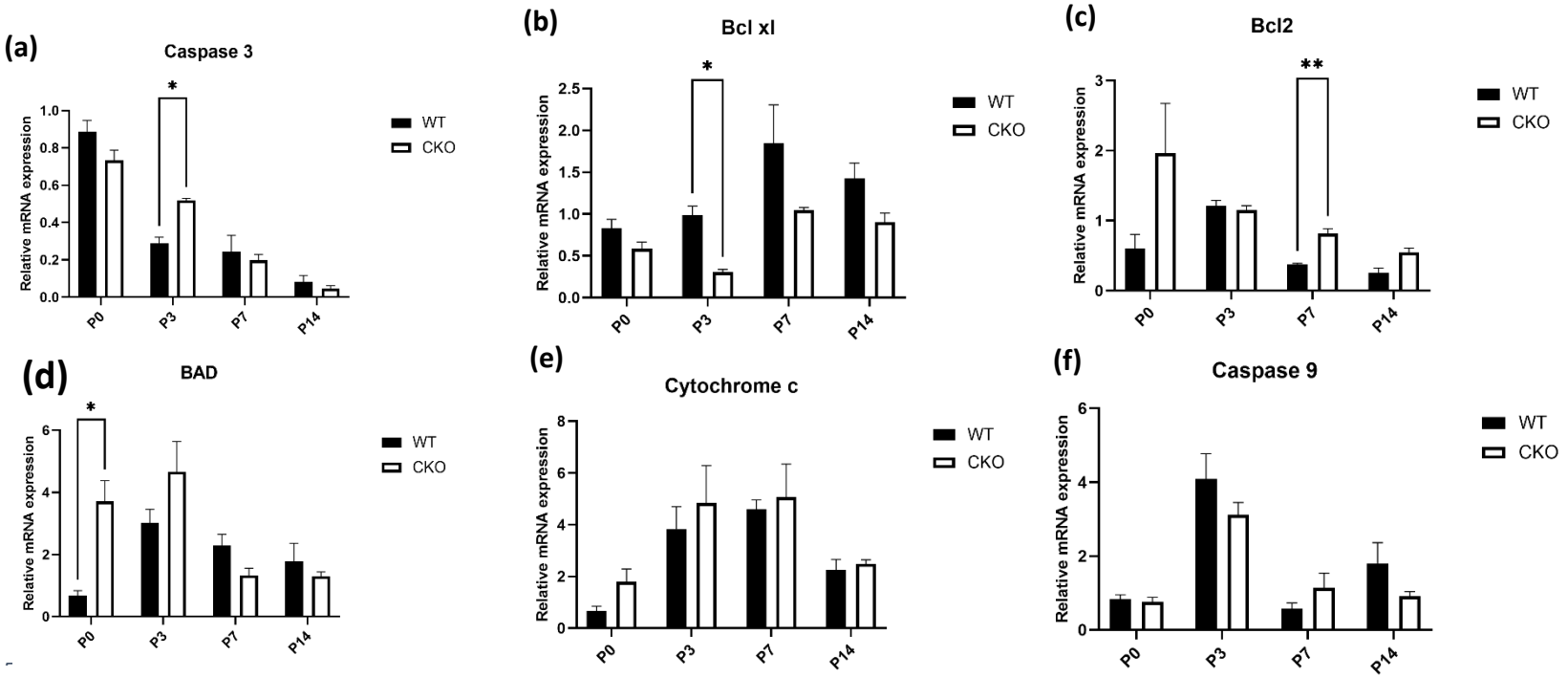

Figure 5.7: Mef2c loss affects normal expression of apoptotic and anti-apoptotic genes in early postnatal mouse striatum. mRNA expression in P0, P3, P7 and P14 postnatal mouse striatum of apoptotic and anti-apoptotic genes: **(a)** Caspase 3; **(b)** Bcl xl; **(c)** Bcl2; **(d)** BAD; **(e)** Cytochrome c; **(f)** Caspase 9. * = $p<0.05$, ** = $p<0.01$. Bars on the charts represent means ± SEM.

5.4.6 The effect of Mef2c CKO on the proliferation, maturation, and survival of MSNs *in vitro*

Next, an *in vitro* approach was used to investigate the consequences of Mef2c loss on primary striatal NPCs, by looking specifically at proliferation, neurogenesis, maturation, and survival of MSNs at cellular level in culture, to reduce the masking of any effect by biological compensatory mechanisms that may occur in the whole organism. Furthermore, data in the previous two chapters demonstrated that Mef2c expression starts to be detected at E14 and it is associated with matrix MSNs. Therefore, the focus of the culture experiment was on E14 and E16 MSNs to obtain cell cultures enriched with striatal matrix MSNs. RFP expression was used as a marker of MSNs in the rest of this section. The experimental plan is shown in **Figure 5.8a.**

In the literature, various concentrations of EdU were recommended to be added to the neuronal growth medium (Chehrehasa et al., 2009). Here, a pilot experiment was performed to optimize the dose of EdU. Two concentrations, 10 and 20 µM, were tested and no difference in the detection of proliferating cells in either WGE or cortex cultures 24 hours post EdU administration was observed **(Figure 5.8b)**. Therefore, 10 µM was used throughout these *in vitro* proliferation studies to minimize the exposure of cells to extrinsic factors that could affect their ability to proliferate and differentiate normally.

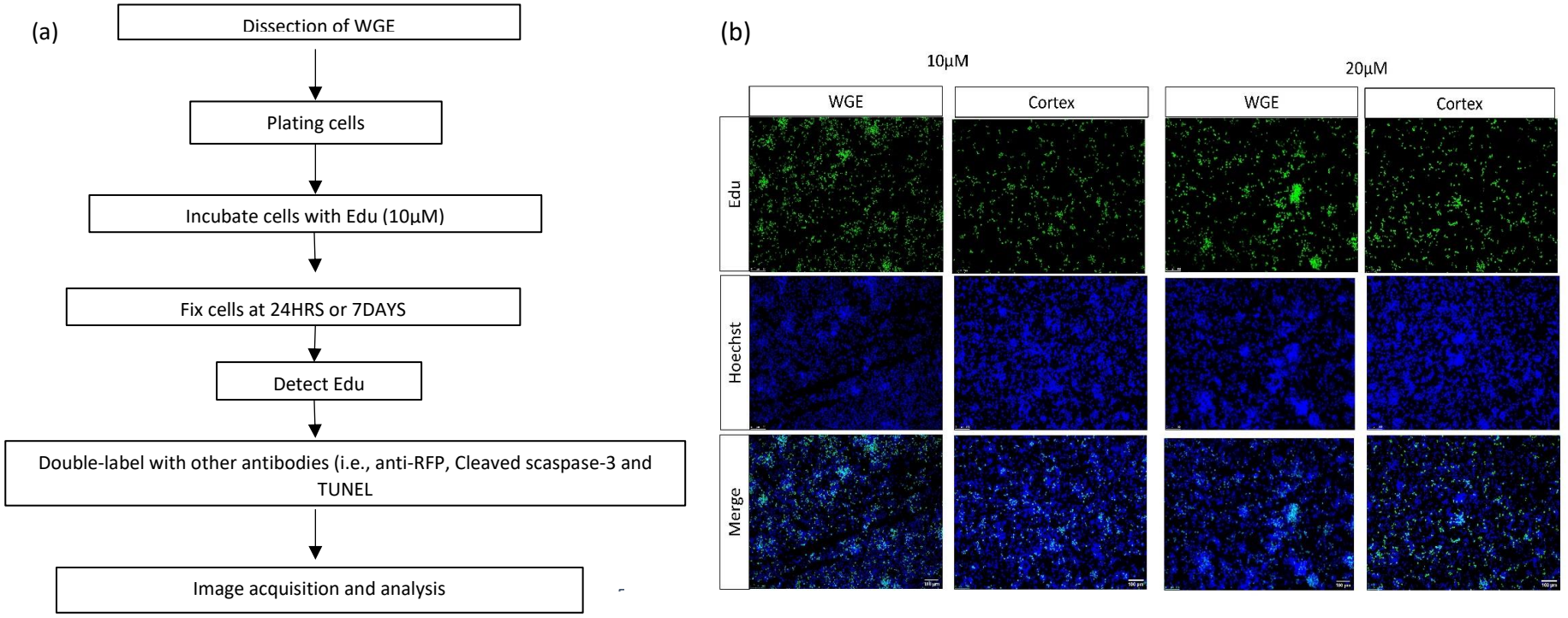

Figure 5.8: A summary of the experimental plan of the culture experiment using the proliferative marker Edu. **(a)** flow diagram for experimental plan. **(b)** Detection of Edu (green) and Hoechst (blue) of the pilot experiment performed for optimizing the dose of EdU used. No obvious difference was noticed in the overall proliferation between the two doses (10µM and 20µM) added to the medium of the cultured cells fixed at 24hrs in WGE and cortex. Scale bars = 100µm.

Gsx-2 cre reporter was shown to be strongly expressed in MSNs in chapter 3, therefore, in this chapter, the expression of TdTomato was used to represent MSNs, **Figure 5.9a.** All TdTomato positive cells were MAP2 positive **Figure 5.9b.**

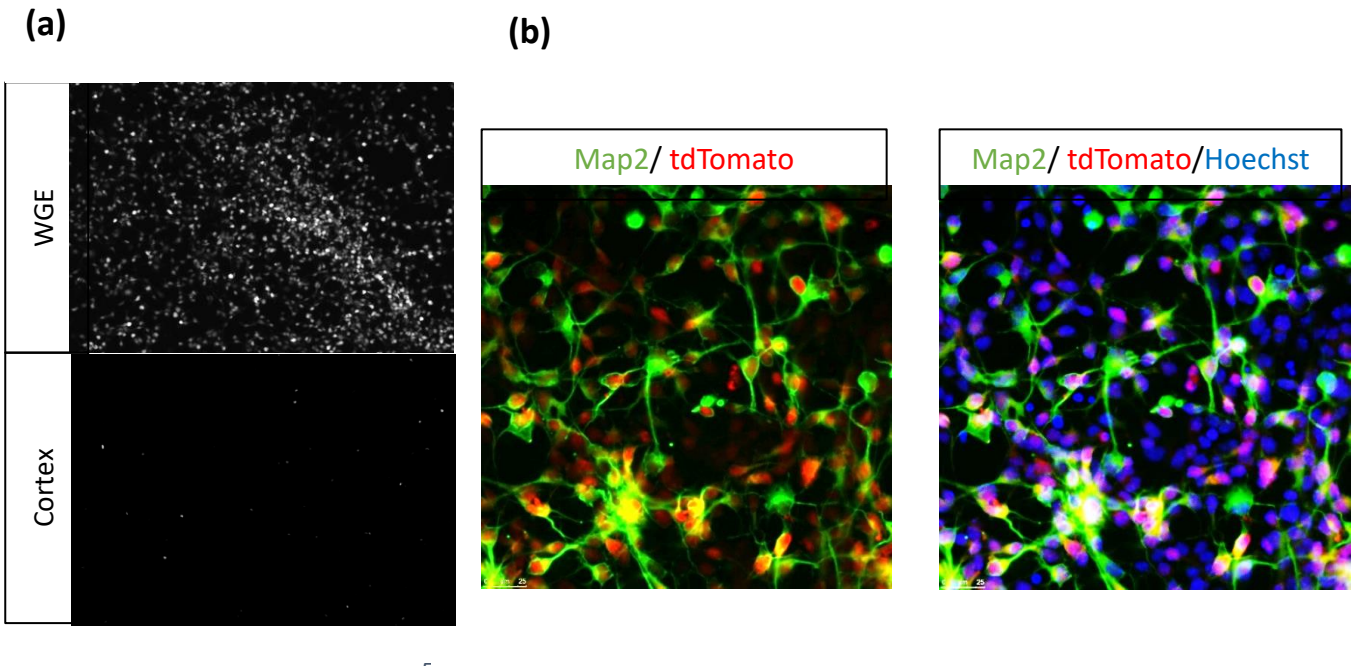

Figure 5.9: Confirmation of tdTomato expression in E16 LGE cultured cells, with minimal expression in cortical tissue. **(a)** Autofluorescence of tdTomato in Gsx2-Cre positive LGE and cortex in E16 cultured cells after 24 hours. **(b)** Immunocytochemistry of the neuronal marker MAP2 (green) and tdTomato (red) shows complete double-labelling between them, indicating that tdTomato is expressed only in neurons.

5.4.7 No significant difference in the proliferation index of *Mef2c CKO* and *WT* E16 LGE and cortex cells at 24hrs *in vitro*.

During embryonic development, NPCs proliferate in the GZ of the LGE and then the postmitotic neurons migrate to their destination to the mantle zone (Brazel et al., 2003; Lebouc et al., 2020). The aim of this experiment was to assess the proliferation index of cultured E16 cells in both WT and CKO, that are fixed 24 hours after adding EdU to the growth medium in LGE and cortical cultures. EdU uptake can be visualized using specific detecting reagents and immunocytochemistry (as described in Methods Chapter 2), and the percentage of EdU positive cells relative to the total number of Hoechst cells represents the overall rate of cell division, **Figure 5.10.**

Mef2c loss had no significant effect on proliferation between WT and CKO in either WGE or cortical E16 cells (Genotype x Dissected part: $F_{(1, 8)} = 1.016$, p=0.3429, two-way ANOVA) **Figure 5.10b**. There was also no significant effect of genotype ($F_{(1, 8)} = 0.3008$, p=0.5984). The overall percentage of proliferative cells in WGE cultures was significantly higher compared to cortical cultures ($F_{(1, 8)} = 76.86$, p<0.0001).

This is the only experiment that involved cortical tissue, the remaining work was restricted to WT and CKO striatal cells.

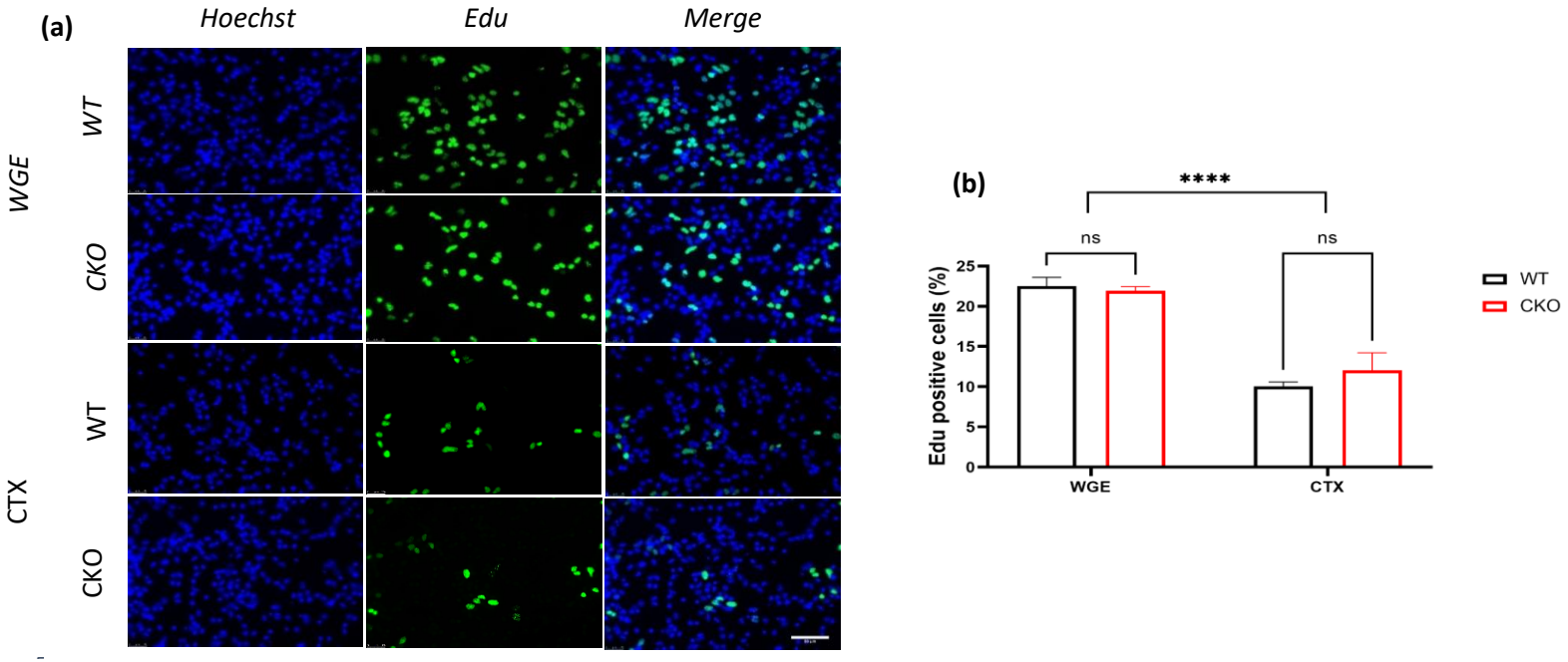

Figure 5.10: No significant difference in the overall proliferation between WT and CKO LGE and cortex E16 cultured cells within the first 24 hours in vitro **(a)** Immunocytochemistry of EdU and Hoechst in WGE (left) and cortex (right) cultures. **(b)** No significant difference was seen in the percentage of EdU positive cells (green) in the WT and CKO cells in either WGE or cortex (p not significant). Overall, there were more proliferating cells in cultured WGE cells compared with cortical cells (P<0.0001). Bars represent mean ± SEM. **** = p < 0.0001. Total n per group is 3 with two biological replicates per sample. Scale bar is 50µm.

5.4.8 There was no significant difference in the proliferation index of MSN progenitors

The proliferation of E16 MSN progenitors was investigated, and unpaired t test was performed to see if there is any significant difference between WT and CKO *in vitro*, **Figure 5.11**.

No significant difference was observed in the total percentage of Edu positive cells (% of total Hoechst cells) between WT (23.2%± 1.26%) and CKO (23.9%±0.64%), ($t_{(4)}$ =0.5368, p=0.619), **Figure 5.11b**, nor in the percentage of $TdTomato^{+}/EdU^{+}$ cells ($t_{(4)}$ =1.237, p=0.283), **Figure 5.11d.**

The percentage of tdTomato positive cells in both genotypes was also quantified and it was significantly lower in CKO ($t_{(4)}$ = 3.529, p =0.024), in CKO (46.1%± 0.9%) compared with WT (56.4%±2.8), **Figure 5.11c.**

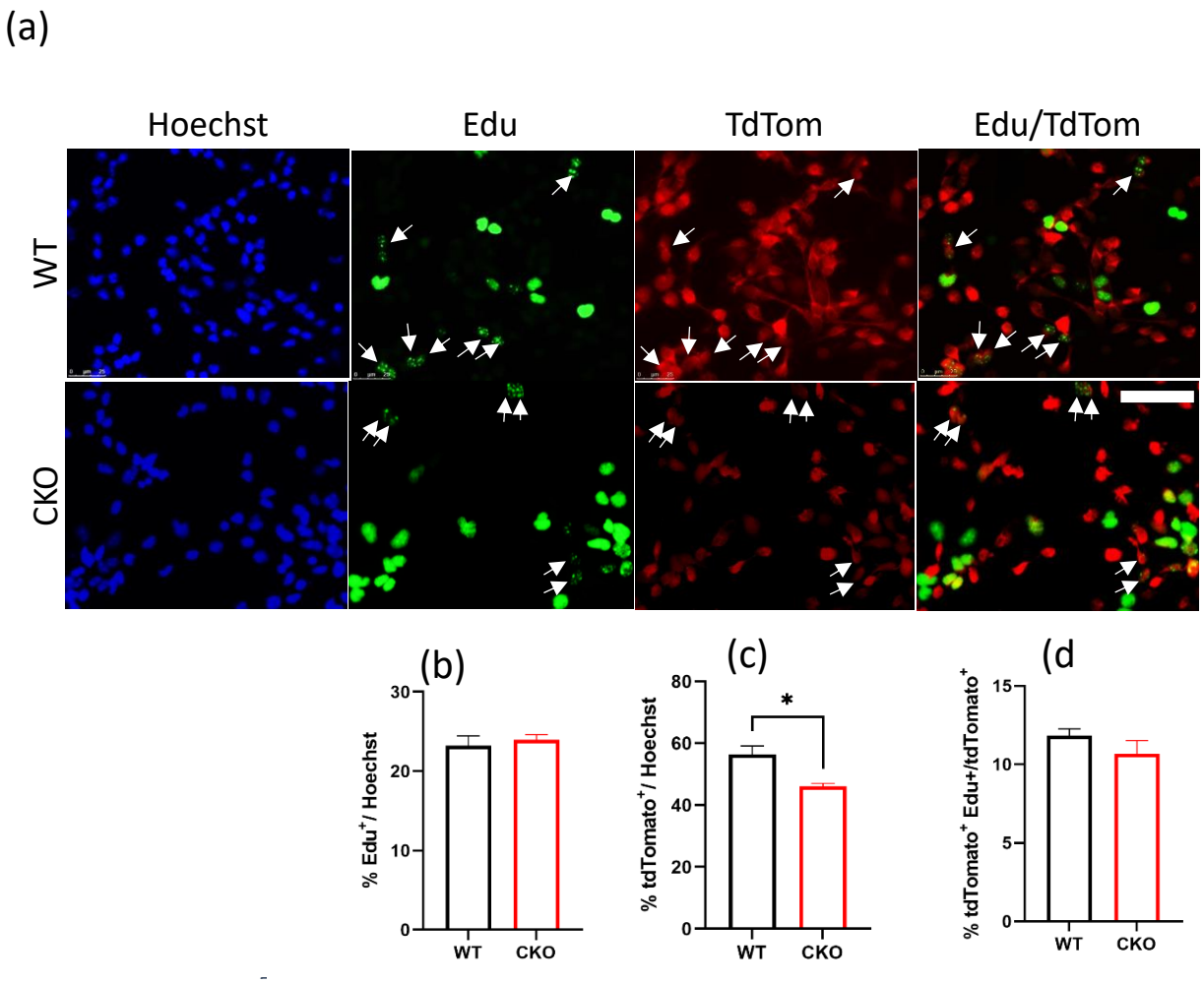

Figure 5.11: No significant difference in the proliferation of MSNs was observed between WT and CKO in E16 cultured cells after 24 hours.

(a) immunocytochemistry of EdU and tdTomato in WT (upper panel) and CKO (lower panel) in E16 cultured WGE. **(b)** No significant difference (p =ns) was seen in the percentage of total proliferative cells as a percentage of total Hoechst, nor in the percentage of proliferating neurons **(d)** between Mef2c CKO and WT represented by TdTom+/Edu+ cells. **(c)** the percentage of TdTom positive cells (as a percentage of Hoechst) was significantly lower in CKO (p=0.024). n=3 per group (two biological replicate per sample). Bar graphs are means ± SEM. Scale bar is 50µm. * = p<0.05.

5.4.9 Cell death was increased in MSN progenitors in E16 culture after 24hrs *in vitro*.

The overall cell death by apoptosis was measured using the TUNEL assay. The aim of this experiment was to assess if the percentage reduction in TdTomato positive cells in the Mef2c CKO resulted from increased cell death.

A significant increase in the percentage of apoptotic cells was found in CKO mice (3.85% ±0.64%), compared with only (1.41%± 0.06%) in WT ($t_{(4)}$ =3.802, p=0.019). The percentage of MSNs undergoing apoptosis measured as a percentage of $TUNEL^{+}$ $tdTomato^{+}$ was also significantly higher in CKO (2.7% ±0.48%) compared with WT (0.91% ±0.07%), (t (4) = 3.683, p=0.020), **(Figure 5.12b).**

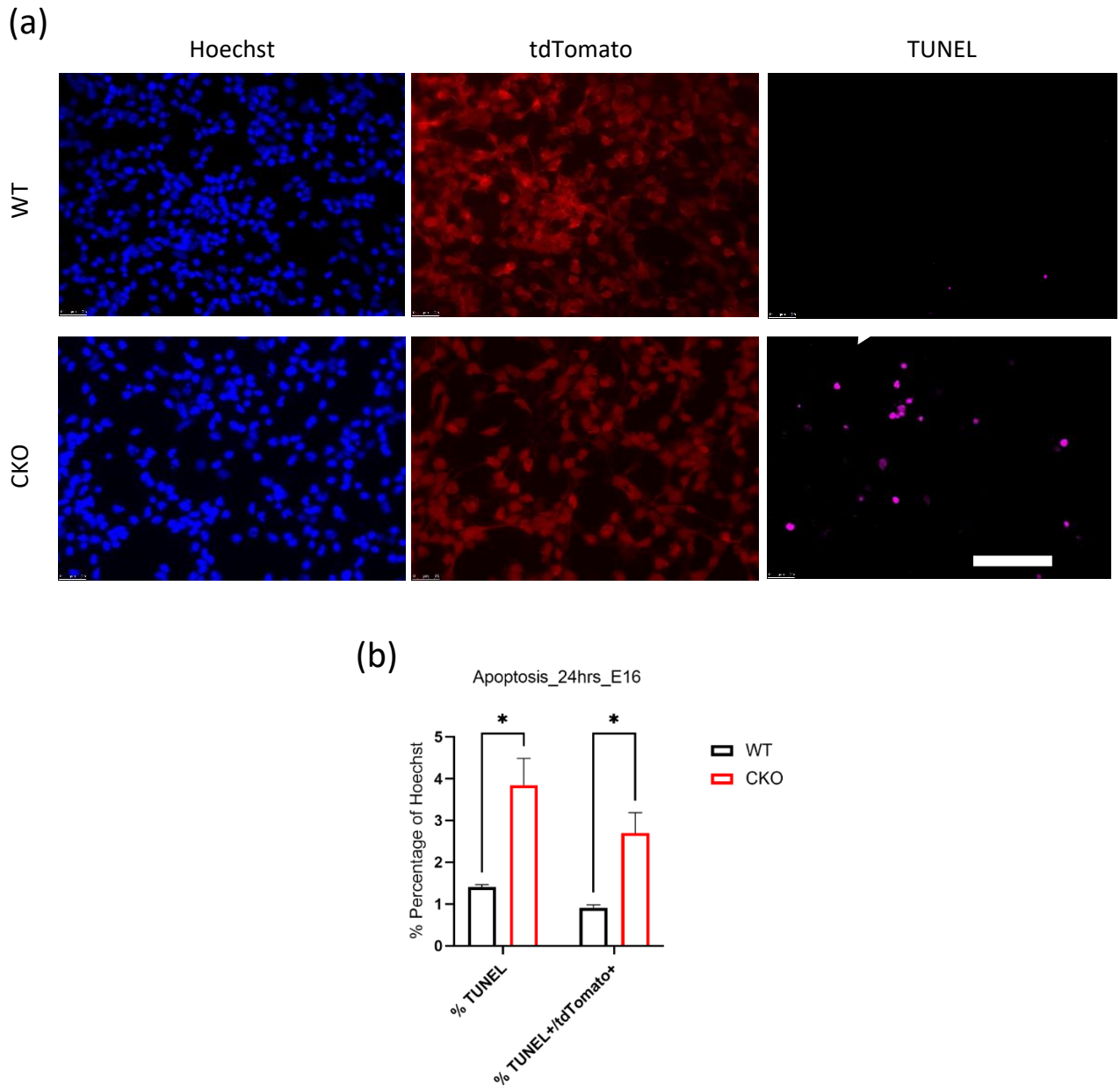

Figure 5.12: Increased apoptotic activity in CKO E16 cultured striatal MSNs compared with

(a) Detection of apoptosis in *WT* and *CKO* E16 LGE was performed using TUNEL assay. TUNEL positive cells (purple) represent cells undergoing apoptosis while *tdTomato* positive (red) are MSNs. **(b)** There was a significant increase in the percentage of TUNEL positive cells (**p*=0.019) and $TUNEL^{+}/tdTomato^{+}$ cells (*p*=0.020) in *CKO* cells (lower panel) compared with *WT* (upper panel). White arrow in higher magnification shows MSN positive for TUNEL. n per group =3, multiple t tests with Holm-Sidak correction. Scale bars are 200µm in low magnification and 100µm in high magnification, * = p<0.05.

5.4.10 Proliferation and apoptosis were significantly impaired in E14 cultured LGE within the first 24 hours.

The survival of E16 cultured MSNs was suboptimal with very poor survival of cells at 6DIV. Therefore, E14 LGE was collected, first to enhance the survival of MSNs to allow identification and analysis of MSNs at later time points, and in addition, to assess the proliferation and neurogenesis at a time point when activity of matrix MSN neurogenesis is at its highest level (Lebouc et al., 2020).

Analysis was performed at 24hrs and 6DIV. At 24hrs, proliferation, neurogenesis and survival of MSNs were assessed (**Figure 5.13a).**

Although a comprehensive analysis of Mef2c expression was conducted in mouse striatum from embryonic through to adulthood in chapter 3, little is known about Mef2c expression in vitro at the two time points of interest in this chapter. Therefore, Mef2c mRNA levels were assessed at 0, 24hrs and 6DIV in WT cultured E14 cells. RT qPCR analysis showed that *Mef2c* levels were significantly increased over time in culture ($F_{(2, 7)}$ = 23.35, p<0.0001, one-way ANOVA) **Figure 5.13b**. Post hoc multiple comparison using Tukey's test showed that *Mef2c* had significantly increased between 0hrs and 24hrs (p=0.0044), and then further increased at 6DIV (p=0.0005).

Unlike E16, proliferation at E14 was significantly higher (unpaired t test: $t_{(5)}$ =3.228, p=0.023) in WT (52.4% ±1.23%) compared to CKO (41.6% ±2.9%), **Figure 5.13c**. The percentage of MSNs represented by the percentage of tdTomato cells was not significantly different between CKO (38.2%±2.18%) compared to WT (42.3%±1.15%) (unpaired t test: $t_{(5)}$ =1.467, p=0.199) **Figure 5.13d**, nor the percentage of the proliferating MSNs represented by the percentage of tdTomato + and EdU+ cells (WT; 20.55% ± 4.65%, CKO; 15.18% ± 1.52), ($t_{(5)}$=1.251, p=0.133) **Figure 5.13e**.

A significant increase in the percentage of TUNEL positive cells was observed in CKO E14 cultured cells (7.69%±1.39%) compared to WT (3.06%±0.48%), ($t_{(5)}$ =2.743, p=0.0203) **Figure 5.13f.** A in CKO (3.09%±0.39%) compared with WT (1.58%±0.29%) ($t_{(5)}$ =2.915, p=0.0166) **Figure 5.13g.**

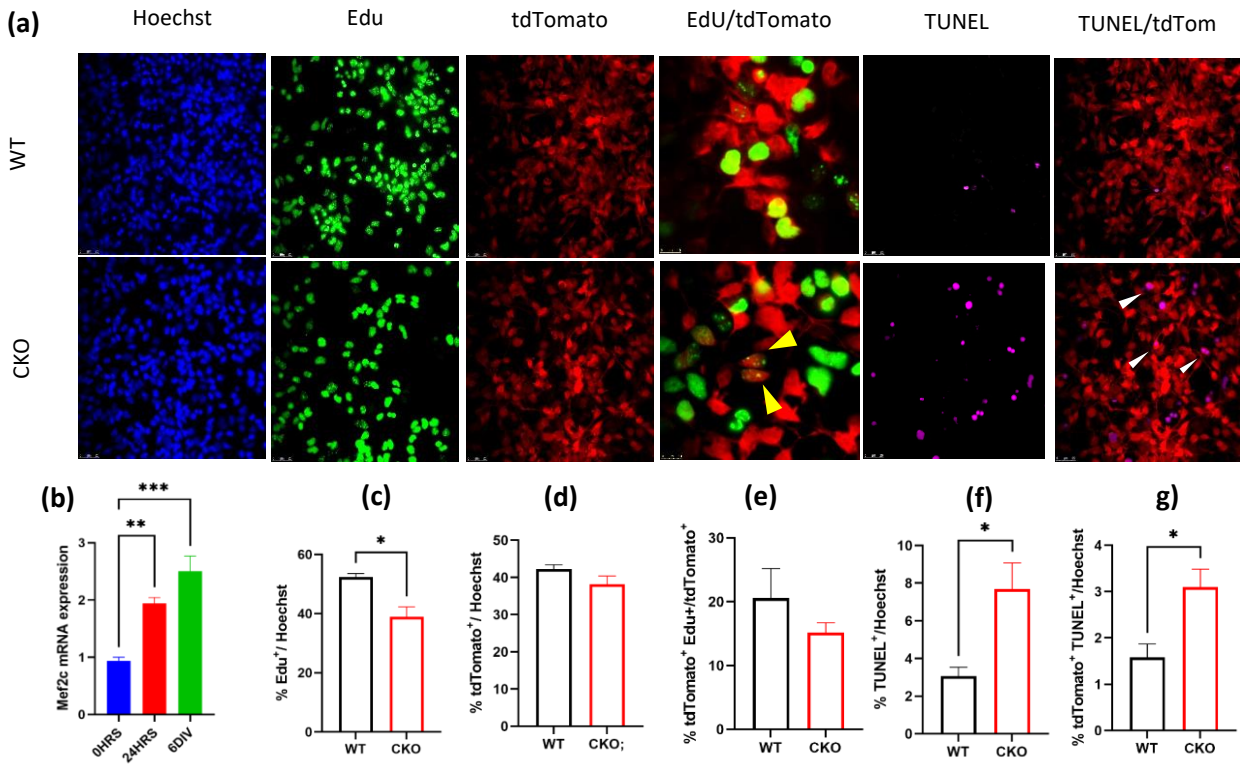

Figure 5.13: Mef2c loss has significant effects on proliferation and survival of E14 cultured LGE cells after 24 hours.

(a) Immunocytochemistry of EdU (green), tdTomato (red) and TUNEL (purple) in WT (upper panel) and CKO (lower panel). (**b**) Mef2c levels increased significantly between 0hrs and 24hrs (**p=0.0044) with a further increase at 6DIV (*** p<0.0001). **(c, d, e)** A significant reduction in proliferation was observed in CKO cells (p=0.023), however, there was no effect on overall tdTomato (p=0.199)**,** nor in Edu+ tdTomato+ cells (p=0.133). **(f, g)** The overall number of apoptotic cells was significantly higher in CKO (p=0.0203) and the percentage of MSNs undergoing apoptosis was significantly higher in CKO (p= p=0.0166). Yellow arrow heads show double labelling of EdU and tdTomato; white arrow heads show double labelling of TUNEL and tdTomato. Bars are means ± S.E.M. n per group is WT =3 and CKO=4, with two biological replicates each. * = p<0.05, ** = p<0.01, *** = p<0.001

5.4.11 The consequences of Mef2c loss on MSNs at 6DIVs were significantly less compared to 24hours.

MSNs were maintained in culture until 6DIV to assess their survival at this time point. Overall, there were more dead cells and cells undergoing apoptosis with small condensed or fragmented nuclei in all conditions. Therefore, the quantification was restricted only to cells that appeared intact based on Hoechst staining.

First, the percentage of tdTomato positive cells was quantified in both WT and CKO and the results showed no significant difference between them ($t_{(4)}$ =0.7081, p=0.518) **Figure 5.14a.**

The significant difference in EdU positive cells was still observed at 6DIV ($t_{(4)}$ =4.036, p=0.016), with (53.3% ± 2.01%) in WT compared to (34.9% ± 2.86%) in CKO, but there was no difference in the percentage of EdU /tdTomato positive cells ($t_{(4)}$ =1.506, p=0.206), (**Figure 5.14b).**

The percentage of apoptotic cells ($TUNEL^+$) and MSNs undergoing apoptosis ($TdTomato^+/TUNEL^+$), at 6DIV was estimated as a percentage of Hoechst cells and the results showed no significant different in both (p=0.217 and p=0.214, respectively). Although the numbers of TUNEL positive cells appeared higher in CKO cells, the difference was not significant **(Figure 5.14c).**

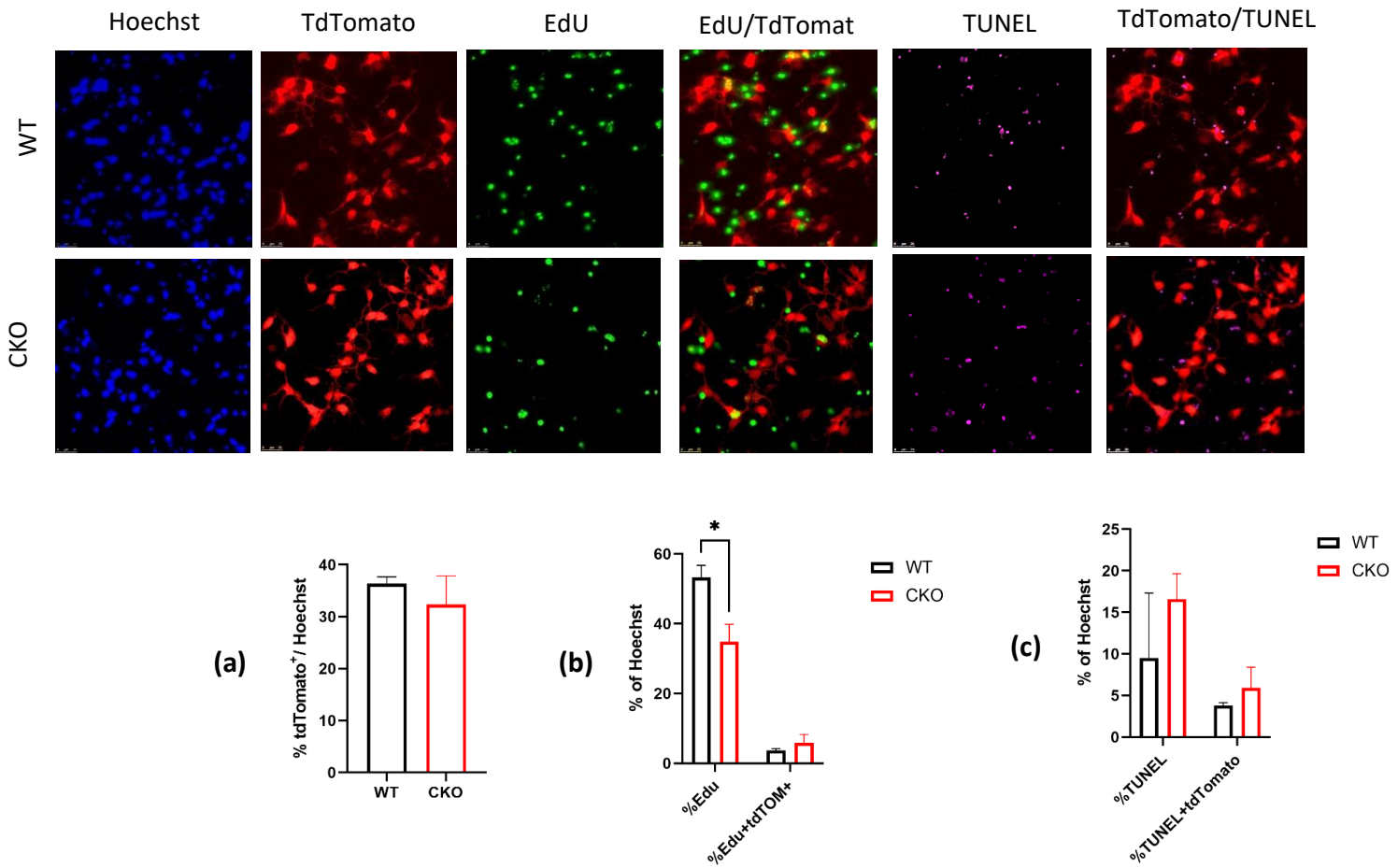

Figure 5.14: Mef2c loss did not cause any further consequences in CKO E14 cultured cells at 6DIV. (a) No significant difference between WT and CKO in tdTomato expression was observed at 6DIV. (b) the significant reduction between WT and CKO in the overall proliferating cells was still observed (p=0.016), but no significant difference in the neurogenesis (p=0.206). (c) No significant difference in the percentage of apoptotic cells and MSNs undergoing apoptosis was observed between WT and CKO (p=0.217 and p=0.214, respectively). Scale bar is 100 µm. Graph bars are means ± SEM. * = p<0.05.

5.5 Discussion

Understanding the biological processes involved in striatal NPC proliferation, differentiation and survival are central in enhancing our knowledge of normal striatal development and provide valuable information of pathological problems in the striatum such as PD and HD. In this chapter, biological mechanisms underlying how Mef2c TF plays an important role in the survival of matrix MSNs in the late embryonic and early postnatal were explored, using *in vivo* and *in vitro* approaches. Although no effect was observed on embryonic proliferation in *Mef2c CKO* mice, an increase in apoptotic activity in early postnatal striatum was observed, accompanied with a decrease in one of the anti-apoptotic factors; Bcl-xl.

Proliferation in the adult mouse brain has been extensively studied in many published works, especially in areas of continuous production of neurons, such as the SVZ and SGZ of the hippocampus (Bordiuk et al., 2014). Despite the significant amount of research on the proliferation and neurogenesis in these two niches of the mouse brain, little is known about the early postnatal proliferation in the mouse striatum.

Both BrdU and EdU are effective and robust proliferative markers that are incorporated permanently in proliferating cells (Chehrehasa et al., 2009; Hill et al., 2005), but a key practical difference is that EdU does not require the harsh HCL pre-treatment to visualize proliferative cells, making its use ideal for the processing of delicate brain tissue at embryonic or early postnatal stages and for cells in culture.

The analysis of overall striatal proliferation in the postnatal mouse striatum performed in this chapter showed no significant difference between *WT* and *CKO*. The proliferation in groups 3 and 4 was very minimum (almost negligible compared to groups 1 and 2. Indicating that it is the proliferation within the first two weeks of mouse striatum that contributes most to the significant increase in striatal volume during early postnatal development that was described in chapter 4. The proliferation spurt occurred in Group1 that received BrdU injections at P6, P7, and P8 are in line with previous reports that showed maximum brain growth in rodents' brain at P7 (Dobbing and Sands, 1979; Bockhorst et al., 2008). Neurogenesis in the mouse brain is thought to be completed during embryonic development and maintained throughout life. After birth, most of

postnatal proliferation in the mouse brain is astrocytes and oligodendrocytes, while microglial cells migrate early postnatally from outside the CNS. RGCs in the SVZ proliferate and the number of astrocytes increases more than six folds during the early postnatal period.(Bandeira et al., 2009a). Several TFs, such as Olig2, regulate this neuronal-glial (Petryniak et al., 2007). Mef2c is not expressed in striatal astrocytes as shown in chapter 3 and its loss does not cause any indirect effects on postnatal proliferation in mouse striatum which indicates that Mef2 is only affecting MSNs.

Several TFs involved in the neurogenesis and differentiation of striatal MSNs are expressed in distinct and overlapping patterns in the VZ, SVZ, and mantle zone, among these Ebfa1, Ctip2 and Ikaros are expressed in mantle zone and are required for the differentiation of MSNs (Eisenstat et al., 1999). Mef2 transcription factors in general are found to be implicated in neurogenesis throughout development particularly, Mef2a and Mef2c, (Cho et al., 2011; Zhu et al., 2018). However, based on our knowledge of the spatial and temporal expression of Mef2c from chapter 3, it is very unlikely that Mef2c could be necessary for the proliferation of NPCs during embryonic development. Mef2c was not shown to be expressed in the neurogenic area of the LGE, the GZ and SVZ, but rather it was first detected at the mantle zone, where the postmitotic neurons migrate. This assumption has been confirmed here by undertaking a comprehensive assessment of proliferation of NPCs in the developing LGE using EdU. The results showed no significant difference in EdU uptake between WT and CKO and that the postmitotic neurons survived normally until P0 (the time at which the analysis was done). This indicates that in mouse striatum, Mef2c is not predominantly required for the generation of striatal MSNs.

Mef2c is known as an antiapoptotic factor that enhances neuronal development and plays a crucial protective role both *in vitro* and *in vivo* (Li et al., 2008; Okamoto et al., 2000). In this chapter, it was shown that expression of cleaved caspase 3, an apoptotic marker, was increased significantly at postnatal day 3. It is well-known that neurons in the CNS undergo apoptosis during early postnatal development as a normal physiological process important for CNS growth and development in mammals (Kuida et al., 1996; Cecconi et al., 1998). Apoptosis in neonatal and early postnatal brain was assessed in *Mef2c WT* and *CKO* mice by using IHC of cleaved caspase 3 and RT qPCR of a

panel of apoptotic and anti-apoptotic genes at four time points P0, P3, P7 and P14. These age groups were chosen to test the hypothesis that Mef2c is important for the survival of a subpopulation of MSNs during the first two weeks of postnatal life.

Two waves of neuronal death in the developing mouse brain have been appreciated in the CNS of mammals. The first one includes NPCs that reside in the VZ and SVZ and causes death of these cells soon after birth (Blaschke et al., 1996; Blaschke et al., 1998; Thomaidou et al., 1997). The second one involves apoptosis of postmitotic neurons that differentiated and started receiving nerve terminals to establish connections with other brain regions (Oppenheim, 1985; Buss et al., 2006). The pattern of cleaved caspase 3 expression in *WT* mouse? striatum in the experiment described in this chapter is consistent with (Mosley et al., 2017) in which they showed an abrupt increase in cell death from P0 to P1 that remained high at P3 and then reduced significantly at P7 with further reduction toward P11. Here I show, in postnatal mouse striatum, an increase in cleaved caspase 3 expression from P0 to P3, with a peak at P3 and then abrupt reduction until expression becomes minimal at P14. The results show that the levels of cleaved caspase 3, the most-known apoptotic initiator, increased significantly in *CKO* P3 mouse striatum compared with *WT*, while it normalized at P7 and P14 between *WT* and *CKO* with no significant difference between genotypes. Mef2c expression was shown to peak in neonatal striatum at P0 (as shown here in Chapter 3), nonetheless, no significant difference was noticed at P0 in apoptotic activity and neurons that proliferated during embryonic development survived normally until P0 as shown in the results section above. Another interesting observation was that the morphology of the apoptotic cells was greatly variable across the four age groups. At P3, cleaved caspase 3 immunoreactive neurons looked like Golgi-stained cells with the dendritic tree clearly shown, indicating that these cells were at early stages of apoptosis as described in (Lossi et al., 2004). While at P7 and P14, the immunoreactivity in the apoptotic cells was within the soma only.

Mef2c *TF* acts during a period consistent with the differentiation and maturation of striatal MSNs and downregulates largely postnatally at P14 onward except for the minimum expression at DM aspects of the striatum. Mef2c shares this characteristic pattern of expression (downregulation in mouse striatum after birth) with different TFs

in the literature, for example, Helios is expressed at E14.5, peaks somewhere between E18 and P3 and then downregulates significantly to P15, until it is completely absent in adult mouse striatum and it is expressed in both GZ and MZ (Martín-Ibáñez et al., 2012; Martín-Ibáñez et al., 2017). Ikaros-1 TF also showed transient expression in the developing striatum with peak at E20 and then complete loss after P2 (Agoston et al., 2007; Kiehl et al., 2008; Martín-Ibáñez et al., 2010). Zfhx3 TF was also described in (Zhang et al., 2019a) as highly expressed during striatal development but then completely lost after P15.

The loss of Helios in the developing mouse striatum has caused increased cell death in enkephalin-expressing D2 MSNs at P3, (Martín-Ibáñez et al., 2017). Furthermore, knockout of Zfhx3 CKO was shown to increase cell death in early postnatal striatum over the postnatal period that extends between P0 and P7, but normalizes at P11 (Zhang et al., 2019a). In this thesis, the apoptotic activity in *Mef2c CKO* mice was shown to be significantly higher compared to WT at P3 only, but not after this. Taken together, these findings suggest that the first postnatal week is critical for maturation of striatal MSNs and Mef2c TF is required for MSNs survival and maintenance during this period.

To further investigate the anti-apoptotic role of Mef2c, the expression levels of Caspase 3, Bcl xl, Bcl2, BAD, Cytochrome c and caspase 9 were measured and normalized to the expression of two housekeeping genes. Caspase 3 was shown to be significantly increased at P3 consistent with the increase in cleaved caspase 3 expression immunoreactivity observed in P3 CKO striatum. Bcl xl is a post-mitotic anti-apoptotic factor and a member of Bcl2 family and is expressed in embryonic and adult neurons in mouse brain (Opferman and Kothari, 2018). Bcl xl levels were decreased in CKO across the four age groups, but this was not significant compared to WT except at P3 in CKO mice. This suggests that Mef2c CKO MSNs are more vulnerable to apoptosis, probably due to reduced levels of this anti-apoptotic factor. Although the reduction seems relatively high, the neuronal loss in Mef2c CKO was about 18% compared to WT. This could be contributed to the specific functions of Bcl xl since its knockout in dorsal telencephalon did not cause global loss in neurons, but rather an increase in cell death in only postmitotic neurons early postnatally (Nakamura et al., 2016). BAD is an pro-apoptotic protein and a cell death promotor (Li et al., 2020), it suppresses the activity of

Bcl xl by forming heterodimers with it (Jiang et al., 2013). In CKO mice, BAD levels were significantly increased at P0, but not at P3. This could indicate that although no significant increase in apoptotic activity was observed at P0, the changes in the normal expression of genes important for the survival of MSNs starts early at P0. Also, at P0 and P3 a triple increase in cytochrome c was observed, however, this difference was not statistically significant. but it could indicate a mitochondrial-mediated apoptosis.

The results in this research work strongly suggest that Mef2c could have binding sites for *Bcl xl*, and its loss results in suppression of neural protection mediated by Bcl xl pathways. S-nitrosylation of *Mef2c* was found to induce cell death in mouse cortex through suppression of *Bcl xl* pathways and decreasing neuronal *Bcl xl* levels (Okamoto, Nakamura et al. 2014). Furthermore, Mef2c loss in B cells caused reduced transcription of the anti-apoptotic genes Bcl xl and cyclins, although these genes lack binding sites for Mef2c it was suggested that Mef2c could control this process indirectly (Andrews et al., 2012). In contrary, in neuronal cells, Mef*2c* was found to have binding sites in the regulatory region of Bcl-xl gene in (Li et al., 2008d).

Primary neuronal cultures are powerful tools to study biological processes to reflect events occurring in mouse models as adequately as possible. One of the earliest reports of Mef2c roles in neurogenesis and survival was assessed in rodents ESCs using *in vitro* approach *(Li et al., 2008d)*. Cells overexpressing *Mef2c* were destined for a neuronal fate and their survival was enhanced even after withdrawal of growth factors. Subsequent reports have also shown a significant role of Mef2c in hESCs development and survival in cell culture (Li et al., 2008b). Therefore, to further characterize the functional roles of Mef2c in the development of the mouse striatum, an *in vitro* analysis was performed using specific proliferation and cell death assays. The work outlined here in this chapter was carried out alongside an *in vivo* experiment to assess the same biological events *in vitro*.

E16 was the time point at which primary striatal tissue was collected as I am interested in studying any potential effect of Mef2c loss on matrix MSNs while at the same time make sure that Mef2c level started to be adequately expressed in the developing LGE. Unfortunately, I could not keep these cells alive for more than 4 DIV, which made

analysis of differentiation and maturation using Darpp32 expression very difficult. To overcome the issue of lack of survival at E16, we collected E14 LGE at which matrix MSNs neurogenesis peaks (Gerfen, 1992; Mason et al., 2005), as the earliest the gestational stage the more surviving neurons we will get.

Within the first 24hours, the percentage of TUNEL positive cells was significantly increased in Mef2c CKO E16 cultured cells within the first 24hours, this strongly supported the previous finding that Mef2c is important during early development to prevent cell death. The increase in the percentage of apoptotic cells combined with the reduction of the percentage of tdTomato positive cells means that the lost cells and those undergoing apoptosis are very likely to be MSNs. It has been shown that the time required for TUNEL positive nuclei to be cleared is about 2hours and 20 minutes, (Thomaidou et al., 1997) this could explain having 10% reduction in the percentage of tdTomato positive cells in CKO with overall apoptotic activity of ~4%. This reduced survival is in line with (Cho et al., 2011) in which a significant increase (doubled) in the cell death was observed in hNPCs lenti-shMEF2C infected cells at 14 DIV, while no significant difference was noticed in cell viability by 33 dpi. Which means that Mef2c is important for cell survival through development but not at later stages. This indicates that Mef2c could play an important neuroprotective role early during the 24hrs of striatal NPCs development as its loss caused increased neuronal loss.

5.6 Conclusion

To conclude, I showed here in this chapter that *Mef2c* striatal-specific loss is implicated with increased cell death in matrix compartment in early postnatal development, particularly at P3. But it had no significant effect on the proliferation of NPCs during embryonic development nor on postnatal proliferation in the mouse striatum. I have also shown that Mef2c CKO has affected the normal expression of the apoptotic and anti-apoptotic factors caspase 3, Bcl xl, Bcl2 and BAD. Indicating that the increased apoptotic activity might be associated with alterations in Bcl-xl pathways.

Further investigation is required to assess the exact role of *Mef2c* in Bcl-xl induced anti-apoptotic pathway using transcriptomic analysis of WT and CKO mouse striatum at P3 and P0. In addition, the finding that Mef2c loss resulted in less EdU positive cells in CKO E14 cultured LGE raised the question whether Mef2c plays an important secondary role in proliferation *in vitro* but not *in vivo,* which also needs further investigation.

Chapter 6: The functional consequences of embryonic striatal Mef2c CKO

6.1 Summary

Previous publications have shown that alterations in normal striatal development using genetic ablation of certain genes resulted in behavioural impairment in knockout mice. Here I assessed whether Mef2c loss in the mouse striatum during embryonic development resulted in any functional consequences. For this I analysed the performance of Mef2c CKO mice and their WT controls using tests of balance, coordinated motor skills and locomotor activity, in addition to other simple rodent behaviour tasks, nesting and marble burying.

Mef2c CKO mice exhibited impairments in some motor tests and showed significantly reduced exploratory behaviour when introduced to a new environment. They reared significantly less in open field testing and failed to acquire the same motor performance of WT mice on accelerated rotarod testing.

These functional abnormalities may be a consequence of the histological abnormalities described in chapter 4, manifested by matrix MSNs loss and abnormal dendritic tree development.

6.2 Introduction

Mef2c loss during embryonic striatal development was shown to result in significant changes in normal development of MSNs, particularly reduced striatal volume, and significant loss of MSNs. Furthermore, these effects seemed to predominantly affect the matrix, rather than striosome, compartment. This prompted the need to assess whether there is a functional consequence of *Mef2c CKO* on motor functions, especially as these two compartments serve different functions in the mouse striatum.

The striatum can be organized functionally based on the topographic distribution of the glutamatergic and monoaminergic projections into dorsolateral, dorsomedial, and ventral portions of the striatum which are associated with sensorimotor, associative, and limbic functions, respectively. The dorsal striatum, a key regulator of motor and motor learning functions, can be divided anatomically and functionally into two main parts; the matrix which receives input from the sensorimotor cortex and is responsible for motor functions and adaptive behaviour to environment, and the striosomes which receive input from the limbic system and amygdala and is responsible for habituation, motivation and reward-associated functions (Bolam et al., 1988; Canales and Graybiel, 2000; McDonald, 1992; Brimblecombe and Cragg, 2017). Although these two segments are anatomically and neurochemically distinct in the adult mouse striatum (Graybiel, 1990), the balance between them is crucial to control motor and non-motor behaviour(Canales and Graybiel, 2000a). Striosomes in the lateral aspect of the dorsal striatum were also shown to play role in the development of habitual behaviour (Jenrette et al., 2019).

As discussed in the general introduction, Mef2c *loss* in cortical neurons using different *CKO* mouse models resulted in various behavioural phenotypes. *Mef2c het* mice showed reduced viability, i.e., reduced lifespan, and a significant increase in paw clasping (Tu et al., 2017a). Harrington et al, found that Emx1-cre *Mef2c CKO* mice compared with WT mice showed significant hyperactivity and repetitive behaviour represented by increased beam breaks and movement time in activity cage assessments. However these CKO animals were not seen to be impaired in rotarod testing, assessed by latency to fall (Harrington et al., 2016c). Another publication from the same author reported that only male *CKO* mice showed significant hyperactivity, but still no significant effect on latency

to fall on the rotarod (Harrington et al., 2020b). Mice with Mef2c loss in nestin expressing cre cells did not exhibit any significant difference in locomotor activity, however, these mice presented with possible alterations in anxiety-like behaviour and cognition (Li et al., 2008a). There was postnatal Mef2c loss between P10-P14 in the granule cells of the hippocampus using a CaMKII cre mouse line which showed significant motor deficits including increased paw clasping, increased beam breaks and a reduction in latency to fall on rotarod testing. In addition, these mice showed impairment in nest building, wherein they were seen to build significantly smaller and lower quality nests compared to control animals(Adachi et al., 2016b). In contrast, *Mef2c* deletion during late embryogenesis in cortex and hippocampus under the control of the hGFAP cre resulted in no effect on beam breaks or on performance of *CKO* mice on rotarod (Barbosa et al., 2008b). Variations in behavioural outcomes between different mouse models indicates an important effect of the timing of Mef2c loss on functional outcomes.

Mef2c loss in mice has also shown impairments in cognitive functions like ''anxiety-like'' behaviour. For example, *nestin-Cre*$^{+}$*/Mef2c* $^{loxP/null}$ mice did not fear open arms of open maze and showed reduced rearing frequencies compared to controls (Li et al., 2008a).

the main objective of this chapter was to assess the behavioural functions in our Gsx2-Cre *Mef2c CKO* mice using a battery of motor behavioural testing comprising motor testing, including rotarod, open field arena and in activity boxes to assess coordinated movement and locomotor functions, as well as assessment of nesting and marble burying.

6.3 Experimental procedures

A total of 16 WT and 14 CKO mouse aged 12-months at the time of testing were used for behavioural assessment conducted in this chapter. In general, mice were acclimatised to the testing room for at least two hours before starting the test. Nesting and marble burying tests were performed as described in sections **2.6.1** and **2.6.2** respectively. Coordinated motor assessment on rotarod was conducted as described in **2.4.6** and spontaneous locomotor assessment in an open field arena was performed at 11:00 am as in **2.6.5**. light/dark activity was conducted as in **2.6.3.**

All statistical tests were done using prism software. Two-way repeated measures ANOVA test was conducted to analyse the effect of trial and genotype on rotarod or time and genotype in activity boxes followed by simple main effects analysis when there is a significant interaction between the two main factors tested. Unpaired t test was conducted to analyse nesting and marble burying results, in addition to the parameters assessed in the open field test.

6.4 Results

General observations

At the time of testing there were no observed differences between *Mef2c CKO* mice and their WT controls. The transgenic mice in this project bred normally, and a mendelian frequency was observed following mating, suggesting the absence of foetal lethality. 12-month-old *Mef2c CKO* and *WT* littermate control mice were tested to explore any effect of the *CKO*. Data from male and female mice were pooled to increase statistical power.

6.4.1 Animal weights and survival of *CKO* mice

There were no differences in body weight between 12-month-old *Mef2c CKO* mice and *WT* controls for both males and females (unpaired t tests: both genders combined: $t_{(28)}$ =0. 6741, p =0. 5058; females: $t_{(21)}$ =0.1627, p=0.87; Males: $t_{(5)}$ =0.9456, p=0.39), **Figure 6.1**. There were also no distinguishable morphological differences between *Mef2c* CKO and WT littermate controls.

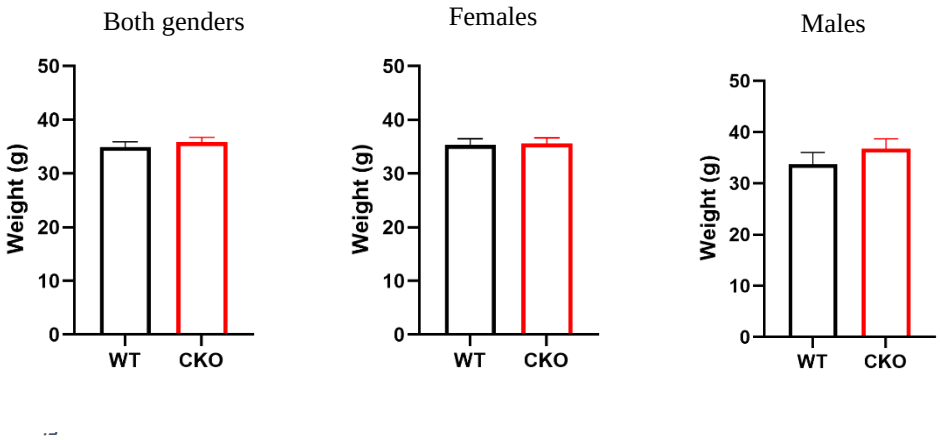

Figure 6.1: No significant difference between *WT* and *CKO* in the mean weight in (g) of 12-months old mice *in both males and females*. Bars are means ± SEM. WT n = 14; CKO n = 16.

6.4.2 Nesting

To assess nest building, mice were placed individually in new cages with equal sized square-shaped nesting material in each cage and left for two hours. The amount of shredded and non-shredded material was collected and weighed as described in Chapter 2, section 2.6.1. there was no significant difference between *Mef2c KO* mice and their *WT* littermates in the percentage of material shredded (Unpaired t-test; t $(_{32})$ = -1.499, p = 0.1437), **Figure 6.2**.

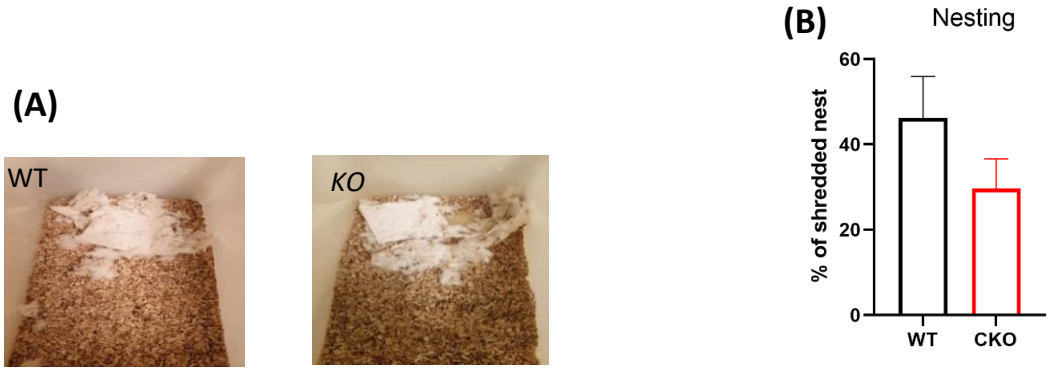

Figure 6.2 No significant difference between WT and CKO in the amount of shredded nest material.

(A): Representative photographs of the nesting test from *WT* and *CKO* mice. **(B)** Bar graphs show no significant difference in the percentage of material shredded between the two groups *p*=0.1437. Bars are means ± SEM.*n for each group: WT*=17, *CKO*=17.

6.4.3 Marble burying test

The marble burying task tests a normal rodent behaviour to bury unknown objects. This behaviour is assumed to be related to fear of foreign objects in rodents (neophobia) and thus any aberration in this behaviour could be interpreted as demonstrating the presence of anxiety -like behaviour and may also impact on planning for further experiments. In this test marbles were placed in rows (5 rows of 4 marbles per row) on deep sawdust in large cages as described in chapter 2. Individual mice were placed in the cages with plastic lids and left for 30 minutes. After 30 minutes, marbles were scored based on how much were buried i.e, more than 50% buried or less than 50% buried. There was no significant difference in the number of marbles buried between *Mef2c CKO* mice and *WT* controls (t $_{(32)}$ = .3493, *p* =0.7291), **Figure 6.3.**

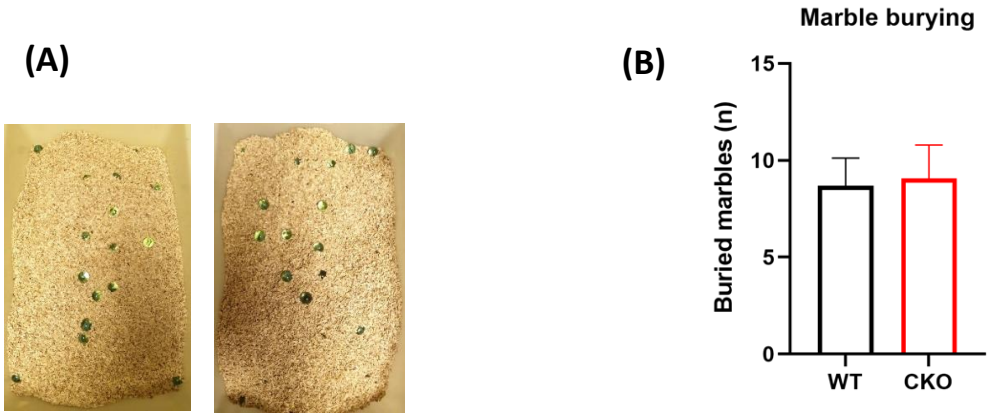

Figure 6.3 No significant difference between WT and CKO in the percentage of marbles buried.

(**A**): Representative photographs from the marble burying test from a *WT* (left) and *CKO* mice (right). (**B**): bar graph represents the mean number of marbles that were more than 505 buried. Bars are means ± SEM. *Mef2c* CKO (n=14) and WT (n=16).

6.4.4 Inverted grip strength test

This test is used to measure the strength of the fore and hind limbs. The time the mouse spent grasping the grid without falling was recorded as latency to fall. A cut off point of a maximum 1 minute was used. No significant difference between Mef2c CKO mice and their WT littermates was observed (unpaired t-test; $t_{(30)} = -.796$, $P = .432$**), Figure 6.4.**

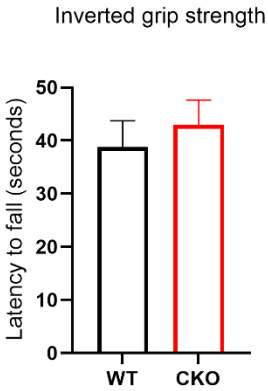

Figure 6.4 No significant difference between WT and CKO in latency to fall in inverted grip strength test. No difference between Mef2c CKO and WT controls. Bars are means ± SEM. Mef2c CKO (n=14) and WT (n=16).

Open field

6.4.5 Open field testing showed that *Mef2c CKO* mice are significantly less active than WT littermates and their movement path shape was significantly different.

Open field activity was carried out to assess locomotor activity in an open arena using overhead video tracking software Ethovision (Noldus). This software allowed velocity, distance travelled and rearing to be recorded over a 10-minute period.

The overall activity of *CKO* mice was significantly reduced compared to WT mice**, Figure 6.5.** *CKO* mice travelled less distance in the arena (distance moved: $t_{(28)} = 2.562$, $p = 0.016$); their velocity was also significantly less (velocity: $t(28) = 2.560$, $p = 0.016$); and they reared significantly less (rearing: $t_{(28)} = 2.936$, $p = 0.006$). All four parameters were analysed using t tests with Holm-Sidak correction. No significant difference was found in the duration of time spent in the centre zone, ($t_{(28)} = -.992$, $p = 0.33$), **Figure 6.5 a-d**. Representative traces are shown in **Figure 6.5 e.**

Data about the shape of movement (path-shape variables) were also recorded using the tracking software, multiple variables were defined and recorded as below according to (Gale et al., 2009):

Turn angle	average change in heading, in degrees across two consecutive samples
Heading	the direction of movement relative to a reference line established over two samples (nose tip, tail base….).
Angular velocity	the average turn angle per unit time.
Meander	average turn angle per distance moved

Table 6.1 locomotor path-shape variables analysed. according to (Gale et al., 2009)

Among these measurements, a significant difference was found between *WT* and *CKO* in Turn angle ($t_{(28)} = 2.050$, $p=0.049$), angular velocity ($t_{(28)} = 2.217$, $p=0.034$), meander ($t_{(28)} = 2.212$, $p=0.035$), and heading ($t_{(28)} = 2.349$, $p=0.026$), Figure **6.5 f**.

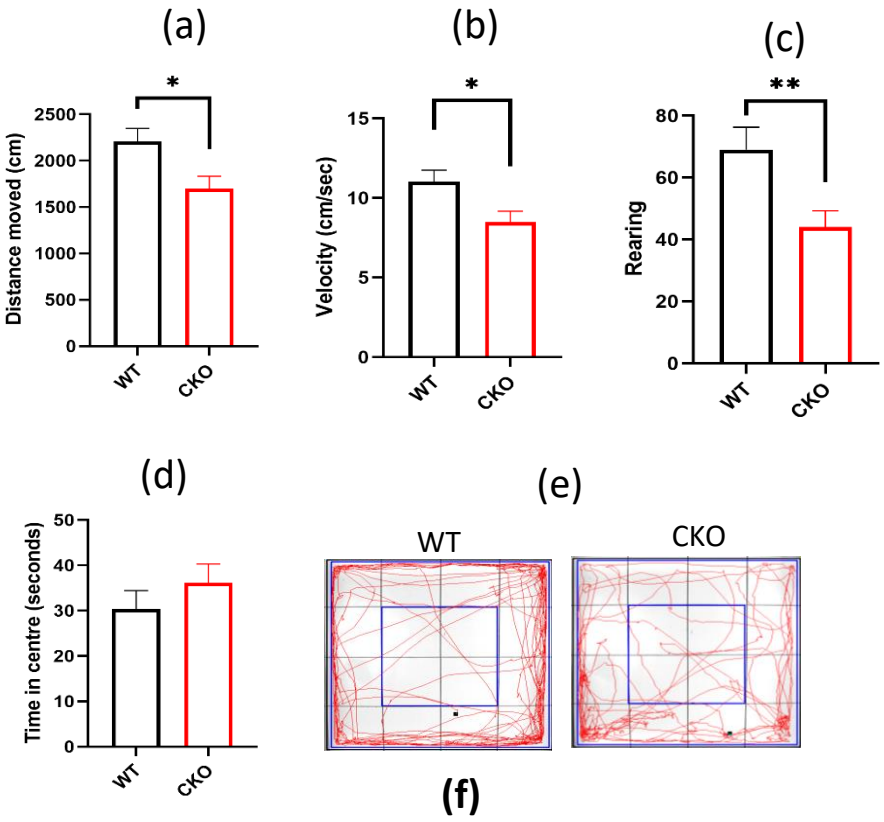

	WT	*CKO*	*P value*	*Difference*	*t ratio*	*df*
Turn angle (degrees)	128.7	203.5	0.049	74.80-	2.050	28.00
Angular velocity (degrees/seconds)	48.30	53.47	0.034	5.177-	2.217	28.00
Meander (degrees/cm)	-25.93	-38.93	0.035	12.99	2.212	28.00
Heading (degrees)	-18.14	-28.61	0.026	10.47	2.349	28.00

Figure 6.5: *Mef2c CKO* mice showed reduced locomotor activity in the open field test during a 10-minute period using Ethovision. Compared to their WT littermates, *Mef2c CKO* had lower total distance moved **(a),** lower velocity **(b),** and reared less **(c),** but there was no difference in time spent in the centre zone **(d). (e)** shows representative tracings of mouse movement during the test period. **(f)** This table shows a summary of the results of path shape analysis, with Mef2c CKO mice showing significant increase in Turn angle and angular velocity and a significant decrease in meander and heading. *CKO* (n) =14, WT (n) = 16. Bars represent mean ± S.E.M. * = p<0.05, **= p<0.01.

6.4.6 Rotarod

Rotarod is used to test motor coordination and balance in mice (Sedelis et al., 2001). *Mef2c CKO* mice spent significantly less time on the rotarod compared with WT controls, and a reduced latency to fall was observed compared to *WT* littermate mice, suggesting the presence of impaired motor coordination due to motor impairment **(Figure 6.6).** A two-way ANOVA with genotype and number of trials as the two main factors, confirmed a significant main effect of genotype ($F_{(1, 29)} = 6.442$; $p = 0.0053$), although there was no significant interaction between genotype and trial (Genotype x trial; $F_{(9, 261)} = 1.343$, $p = 0.216$), suggesting that this change did not vary significantly over time, **(Figure 6.6, a).** Cumulative data of the latency to fall for *WT* and *CKO* are shown in **(Figure 6.6, b).**

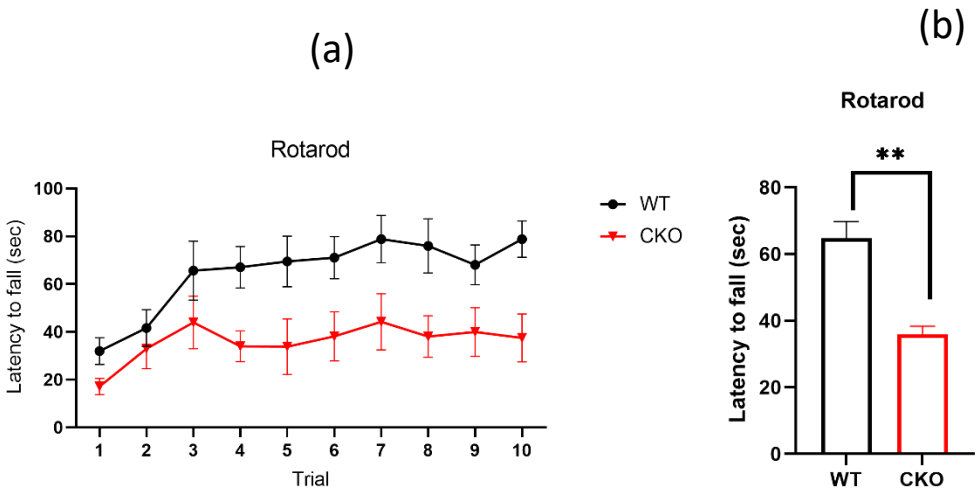

Figure 6.6 Mef2c CKO mice spent less time on the rotating rod compared with wildtype littermates.

(A): line graph shows the means of latency to fall of *Mef2c CKO* and *WT* controls over nine attempts; the first two were initial testing and the remaining eight are the experimental trials (in seconds). **(B):** This bar graph shows the averaged latency to fall for each genotype p =.0053. Mef2c CKO (n=14) and WT (n=16). Data are presented as means ± SEM.

6.4.7 Automated activity boxes

Mef2c CKO mice were tested for spontaneous motor activity to see if there were any phenotypic differences compared to *WT* over testing period as observed in rotarod and open field testing in the previous sections. Mice were placed in automated activity boxes and the total number beam breaks was averaged per 5 minutes.

Over 30 minutes, *CKO* mice were significantly hypo-active compared to WT (two-way repeated measures ANOVA gave a main effect of Genotype: $F_{(1, 28)} = 8.000$, p= 0.0085) **Figure 6.7 a**. There was no significant interaction between time and genotype ($F_{(5, 140)} = 0.7222$, p=0.6078).

To assess whether this hypo-activity persisted over the circadian cycle, I placed *Mef2c CKO* mice and WT controls in the activity boxes for 32 hours (only the first 27 hours were analysed). This period was subdivided as follows: a three-hour habituation phase, 12 hours light cycle and 12 hours dark cycle. There was a significant effect of Mef2c loss over the testing period (Two-way repeated measures ANOVA of genotype x time: $F_{(30, 840)} = 1.597$, *P*=0.0229) **Figure 6.7 b**.

Therefore, the total beam-breaks of both genotypes during the first three hours, light cycle and dark cycle were averaged, and two-way repeated measures ANOVA with Bonferroni correction was conducted. Mef2c loss was found to significantly affect the number of beam breaks over the three phases tested (Genotype X time; $F_{(2, 56)} = 7.503$, *p*=0.0013) **Figure 6.7 c**. Pairwise comparison showed that *CKO* mice were significantly less active compared with *WT* controls over the habituation period only (*p*=0.0173) while no significant difference was observed over dark and light phases (*p*>0.9999 and >0.9999, respectively).

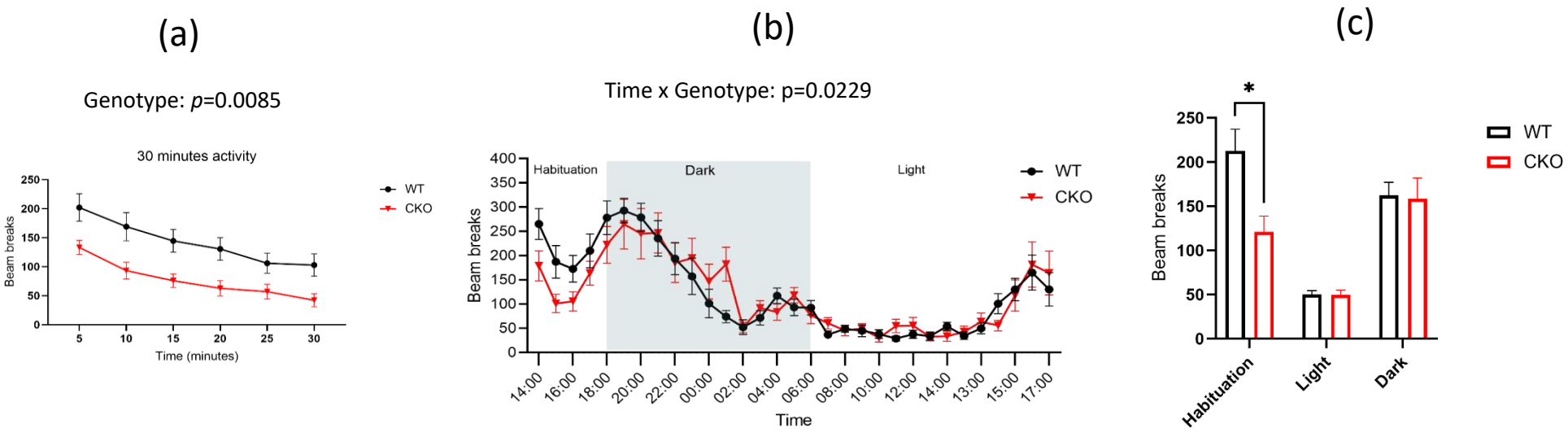

Figure 6.7: 12-month-old *Mef2c CKO* mice showed significant reduction in activity during habituation in automated activity testing. (a) Graphical representation of beam-breaks made by *Mef2c CKO* and *WT* mice over a 30 min period, measured at 5 minutes intervals. Analysis revealed a significant reduction in beam breaks in CKO mice (Genotype: *p*=0.0085). **(b)** Activity of *Mef2c CKO* mice and *WT* controls plotted hour-by–hour over the 24-hour period showed a significant difference in the number of beam breaks between *CKO* mice and controls (*p*=0.0229). The dark phase of the activity task (18:00-06:00) is highlighted in grey. **(c)** Overall activity over the first three hours of activity box testing showed that *Mef2c CKO* mice were significantly less active compared with *WT (p*=0.0173). Bars and lines represent the means of non- perseverative beam breaks. Mef2c CKO (n=14) and WT (n=16). Error bars are SEM.

6.5 Discussion

The striatum is a key regulator of motor and cognitive functions in the mouse brain, and is responsible for learning, habits, and motivation (Graybiel, 2008). For the successful generation of movement, a balance in neuronal coordination between cortex, striatum and thalamus is required and any genetic alteration in the development of the mouse striatum is likely to disrupt these functions (Shepherd, 2013). Early targeted lesion studies revealed that the dorsolateral striatum is important for the development of habitual behaviour (Yin et al., 2004, Vandaele et al., 2019). Therefore, it was important to test whether Mef2c striatal loss during development led to behavioural deficits in adulthood. The disturbance of behavioural phenotypes in *CKO* mice shown in this chapter demonstrate that the Mef2c TF plays an important functional role in the mouse striatum, as its loss during embryonic development has resulted in significant alterations in normal mouse behaviour.

Mef2c CKO animals had normal survival to at least 12-months without any overt morphological or behavioural changes on general observation in their home cages. They also performed normally on grip strength testing, which was an important screening test as Mef2c is known to be crucial for muscle development, the absence of any deficit in grip strength implies normal muscle development and further evidence of the specificity of the conditional knockout.

However, in a specific battery of functional tests, *Mef2c CKO* mice showed motor impairments related to habituation to novelty and in exploratory behaviour, but no clear signs of anxiety-like behaviour as they did not perform differently in the marble burying test and did not spend less time in the centre of an open field arena when compared to WT controls. CKO mice also did not significantly differ in nest building.

I show here that *CKO* mice motor functions have been significantly affected by the loss of Mef2c in the mouse striatum, mainly by impaired motor coordination when tested on accelerated rotarod compared with *WT littermates*. *Mef2c CKO* and *WT* mice showed improvement in performance within the first three trials after which both groups reached a plateau with *CKO* showing significantly lower latency to fall that did not worsen with time. The striatal connections involved in motor coordination are very

complex. The mouse striatum receives dopaminergic projection from SNc and projects to the internal part of globus pallidus and SNr through the direct pathway and the globus pallidus externus and STN through the indirect pathway. This indicates that the reduced performance and motor impairment observed in this test could result partially from the loss of neurons described in chapter 4 that have caused imbalance in this complex organisation. Rotarod testing outcomes showed that, while WT and CKO have comparable motor learning patterns, the overall performance of CKO was significantly reduced compared to WT levels. CKO mice do seem to learn this task but cannot reach same levels of performance as the WT mice.

The results of the rotarod could be also interpreted as reduced motivation to perform the task, so *CKO* mice could have found it easier to jump off the rotating rotarod rather than completing the test. This could be linked to the specification of DM striatum in the goal-directed motor functions (Vandaele et al., 2019) and having Mef2c highly expressed at the DM aspect and thus its loss might affect these functions. However, this interpretation requires further testing.

Our results are in line with the outcomes of rotarod testing of *CaMKII* cre *Mef2c CKO* mice in which Mef2c is lost in the cortex and hippocampus during postnatal development; testing these mice showed significantly reduced latency to fall (Adachi et al., 2016a). Rotarod testing showed impairment in motor functions that was linked to neuronal loss in mouse striatum (Martín-Ibáñez et al., 2017), substantia nigra (SNc) (Lei et al., 2014) or globus pallidus (He et al., 2016; Martín-Ibáñez et al., 2017; Lei et al., 2014). On the other hand, our results contradict reports of *Mef2c loss* in the cortex in which it was found that *Mef2c* loss during early embryonic development in *Mef2c het null* mice and in the *Emx1-Cre CKO* led to normal performance on the accelerated rotarod but cognitive deficits and autistic-type behaviours (Harrington et al., 2016; Harrington et al., 2020). Cognition and autistic-like behaviours were not assessed in our study, however, the differences in rotarod performance illustrate the differential effect of Mef2c loss in these two brain regions. This could simply be the result of Mef2c loss leading to alterations in different neural circuits, but it could also be consistent with Mef2c loss having fundamentally different effects on neural cells in the two regions. The

varying results of Mef2c CKO in the cortex at embryonic or postnatal could also suggest an important effect of the developmental timing of Mef2c loss.

When mice were placed in the open field arena for 10 minutes, *CKO* mice showed significantly reduced movement and rearing, indicating that *they* exhibited less exploratory and novelty-induced motor activity when placed in a new environment (the testing arena). The number of times an animal rears can be used as a measure to estimate exploratory behaviour in rodents (Barrós-Loscertales et al., 2011; Seibenhener and Wooten, 2015; Sturman et al., 2018; Zhuang et al., 2001). *Mef2c CKO* were found to travel significantly less far and to travel slower than WT littermate mice. The open field test is considered to provoke a moderate level of anxiety in the unescapable arena test (Belzung, 1992). The time *Mef2c CKO* mice spent in the centre was unchanged compared to *WT*, suggesting that these mice showed a normal fear of the centre and showed no significant anxiety-like behaviour.

Loss of MSNs in striatal striosomes in a transgenic mice expressing Cre recombinase in striosomes with a virus driving Cre-dependent expression of caspase 3 showed no effect on motor functions using rotarod and OFT (Nadel et al., 2020). However, these mice showed a significant impairment in behavioural stability and habit formation with a stereotyped movement. Since Mef2c was shown in this thesis to be expressed only in matrix MSNs but not in striosomes, and its loss caused impairment in motor functions on rotarod and OFT, this strongly indicates the different functional roles of matrix and striosomes compartments in the mouse striatum. Furthermore, the results of OFT were variable in different FoxP1 CKO mouse models depending on loss of FoxP1 in D1, D2, or in D1and D2 expressing MSNs as described in (Anderson et al., 2020a), with no significant difference in velocity between D1 FoxP1 CKO and controls, while this was significantly increased in in D2 and D1D2 FoxP1 CKO mice compared to controls. Similarly, motor impairment on rotarod testing, manifested by a significant reduction in latency to fall, was only reported in FoxP1 loss in D2 CKO and in D1D2 CKO, indicating that the loss of FoxP1 in D1 expressing MSNs that are enriched in striosomes does not trigger motor dysfunction.

To further assess changes in locomotor activity observed in open field test, *Mef2c CKO* mice were placed in activity boxes over 30 minutes. These results were confirmatory to the open field test. The activity of *CKO* mice was significantly reduced within the habituation phase, although no significant difference was found over the whole 24-hour light/dark cycle. The habituation phase was defined as the first three hours of the test, bearing in mind that these mice are in their late adulthood when they were tested, and therefore, learning new environments could take longer time that when testing younger mice.

Variable results in activity testing were found when cortical Mef2c levels were altered. For example, mice with selective Mef2c loss in excitatory cortical neurons, using Emx1^{Cre,} showed significant increase in the number of beam breaks when monitored over one hour. This indicates that these mice have hyperactive behaviours though no data about motor functions during habituation were provided (Harrington et al., 2016a). Mef2c heterozygous mice also showed hyperactivity, but this was only observed in males, in addition to reduced social behaviour (Harrington et al., 2020a). As discussed above, these differences may be caused by differential expression of Mef*2c* in the striatum and cortex of the adult mouse described in chapter 3 and/or to the different roles of the cortex and striatum in these behaviours and hence a differential impact following *CKO* of *Mef2c* in each area.

The striatal connections involved in motor coordination are very complex. The striatum can be organized functionally based on the topographic distribution of the glutamatergic projections from sensorimotor and associative cortical regions to matrix MSNs and conversely limbic domains to striosome MSNs (Gerfen, 1984; Bolam et al., 1988; Ragsdale Jr and Graybiel, 1988; Flaherty and Graybiel, 1994). Alterations in GABA signalling in mouse matrix MSNs were shown to cause motor deficits similar to those seen in HD (Reinius et al., 2015b). *Mef2c* CKO significantly altered normal striatal development and resulted in a partial non-progressive loss of striatal MSNs in the matrix compartment during development. Significant alterations in the dendritic tree arborisation were seen in *Mef2c* CKO mice, where afferents from cortical and thalamic areas form synapses with MSNs. Striatal neuronal loss has been previously associated with HD-like behavioural phenotypes and contributes to the motor deficits described in

HD (Fernagut et al., 2003; Rosser and Dunnett, 2003). The *Mef2c CKO* mice described in this chapter generally showed significant motor impairment compared with WT controls, as manifested in rotarod testing in which *CKO* mice failed to perform as well as WT controls and displayed slower habituation when introduced to new places. These findings are in line with the proposed role of matrix MSNs in motor functions, and in adaptive motor behaviour to the environment (Bolam et al., 1988, Canales and Graybiel, 2000b)

Exploring new environments is a normal mouse behaviour (Leussis and Bolivar, 2006) and habituation to new environments is a form of learning in rodents, thus when a mouse is introduced to new surroundings, it starts exploring until it becomes ''habituated'' to the new environment. In rodents this behaviour has been tested using various methods; open field through measuring overall activity and number of rearings as described in (Bolam et al., 1988; Zhuang et al., 2001) , and vertical and horizontal beam breaks in activity boxes and Y mazes (Malleret et al., 1999; Dellu et al., 2000). CKO mice in this chapter showed significant reduction in locomotor activity during the first three-hour habituation period of testing but no difference in nocturnal and day activity, once habituated, indicating a reduced response to novelty only. The results of the OFT could also indicate reduced activity to novelty, however, this might require testing Mef2c CKO over several days to see if the hypoactive behaviour can be ameliorated by frequent exposure to the testing arena.

6.6 Conclusion

To conclude, the findings of motor behavioural testing suggest that *Mef2c* could play an important role in motor function, and its loss early during embryonic development in the mouse striatum has significantly affected motor functions, mainly through reduced motor activity during habituation in new environments. This adds to the existing literature suggesting that MSNs in the matrix compartment are required for proper motor functions, and that the MSN loss in matrix could have resulted in an imbalance

between matrix and striosomes MSNs that contributed to the behaviour deficits reported in this chapter. Future work should investigate the effects of Mef2c loss on cognitive functions to rule out any effect of Mef2c striatal loss on these functions.

Chapter 7: General Discussion

7.1 General discussion

The focus of this thesis was studying and investigating the functional roles of Mef2c TF in the development of MSNs. Mef2c TF was first described as being involved in the development and differentiation of myocytes but was found later to play important functional roles in the mouse cortex and hippocampus. Although previous research has explored the functional roles of Mef2c in various regions of the mouse brain, its roles in striatal development has received limited attention to date. Mef2c TF was amongst the most upregulated TFs (the fifth) during embryonic striatal development (between E12 and E16) in a gene analysis survey performed in the host lab (Precious et al., 2016).

Mef2c expression was known to be enriched in the cortex of the developing and adult mouse brain, but little was known about the pattern of its expression in the developing and adult mouse striatum. Therefore, the key findings in chapter 3 of this thesis were the characterization of Mef2c expression pattern in mouse striatum and findings in chapters 4, 5, and 6, using *Gsx2-Cre-loxP* induced recombination to generate a Mef2c CKO mouse model, investigated the anatomical and functional consequences of Mef2c loss in the development of MSNs and potential underlying biological mechanisms.

In chapter 3, the spatiotemporal expression of Mef2c was established in the embryonic and postnatal mouse striatum and showed that Mef2c was expressed mostly between E14 and P14 with peak expression observed at P0. Despite this relatively short window of expression, the onset of Mef2c expression is coincident with a critical period of dynamic changes in early postnatal development, the first postnatal weeks.

Furthermore, I showed that Mef2c is colocalized with Ctip2 in P0 mouse striatum that is expressed in matrix and striosomes MSNs. However, it does not colocalize with the striosome marker in P0 striatum, Darpp32, indicating that Mef2c is specifically expressed in the matrix MSNs. This was the first observation in this thesis suggesting that Mef2c is predominantly expressed only in matrix MSNs and hence might be important for their development. This observation was further confirmed in the birth-dating experiment

performed in chapter 4 that showed, at P0, Mef2c was significantly upregulated in MSNs born at E14 and E16, but not those born at E12.

The mouse striatum is a heterogenous structure. In adult mouse it consists of multiple populations of MSNs that are distributed over two compartments: striosomes and matrix. Matrix and striosomes compartments are largely identified by their expressing genes. Transcriptomic analysis of different mouse striatal CKO models targeting specific populations have provided valuable information about novel TFs involved in MSNs differentiation and compartmentation (Anderson et al., 2020; Gokce et al., 2016; Ho et al., 2018)..Identifying markers differentially expressed in these two striatal compartments provides valuable basic knowledge that can be used for different purposes.

Dysregulation of specific matrix or striosomes markers in mouse striatum during development by genetic deletion or overexpression in mouse models has significantly enhanced our understanding of their functional roles in striatal development. Transgenic mice that induce recombination in specific striatal compartments were generated based on the basic knowledge of matrix-striosomes specific markers. For example, targeting striosomes MSNs was performed using Nr4a1 and the tyrosine hydroxylase-eGFP mice (Davis and Puhl, 2011; Miura et al., 2007). Nr4a1 is a specific marker of striosomes that was shown to be co-expressed with the striosomes marker MOR1. Nr4a1 -GFP reporter mice were used in another study to identify more striosomes markers using RNA- and ATAC-seq with sorted striosome and matrix cells at postnatal day 3 (Cirnaru et al., 2021). Furthermore, a transgenic mouse line Gpr101-cre with cre-recombinase activity localised to matrix D1 and D2 MSNs was generated to specifically delete genes in matrix MSNs (Reinius et al., 2015a) and proenkephalin-eGFP transgenic mice were found also to label matrix MSNs (Koshimizu et al., 2008b).

Some neurodegenerative diseases affecting striatum have been shown through histological analysis to affect matrix-striosomes compartment differentially. For example, histological analysis of post-mortem tissue from HD patients showed a significant loss of striosomes MSNs at the early stages of the disease while both matrix

and striosomes MSNs become equally involved in the degenerative process at later stages of HD (Moratalla et al., 1992; Morton et al., 1993; Tippett et al., 2007). HD mouse models have also shown preferential loss of striosomes MSNs (Lawhorn et al., 2008). These results are consistent with a recent investigation using transcriptomic analysis using scRNA sequencing of two HD mouse models, R6/2 (at 9 weeks of age) and zQ175 (at 6 months of age), and human HD striata (grade 1) that showed MSNs in striosomes and matrix, and in D1-D2 pathways are differentially susceptible to degeneration through the course of the disease, with the earliest degeneration in striosome MSNs that express D2 receptor followed by those expressing D1 receptor and then matrix MSNs that express D2 receptor (Matsushima et al., 2022). In PD, a preferential loss of dopaminergic terminals was observed in striosomes, but more interestingly, a preferential loss of cells in ''nigrosomes'', structures in SNc that resemble the striatal striosome compartments in lacking immunoreactivity to CB, was observed in humans and monkeys (Damier et al., 1999; Iravani et al., 2005). In addition, a significant upregulation of prodynorphin in striosomes was observed in PD patients and in monkeys with L-dopa-induced dyskinesia (Henry et al., 2003).

The role of Mef2c in the development of MSNs from early postnatal development until 12 months of age was explored using Gsx2-Cre driven loxP mouse model to knockout Mef2c specifically in the mouse striatum. I found that the loss of Mef2c resulted in a reduction of striatal volume and reduction in MSNs neuronal count in striatal matrix compartment. Interestingly, the reduction in NeuN, FoxP1, Ctip2 and Darpp32 was stable in P14 CKO mouse striatum through to 12 months, indicating that Mef2c does not cause any degenerative effects beyond P14. Reduction in brain and caudo-putamen volume is evident in many pathological conditions in human brain, such as HD, PD, schizophrenia (Bogerts et al., 1985; Pitcher et al., 2012; Rosas et al., 2001) and in patients with cocaine dependence (Barrós-Loscertales et al., 2011). The percentage reduction in Darpp32 expression in CKO mouse striatum at 3-months (28%) was higher compared to the reduction in FoxP1 and Ctip2 at the same time point (~ 18% in both); this does not necessarily mean that there is more reduction in Darpp32 compared to other MSNs, as Darpp32 was only expressed in about 60% of the MSNs, but it could

suggest that there is more tendency of Mef2c to influence the survival of MSNs that will reach full maturity later through adulthood.

Since, Mef2c expression was compartmentalized, i.e., it is expressed in one striatal compartment which is the matrix, but it is absent in the striosomes, it was assumed that this TF is not required in the formation and maturation of striosome MSNs. To confirm this, part of the experiments performed in chapter 4 aimed to see whether Mef2c loss impaired normal development of the striosome and matrix MSNs. Therefore, the immunohistochemical analysis using MOR1 and CB as markers of striosomes and matrix respectively was performed and the results revealed that Mef2c CKO striosomes developed normally with no obvious anatomical or structural changes in the organization of the striosome compartment, however, after quantifying the percentage area of striosomes it was significantly increased. Along with the significant reduction in striatal volume described in chapter 4, I hypothesized that this percentage increase in striosome area was likely due to the cellular loss from one compartment more than the other. The significant reduction in the percentage of CB^{+} area confirmed the conclusion that the loss in CKO mice is indeed matrix MSNs, but not striosomes.

In the literature Mef2c loss has been shown to be associated with dramatic morphological changes in dendritic spines and dendritic tree in the cortical and hippocampal neurons (Barbosa et al., 2008; Adachi et al., 2016; Harrington et al., 2016; Kamath and Chen, 2019; Puang et al., 2020), however, in this thesis, Mef2c was not found to cause any effect on dendritic spines density but a significant effect in dendritic tree complexity was observed in line with the increase in dendritic tree complexity observed in (Kamath and Chen, 2019b). This indicates that Mef2c loss during embryonic development might not be important for dendritic spine development that occurs later in postnatal life. Furthermore, the timing of Mef2c loss might be a contributing factor on striatal dendritic spines development, as postnatal loss at P2 described in (Chen et al., 2016) showed a significant increase in spines density while in this thesis embryonic CKO of Mef2c in mouse striatum did not. The significant alterations in dendritic spine density associated with Mef2c loss in cortical and hippocampal neurons were associated with a significant increase in locomotor movement compared to controls (Harrington et al., 2016; Harrington et al., 2020), Here, I show that Gsx2-Cre $Mef2c^{fl/fl}$ mice showed

significant reduction in activity only when placed in new environment. Taken together, this indicates that Mef2c has different functional roles in striatum, and this is very likely to be associated with motor functions.

As outlined earlier in this chapter Mef2c expression is coincident with an extensive developmental change especially during the first two postnatal weeks. These include, cessation of neurogenesis, the initiation of gliogenesis, early postnatal physiological neuronal turnover process and formation of dendritic spines (Miller and Gauthier, 2007; Catalani et al., 2002; Kriegstein and Alvarez-Buylla, 2009; Cowan, 1979; Bockhorst et al., 2008; Baloch et al., 2009; Ahern et al., 2013) (Miller and Gauthier, 2007, Catalani et al., 2002b, Kriegstein and Alvarez-Buylla, 2009, Cowan, 1979, Bockhorst et al., 2008, Baloch et al., 2009, Ahern et al., 2013). The shift between neurogenesis and gliogenesis, is a process necessary for the production of oligodendrocytes and astrocytes responsible for myelination and support for neuronal cells (Bergmann and Frisén, 2013). Gliogenesis becomes evident at P0 and continues until the first two weeks after birth, with a peak between P7 and P10 in line with the results of the BrdU experiment in chapter 5 that showed peak BrdU uptake in group1, where administration of BrdU was between P5-P7.

In addition, the formation of synapses in matrix MSNs with axon terminals from cortex, thalamus, and substantia nigra first become evident by the end of P7 (Rice and Barone, 2000; Li et al., 2010). Also, one of the most important events taking place during this period is the physiological neuronal turnover that contributes to the loss of about 50% of neurons born during embryonic development (Oppenheim, 1985; Buss et al., 2006). This process terminates in the mouse striatum at P7, as shown in chapter 5, a time point at which a peak in gliogenesis occurs. Due to the dynamic biological events taking place during this period the effect of Mef2c loss on early mouse striatum could have been masked, so that it was not until P14 or 3 months that the first significant difference between *WT* and *CKO* was detected. The increased proliferative activity in P7 mouse brain could have balanced the neuronal loss that occurred earlier and the significant increase in the anti-apoptotic factor Bcl2 in P7 CKO mouse striatum could suggest a compensatory mechanism in CKO mice, however, this requires further investigations.

Interestingly, Mef2c that was described extensively in the previous literature as being involved in proliferation and neurogenesis (Skerjanc and Wilton, 2000; Cho et al., 2011;

Tu et al., 2017), did not cause any significant effect on overall proliferation in postnatal mouse striatum nor on proliferation of NPCs in the LGE during embryonic development. Based on my findings in chapter 4, it was likely that the neuronal loss would occur at a time point between P7 and P14, however, experiments performed in chapter 5 showed a significant increase in the apoptotic activity manifested by the significant increase in caspase 3 positive cells at P3. This was potentially initiated by alterations in the anti-apoptotic mechanisms mediated by Bcl xl. Changes in gene expression were mostly at P0 and P3, with no significant effects observed at P7 and P14 except for the significant increase in the anti-apoptotic factor Bcl2 at P7. This suggests that the effects of Mef2c loss are taking place early after birth, earlier than P7, but it was not observed histologically and statistically until the period of neuronal maturation has completed by the end of the second postnatal week.

Mutations of MEF2C in humans causes abnormalities in motor movement (Le Meur et al., 2010b). Mef2c CKO mice in this research work showed a significant hypoactivity and reduced exploratory behaviour when placed in a new environment. The significant reduction in NeuN counts in CKO mice in the matrix compartment could be a contributing factor for these alterations in behaviour. This mild non-progressive neuronal loss might cause neuroanatomical and neurochemical changes in cortico-striatal and striato-nigral circuitries and consequently, alterations in behavioural functions. Neuronal loss in the mouse striatum, globus pallidus, STN and cortex contribute to the motor dysfunction observed in HD mouse models (Albin, 1995; Vonsattel et al., 1985; Lange et al., 1992). Helios CKO mice exhibited an significant increase in cell death at postnatal day 3 which was associated with a significant impairment of motor functions manifested by an increase in the number of falls on balance beam and rotarod tests (Martín-Ibáñez et al., 2017). Although Mef2c and Helios regulate different roles in MSN development, they are both expressed within the same developmental window, between E14 and P14, and CKO of both results in neuronal loss and impairment in motor functions. The functional implications are highly dependent on the cell population affected, for example matrix-striosomes organisation receives different input from the cortex, with striosomes mainly receiving input from limbic cortex and therefore the motor deficits shown in mouse models with deletion of

striosomes MSNs or in lesions targeting striosomes MSNs present with impairments cognitive functions (Beste et al., 2018) while lesions targeting matrix MSNs at the dorsolateral aspect of the striatum present with motor impairments and alterations in the development of habitual behaviour (Atallah et al., 2007; Yin et al., 2004).

Part of this research work was to investigate the consequences of Mef2c loss during late embryonic development using *in vitro* approaches. The results of these experiments were consistent with what had been seen *in vivo*, except for the interesting finding that showed significant reduction in proliferating cells in E14 CKO cultured cells. Due to lack of time, I was unable to undertake any further experiment to see if Mef2c impacted the proliferation of certain non-neuronal cell types *in vitro*, given that no significant effect was observed on neurogenesis between WT and CKO at E14. Other than that, Mef2c was shown in this thesis to play a crucial role in neuronal survival both *in vivo* and *in vitro* in line with (Akhtar et al., 2012; Li et al., 2008).

7.2 What is next?

Lack of data on whether the neuronal loss described in this thesis is in D1 or D2 MSNs is one of the limitations in this thesis. Most of the commercially available D1 and D2 antibodies are very poor, and therefore, results in research work that used them were non-conclusive. This issue was addressed in other research work by using D1, D2, or both D1D2 expressing transgenic GFP mice as described in (Anderson et al., 2020b), unfortunately these mouse lines were not available through the work of this thesis. Otherwise, they could be very helpful in determining the precise effect of Mef2c loss on direct and indirect pathways.

Since Mef2c has been identified as expressed in matrix MSNs only, single cell analysis of MSNs populations in Mef2c CKO in mouse striatum could contribute to discovering novel genes and cell markers that will help in gaining insights about matrix MSNs maturation and survival.

Mef2c was shown to be an important TF for the survival of MSNs, and this makes it of interest in pre-clinical studies that use human stem cells in replacement therapies in HD and PD. hESCs are a potential source of cell-based therapy to treat these neurodegenerative diseases, however, current protocols are still required to be improved for optimum differentiation of hESCs into functioning MSNs. A reduced motor deficit, and enhanced survival of grafts that are more enriched with dopaminergic neurons were observed in Mef2c -overexpressing NPC transplanted into 6-hydroxydopamine—lesioned PD rat model (Cho et al., 2011). No similar studies have been conducted in HD animal models so far, although in HD the complexity of the basal ganglia circuits is one of the biggest challenges and limitations to determine the best cell type to replace (Dunnett and Rosser, 2004; Shannon and Kordower, 1996). Given the findings in this thesis, Mef2c can be considered as a potential factor in enhancing the survival of transplanted grafts and based on our knowledge of the spatiotemporal expression of this TF, replacing lesioned or damaged matrix MSNs are very likely to be the area of function of Mef2c.

The focus of the behavioural work in this thesis was on performing motor assessment of Mef2c CKO mice, and the results showed that these functions have been significantly

impacted. However, this does not exclude the presence of other consequences or impairment related to cognitive functions.

7.3 Concluding remarks

The striatum is a heterogenous structure and genes involved in the development and differentiation of MSNs are not fully known. Therefore, full understanding of the mechanisms involved in MSNs differentiation could be fundamental for improving cell protocols in cell-based transplantation therapy of HD. Neurodegeneration of MSNs is a hallmark of HD and transplanting human foetal tissue has showed a proof of concept in clinical trials. However, obtaining human foetal tissue is associated with many ethical and practical issues that necessitates the need to improve protocols that use stem cells.

The key findings in this thesis are that CKO of Mef2c in the mouse striatum disturbs normal development of striatal MSNs, in particular the survival of matrix MSNs. The period over which Mef2c appears to be exerting this role is early postnatal development. Indicating that Mef2c could be of great functional importance for the survival of matrix MSNs. I have shown in this thesis data on the expression pattern of Mef2c in the developing and adult mouse striatum that was not known before. Furthermore, I have confirmed that in MSNs, Mef2c is a marker of matrix MSNs, and is not expressed in striosomes, novel data that could help with identifying and manipulating MSNs compartmentalisation into matrix and striosomes.

The data in this thesis has also suggested that Mef2c loss in Gsx-2 expressing lineage of NPCs during embryonic development of the LGE is impacting the maturation and survival of a subset of matrix MSNs during early postnatal development. Furthermore, I have shown that Mef2c CKO does not markedly affect the density of dendritic spines, a classical consequence of Mef2c loss in the cortex and hippocampus of the mouse brain.

To conclude, my findings provide novel data about the role of Mef2c TF in the development of matrix MSNs. Mef2c should be considered as a potential factor in protocols aiming to use human iPSC-derived striatal neurons to generate functional MSNs for grafting purposes, as this could potentially enhance the survival of these cells and subsequently enhancing the grafts survival in pre-clinical trials.

References

ADACHI, M., LIN, P.-Y., PRANAV, H. & MONTEGGIA, L. M. 2016a. Postnatal Loss of Mef2c Results in Dissociation of Effects on Synapse Number and Learning and Memory. *Biological psychiatry (1969),* 80**,** 140-148.

AHERN, T. H., KRUG, S., CARR, A. V., MURRAY, E. K., FITZPATRICK, E., BENGSTON, L., MCCUTCHEON, J., DE VRIES, G. J. & FORGER, N. G. 2013. Cell death atlas of the postnatal mouse ventral forebrain and hypothalamus: effects of age and sex. *The Journal of comparative neurology,* 521**,** 2551-2569.

ANDERSON, A. G., KULKARNI, A., HARPER, M. & KONOPKA, G. 2020a. Single-Cell Analysis of Foxp1-Driven Mechanisms Essential for Striatal Development. *Cell Rep,* 30**,** 3051-3066.e7.

ANDERSON, S. A., QIU, M., BULFONE, A., EISENSTAT, D. D., MENESES, J., PEDERSEN, R. & RUBENSTEIN, J. L. R. 1997. Mutations of the Homeobox Genes Dlx-1 and Dlx-2 Disrupt the Striatal Subventricular Zone and Differentiation of Late Born Striatal Neurons. *Neuron (Cambridge, Mass.),* 19**,** 27-37.

ANDERSON, S. A. & WONDERS, C. P. 2006. The origin and specification of cortical interneurons. *Nature reviews. Neuroscience,* 7**,** 687-696.

ANDREWS, S. F., DAI, X., RYU, B. Y., GULICK, T., RAMACHANDRAN, B. & RAWLINGS, D. J. 2012. Developmentally regulated expression of MEF2C limits the response to BCR engagement in transitional B cells. *Eur J Immunol,* 42**,** 1327-36.

ANGELOZZI, M., DE CHARLEROY, C. R. & LEFEBVRE, V. 2021. EdU-Based Assay of Cell Proliferation and Stem Cell Quiescence in Skeletal Tissue Sections. *In:* HILTON, M. J. (ed.) *Skeletal Development and Repair: Methods and Protocols.* New York, NY: Springer US.

ARLOTTA, P., MOLYNEAUX, B. J., CHEN, J., INOUE, J., KOMINAMI, R. & MACKLIS, J. D. 2005. Neuronal subtype-specific genes that control corticospinal motor neuron development in vivo. *Neuron,* 45**,** 207-21.

ARLOTTA, P., MOLYNEAUX, B. J., JABAUDON, D., YOSHIDA, Y. & MACKLIS, J. D. 2008. Ctip2 Controls the Differentiation of Medium Spiny Neurons and the Establishment of the Cellular Architecture of the Striatum. *The Journal of neuroscience,* 28**,** 622-632.

ARNOLD, M. A., KIM, Y., CZUBRYT, M. P., PHAN, D., MCANALLY, J., QI, X., SHELTON, J. M., RICHARDSON, J. A., BASSEL-DUBY, R. & OLSON, E. N. 2007. MEF2C Transcription Factor Controls Chondrocyte Hypertrophy and Bone Development. *Developmental Cell,* 12**,** 377-389.

ASSALI, A., HARRINGTON, A. J. & COWAN, C. W. 2019. Emerging roles for MEF2 in brain development and mental disorders. *Current opinion in neurobiology,* 59**,** 49-58.

AYLWARD, E. H., LIU, D., NOPOULOS, P. C., ROSS, C. A., PIERSON, R. K., MILLS, J. A., LONG, J. D. & PAULSEN, J. S. 2012. Striatal Volume Contributes to the Prediction of Onset of Huntington Disease in Incident Cases. *Biological psychiatry (1969),* 71**,** 822-828.

BACON, C., SCHNEIDER, M., LE MAGUERESSE, C., FROEHLICH, H., STICHT, C., GLUCH, C., MONYER, H. & RAPPOLD, G. A. 2015. Brain-specific Foxp1 deletion impairs neuronal development and causes autistic-like behaviour. *Molecular psychiatry,* 20**,** 632-639.

BALOCH, S., VERMA, R., HUANG, H., KHURD, P., CLARK, S., YAROWSKY, P., ABEL, T., MORI, S. & DAVATZIKOS, C. 2009. Quantification of brain maturation and growth patterns in C57BL/6J mice via computational neuroanatomy of diffusion tensor images. *Cereb Cortex,* 19**,** 675-87.

BANDEIRA, F., LENT, R. & HERCULANO-HOUZEL, S. 2009. Changing numbers of neuronal and non-neuronal cells underlie postnatal brain growth in the rat. *Proceedings of the National Academy of Sciences of the United States of America,* 106**,** 14108-14113.

BAQUET, Z. C., GORSKI, J. A. & JONES, K. R. 2004. Early Striatal Dendrite Deficits followed by Neuron Loss with Advanced Age in the Absence of Anterograde Cortical Brain-Derived Neurotrophic Factor. *The Journal of neuroscience,* 24**,** 4250-4258.

BARBOSA, A. C., KIM, M.-S., ERTUNC, M., ADACHI, M., NELSON, E. D., MCANALLY, J., RICHARDSON, J. A., KAVALALI, E. T., MONTEGGIA, L. M., BASSEL-DUBY, R. & OLSON, E. N. 2008. MEF2C, a Transcription Factor That Facilitates Learning and Memory by Negative Regulation of Synapse Numbers and Function. *Proceedings of the National Academy of Sciences - PNAS,* 105**,** 9391-9396.

BARRÓS-LOSCERTALES, A., GARAVAN, H., BUSTAMANTE, J. C., VENTURA-CAMPOS, N., LLOPIS, J. J., BELLOCH, V., PARCET, M. A. & ÁVILA, C. 2011. Reduced striatal volume in cocaine-dependent patients. *NeuroImage,* 56**,** 1021-1026.

BELZUNG, C. 1992. Hippocampal mossy fibres: implication in novelty reactions or in anxiety behaviours? *Behav Brain Res,* 51**,** 149-55.

BENTHALL, K. N., CORDING, K. R., AGOPYAN-MIU, A. H. C. W., CHEN, E. Y. & BATEUP, H. S. 2020. Loss of Tsc1 from striatal direct pathway neurons impairs endocannabinoid-LTD and enhances motor routine learning. *bioRxiv***,** 2019.12.15.877126.

BERGMANN, O. & FRISÉN, J. 2013. Why Adults Need New Brain Cells. *Science,* 340**,** 695-696.

BESTE, C., MOLL, C. K. E., PÖTTER-NERGER, M. & MÜNCHAU, A. 2018. Striatal Microstructure and Its Relevance for Cognitive Control. *Trends Cogn Sci,* 22**,** 747-751.

BJORNESS, T. E., KULKARNI, A., RYBALCHENKO, V., SUZUKI, A., BRIDGES, C., HARRINGTON, A. J., COWAN, C. W., TAKAHASHI, J. S., KONOPKA, G. & GREENE, R. W. 2020. An essential role for mef2c in the cortical response to loss of sleep in mice. *eLife,* 9**,** 1-46.

BOCKHORST, K. H., NARAYANA, P. A., LIU, R., AHOBILA-VIJJULA, P., RAMU, J., KAMEL, M., WOSIK, J., BOCKHORST, T., HAHN, K., HASAN, K. M. & PEREZ-POLO, J. R. 2008. Early postnatal development of rat brain: in vivo diffusion tensor imaging. *J Neurosci Res,* 86**,** 1520-8.

BOLAM, J. P., IZZO, P. N. & GRAYBIEL, A. M. 1988. Cellular substrate of the histochemically defined striosome/matrix system of the caudate nucleus: a combined Golgi and immunocytochemical study in cat and ferret. *Neuroscience,* 24**,** 853-75.

BORDIUK, O. L., SMITH, K., MORIN, P. J. & SEMËNOV, M. V. 2014. Cell proliferation and neurogenesis in adult mouse brain. *PloS one,* 9**,** e111453-e111453.

BRIMBLECOMBE, K. R. & CRAGG, S. J. 2017. The Striosome and Matrix Compartments of the Striatum: A Path through the Labyrinth from Neurochemistry toward Function. *ACS Chemical Neuroscience,* 8**,** 235-242.

BUCKANOVICH, R. J., POSNER, J. B. & DARNELL, R. B. 1993. Nova, the paraneoplastic Ri antigen, is homologous to an RNA-binding protein and is specifically expressed in the developing motor system. *Neuron,* 11**,** 657-72.

BURTON, T. R., DIBROV, A., KASHOUR, T. & AMARA, F. M. 2002. Anti-apoptotic wild-type Alzheimer amyloid precursor protein signaling involves the p38 mitogen-activated protein kinase/MEF2 pathway. *Molecular Brain Research,* 108**,** 102-120.

CANALES, J. J. & GRAYBIEL, A. M. 2000. A measure of striatal function predicts motor stereotypy. *Nature neuroscience,* 3**,** 377-383.

CATALANI, A., SABBATINI, M., CONSOLI, C., CINQUE, C., TOMASSONI, D., AZMITIA, E., ANGELUCCI, L. & AMENTA, F. 2002. Glial fibrillary acidic protein immunoreactive astrocytes in developing rat hippocampus. *Mechanisms of ageing and development,* 123**,** 481-490.

CHAN, S. F., HUANG, X., MCKERCHER, S. R., ZAIDI, R., OKAMOTO, S.-I., NAKANISHI, N. & LIPTON, S. A. 2015. Transcriptional profiling of MEF2-regulated genes in human neural progenitor cells derived from embryonic stem cells. *Genomics data,* 3**,** 24-27.

CHEHREHASA, F., MEEDENIYA, A. C. B., DWYER, P., ABRAHAMSEN, G. & MACKAY-SIM, A. 2009. EdU, a new thymidine analogue for labelling proliferating cells in the nervous system. *Journal of neuroscience methods,* 177**,** 122-130.

CHEN, Y.-C., KUO, H.-Y., BORNSCHEIN, U., TAKAHASHI, H., CHEN, S.-Y., LU, K.-M., YANG, H.-Y., CHEN, G.-M., LIN, J.-R., LEE, Y.-H., CHOU, Y.-C., CHENG, S.-J., CHIEN, C.-T., ENARD, W., HEVERS, W., PÄÄBO, S., GRAYBIEL, A. M. & LIU, F.-C. 2016. Foxp2 controls synaptic wiring of corticostriatal circuits and vocal communication by opposing Mef2c. *Nature neuroscience,* 19**,** 1513-1522.

CHO, E.-G., ZAREMBA, J. D., MCKERCHER, S. R., TALANTOVA, M., TU, S., MASLIAH, E., CHAN, S. F., NAKANISHI, N., TERSKIKH, A. & LIPTON, S. A. 2011. MEF2C enhances dopaminergic neuron differentiation of human embryonic stem cells in a parkinsonian rat model. *PloS one,* 6**,** e24027-e24027.

CHO, Y., ASSALI, A., TSVETKOV, E. & COWAN, C. W. 2022. 411 Essential role for the neurodevelopmental disorder-linked gene, MEF2C, in inhibitory neuron function and neurotypical behaviors. *Journal of Clinical and Translational Science,* 6**,** 79-80.

CIRNARU, M.-D., SONG, S., TSHILENGE, K.-T., CORWIN, C., MLECZKO, J., GALICIA AGUIRRE, C., BENLHABIB, H., BENDL, J., APONTES, P., FULLARD, J., CREUS-MUNCUNILL, J., REYAHI, A., NIK, A. M., CARLSSON, P., ROUSSOS, P., MOONEY, S. D., ELLERBY, L. M. & EHRLICH, M. E. 2021. Unbiased identification of novel transcription factors in striatal compartmentation and striosome maturation. *eLife,* 10**,** e65979.

COHEN, G. M. 1997. Caspases: the executioners of apoptosis. *Biochem J,* 326 (Pt 1)**,** 1-16.

COSGROVE, D., WHITTON, L., FAHEY, L., Ó BROIN, P., DONOHOE, G. & MORRIS, D. W. 2019. Genes influenced by MEF2C contribute to neurodevelopmental disease via gene expression changes that affect multiple types of cortical excitatory neurons. *bioRxiv***,** 2019.12.16.877837.

COWAN, W. M. 1979. The development of the brain. *Sci Am,* 241**,** 113-33.

CRITTENDEN, J. R., DUNN, D. E., MERALI, F. I., WOODMAN, B., YIM, M., BORKOWSKA, A. E., FROSCH, M. P., BATES, G. P., HOUSMAN, D. E., LO, D. C. & GRAYBIEL, A. M. 2010. CalDAG-GEFI down-regulation in the striatum as a neuroprotective change in Huntington's disease. *Human molecular genetics,* 19**,** 1756-1765.

CRITTENDEN, J. R. & GRAYBIEL, A. M. 2011. Basal ganglia disorders associated with imbalances in the striatal striosome and matrix compartments. *Frontiers in neuroanatomy,* 5**,** 59.

DANG, M. T., YOKOI, F., YIN, H. H., LOVINGER, D. M., WANG, Y. & LI, Y. 2006. Disrupted Motor Learning and Long-Term Synaptic Plasticity in Mice Lacking NMDAR1 in the Striatum. *Proceedings of the National Academy of Sciences - PNAS,* 103**,** 15254-15259.

DAVIS, M. I. & PUHL, H. L. 2011. Nr4a1-eGFP is a marker of striosome-matrix architecture, development and activity in the extended striatum. *PloS one,* 6**,** e16619-e16619.

DEACON, T. W., PAKZABAN, P. & ISACSON, O. 1994. The lateral ganglionic eminence is the origin of cells committed to striatal phenotypes: neural transplantation and developmental evidence. *Brain research,* 668**,** 211-219.

DECZKOWSKA, A., MATCOVITCH-NATAN, O., TSITSOU-KAMPELI, A., BEN-HAMO, S., DVIR-SZTERNFELD, R., SPINRAD, A., SINGER, O., DAVID, E., WINTER, D., SMITH, L., KERTSER, A., BARUCH, K., ROSENZWEIG, N., TEREM, A., PRINZ, M., VILLEDA, S., CITRI, A., AMIT, I. & SCHWARTZ, M. 2017. Mef2C restrains microglial inflammatory response and is lost in brain ageing in an IFN-I-dependent manner. *Nat Commun,* 8**,** 717-717.

DESPLATS, P. A., KASS, K. E., GILMARTIN, T., STANWOOD, G. D., WOODWARD, E. L., HEAD, S. R., SUTCLIFFE, J. G. & THOMAS, E. A. 2006. Selective deficits in the expression of striatal-enriched mRNAs in Huntington's disease. *J Neurochem,* 96**,** 743-57.

DRAGATSIS, I. & ZEITLIN, S. 2000. CaMKII alpha-Cre transgene expression and recombination patterns in the mouse brain. *Genesis,* 26**,** 133-5.

DUNNETT, S. B. & BJÖRKLUND, A. 1992. *Neural transplantation*, IRL Press.

DUQUE, A. & RAKIC, P. 2011. Different effects of bromodeoxyuridine and [3H] thymidine incorporation into DNA on cell proliferation, position, and fate. *The Journal of neuroscience : the official journal of the Society for Neuroscience,* 31**,** 15205-15217.

EISENSTAT, D. D., LIU, J. K., MIONE, M., ZHONG, W., YU, G., ANDERSON, S. A., GHATTAS, I., PUELLES, L. & RUBENSTEIN, J. L. 1999. DLX-1, DLX-2, and DLX-5 expression define distinct stages of basal forebrain differentiation. *J Comp Neurol,* 414**,** 217-37.

ERIKSSON, P. S., PERFILIEVA, E., BJÖRK-ERIKSSON, T., ALBORN, A.-M., NORDBORG, C., PETERSON, D. A. & GAGE, F. H. 1998. Neurogenesis in the adult human hippocampus. *Nature Medicine,* 4**,** 1313-1317.

ERNST, A., ALKASS, K., BERNARD, S., SALEHPOUR, M., PERL, S., TISDALE, J., POSSNERT, G., DRUID, H. & FRISÉN, J. 2014. Neurogenesis in the Striatum of the Adult Human Brain. *Cell,* 156**,** 1072-1083.

FIENBERG, A. A., HIROI, N., MERMELSTEIN, P. G., SONG, W., SNYDER, G. L., NISHI, A., CHERAMY, A., O'CALLAGHAN, J. P., MILLER, D. B., COLE, D. G., CORBETT, R., HAILE, C. N., COOPER, D. C., ONN, S. P., GRACE, A. A., OUIMET, C. C., WHITE, F. J., HYMAN, S. E., SURMEIER, D. J., GIRAULT, J., NESTLER, E. J. & GREENGARD, P. 1998. DARPP-32: regulator of the efficacy of dopaminergic neurotransmission. *Science,* 281**,** 838-42.

FISHELL, G. & VAN DER KOOY, D. 1989. Pattern formation in the striatum: developmental changes in the distribution of striatonigral projections. *Brain Res Dev Brain Res,* 45**,** 239-55.

FJODOROVA, M., LOUESSARD, M., LI, Z., DE LA FUENTE, D. C., DYKE, E., BROOKS, S. P., PERRIER, A. L. & LI, M. 2019. CTIP2-Regulated Reduction in PKA-Dependent DARPP32 Phosphorylation in Human Medium Spiny Neurons: Implications for Huntington Disease. *Stem Cell Reports,* 13**,** 448-457.

FLAVELL, S. W., COWAN, C. W., KIM, T.-K., GREER, P. L., LIN, Y., PARADIS, S., GRIFFITH, E. C., HU, L. S., CHEN, C. & GREENBERG, M. E. 2006. Activity-Dependent Regulation of MEF2 Transcription Factors Suppresses Excitatory Synapse Number. *Science (American Association for the Advancement of Science),* 311**,** 1008-1012.

FOSTER, G. A., SCHULTZBERG, M., HÖKFELT, T., GOLDSTEIN, M., HEMMINGS, H. C., JR., OUIMET, C. C., WALAAS, S. I. & GREENGARD, P. 1987. Development of a dopamine- and cyclic adenosine 3':5'-monophosphate-regulated phosphoprotein (DARPP-32) in the prenatal rat central nervous system, and its relationship to the arrival of presumptive dopaminergic innervation. *J Neurosci,* 7**,** 1994-2018.

FUJII, T., MURATA, K., MUN, S.-H., BAE, S., LEE, Y. J., PANNELLINI, T., KANG, K., OLIVER, D., PARK-MIN, K.-H. & IVASHKIV, L. B. 2021. MEF2C regulates osteoclastogenesis and pathologic bone resorption via c-FOS. *Bone Research,* 9**,** 4.

GALE, G. D., YAZDI, R. D., KHAN, A. H., LUSIS, A. J., DAVIS, R. C. & SMITH, D. J. 2009. A genome-wide panel of congenic mice reveals widespread epistasis of behavior quantitative trait loci. *Molecular psychiatry,* 14**,** 631-645.

GERFEN, C. R. 1992. The neostriatal mosaic: multiple levels of compartmental organization. *Trends in Neurosciences,* 15**,** 133-139.

GRAVELAND, G. A. & DIFIGLIA, M. 1985. The frequency and distribution of medium-sized neurons with indented nuclei in the primate and rodent neostriatum. *Brain Res,* 327**,** 307-11.

GRAYBIEL, A. M. 1990. Neurotransmitters and neuromodulators in the basal ganglia. *Trends in Neurosciences,* 13**,** 244-254.

GRAYBIEL, A. M. 2008. Habits, rituals, and the evaluative brain. *Annual review of neuroscience,* 31**,** 359-387.

GRAYBIEL, A. M., BAUGHMAN, R. W. & ECKENSTEIN, F. 1986. Cholinergic neuropil of the striatum observes striosomal boundaries. *Nature (London),* 323**,** 625-627.

GRITTON, H. J., HOWE, W. M., ROMANO, M. F., DIFELICEANTONIO, A. G., KRAMER, M. A., SALIGRAMA, V., BUCKLIN, M. E., ZEMEL, D. & HAN, X. 2019. Unique contributions of parvalbumin and cholinergic interneurons in organizing striatal networks during movement. *Nat Neurosci,* 22**,** 586-597.

GU, X., FU, C., LIN, L., LIU, S., SU, X., LI, A., WU, Q., JIA, C., ZHANG, P., CHEN, L., ZHU, X. & WANG, X. 2018. miR-124 and miR-9 mediated downregulation of HDAC5 promotes neurite development through activating MEF2C-GPM6A pathway. *Journal of cellular physiology,* 233**,** 673-687.

GUSEL'NIKOVA, V. V. & KORZHEVSKIY, D. E. 2015. NeuN As a Neuronal Nuclear Antigen and Neuron Differentiation Marker. *Acta Naturae,* 7**,** 42-7.

HAKIM, N. H., KOUNISHI, T., ALAM, A. H., TSUKAHARA, T. & SUZUKI, H. 2010. Alternative splicing of Mef2c promoted by Fox-1 during neural differentiation in P19 cells. *Genes Cells,* 15**,** 255-67.

HARRINGTON, A. J., BRIDGES, C. M., BERTO, S., BLANKENSHIP, K., CHO, J. Y., ASSALI, A., SIEMSEN, B. M., MOORE, H. W., TSVETKOV, E., THIELKING, A., KONOPKA, G., EVERMAN, D. B., SCOFIELD, M. D., SKINNER, S. A. & COWAN, C. W. 2020. MEF2C Hypofunction in Neuronal and Neuroimmune Populations Produces MEF2C Haploinsufficiency Syndrome–like Behaviors in Mice. *Biological psychiatry (1969),* 88**,** 488-499.

HARRINGTON, A. J., RAISSI, A., RAJKOVICH, K., BERTO, S., KUMAR, J., MOLINARO, G., RADUAZZO, J., GUO, Y., LOERWALD, K., KONOPKA, G., HUBER, K. M. & COWAN, C. W. 2016. MEF2C regulates cortical inhibitory and excitatory synapses and behaviors relevant to neurodevelopmental disorders. *eLife,* 5.

HASTINGS, M. L. & KRAINER, A. R. 2001. Pre-mRNA splicing in the new millennium. *Curr Opin Cell Biol,* 13**,** 302-9.

HATTEN, M. E., HEINTZ, N., GONG, S., ZHENG, C., DOUGHTY, M. L., LOSOS, K., DIDKOVSKY, N., SCHAMBRA, U. B., NOWAK, N. J., JOYNER, A. & LEBLANC, G. 2003. A gene expression atlas of the central nervous system based on bacterial artificial chromosomes. *Nature,* 425**,** 917-925.

HENRY, B., DUTY, S., FOX, S. H., CROSSMAN, A. R. & BROTCHIE, J. M. 2003. Increased striatal pre-proenkephalin B expression is associated with dyskinesia in Parkinson's disease. *Exp Neurol,* 183**,** 458-68.

HERKENHAM, M. & PERT, C. B. 1981. Mosaic distribution of opiate receptors, parafascicular projections and acetylcholinesterase in rat striatum. *Nature (London),* 291**,** 415-418.

HEYSER, C. J., FIENBERG, A. A., GREENGARD, P. & GOLD, L. H. 2000. DARPP-32 knockout mice exhibit impaired reversal learning in a discriminated operant task. *Brain Research,* 867**,** 122-130.

HINTIRYAN, H., FOSTER, N. N., BOWMAN, I., BAY, M., SONG, M. Y., GOU, L., YAMASHITA, S., BIENKOWSKI, M. S., ZINGG, B., ZHU, M., YANG, X. W., SHIH, J. C., TOGA, A. W. & DONG, H.-W. 2016. The mouse cortico-striatal projectome. *Nature Neuroscience,* 19**,** 1100-1114.

HISATSUNE, C., OGAWA, N. & MIKOSHIBA, K. 2013. Striatum-specific expression of Cre recombinase using the Gpr88 promoter in mice. *Transgenic Res,* 22**,** 1241-7.

HUNNICUTT, B. J., JONGBLOETS, B. C., BIRDSONG, W. T., GERTZ, K. J., ZHONG, H. & MAO, T. 2016. A comprehensive excitatory input map of the striatum reveals novel functional organization. *eLife,* 5**,** e19103.

HYO JUNG, K., YUKA IMAMURA, K., FENG, C., YING, Z., XUMING, X., MINGFENG, L., ANDRÉ, M. M. S., MIHOVIL, P., KYLE, A. M., GORAN, S., TOBIAS, G., YURAE, S., MATTHEW, B. J., ŽELJKA, K., SIMONE, M., SOFIA, F., SHEILA, U., STEVEN, N. L., ALEXANDER, V., DANIEL, R. W., SHRIKANT, M., THOMAS, M. H., ANITA, H., MARK, R., JOEL, E. K. & NENAD, Š. 2011. Spatio-temporal transcriptome of the human brain. *Nature,* 478**,** 483.

INFANTINO, V., CONVERTINI, P., MENGA, A. & IACOBAZZI, V. 2013. MEF2C exon α: Role in gene activation and differentiation. *Gene,* 531**,** 355-362.

ITO, H., GOTO, S., SAKAMOTO, S. & HIRANO, A. 1992. Calbindin-D28K in the basal ganglia of patients with parkinsonism. *Annals of neurology,* 32**,** 543-550.

IVKOVIC, S. & EHRLICH, M. E. 1999. Expression of the striatal DARPP-32/ARPP-21 phenotype in GABAergic neurons requires neurotrophins in vivo and in vitro. *J Neurosci,* 19**,** 5409-19.

JAIN, M., ARMSTRONG, R. J. E., BARKER, R. A. & ROSSER, A. E. 2001. Cellular and molecular aspects of striatal development. *Brain Research Bulletin***,** 533–540.

JENRETTE, T. A., LOGUE, J. B. & HORNER, K. A. 2019. Lesions of the Patch Compartment of Dorsolateral Striatum Disrupt Stimulus-Response Learning. *Neuroscience,* 415**,** 161-172.

JENSEN, K. B., DREDGE, B. K., STEFANI, G., ZHONG, R., BUCKANOVICH, R. J., OKANO, H. J., YANG, Y. Y. & DARNELL, R. B. 2000. Nova-1 regulates neuron-specific alternative splicing and is essential for neuronal viability. *Neuron,* 25**,** 359-71.

JIANG, L., LUO, M., LIU, D., CHEN, B., ZHANG, W., MAI, L., ZENG, J., HUANG, N., HUANG, Y., MO, X. & LI, W. 2013. BAD overexpression inhibits cell growth and induces apoptosis via mitochondrial-dependent pathway in non-small cell lung cancer. *Cancer cell international,* 13**,** 53-53.

KAMATH, S. P. & CHEN, A. I. 2019. Myocyte Enhancer Factor 2c Regulates Dendritic Complexity and Connectivity of Cerebellar Purkinje Cells. *Molecular neurobiology,* 56**,** 4102-4119.

KELLY, S. M., RAUDALES, R., HE, M., LEE, J. H., KIM, Y., GIBB, L. G., WU, P., MATHO, K., OSTEN, P., GRAYBIEL, A. M. & HUANG, Z. J. 2018. Radial Glial Lineage Progression and Differential Intermediate Progenitor Amplification Underlie Striatal Compartments and Circuit Organization. *Neuron,* 99**,** 345-361.e4.

KELM-NELSON, C. A., BRAUER, A. F. L., BARTH, K. J., LAKE, J. M., SINNEN, M. L. K., STEHULA, F. J., MUSLU, C., MARONGIU, R., KAPLITT, M. G. & CIUCCI, M. R. 2018. Characterization of early-onset motor deficits in the Pink1−/− mouse model of Parkinson disease. *Brain research,* 1680**,** 1-12.

KESSARIS, N., RICHARDSON, W. D., FOGARTY, M., IANNARELLI, P., GRIST, M. & WEGNER, M. 2006. Competing waves of oligodendrocytes in the forebrain and postnatal elimination of an embryonic lineage. *Nature neuroscience,* 9**,** 173-179.

KIM, D. S., FROELICK, G. J. & PALMITER, R. D. 2002. Dopamine-Dependent Desensitization of Dopaminergic Signaling in the Developing Mouse Striatum. *The Journal of neuroscience,* 22**,** 9841-9849.

KOSHIMIZU, Y., WU, S.-X., UNZAI, T., HIOKI, H., SONOMURA, T., NAKAMURA, K. C., FUJIYAMA, F. & KANEKO, T. 2008. Paucity of enkephalin production in neostriatal striosomal neurons: analysis with preproenkephalin-green fluorescent protein transgenic mice. *The European journal of neuroscience,* 28**,** 2053-2064.

KOSHIMIZU, Y., WU, S. X., UNZAI, T., HIOKI, H., SONOMURA, T., NAKAMURA, K. C., FUJIYAMA, F. & KANEKO, T. 2008b. Paucity of enkephalin production in neostriatal striosomal neurons: analysis with preproenkephalin-green fluorescent protein transgenic mice. *Eur J Neurosci,* 28**,** 2053-64.

KRIEGSTEIN, A. & ALVAREZ-BUYLLA, A. 2009. The glial nature of embryonic and adult neural stem cells. *Annu Rev Neurosci,* 32**,** 149-84.

KUPFERSCHMIDT, D. A., JUCZEWSKI, K., CUI, G., JOHNSON, K. A. & LOVINGER, D. M. 2017. Parallel, but Dissociable, Processing in Discrete Corticostriatal Inputs Encodes Skill Learning. *Neuron,* 96**,** 476-489.e5.

LANCIEGO, J. L., LUQUIN, N. & OBESO, J. A. 2012 Functional Neuroanatomy of the Basal Ganglia. *Cold Spring Harb Perspect Med*.

LATCHNEY, S. E., JIANG, Y., PETRIK, D. P., EISCH, A. J. & HSIEH, J. 2015. Inducible knockout of Mef2a, -c, and -d from nestin-expressing stem/progenitor cells and their progeny unexpectedly uncouples neurogenesis and dendritogenesis in vivo. *FASEB journal : official publication of the Federation of American Societies for Experimental Biology,* 29**,** 5059-5071.

LAWHORN, C., SMITH, D. M. & BROWN, L. L. 2008. Striosome-matrix pathology and motor deficits in the YAC128 mouse model of Huntington's disease. *Neurobiol Dis,* 32**,** 471-8.

LE MEUR, N., HOLDER-ESPINASSE, M., JAILLARD, S., GOLDENBERG, A., JORIOT, S., AMATI-BONNEAU, P., GUICHET, A., BARTH, M., CHAROLLAIS, A. & JOURNEL, H. 2010. MEF2C haploinsufficiency caused by either microdeletion of the 5q14. 3 region or mutation is responsible for severe mental retardation with stereotypic movements, epilepsy and/or cerebral malformations. *Journal of medical genetics,* 47**,** 22-29.

LEBOUC, M., RICHARD, Q., GARRET, M. & BAUFRETON, J. 2020. Striatal circuit development and its alterations in Huntington's disease. *Neurobiology of Disease,* 145**,** 105076.

LEE, K., HOLLEY, S. M., SHOBE, J. L., CHONG, N. C., CEPEDA, C., LEVINE, M. S. & MASMANIDIS, S. C. 2017. Parvalbumin Interneurons Modulate Striatal Output and Enhance Performance during Associative Learning. *Neuron,* 93**,** 1451-1463.e4.

LEI, P., AYTON, S., MOON, S., ZHANG, Q., VOLITAKIS, I., FINKELSTEIN, D. I. & BUSH, A. I. 2014. Motor and cognitive deficits in aged tau knockout mice in two background strains. *Molecular neurodegeneration,* 9**,** 29-29.

LEID, M., ISHMAEL, J. E., AVRAM, D., SHEPHERD, D., FRAULOB, V. & DOLLÉ, P. 2004. CTIP1 and CTIP2 are differentially expressed during mouse embryogenesis. *Gene Expr Patterns,* 4**,** 733-9.

LEUSSIS, M. P. & BOLIVAR, V. J. 2006. Habituation in rodents: A review of behavior, neurobiology, and genetics. *Neuroscience and biobehavioral reviews,* 30**,** 1045-1064.

LI, H., RADFORD, J. C., RAGUSA, M. J., SHEA, K. L., MCKERCHER, S. R., ZAREMBA, J. D., SOUSSOU, W., NIE, Z., KANG, Y.-J., NAKANISHI, N., OKAMOTO, S.-I., ROBERTS, A. J., SCHWARZ, J. J. & LIPTON, S. A. 2008. Transcription factor MEF2C influences neural stem/progenitor cell differentiation and maturation <em>in vivo</em&gt. *Proceedings of the National Academy of Sciences,* 105**,** 9397.

LI, H., ZHONG, X., CHAU, K. F., WILLIAMS, E. C. & CHANG, Q. 2011. Loss of activity-induced phosphorylation of MeCP2 enhances synaptogenesis, LTP and spatial memory. *Nat Neurosci,* 14**,** 1001-8.

LI, M., WANG, D., HE, J., CHEN, L. & LI, H. 2020. Bcl-XL: A multifunctional anti-apoptotic protein. *Pharmacological Research,* 151**,** 104547.

LI, Z., MCKERCHER, S. R., CUI, J., NIE, Z., SOUSSOU, W., ROBERTS, A. J., SALLMEN, T., LIPTON, J. H., TALANTOVA, M., OKAMOTO, S.-I. & LIPTON, S. A. 2008. Myocyte Enhancer Factor 2C as a Neurogenic and Antiapoptotic Transcription Factor in Murine Embryonic Stem Cells. *The Journal of neuroscience,* 28**,** 6557-6568.

LIN, Q., SCHWARZ, J., BUCANA, C. & OLSON, E. N. 1997. Control of Mouse Cardiac Morphogenesis and Myogenesis by Transcription Factor MEF2C. *Science (American Association for the Advancement of Science),* 276**,** 1404-1407.

LINGLEY, A. J., BOWDRIDGE, J. C., FARIVAR, R. & DUFFY, K. R. 2018. Mapping of neuron soma size as an effective approach to delineate differences between neural populations. *J Neurosci Methods,* 304**,** 126-135.

LIU, F. C. & GRAYBIEL, A. M. 1992. Heterogeneous development of calbindin-D28K expression in the striatal matrix. *J Comp Neurol,* 320**,** 304-22.

LOBO, M. K., YEH, C. & YANG, X. W. 2008. Pivotal role of early B-cell factor 1 in development of striatonigral medium spiny neurons in the matrix compartment. *J Neurosci Res,* 86**,** 2134-46.

LÓPEZ-GIMÉNEZ, J. F., TECOTT, L. H., PALACIOS, J. M., MENGOD, G. & VILARÓ, M. T. 2002. Serotonin 5- HT (2C) receptor knockout mice: autoradiographic analysis of multiple serotonin receptors. *Journal of neuroscience research,* 67**,** 69-85.

LOSSI, L., TAMAGNO, I. & MERIGHI, A. 2004. Molecular morphology of neuronal apoptosis: Analysis of caspase 3 activation during postnatal development of mouse cerebellar cortex. *Journal of molecular histology,* 35**,** 621-629.

LOUIS SAM TITUS, A. S. C., YUSUFF, T., CASSAR, M., THOMAS, E., KRETZSCHMAR, D. & D'MELLO, S. R. 2017. Reduced Expression of Foxp1 as a Contributing Factor in Huntington's Disease. *The Journal of neuroscience: the official journal of the Society for Neuroscience,* 37**,** 6575-6587.

LUK, K. C. & SADIKOT, A. F. 2001. GABA promotes survival but not proliferation of parvalbumin-immunoreactive interneurons in rodent neostriatum: an in vivo study with stereology. *Neuroscience,* 104**,** 93-103.

LYONS, G. E., MICALES, B. K., SCHWARZ, J., MARTIN, J. F. & OLSON, E. N. 1995. Expression of mef2 genes in the mouse central nervous system suggests a role in neuronal maturation. *The Journal of neuroscience,* 15**,** 5727-5738.

MAJIDI, S. P., REDDY, N. C., MOORE, M. J., CHEN, H., YAMADA, T., ANDZELM, M. M., CHERRY, T. J., HU, L. S., GREENBERG, M. E. & BONNI, A. 2019. Chromatin Environment

and Cellular Context Specify Compensatory Activity of Paralogous MEF2 Transcription Factors. *Cell Rep,* 29**,** 2001-2015.e5.

MARIN, O., ANDERSON, S. A. & RUBENSTEIN, J. L. R. 2000. Origin and Molecular Specification of Striatal Interneurons. *The Journal of neuroscience,* 20**,** 6063-6076.

MARTÍN-IBÁÑEZ, R., CRESPO, E., URBÁN, N., SERGENT-TANGUY, S., HERRANZ, C., JAUMOT, M., VALIENTE, M., LONG, J. E., PINEDA, J. R., ANDREU, C., RUBENSTEIN, J. L. R., MARÍN, Ó., GEORGOPOULOS, K., MENGOD, G., FARIÑAS, I., BACHS, O., ALBERCH, J. & CANALS, J. M. 2010. Ikaros-1 couples cell cycle arrest of late striatal precursors with neurogenesis of enkephalinergic neurons. *Journal of comparative neurology (1911),* 518**,** 329-351.

MARTÍN-IBÁÑEZ, R., PARDO, M., GIRALT, A., MIGUEZ, A., GUARDIA, I., MARION-POLL, L., HERRANZ, C., ESGLEAS, M., GARCIA-DÍAZ BARRIGA, G., EDEL, M. J., VICARIO-ABEJÓN, C., ALBERCH, J., GIRAULT, J.-A., CHAN, S., KASTNER, P. & CANALS, J. M. 2017. Helios expression coordinates the development of a subset of striatopallidal medium spiny neurons. *Development (Cambridge, England),* 144**,** 1566.

MATSUSHIMA, A., PINEDA, S. S., CRITTENDEN, J. R., LEE, H., GALANI, K., MANTERO, J., KELLIS, M., HEIMAN, M. & GRAYBIEL, A. M. 2022. Huntington's Disease Produces Multiplexed Transcriptional Vulnerabilities of Striatal D1-D2 and Striosome-Matrix Neurons. *bioRxiv***,** 2022.04.25.489455.

MCDONALD, A. J. 1992. Projection neurons of the basolateral amygdala: a correlative Golgi and retrograde tract tracing study. *Brain Res Bull,* 28**,** 179-85.

MCGUIRT, A. F., POST, M. R., PIGULEVSKIY, I., SULZER, D. & LIEBERMAN, O. J. 2021. Coordinated Postnatal Maturation of Striatal Cholinergic Interneurons and Dopamine Release Dynamics in Mice. *J Neurosci,* 41**,** 3597-3609.

MILLER, F. D. & GAUTHIER, A. S. 2007. Timing is everything: making neurons versus glia in the developing cortex. *Neuron,* 54**,** 357-69.

MIYAMOTO, Y., KATAYAMA, S., SHIGEMATSU, N., NISHI, A. & FUKUDA, T. 2018. Striosome-based map of the mouse striatum that is conformable to both cortical afferent topography and uneven distributions of dopamine D1 and D2 receptor-expressing cells. *Brain structure & function,* 223**,** 4275-4291.

MIYOSHI, G., YOUNG, A., PETROS, T., KARAYANNIS, T., MCKENZIE CHANG, M., LAVADO, A., IWANO, T., NAKAJIMA, M., TANIGUCHI, H., HUANG, Z. J., HEINTZ, N., OLIVER, G., MATSUZAKI, F., MACHOLD, R. P. & FISHELL, G. 2015. Prox1 Regulates the Subtype-Specific Development of Caudal Ganglionic Eminence-Derived GABAergic Cortical Interneurons. *J Neurosci,* 35**,** 12869-89.

MOSLEY, M., SHAH, C., MORSE, K. A., MILORO, S. A., HOLMES, M. M., AHERN, T. H. & FORGER, N. G. 2017. Patterns of cell death in the perinatal mouse forebrain: Cell Death in the Perinatal Mouse Brain. *Journal of comparative neurology (1911),* 525**,** 47-64.

NADEL, J. A., PAWELKO, S. S., COPES-FINKE, D., NEIDHART, M. & HOWARD, C. D. 2020. Lesion of striatal patches disrupts habitual behaviors and increases behavioral variability. *PLOS ONE,* 15**,** e0224715.

NAKAMURA, A., SWAHARI, V., PLESTANT, C., SMITH, I., MCCOY, E., SMITH, S., MOY, S. S., ANTON, E. S. & DESHMUKH, M. 2016. Bcl-xL is essential for the survival and function of differentiated neurons in the cortex that control complex behaviors. *The Journal of neuroscience,* 36**,** 5448-5461.

NIKOUEI, K., MUÑOZ-MANCHADO, A. B. & HJERLING-LEFFLER, J. 2016. BCL11B/CTIP2 is highly expressed in GABAergic interneurons of the mouse somatosensory cortex. *Journal of chemical neuroanatomy,* 71**,** 1-5.

OKAMOTO, S.-I., KRAINC, D., SHERMAN, K. & LIPTON, S. A. 2000. Antiapoptotic Role of the p38 Mitogen-Activated Protein Kinase-Myocyte Enhancer Factor 2 Transcription Factor Pathway during Neuronal Differentiation. *Proceedings of the National Academy of Sciences - PNAS,* 97**,** 7561-7566.

OPFERMAN, J. T. & KOTHARI, A. 2018. Anti-apoptotic BCL-2 family members in development. *Cell Death & Differentiation,* 25**,** 37-45.

OSÓRIO, J. & RÉTAUX, S. 2008. The lamprey in evolutionary studies. *Development Genes and Evolution***,** 221–235.

OUIMET, C. C. & GREENGARD, P. 1990. Distribution of DARPP-32 in the basal ganglia: an electron microscopic study. *J Neurocytol,* 19**,** 39-52.

PAI, E. L.-L., CHEN, J., DARBANDI, S. F., CHO, F. S., CHEN, J., LINDTNER, S., CHU, J. S., PAZ, J. T., VOGT, D., PAREDES, M. F. & RUBENSTEIN, J. L. R. 2020. Maf and mafb control mouse pallial interneuron fate and maturation through neuropsychiatric disease gene regulation. *eLife,* 9.

PARIKSHAK, NEELROOP N., LUO, R., ZHANG, A., WON, H., LOWE, JENNIFER K., CHANDRAN, V., HORVATH, S. & GESCHWIND, DANIEL H. 2013. Integrative Functional Genomic Analyses Implicate Specific Molecular Pathways and Circuits in Autism. *Cell,* 155**,** 1008-1021.

PEIXOTO, R. T., WANG, W., CRONEY, D. M., KOZOROVITSKIY, Y. & SABATINI, B. L. 2016. Early hyperactivity and precocious maturation of corticostriatal circuits in Shank3B â '/â ' mice. *Nature neuroscience,* 19**,** 716-724.

PETRYNIAK, M. A., POTTER, G. B., ROWITCH, D. H. & RUBENSTEIN, J. L. 2007. Dlx1 and Dlx2 control neuronal versus oligodendroglial cell fate acquisition in the developing forebrain. *Neuron,* 55**,** 417-33.

PLOTKIN, J. L. & SURMEIER, D. J. 2015. Corticostriatal synaptic adaptations in Huntington's disease. *Curr Opin Neurobiol,* 33**,** 53-62.

POTTHOFF, M. J. & OLSON, E. N. 2007. MEF2: a central regulator of diverse developmental programs. *Development,* 134**,** 4131-40.

PRECIOUS, S. V., KELLY, C. M., REDDINGTON, A. E., VINH, N. N., STICKLAND, R. C., PEKARIK, V., SCHERF, C., JEYASINGHAM, R., GLASBEY, J., HOLEITER, M., JONES, L., TAYLOR, M. V. & ROSSER, A. E. 2016. FoxP1 marks medium spiny neurons from precursors to maturity and is required for their differentiation. *Experimental neurology,* 282**,** 9-18.

PUANG, SHU J., ELANGGOVAN, B., CHING, T. & SNG, JUDY C. G. 2020. MEF2C and HDAC5 regulate Egr1 and Arc genes to increase dendritic spine density and complexity in early enriched environment. *Neuronal signaling,* 4**,** NS20190147-NS20190147.

QIN, S., MADHAVAN, M., WACLAW, R. R., NAKAFUKU, M. & CAMPBELL, K. 2016. Characterization of a new Gsx2-cre line in the developing mouse telencephalon. *Genesis (New York, N.Y. : 2000),* 54**,** 542-549.

QIN, S., WARE, S. M., WACLAW, R. R. & CAMPBELL, K. 2017. Septal contributions to olfactory bulb interneuron diversity in the embryonic mouse telencephalon: role of the homeobox gene Gsx2. *Neural Development,* 12**,** 13.

RAJKOVICH, K. E., LOERWALD, K. W., HALE, C. F., HESS, C. T., GIBSON, J. R. & HUBER, K. M. 2017. Experience-Dependent and Differential Regulation of Local and Long-Range Excitatory Neocortical Circuits by Postsynaptic Mef2c. *Neuron (Cambridge, Mass.),* 93**,** 48-56.

REINIUS, B., BLUNDER, M., BRETT, F. M., ERIKSSON, A., PATRA, K., JONSSON, J., JAZIN, E. & KULLANDER, K. 2015. Conditional targeting of medium spiny neurons in the striatal matrix. *Frontiers in Behavioral Neuroscience,* 9.

RIVERA, A., CUÉLLAR, B., GIRÓN, F. J., GRANDY, D. K., DE LA CALLE, A. & MORATALLA, R. 2002. Dopamine D4 receptors are heterogeneously distributed in the striosomes/matrix compartments of the striatum. *Journal of neurochemistry,* 80**,** 219-229.

RIVERA, P., SILVA-PEÑA, D., BLANCO, E., VARGAS, A., ARRABAL, S., SERRANO, A., PAVÓN, F. J., BINDILA, L., LUTZ, B., RODRÍGUEZ DE FONSECA, F. & SUÁREZ, J. 2019. Oleoylethanolamide restores alcohol-induced inhibition of neuronal proliferation and microglial activity in striatum. *Neuropharmacology,* 146**,** 184-197.

ROBBINS, T. W. & COSTA, R. M. 2017. Habits. *Current Biology,* 27**,** R1200-R1206.

RODGERS, K. M., AHRENDSEN, J. T., PATSOS, O. P., STRNAD, F. A., YONCHEK, J. C., TRAYSTMAN, R. J., MACKLIN, W. B. & HERSON, P. S. 2018. Endogenous Neuronal Replacement in the Juvenile Brain Following Cerebral Ischemia. *Neuroscience,* 380**,** 1-13.

ROSS, C. A. & TABRIZI, S. J. 2011. Huntington's disease: from molecular pathogenesis to clinical treatment. *Lancet Neurol,* 10**,** 83-98.

ROSSER, A. E. & BACHOUD-LÉVI, A.-C. 2012. Chapter 17 - Clinical trials of neural transplantation in Huntington's disease. *In:* DUNNETT, S. B. & BJÖRKLUND, A. (eds.) *Progress in Brain Research.* Elsevier.

RUBIN, A. N., ALFONSI, F., HUMPHREYS, M. P., CHOI, C. K., ROCHA, S. F. & KESSARIS, N. 2010. The germinal zones of the basal ganglia but not the septum generate GABAergic interneurons for the cortex. *J Neurosci,* 30**,** 12050-62.

SAKA, E., GOODRICH, C., HARLAN, P., MADRAS, B. K. & GRAYBIEL, A. M. 2004. Repetitive behaviors in monkeys are linked to specific striatal activation patterns. *J Neurosci,* 24**,** 7557-65.

SANDAU, M. M., NAKAGAWA, O., ALBRING, J. C., KOHYAMA, M., MURPHY, K. M., WILKER, P. R. & SCHWARZ, J. J. 2008. Transcription factor Mef2c is required for B cell proliferation and survival after antigen receptor stimulation. *Nature immunology,* 9**,** 603-612.

SATO, K., SUMI-ICHINOSE, C., KAJI, R., IKEMOTO, K., NOMURA, T., NAGATSU, I., ICHINOSE, H., ITO, M., SAKO, W., NAGAHIRO, S., GRAYBIEL, A. M. & GOTO, S. 2008. Differential involvement of striosome and matrix dopamine systems in a transgenic model of dopa-responsive dystonia. *Proceedings of the National Academy of Sciences,* 105**,** 12551-12556.

SEDELIS, M., SCHWARTING, R. K. & HUSTON, J. P. 2001. Behavioral phenotyping of the MPTP mouse model of Parkinson's disease. *Behav Brain Res,* 125**,** 109-25.

SEKIYAMA, Y., SUZUKI, H. & TSUKAHARA, T. 2012. Functional gene expression analysis of tissue-specific isoforms of Mef2c. *Cell Mol Neurobiol,* 32**,** 129-39.

SHEPHERD, G. M. G. 2013. Corticostriatal connectivity and its role in disease. *Nature reviews. Neuroscience,* 14**,** 278-291.

SKERJANC, I. S. & WILTON, S. 2000. Myocyte enhancer factor 2C upregulates MASH-1 expression and induces neurogenesis in P19 cells. *FEBS Lett,* 472**,** 53-6.

SOLEILHAVOUP, C., TRAVAGLIO, M., PATRICK, K., GARÇÃO, P., BOOBALAN, E., ADOLFS, Y., SPRIGGS, R. V., MOLES-GARCIA, E., DHIRAJ, D., OOSTERVEEN, T., FERRI, S. L., ABEL, T., BRODKIN, E. S., PASTERKAMP, R. J., BROOKS, B. P. & PANMAN, L. 2020. Nolz1 expression is required in dopaminergic axon guidance and striatal innervation. *Nature Communications,* 11**,** 3111.

SOUSA, V. H. & FISHELL, G. 2010. Sonic hedgehog functions through dynamic changes in temporal competence in the developing forebrain. *Curr Opin Genet Dev,* 20**,** 391-9.

SPELIOTES, E. K., KOWALL, N. W., SHANTI, B. F., KOSOFSKY, B., FINKLESTEIN, S. P. & LEIFER, D. 1996. Myocyte-specific enhancer binding factor 2C expression in gerbil brain following global cerebral ischemia. *Neuroscience,* 70**,** 67-77.

TAMURA, S., MORIKAWA, Y., IWANISHI, H., HISAOKA, T. & SENBA, E. 2004. Foxp1 gene expression in projection neurons of the mouse striatum. *Neuroscience,* 124**,** 261-267.

TAYLOR, M. V. & HUGHES, S. M. 2017. Mef2 and the skeletal muscle differentiation program. *Semin Cell Dev Biol,* 72**,** 33-44.

TEPPER, J. M., TECUAPETLA, F., KOÓS, T. & IBÁÑEZ-SANDOVAL, O. 2010. Heterogeneity and diversity of striatal GABAergic interneurons. *Front Neuroanat,* 4**,** 150.

THOMAIDOU, D., MIONE, M. C., CAVANAGH, J. F. & PARNAVELAS, J. G. 1997. Apoptosis and its relation to the cell cycle in the developing cerebral cortex. *J Neurosci,* 17**,** 1075-85.

TORESSON, H., POTTER, S. S. & CAMPBELL, K. 2000. Genetic control of dorsal-ventral identity in the telencephalon: opposing roles for Pax6 and Gsh2. *Development,* 127**,** 4361-71.

TSAI, H.-H., LI, H., FUENTEALBA, L. C., MOLOFSKY, A. V., TAVEIRA-MARQUES, R., ZHUANG, H., TENNEY, A., MURNEN, A. T., FANCY, S. P. J., MERKLE, F., KESSARIS, N., ALVAREZ-BUYLLA, A., RICHARDSON, W. D. & ROWITCH, D. H. 2012. Regional Astrocyte Allocation Regulates CNS Synaptogenesis and Repair. *Science (American Association for the Advancement of Science),* 337**,** 358-362.

TU, S., AKHTAR, M. W., ESCORIHUELA, R., AMADOR-ARJONA, A., SWARUP, V., PARKER, J., ZAREMBA, J., HOLLAND, T., BANSAL, N., HOLOHAN, D., LOPEZ, K., RYAN, S., CHAN, S., YAN, L., ZHANG, X., HUANG, X., SULTAN, A., MCKERCHER, S., AMBASUDHAN, R., XU, H., WANG, Y., GESCHWIND, D., ROBERTS, A., TERSKIKH, A., RISSMAN, R., MASLIAH, E., LIPTON, S. & NAKANISHI, N. 2017. NitroSynapsin therapy for a mouse MEF2C haploinsufficiency model of human autism. *Nat Commun,* 8**,** 1488-1488.

VANDAELE, Y., MAHAJAN, N. R., OTTENHEIMER, D. J., RICHARD, J. M., MYSORE, S. P. & JANAK, P. H. 2019. Distinct recruitment of dorsomedial and dorsolateral striatum erodes with extended training. *eLife,* 8**,** e49536.

VOINEAGU, I., WANG, X., JOHNSTON, P., LOWE, J. K., TIAN, Y., HORVATH, S., MILL, J., CANTOR, R. M., BLENCOWE, B. J. & GESCHWIND, D. H. 2011. Transcriptomic analysis of autistic brain reveals convergent molecular pathology. *Nature,* 474**,** 380-384.

WACLAW, R. R., WANG, B., PEI, Z., EHRMAN, L. A. & CAMPBELL, K. 2009. Distinct temporal requirements for the homeobox gene Gsx2 in specifying striatal and olfactory bulb neuronal fates. *Neuron,* 63**,** 451-65.

WALAAS, S. I. & GREENGARD, P. 1984. DARPP-32, a dopamine- and adenosine 3':5'-monophosphate-regulated phosphoprotein enriched in dopamine-innervated brain regions. I. Regional and cellular distribution in the rat brain. *The Journal of neuroscience,* 4**,** 84-98.

WANG, J., ZHANG, Q., CHEN, Y., YU, S., WU, X. & BAO, X. 2019. Rett and Rett-like syndrome: Expanding the genetic spectrum to KIF1A and GRIN1 gene. *Molecular genetics & genomic medicine,* 7**,** e968-e968.

WELSH, C. A., STEPHANY, C.-É., SAPP, R. W. & STEVENS, B. 2020. Ocular dominance plasticity in binocular primary visual cortex does not require C1q. *The Journal of neuroscience,* 40**,** 769-783.

WEXLER, A., WILD, E. J. & TABRIZI, S. J. 2016. George Huntington: a legacy of inquiry, empathy and hope. *Brain,* 139**,** 2326-33.

WICHTERLE, H., TURNBULL, D. H., NERY, S., FISHELL, G. & ALVAREZ-BUYLLA, A. 2001. In utero fate mapping reveals distinct migratory pathways and fates of neurons born in the mammalian basal forebrain. *Development,* 128**,** 3759-71.

WRIGHT, J., STANIC, D. & THOMPSON, L. H. 2013. Generation of striatal projection neurons extends into the neonatal period in the rat brain. *Journal of Physiology,* 591**,** 67-76.

WU, S., ESUMI, S., WATANABE, K., CHEN, J., NAKAMURA, K. C., NAKAMURA, K., KOMETANI, K., MINATO, N., YANAGAWA, Y., AKASHI, K., SAKIMURA, K., KANEKO, T. & TAMAMAKI, N. 2011. Tangential migration and proliferation of intermediate progenitors of GABAergic neurons in the mouse telencephalon. *Development,* 138**,** 2499-509.

WU, W., FOLTER, S. D., SHEN, X., ZHANG, W. & TAO, S. 2011. Vertebrate paralogous MEF2 genes: origin, conservation, and evolution. *PloS one,* 6**,** e17334.

WU, Y., DEY, R., HAN, A., JAYATHILAKA, N., PHILIPS, M., YE, J. & CHEN, L. 2010. Structure of the MADS-box/MEF2 domain of MEF2A bound to DNA and its implication for myocardin recruitment. *Journal of molecular biology,* 397**,** 520-533.

XU, Q., COBOS, I., DE LA CRUZ, E., RUBENSTEIN, J. L. & ANDERSON, S. A. 2004. Origins of cortical interneuron subtypes. *Journal of Neuroscience,* 24**,** 2612-2622.

XUE, L., JIAN, X., HENNING, F., XIAOMENG, T., LIANLIAN, L., YUE, X., HUATENG, C., JIA, Q., GUDRUN, A. R. & JIE-GUANG, C. 2015. Foxp1 regulates cortical radial migration and neuronal morphogenesis in developing cerebral cortex. *PloS one,* 10**,** e0127671.

Y, K. 2013. The unending fascination with the Golgi method. *OA Anatomy,* 1(3)**,** 24.

YGER, M. & GIRAULT, J.-A. 2011. DARPP-32, Jack of All Trades… Master of Which? *Frontiers in Behavioral Neuroscience,* 5.

YIN, H. H., KNOWLTON, B. J. & BALLEINE, B. W. 2004. Lesions of dorsolateral striatum preserve outcome expectancy but disrupt habit formation in instrumental learning. *Eur J Neurosci,* 19**,** 181-9.

YIN, H. H., KNOWLTON, B. J. & BALLEINE, B. W. 2005. Blockade of NMDA receptors in the dorsomedial striatum prevents action-outcome learning in instrumental conditioning. *Eur J Neurosci,* 22**,** 505-12.

YING, C. Y., DOMINGUEZ-SOLA, D., FABI, M., LORENZ, I. C., HUSSEIN, S., BANSAL, M., CALIFANO, A., PASQUALUCCI, L., BASSO, K. & DALLA-FAVERA, R. 2013. MEF2B mutations lead to deregulated expression of the oncogene BCL6 in diffuse large B cell lymphoma. *Nat Immunol,* 14**,** 1084-92.

YOUNG, K. M., FOGARTY, M., KESSARIS, N. & RICHARDSON, W. D. 2007. Subventricular zone stem cells are heterogeneous with respect to their embryonic origins and

neurogenic fates in the adult olfactory bulb. *The Journal of neuroscience: the official journal of the Society for Neuroscience,* 27**,** 8286-8296.

ZENG, C., PAN, F., JONES, L. A., LIM, M. M., GRIFFIN, E. A., SHELINE, Y. I., MINTUN, M. A., HOLTZMAN, D. M. & MACH, R. H. 2010. Evaluation of 5-ethynyl-2'-deoxyuridine staining as a sensitive and reliable method for studying cell proliferation in the adult nervous system. *Brain Research,* 1319**,** 21-32.

ZHANG, J., DUBLIN, P., GRIEMSMANN, S., KLEIN, A., BREHM, R., BEDNER, P., FLEISCHMANN, B. K., STEINHÄUSER, C. & THEIS, M. 2013. Germ-line recombination activity of the widely used hGFAP-Cre and nestin-Cre transgenes. *PloS one,* 8**,** e82818-e82818.

ZHANG, M., ZHU, B. & DAVIE, J. 2015. Alternative splicing of MEF2C pre-mRNA controls its activity in normal myogenesis and promotes tumorigenicity in rhabdomyosarcoma cells. *J Biol Chem,* 290**,** 310-24.

ZHANG, Z., WEI, S., DU, H., SU, Z., WEN, Y., SHANG, Z., SONG, X., XU, Z., YOU, Y. & YANG, Z. 2019. Zfhx3 is required for the differentiation of late born D1-type medium spiny neurons. *Experimental Neurology,* 322**,** 113055.

ZHANG, Z. & ZHAO, Y. 2022. Progress on the roles of MEF2C in neuropsychiatric diseases. *Molecular brain,* 15**,** 8-8.

ZHAO, Z., ZHANG, D., YANG, F., XU, M., ZHAO, S., PAN, T., LIU, C., LIU, Y., WU, Q., TU, Q., ZHOU, P., LI, R., KANG, J., ZHU, L., GAO, F., WANG, Y. & XU, Z. 2022. Evolutionarily conservative and non-conservative regulatory networks during primate interneuron development revealed by single-cell RNA and ATAC sequencing. *Cell research,* 32**,** 425-436.

ZHU, B. & GULICK, T. 2004. Phosphorylation and alternative pre-mRNA splicing converge to regulate myocyte enhancer factor 2C activity. *Mol Cell Biol,* 24**,** 8264-75.

ZHU, B., RAMACHANDRAN, B. & GULICK, T. 2005. Alternative pre-mRNA splicing governs expression of a conserved acidic transactivation domain in myocyte enhancer factor 2 factors of striated muscle and brain. *J Biol Chem,* 280**,** 28749-60.